INTERNATIONAL DOCTORAL
SCHOOL OF THE USC

Sandra Natalia
Díaz Arias

PhD Thesis

Exploring the self-assembly of cyclic peptides into multidimensional nanostructures

Santiago de Compostela, 2024

Doctoral Programme in Chemical Science and Technology

INTERNATIONAL DOCTORAL
SCHOOL OF THE USC

DOCTORAL THESIS

EXPLORING THE SELF-ASSEMBLY OF CYCLIC PEPTIDES INTO MULTIDIMENSIONAL NANOSTRUCTURES

Sandra Natalia Díaz Arias

Supervisors: Javier Montenegro García and Ignacio Insua López

Tutor: Juan Ramón Granja Guillán

PHD PROGRAMME IN CHEMICAL SCIENCE AND TECHNOLOGY

SANTIAGO DE COMPOSTELA

2024

AGRADECIMIENTOS

En primer lugar, me gustaría expresar mi agradecimiento a los directores y tutor de esta tesis doctoral por su apoyo, orientación y dedicación durante estos años. Javier Montenegro, gracias por haberme dado la oportunidad de trabajar en tu grupo de investigación y por depositar tu confianza en mí para llevar a cabo este trabajo. Ignacio Insua, gracias por adentrarme en el mundo del ensamblaje y enseñarme a hacer investigación de calidad, cuestionando y siendo siempre muy críticos con cada paso dado. Juan Granja, gracias por tu pasión por la investigación y tu gran conocimiento sobre los ciclo péptidos que sin duda ha sido clave en el transcurso de esta tesis.

A las diferentes instituciones que han financiado todos los medios de los que disponemos en el grupo de investigación y que han permitido llevar a cabo el trabajo recogido en este manuscrito. A la Agencia Estatal de Investigación (SAF2017-89890-R, PCI2019-103400, PID2020-117143RB-I00, RYC2021-031367-I, RYC2021-034705-I), al Consejo Europeo de Investigación (ERC-Stg DYNAP-677786 y ERC-PoC TraffikGene, 838002), a la Organización Internacional HFSP (RGY0066/2017) y a los Fondos Europeos (ERDF y MSCA-IF 2018-84332). Finalmente, a la Xunta de Galicia por sus financiaciones al grupo (ED431G 2019/03, ED431C 2017/25 y 2016-AD031) y la financiación a nivel personal (ED481A-2020/137) de una de las becas que me concedieron y que me permitió realizar una estancia predoctoral en Cambridge.

Al Prof. Oren Scherman y a la Dr. Jade MacCune por brindarme la oportunidad de realizar la estancia predoctoral en su grupo de investigación. Participar en sus seminarios y trabajar en su laboratorio fue una experiencia enriquecedora tanto a nivel personal como profesional. Gracias a todos los miembros del grupo por su gran acogida durante esos meses. Al Prof. Giovanni Pavan y a la Dr. Annalisa Cardellini por la preciada colaboración que nos ha permitido ampliar nuestro conocimiento sobre el ensamblaje de los ciclo péptidos.

A todos mis compañeros de laboratorio, por la gran familia que formamos dentro y fuera de él, su apoyo ha sido fundamental para no perder la cabeza estos años. También me gustaría agradecer a los miembros más senior del grupo de investigación, ya que sus discusiones científicas y sugerencias durante los seminarios han sido fundamentales a lo largo de la tesis.

A la RIAIDT de la USC que pone a nuestra disposición un gran catálogo de servicios y equipos fundamentales para el correcto desarrollo de nuestra investigación. Al CIQUS y a todas las personas que pertenecen a él, desde los diferentes directivos y técnicos que permiten el buen funcionamiento del centro a todos los profesores e investigadores que siempre están dispuestos a ayudar.

INDEX

1. ABBREVIATIONS & ACRONYMS

δ	Chemical Shift
λ_{exc}	Excitation Wavelength
λ_{max}	Maximum Emission Wavelength
0D	Zero Dimensional
1D	One Dimensional
^{1}H-NMR	Proton Nuclear Magnetic Resonance
2-CTC	2-Chlorotrytil Chloride Resin
2D	Two Dimensional
3D	Three Dimensional
Å	Armstrong
a.u.	Arbitrary units
AA	All-Atoms
aa	Amino Acid
Abs	Absorbance
AFM	Atomic Force Microscopy
Ala	Alanine
Amp	(2S, 4R)-4-aminoproline
amp	(2S, 4S)-4-aminoproline
Asn	Asparagine
ATR	Attenuated total Reflectance
CAC	Critical Aggregation Concentration
CD	Circular Dichroism
CG	Coarse-Grained
CMP	Collagen Mimetic Peptide
CP	Cyclic Peptide
d	doblet
DCM	Dichloromethane
dd	Doublet of Doublets
DFT	Density Functional Theory
DIPEA	N,N-Diisopropylethylamine
DMAP	4-Dimethylaminopyridine
DMF	Dimethylformamide

DNA	Deoxyribonucleic Acid
Equiv	Equivalent
ESI	Electrospray Ionization
FF	Diphenylalanine
Fmoc	Fluorenylmethoxycarbonyl
FTIR	Fourier Transform Infrared Spectroscopy
Gln	Glutamine
Glu	Glutamic Acid
Gly	Glycine
HFIP	1,1,1,3,3,3-Hexafluoro-2-propanol
His	Histidine
HOBt	1-Hydroxybenzotriazole
HPLC	High Performance Liquid Chromatography
HRMS	High Resolution Mass Spectrometry
Hyp	Hydroxiproline
J	Coupling Constant
Leu	Leucine
Lys	Lysine
m	Multiplet
m/z	Mass-to-Charge ratio
MD	Molecular Dynamic
MS	Mass Spectrometry
N-HBTU	N,N,N′,N′-Tetramethyl-O-(1H-benzotriazol-1-yl)uronium hexafluorophosphate
NMM	N-Methylmorpholine
NT	Nanotube
PA	Peptide Amphiphile
Phe	Phenylalanine
PMF	Potential of Mean Force
Pro	Proline
PyAOP	(7-Azabenzotriazol-1-yloxy)tripyrrolidinophosphonium hexafluorophosphate

RNA	Ribonucleic Acid
RT	Room Temperature
s	Singlet
SAXS	Small-Angle X-Ray Scattering
SCPN	Supramolecular Cyclic Peptide Nanotube
SLP	Surfactant-Like Peptide
SP	Supramolecular Polymerization
STEM	Scanning Transmission Electron Microscopy
t	triplet
TEM	Transmission Electron Microscopy
TFA	Trifluoroacetic Acid
ThT	Thioflavin-t
TIPS	Triisopropylsilane
TMV	Tobacco Mosaic Virus
Trp	Tryptophan
US	Umbrella Sampling
UV-Vis	Ultraviolet-visible Spectroscopy

2. RESUMO

A química supramolecular inspirou novas estratexias cara á conectividade molecular, dende unha perspectiva covalente a unha non covalente. Tradicionalmente, os químicos centráronse na formación e ruptura dos enlaces covalentes para construír novas moléculas, mentres que as interaccións moleculares utilizáronse principalmente para comprender o mecanismo das reaccións químicas. Non obstante, este enfoque foi limitado para a síntese de arquitecturas macromoleculares moi complexas ou para a comprensión de procesos biolóxicos. Atopouse un novo enfoque para este problema na química supramolecular, que foi definida como "química máis aló da molécula".

Esta nova disciplina da química é un campo multidisciplinar que combina as características químicas, físicas e biolóxicas de diferentes especies químicas que interactúan entre sí. O seu fundamento reside no estudo das interaccións moleculares a través de forzas non covalentes, incluíndo enlaces de hidróxeno, π-π stacking, forzas de Van der Waals, efectos solvofóbicos e interaccións Coulombicas. Aínda que a forza destas interaccions é relativamente baixa, a combinación de varias delas dota aos complexos supramoleculares de robustez e integridade estrutural. Aínda que certos procesos supramoleculares poden requirir unha guía ou "input" externa, a especificidade e a selectividade inherentes da unión molecular entre monómeros proporcionan a información esencial necesaria para guiar as interaccións supramoleculares.

Polo xeral, é posible distinguir entre dous procesos principais dependendo do número de monómeros implicados no resultado final supramolecular: o recoñecemento molecular e a autoensamblaxe molecular.

O recoñecemento molecular refírese a un proceso no que as moléculas "host" identifican e interactúan selectivamente con moléculas "guest" formando un complexo supramolecular. Esta unión é moi específica e depende da complementariedade física e química entre ambas moléculas que interactúan.

Por outro lado, a autoensamblaxe molecular refírese a un proceso onde os monómeros organízanse espontáneamente no espazo formando arquitecturas supramoleculares ben definidas. As forzas non covalentes que impulsan este proceso poden ser tanto interaccións intramoleculares como intermoleculares segundo se establezan entre partes dun mesmo monómero ou entre monómeros diferentes, respectivamente. Normalmente, as interaccións intramoleculares dan lugar ao que se coñece como un proceso de "folding", onde unha única molécula adopta unha conformación espacial definida, que se asemella ao pregamento natural das proteínas. Á súa vez, as interaccións intermoleculares están implicadas nun proceso onde varios monómeros interactúan para formar polímeros supramoleculares. Este proceso é similar á polimerización covalente, onde as unidades monoméricas poden ser iguais (homopolímero) ou diferentes (heteropolímero), diferenciándose na reversibilidade inherente das interaccións

non covalentes que permiten a elongación-despolimerización dinámica dos agregados supramoleculares.

Aínda que tanto as interaccións supramoleculares como os enlaces covalentes poden presentar reversibilidade e dinamismo baixo certas condicións, os seus mecanismos e, polo tanto, as súas aplicacións difiren significativamente. A reversibilidade dos enlaces covalentes adoita limitarse a certos tipos de reaccións químicas e moitas veces require unha alta enerxía para romper e unir moléculas. Pola contra, as interaccións supramoleculares pódense formar e romper dinámicamente en condicións suaves, o que facilita o control e manipulación do proceso en comparación cos enlaces covalentes.

Esta propiedade, xunto coa capacidade de crear estruturas máis grandes, fai da autoensamblaxe molecular unha poderosa ferramenta para deseñar materiais con propiedades e funcionalidades adaptadas que doutro xeito serían difíciles de conseguir mediante a síntese covalente. Por ese motivo, a autoensamblaxe destaca como un método versátil para a fabricación "bottom-up" ou ascendente de nanomateriais con capacidade de resposta.

A versatilidade da autoensamblaxe molecular reside na ampla gama de monómeros que se poden empregar, así como nas diferentes condicións ás que se poden someter, modificando as vías de ensamblaxe e, polo tanto, a estrutura supramolecular final. Ao seleccionar monómeros con propiedades estruturais e químicas específicas, é posible controlar as interaccións supramoleculares que impulsan o proceso de ensamblaxe, controlando con precisión a estrutura final ensamblada. Non obstante, a pesar dos avances no campo, este deseño racional segue sendo un reto cando se trata de sistemas multidimensionais, onde os monómeros deben elongarse en direccións ortogonais simultáneamente. Ademáis, estes sistemas máis complexos poden dar lugar a vías de ensamblaxe competitivas, dificultando o control do proceso e dando lugar á formación de estruturas polidispersas e heteroxéneas.

A vida mostra moitos exemplos onde as moléculas se organizan de forma xerárquica e ben definida, formando conxuntos funcionais esenciais para os procesos biolóxicos. A capacidade intrínseca destes sistemas biolóxicos de autoensamblarse con precisión e especificidade reside nas diversas e intrincadas interaccións que as biomoléculas poden establecer. Esta propiedade inherente inspirou aos investigadores a utilizar biomoléculas como monómeros na fabricación de sistemas autoensamblados complexos. Entre eles, os péptidos destacan pola gran diversidade química que ofrecen infinitas combinacións de aminoácidos. Esta diversidade permite deseñar un número infinito de secuencias peptídicas con propiedades específicas que ditarán a súa ensamblaxe final. Os diferentes aminoácidos proteinoxénicos cobren unha ampla gama de propiedades químicas e físicas, incluíndo tamaño, carga, hidrofobicidade e, en xeral, a súa

tendencia a formar certas interaccións non covalentes. Aínda que esta variedade química e estrutural pode axudar no deseño racional de monómeros peptídicos, tamén complicará a fabricación previsible de materiais supramoleculares xa que é necesario controlar que as forzas non covalentes cooperen de forma correcta e ortogonal cara a diferentes direccións de crecemento.

Actualmente, moitos enfoques para a fabricación de nanoestruturas baséanse en métodos de proba e erro, que poden ser complexos e ineficientes. Ademais, moitos enfoques existentes limítanse a secuencias naturais con patróns de pregamento predeterminados, restrinxindo o uso de análogos non naturais.

Un dos principais retos actuais reside en establecer regras xerais de deseño para codificar a nivel molecular (monómeros) que poidan ser aplicadas de xeito universal, posibilitando a fabricación de estruturas ben definidas de forma previsible e selectiva.

Dentro da gran variedade de posibles estruturas peptídicas, nesta tesis centrarémonos nos péptidos cíclicos (CP) formados por D,L-α-aminoácidos. Este tipo de péptidos presentan vantaxes na creación de conxuntos multidimensionais dada a súa xeometría ríxida. Os péptidos cíclicos cun número par de aminoácidos D/L alternados na súa secuencia adoptan unha conformación macrocíclica plana con enlaces peptídicos orientados perpendicularmente ao anel. Esta disposición pode permitir que os péptidos cíclicos se apilen formando estruturas nanotubulares nunha conformación similar ás laminas tipo β. Unha extensa rede de enlaces de hidróxeno entre grupos peptídicos amida impulsa a autoensamblaxe nunha dimensión (é dicir, o alongamento de nanotubos) e fainos altamente estables en ambientes acuosos. Notablemente, as cadeas laterais dos aminoácidos están apuntando cara a fóra do nanotubo, decorando así a súa superficie. Os estudos iniciais revelaron que a estabilidade dos nanotubos está poco influenciada polas súas cadeas laterais, o que abre un amplo abano de posibilidades no deseño de monómeros peptídicos cíclicos. Desde o seu descubrimento, os nanotubos de péptidos cíclicos foron investigados amplamente tanto a nivel estrutural como funcional. Descifráronse unha gran variedade de secuencias capaces de formar nanotubos con, por exemplo, diferentes diámetros internos para a unión selectiva de pequenas moléculas ou decorados con polímeros con potenciais aplicacións en biomedicina. Non obstante, todos estes avances no uso de péptidos cíclicos centráronse nun único conxunto supramolecular, os nanotubos, sen ter en conta outros sistemas superiores.

Nesta tese de doutoramento propoñemos empregar os péptidos cíclicos como monómeros potenciais para construír arquitecturas supramoleculares multidimensionais con xeometrías definidas. Esta proposta xorde das características estruturais anteriormente explicadas destas moléculas, que postulamos como excelentes andamios para deseñar conxuntos xerárquicos. Tendo en conta a potencial rixidez do anel peptídico cíclico e que as cadeas laterais están

apuntando cara a fóra na superficie dos nanotubos unidimensionales, plantexamos a hipótese de que o deseño racional de secuencias peptídicas adaptadas conduciría o empaquetamento lateral dos nanotubos cara a outras direccións, formando, finalmente, máis altas. asembleas ordenadas.

Un traballo publicado recentemente no noso grupo de investigación demostrou a autoensamblaxe secuencial de 1D a 2D dun péptido cíclico anfifílico: **CP$_x$**. Este monómero ten dous dominios segregados, un dominio hidrofóbico formado polo tripéptido Leu-Trp-Leu e outro hidrofílico, composto por aminoácidos polares onde o ácido glutámico e a histidina xogan un papel fundamental como residuos cargados durante o proceso de ensamblaxe. Esta anfifilicidade é amplificada ao longo do conxunto nanotubular 1D, onde as cadeas laterais clasifícanse axialmente cara a rexións ortogonais. Estes nanotubos posteriormente empaquetanse formando nanofollas 2D nun ambiente acuoso impulsado principalmente polo efecto hidrofóbico. As características clave do deseño que dirixen este conxunto xerárquico están codificadas na secuencia primaria. Na rexión hidrófoba, a formación dunha cremalleira de leucina proporciona direccionalidade ao alongamento 2D, organizando os nanotubos nunha configuración escalonada en zig-zag entre capas. Ademais, o empaquetamento hidrofóbico reforzase e dirixe aínda máis polas interaccións de π-π stacking entre os grupos indol do triptófano adxacente dentro do nanotubo. Na rexión hidrofílica, os aminoácidos con carga polar xogan un papel fundamental no mantemento da bicapa xa que o estado de ionización do monómero a pH fisiolóxico ten unha carga neta negativa polos glujtámicos desprotonados. Esta carga tamén se amplifica ao longo da montaxe e a repulsión xerada mantén as nanofollas nun estado illado e estendido evitando que se agreguen. En resumen, CPx adaptouse con motivos supramoleculares ortogonais para que, en condicións axeitadas, puidese presentar un delicado equilibrio entre interaccións non covalentes atractivas (enlaces de hidróxeno e efecto hidrófobo) e repulsivas (electrostáticas), orientando o seu conxunto xerárquico cara á formación de nanofollas 2D.

No primeiro capítulo desta tese, pretendemos estudar a relación entre a secuencia primaria do péptido cíclico anteriormente descrito: **CP$_x$**, e o seu comportamento no autoensamblaxe secuencial de 1D a 2D. Partindo dos coñecementos adquiridos no traballo previo sobre as forzas que impulsan o proceso de autoensamblaxe, cuestionamos aquí, dende unha visión máis específica, que posicións e aminoácidos están a desempeñar un papel fundamental e cales aceptarían modificación. Pretendemos obter unha comprensión máis profunda das contribucións individuais de cada aminoácido na ensamblaxe, xerando así regras de deseño máis xerais e desbloqueando todo o potencial desta estratexia para lograr nanomateriais 2D.

Para este fin, deseñamos unha biblioteca de péptidos con modificacións sistemáticas derivadas do **CP$_x$** orixinal. Cada novo monómero foi meticulosamente

adaptado con pequenos cambios, mediante a substitución dun residuo por outro ou o intercambio de residuos entre diferentes posicións. Estas modificacións individuais axudáronnos a desentrañar a interacción entre o deseño molecular e as forzas intermoleculares que dirixen o proceso de ensamblaxe. Dado que a anfifilicidade é de vital importancia para a segregación de ambos dominios e, polo tanto, para o crecemento ortogonal cara a diferentes direccións, decidimos dividir a exploración estrutural entre os cambios na rexión hidrofóbica e pola rexión.

Inicialmente, deseñamos modificacións no dominio hidrofóbico central, substituíndo tanto o triptófano central como as dúas leucinas flanqueadas por outros residuos aromáticos ou non aromáticos e menos voluminosos. Os resultados amosaron que, en xeral, este dominio tolera ben as modificacións estudadas: a substitución do residuo de triptófano central por alanina (**CP$_A$**), leucina (**CP$_L$**) e fenilalanina (**CP$_F$**) amosaron a formación de nanofollas, concluíndo que un residuo aromático é non estritamente necesario para manter o ensamblaxe. Ademais, substituímos ambas as leucinas por residuos aromáticos (**CP$_{2F}$**) e tamén deseñamos unha variante co mesmo aminoácido nas tres posicións (**CP$_{3F}$**). Os resultados obtidos con estas dúas modificacións adicionais tamén foron positivos, con formación de nanofollas para ambos os casos. Non obstante, observamos o mesmo patrón para os derivados cos mesmos aminoácidos nesta rexión (**CP$_L$** e **CP$_{3F}$**), un maior grao de enrrugamento nas nanofollas formadas e una maior agregación. Polo tanto, postulamos que é necesario un desaxuste hidrofóbico entre os residuos centrais e flanqueados para dirixir o crecemento 2D mediante a asociación ordenada de nanotubos.

En segundo lugar, exploramos modificacións na rexión polar, demostrando a alta dependencia do sistema ensamblado para o estado cargado do monómero. Para avaliar esta rexión polar, deseñamos dous péptidos que varían a posición de ambos aminoácidos cargados: **CP$_{oE}$**, mantén a segregación do ácido glutámico e da histidina en dominios separados pero perde o desaxuste frontal e resulta incapaz de formar nanofollas, mentres que **CP$_{2E2H}$**, con aminoácidos idénticos. ácidos dispostos en dominios homodiméricos ensamblados en nanofollas 2D estendidas. Ampliamos a exploración avaliando a influencia das cargas negativas, deseñando un péptido cíclico totalmente aniónico con catro ácidos glutámicos **CP$_{4E}$** e substituíndo as histidinas por lisinas, **CP$_K$**, para ter unha carga neta cero ao longo do sistema. Estes resultados mostraron que é necesario ter certa repulsión para manter a formación das nanofollas 2D xa que en ambos os casos non se conseguiron nanofollas.

En conclusión, no primeiro capítulo, presentamos que os péptidos cíclicos poden usarse para adaptar materiais bidimensionais controlando as forzas supramoleculares en diferentes direccións de crecemento. Este control pódese conseguir deseñando monómeros con motivos de unión non covalentes situados estratexicamente. En base a este coñecemento, decidimos ampliar a biblioteca e

deseñar novos monómeros peptídicos cíclicos con diferentes motivos de unión para conseguir nanoestruturas diferentes ás bicapas de nanofollas. Polo tanto, nos próximos dous capítulos, mostraremos dúas estratexias adicionais de deseño que nos permiten fabricar diferentes arquitecturas.

No segundo capítulo propuxemos modificar a propagación 2D incorporando motivos de unión en posicións ortogonais ao longo da estrutura monomérica: **CP10**. En concreto, incorporamos dúas caras hidrofóbicas enfrontadas estratexicamente posicionadas nun ángulo de 180º para inducir a asociación de nanotubos cara á formación dunha monocapa. Baseándonos no deseño de **CP$_x$**, queriamos manter o mesmo tripéptido hidrofóbico formado pola secuencia Leu-Trp-Leu e tanto o ácido glutámico como a histidina como aminoácidos con carga polar. Para iso, tivemos que aumentar a dez aminoácidos a secuencia do péptido cíclico. Postulamos que con este deseño, o conxunto monocapa sería impulsado e estabilizado polo mesmo equilibrio de interaccións supramoleculares que **CP$_x$**. Mentres que os enlaces de hidróxeno e o efecto hidrófobo actúan como forzas atractivas entre os péptidos cíclicos e os nanotubos respectivamente, a superficie cargada negativamente estabiliza as monocapas por repulsión electrostática.

A caracterización experimental probou a formación destas novas arquitecturas monocapas que demostran a disposición deseñada de nanotubos empaquetados lateralmente.

Ademais, debido á falta de comprensión mecanicista destes conxuntos xerárquicos a nivel molecular, utilizamos simulacións computacionais para estudar en detalle as diferentes etapas supramoleculares ao longo do proceso de polimerización. Un conxunto de modelos computacionais revelou que o mecanismo de polimerización presenta un sesgo entre a propagación unidimensional (axial) e bidimensional (lateral).

En primeiro lugar, as simulacións de dinámica molecular determinaron a conformación antiparalela como a máis estable. En segundo lugar, utilizouse o modelado in silico para estudar o proceso de autoensamblaxe medindo as enerxías de dimerización de oligómeros de diferentes tamaños cara a ambas as direccións de polimerización: axial e lateral. Os resultados amosaron un claro sesgo na dirección de propagación dependendo do grao de oligomerización nos nanotubos. Os monómeros **CP10** sofren preferentemente un elongamento unidimensional en estados de oligomerización curtos, mentres que os oligómeros máis longos prefiren a propagación en 2D. En terceiro lugar, o modelado de "coarse-grained" revelou que a polimerización é un proceso por pasos no que se forma inicialmente un clúster hidrofóbico de nanotubos orientados aleatoriamente, que posteriormente se realiña mediante contactos laterais formando a monocapa.

Por último, as simulacións metadinámicas demostraron que a formación destas monocapas se mantén debido á flexibilidade que lle confire o tripéptido hidrofóbico: Leu-Trp-Leu. Este motivo de deseño chámouse "triptophan hinge" ou bisagra de triptófano, debido ao papel clave que desempeñan os residuos de triptófano no mantemento da interface dinámica non polar. Ademais, demostramos con éxito a relevancia deste motivo deseñando monómeros peptídicos cíclicos con mutacións seleccionadas na rexión hidrofóbica. Mediante experimentos control, empregando microscopía de epifluorescencia, puidemos confirmar a incapacidade de ensamblar dos monómeros que carecen tanto do residuo de triptófano no medio como de residuos de leucinas a ambos lados. Estes resultados confirmaron ademais a importancia da tríada Leu-Trp-Leu para permitir o contacto flexible entre os nanotubos.

En conclusión, esta investigación demostrou aínda máis o potencial dos péptidos cíclicos como monómeros para adaptar nanoestruturas autoensambladas con morfoloxías específicas. Ademais, a comprensión mecanicista da propagación en diferentes direccións axudará a implementar regras xerais clave no deseño racional de monómeros para ensamblaxes multidimensionais, cambiando así o desenvolvemento empírico de monómeros cara a enxeñaría de deseños moleculares predicibles.

No terceiro e último capítulo desta tese, pretendemos trascender os límites da autoensamblaxe 2D e deseñar un novo monómero capaz de crecer ordenadamente nunha nova dirección de propagación. Partindo dos principios fundamentais establecidos nos capítulos anteriores, deseñamos un novo monómero peptídico cíclico que codificaba a información específica para guiar a súa ensamblaxe con precisión cara á formación de nanofollas 3D multicapa. Este innovador monómero non só mantén os principios de anfifilicidade e cargas controladas, senón que tamén incorpora precisión xeométrica, garantindo un empaquetado eficiente no proceso de ensamblaxe. O novo monómero peptídico cíclico **CP6** está composto por seis aminoácidos, incluíndo dúas leucina consecutivas e catro histidinas e ácidos glutámicos alternados.

No novo deseño, o dominio hidrófobo impulsa a ensamblaxe lateral a través da formación da cremalleira de leucina explicada anteriormente. A estrutura de bicapa resultante expón ao medio acuoso os aminoácidos con carga polar: ácido glutámico e histidina. Polo tanto, formulamos a hipótese de que un equilibrio finamente afinado de estados ionizables sería axeitado para o crecemento ao longo do eixe z. A pH lixeiramente ácido, coa histidina comezando a protonarse, cada cara exposta da bicapa serviría de plataforma para a incorporación sucesiva doutras capas de nanotubos mediante interaccións electrostáticas atractivas, dando lugar á formación de nanoestruturas 3D multicapa. Ademais, tivo que introducirse un nivel adicional de control, en canto á precisión xeométrica, para manter este proceso de autoensamblaxe. A redución do tamaño de **CP6** foi un

movemento calculado que non só acurta o diámetro do péptido cíclico dando lugar a un péptido cíclico máis ríxido e restrinxido, senón que tamén allana o camiño para a complementariedade entre os aminoácidos dos péptidos veciños. Esta complementariedade observada dentro da multicapa de **CP6**, formaría unha rede hexagonal pechada onde cada aminoácido dun péptido cíclico coincide perfectamente cos dun péptido cíclico veciño.

Unha vez deseñado, validamos a formación destas novas arquitecturas mediante diferentes técnicas de microscopía. Ademais, observamos unha tendencia a formar nanofollas homoxéneas, suxerindo unha cinética de crecemento controlada a través das diferentes dimensións, e anticipando a capacidade potencial deste novo deseño para controlar con precisión o tamaño e a forma do conxunto resultante.

Neste último capítulo, amosamos por primeira vez como se poden adaptar os péptidos cíclicos para guiar a súa autoensamblaxe cara á formación de nanoestruturas tridimensionais ordenadas. Este estudo destaca a importancia de tres motivos de deseño específicos: carácter anfifílico, cargas controladas e precisión xeométrica, para orquestrar a formación de nanofollas multicapa. Cada elemento de deseño xoga un papel esencial ao ditar o proceso de autoensamblaxe, contribuíndo colectivamente ao estado final de montaxe.

En conclusión, estes achados proporcionan unha nova visión sobre a autoensamblaxe de péptidos cíclicos. Como só se utilizou para ensamblar nanotubos nunha única dimensión, aquí explotamos o seu potencial como monómeros na fabricación de conxuntos de orde superior. Elucidamos unha disposición racional de aminoácidos que inducirá espontaneamente a autoclasificación axial de dominios anfifílicos ao longo dos nanotubos e impulsará a súa asociación lateral en 2D. Incorporamos diferentes motivos de deseño estrutural en cada capítulo, mantendo os mesmos residuos en todos os casos. Estes resultados destacan a gran riqueza dos péptidos como monómeros, demostrando que pequenos cambios estruturais poden levar a grandes cambios no proceso de ensamblaxe. En xeral, empregamos tres motivos de deseño específicos -carácter anfifílico, carga neta e disposición xeométrica- para orquestrar diferentes tipos de conxuntos de nanofollas. Presentamos a hipótese de que os motivos estruturais e os conceptos supramoleculares presentados nesta tese pódense aplicar amplamente a unha variedade de monómeros autoensamblables, atopando aplicación na enxeñaría de biomateriais e como potenciais ferramentas biomédicas.

3. ABSTRACT

Molecular self-assembly is a fundamental process in supramolecular chemistry where individual molecules spontaneously organize into well-defined architectures. This process is a powerful tool across diverse fields, allowing the fabrication of complex systems that would otherwise be difficult to achieve with traditional covalent synthetic methods. Molecular self-assembly not only helps to understand natural assembly processes but also enables the fabrication of non-canonical architectures with properties and functions not evolved naturally and with great implications in nanotechnology and materials science.

The versatility of molecular self-assembly lies in the wide range of monomers that can be used. By selecting monomers with specific structural and chemical properties, it is possible to control the supramolecular interactions that drive the assembly process, precisely controlling the final assembled structure. However, despite advances in the field, this rational design remains a challenge when dealing with multidimensional systems, where monomers are required to elongate in orthogonal directions simultaneously. In addition, these more complex systems can give rise to competing assembly pathways, making process control difficult and leading to the formation of polydisperse and heterogeneous structures.

Life shows plenty of examples where molecules organize in a hierarchical and well-defined manner, forming functional assemblies essential for biological processes. This inherent propensity has inspired researchers to use biomolecules as monomers in new artificially assembled structures. Among them, peptides stand out because of the high chemical diversity offered by endless combinations of amino acids. This diversity allows to design an infinite number of peptide sequences with specific properties that will dictate their final assembly. However, this chemical and structural variety also complicates the predictable fabrication of supramolecular materials as it is necessary to control that non-covalent forces cooperate correctly and orthogonally towards different directions of growth.

Currently, many approaches for the fabrication of nanostructures are based on trial-and-error methods, which can be complex and inefficient. For that reason, one of the main challenges lies in establishing general design rules to be encoded at the molecular level (monomers) that can be universally applied, enabling the fabrication of well-defined structures predictably and selectively.

Within the great variety of possible peptide structures, in this dissertation, we will focus on cyclic peptides (CP) formed by D,L-α-amino acids. These type of peptides present advantages in the creation of multidimensional assemblies given their rigid geometry. Cyclic peptides with an even number of alternating D/L amino acids can adopt a planar macrocyclic conformation with peptide bonds oriented perpendicularly to the ring. This arrangement allows CPs to stack up forming nanotubular structures in a conformation similar to β-sheets. An extensive network of hydrogen bonds between peptide amide groups drives the

self-assembly in one dimension (i.e. nanotubes) and makes them highly stable in aqueous environments. Notably, the side chains of the amino acids are pointing outward from the nanotube, thus decorating its surface. Initial studies have revealed that the nanotube's stability is usually not influenced by their side chains, opening a wide range of possibilities in the design of cyclic peptide monomers. Since their discovery, cyclic peptide nanotubes have been extensively investigated both structurally and functionally. However, all these advances in using cyclic peptides have focused on a single supramolecular assembly, nanotubes, overlooking other potential assemblies.

In this PhD dissertation, we propose cyclic peptides as potential monomers to build up multidimensional supramolecular architectures with defined geometries. This proposal arises from the previously explained structural characteristics of these molecules, which we postulate as excellent scaffolds to design hierarchical assemblies. Taking into account the potential rigidity of the cyclic peptide ring and that side chains are pointing outward at the surface of one-dimensional nanotubes, we hypothesized that rationally designing tailored peptide sequences would drive the lateral packing of nanotubes toward other directions, ultimately forming higher-ordered assemblies.

A recently published work carried out in our group has demonstrated for the first time the sequential 1D-to-2D self-assembly of an amphiphilic cyclic peptide: **CP$_x$** into nanosheets. This amphiphilicity is amplified along the 1D-nanotubular ensemble by segregating hydrophobic and polar-charged amino acids towards orthogonal faces. This disposition and a delicate balance between attractive and repulsive supramolecular forces can drive lateral ordering by forming bilayers in an aqueous environment. In the hydrophobic domain, the tripeptide formed by leucine-tryptophan-leucine drives the self-assembly through the hydrophobic effect while also imparting directionality and ordering by forming a leucine zipper and tryptophan stacking. The opposite polar face with charged amino acids - glutamic acid and histidine, helps in maintaining the bilayer structure through repulsive electrostatic interaction at optimal pH conditions.

In the first chapter of this thesis, we aimed to study the relationship between the primary sequence of **CP$_x$** and the behavior on its hierarchical self-assembly. Based on the knowledge acquired in the previous work on the forces driving the self-assembly process, we here question, from a more detailed perspective, which positions and amino acids are playing a key role and which would accept modification. Our objective was to obtain a deeper understanding of the individual contributions of each amino acid in the assembly, thus generating more general design rules and unlocking the full potential of this strategy to achieve 2D nanomaterials.

For this purpose, we designed a library of peptides with systematic modifications derived from the original **CP$_x$**. These individual modifications

helped us unravel the interplay between molecular design and intermolecular forces directing the assembly process. Since amphiphilicity is of vital importance for the segregation of both domains and thus for the orthogonal growth toward different directions, we decided to maintain it and divide the structural exploration between mutations in the hydrophobic and polar regions separately.

Changes in the hydrophobic domain were, in general, well tolerated. We have replaced both the central tryptophan and the two flanked leucines with other non-aromatic and less bulky aromatic residues. Although all variations assemble into nanosheets, we have observed a different tendency in monomers with the same residue in the three positions: a higher degree of wrinkling and more aggregates in the background. Therefore, we postulated that a hydrophobic mismatch between central and flanked residues is required to direct 2D growth through ordered nanotube association.

On the contrary, the polar region was less tolerant of changes. We have observed that while glutamic and histidine are placed together, nanosheets are formed but if they are segregated in different positions, the assembly is disrupted. Moreover, we have also designed two variants by replacing both histidines with two more glutamic acids and with lysines to have a fully anionic cyclic peptide and a zero net charge, respectively. None of these mutations have shown a tendency to form nanosheets even by modulating assembly conditions. These results demonstrated the high dependence of the assembled system for the charge state of the monomers.

With the knowledge acquired in the first chapter, we decided to expand the potential of cyclic peptides in assembling new nanostructures. To this end, we modified the 2D propagation by incorporating binding motifs in orthogonal positions along the monomeric structure: **CP10**. We have incorporated two confronted hydrophobic faces at a 180° angle to induce the nanotube association toward the formation of a monolayer. Based on **CP$_x$**'s design, we maintained the same hydrophobic tripeptide and polar charged amino acids, to drive the monolayer assembly with the same balance of supramolecular interactions.

Moreover, due to the lack of mechanistic understanding of these hierarchical assemblies at the molecular level, we have used computational simulations to study in detail the different supramolecular stages along the polymerization process. A set of computational models has revealed that the polymerization mechanism exhibits a bias between one-dimensional (axial) and two-dimensional (lateral) propagation based on the degree of oligomerization of the nanotube. Moreover, coarse-grained modeling demonstrated that polymerization occurs in a stepwise manner, initially forming a hydrophobic cluster of randomly oriented nanotubes that subsequently realign into ordered lateral contacts forming the monolayer. Finally, metadynamics simulations highlighted the key role of

tryptophan in the hydrophobic region in maintaining the assembly thanks to the flexibility impart in lateral contacts. We have named this motif as "tryptophan hinge".

In the third and final chapter, we aimed to transcend the limits of the 2D assembly and design a new monomer capable of orderly growth in a new direction of propagation. Building upon the foundation principles established in the previous chapters, we designed a new cyclic peptide monomer that encoded specific information to guide its assembly with precision toward the formation of 3D multilayered nanosheets.

This innovative monomer was reduced to six amino acids: **CP6**, maintaining both the hydrophobic and polar domains previously described. This specific design was made to maintain amphiphilicity but also to incorporate geometric precision, ensuring efficient packing in the assembly process. The reduction in size results in a more rigid cyclic peptide and allows the formation of a hexagonal-type lattice where all the amino acids are perfectly matched in a complementary way. The propagation toward the third dimension was achieved by decreasing the pH of the medium, thus establishing electrostatic attraction between polar faces.

Once meticulously designed, we have validated the formation of these new multilayered nanosheets and demonstrated for the first time how cyclic peptides can be tailored to guide their self-assembly toward the formation of ordered three-dimensional nanostructures. Moreover, we have observed a tendency to form homogeneous nanosheets, suggesting control growth across different dimensions, and anticipating the potential ability of this new design to precisely control the size and shape of the resulting assembly.

In conclusion, these findings provide new insight into the self-assembly of cyclic peptides. Having only been used to assemble nanotubes in the one-dimension, we here exploited their potential as monomers in the fabrication of higher-ordered assemblies. We have elucidated a rational disposition of amino acids that will spontaneously induce axial self-sorting along nanotubes and drive their lateral propagation across different directions. Overall, we have employed three specific design motifs: amphiphilic character, net charge, and geometric disposition, in orchestrating different types of nanosheet assemblies. We hypothesize that the structural motifs and supramolecular concepts presented in this thesis can be broadly applied to a variety of self-assembling monomers, finding application in biomaterial engineering and as potential biomedical tools.

4. INTRODUCTION

4.1. SUPRAMOLECULAR SELF-ASSEMBLY

4.1.1. Introduction to supramolecular chemistry

Supramolecular chemistry is a highly interdisciplinary field that emerged in the latter half of the 20th century, changing our understanding of molecular interactions. Unlike covalent synthetic chemistry, in which atoms are joined together by covalent bonds, supramolecular chemistry goes one step forward and uses the connection of molecular units (e.g., monomers) linked by non-covalent interactions. This new field stood out by presenting a novel solution for the fabrication of complex macromolecular systems hardly accessible from covalent synthetic chemistry.[1]

Although the implementation of supramolecular chemistry took place less than 40 years ago, its conceptual foundations go back much further in time, when scientists began to study the underlying principles by which molecules interact with each other. A milestone that marked the beginning of this new discipline dates back to 1873, when Diderick van der Waals developed a theory on the state of gases, introducing a new type of intermolecular forces between dipoles, later called Van der Waals forces in his honor.[2] A few years later, Fischer introduced the "lock and key model" for enzyme-substrate interactions, which outlined the importance of the specificity and complementarity between molecules.[3] At the beginning of the 20th century, hydrogen bonds began to be investigated. Initially, Latimer and Rodebush described them as "the hydrogen nucleus contained between two octets constitutes a weak bond",[4] but it was not until 1928 that Linus Pauling called them "hydrogen bonds".[5] Even the word "supermolecule", was first used in the mid-1930s by Wolf and his co-workers to describe small dimers of carboxylic acids linked by hydrogen bonds.[6] Years later, this word was used to define higher entities formed by the non-covalent association between various compounds. This brief retrospective highlights the importance of past discoveries in the development of the new field three decades later, but more importantly, this

[1] J. M. Lehn, *Isr. J. Chem.,* **2018**, *58*, 136–141.
[2] J. D. Van der Waals, *On the Continuity of the Gaseous and Liquid States*, Leiden, **1873**.
[3] E. Fischer, *J. Am. Chem. Soc.,* **1894**, *3*, 2985–2993.
[4] B. M. Wendell Latimer, W. H. Rodebush, *J. Am. Chem. Soc.,* **1920**, *42*, 1419–1433.
[5] L. Pauling, *Chem. Rev.,* **1928**, *5*, 173–213.
[6] K. L. Wolf, H. Prahm, H. Harms, *J. Phys. Chem.,* **1937**, *36B*, 237–287.

story reflects the significance that isolated discoveries, regardless of their current relevance, could lead to future great advances.

The journey continued with the characterization of new molecular interactions, which allowed the design of supramolecular architectures of increasing complexity. These new discoveries were also beneficial to complementary emerging fields such as molecular biology or nanotechnology.[7,8] A defining breakthrough came when the Swedish Academy awarded with the Nobel Prize in Chemistry to Cram, Lehn, and Pedersen in 1987 "for their development and use of molecules with structure-specific interactions of high selectivity". Charles J. Pedersen described the synthesis of crown ethers (Figure 1), which are cyclic polyethers able to bind alkaline metal ions with high affinity and selectivity.[9] Expanding upon Pedersen's discoveries, Jean-Marie Lehn introduced three-dimensionality to crown ethers by synthesizing bicyclic cryptand (Figure 1).[10,11] These new compounds were also capable of selectively complexing guest molecules, improving affinity over crown ethers because of their trigonal geometry, a property that also allowed the binding of other species beyond metal ions. Donald J. Cram contributed with new macrocycle hosts with rigid cavities termed spherands (Figure 1).[12,13] This new class of macrocycles improved the affinity for the ligand because they were conformationally preorganized changes to form the supramolecular complex, thus decreasing the energy required for the binding. In their Nobel lectures, Cram named this new field of research "host-guest chemistry", where the larger "host" molecules are designed to interact specifically with smaller "guest" molecules forming a supramolecular complex.[14] At the same time, Lehn coined the term supramolecular chemistry, a concept that gave name to a new area of chemistry, defined as "chemistry beyond the molecule".[15] The objective of this new field is the design of complex assemblies based on molecular components held together by intermolecular non-covalent interactions.

In the past decades, scientists have uncovered and crafted a vast array of supramolecular systems, employing them to perform intricate functions. With the growth of the field, different terms have emerged within supramolecular chemistry, based on the different supramolecular complexes formed or the processes followed to obtain them. The following sections will provide a concise

[7] A. Werner, *Z. Anorg. Chem.,* **1893**, *3*, 267–330.
[8] J. Watson, F. Crick, *Nature*, **1953**, *171*, 737–738.
[9] C. J. Pedersen, *J. Am. Chem. Soc.,* **1967**, *89*, 7017–7036.
[10] B. Dietrich, J.M. Lehn, J.P. Sauvage, *Tetrahedron Lett.,* **1969**, *10*, 2889–2892.
[11] B. Dietrich, J. M. Lehn, J. P. Sauvage, *Tetrahedron Lett* **1969**, *10*, 2885–2888.
[12] K. N. Trueblood, C. B. Knobler, E. Maverick, R. C. Helgeson, S. B. Brown, D. J. Cram, *J. Am. Chem. Soc.,* **1981**, *103*, 5594–5596.
[13] D. J. Cram, T. Kaneda, R. C. Helgeson, G. M. Lein, *J. Am. Chem. Soc.,* **1979**, *101*, 6752–6754.
[14] D. J. Cram, *The Design of Molecular Hosts, Guests, and Their Complexes (Nobel Lecture)*, **1988**.
[15] J. M. Lehn, *Supramolecular Chemistry-Scope and Perspectives Molecules, Supermolecules, and Molecular Devices (Nobel Lecture)*, **1988**.

overview of the fundamental concepts that underpin this younger field of chemistry and will help understand the work addressed throughout this dissertation.

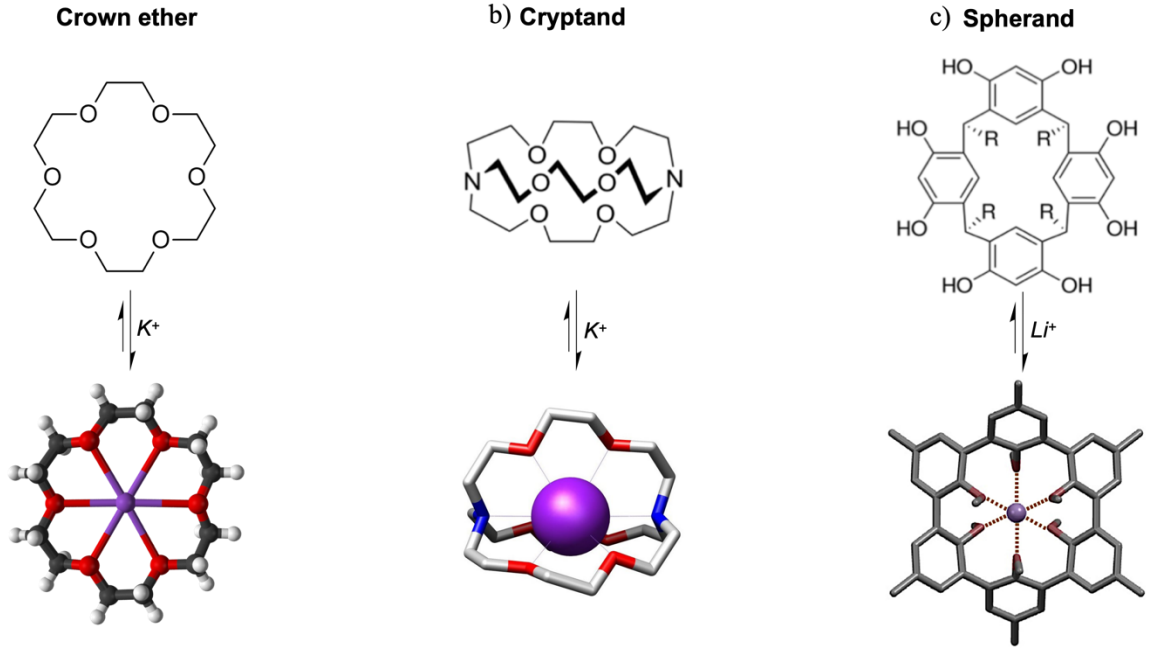

Figure 1. Chemical structure (upper row) and host-guest complexes (bottom row) for: a) crown ether, b) cryptand and c) spherand.

4.1.2. Concepts in supramolecular chemistry

Supramolecular chemistry uses the information encoded in molecules to form assembled systems through well-defined non-covalent interactions. The basic units or molecules employed by supramolecular chemists are known as "**monomers**" or "**building blocks**" (Figure 2, left), and it is the information contained in these compounds, both the inherent properties and structural features, that dictates the supramolecular interactions that give rise to more complex architectures (Figure 2, right).[16] The richness that chemistry offers allow a vast diversity of monomers to create a wide range of supramolecular structures with varying properties and functions. However, it is important to point out that subsequent sections will focus on a specific subset of monomers -rooted in biomolecules, with a particular focus on amino acids since they are the main characters in this work.

Generally, the different types of supramolecular entities developed allow the division of supramolecular chemistry into two broads, partially overlapping areas: **molecular recognition** and **molecular self-assembly**.[17] Both concepts are

[16] J. Rebek, *Proc Natl Acad* , **2009**, *106*, 10423–10424.
[17] J. M. Lehn, Makromolekulare Chemie. Macromolecular Symposia, **1993,** *69*, 1-17.

based on the organization of molecules into ordered structures, but the main difference is the number of monomers involved in the process and how the binding occurs. While molecular recognition is based on a small number of components, usually two, that specifically join together to form a single entity, self-assembly involves a larger number of monomer units that spontaneously arrange to generate larger entities.

Molecular recognition (Figure 2, top), previously named "host-guest chemistry" by Cram,[14] can be defined as a process that occurs when two or more molecules or ions are held together to form a complex with a unique structural relationship. Molecules designated as hosts are typically characterized by macrocycles with "pore-like" structure that allows them to behave as receptors with high affinity and selectivity for guest molecules, often smaller in size, also called substrates or ligands.[18] The selective binding between these components is a result of the high affinity observed at the binding sites inherent in their structures. The field started with the discovery of macrocycles exemplified by the previously mentioned Nobel Prize winner crown ethers, cryptands, and spherands, which promoted the development of novel host molecules like cucurbiturils,[19] cavitands,[20] or carcerands.[21] As the field evolved, the synthesis of more sophisticated host molecules lead to the creation of more complex structures like molecular machines, for which J. P. Sauvage (catenane),[22] J. F. Stoddart (rotaxane)[23] and B. L. Feringa (molecular motor)[24] received the Nobel Prize in Chemistry in 2016.

On the other hand, molecular self-assembly refers to the process by which monomers spontaneously interact and organize themselves into well-defined large architectures (Figure 2, middle).[25] This spontaneous but controlled assembly relies on the collective behavior of the individual components since the information encoded at their molecular level directs the supramolecular interactions. These interactions can be both intra- or intermolecular, depending on whether they occur between units of the same monomer or between different monomers, respectively. For example, "**folding**" is a process guided solely by intramolecular interactions in which a single molecule arranges its different units into specific three-dimensional shapes (Figure 2, bottom). The self-assembly process involves intermolecular interactions ans could also be considered as a supramolecular polymerization, since it consists of successive organization of monomers into larger structures.

[18] J. F. Stoddart, *Org. Chem. Annual Reports Section B,* **1988**, *85*, 353–386.
[19] W. A. Freeman, W. L. Mock, N. Y. Shih, *J. Am. Chem. Soc.,* **1981**, *103*, 7367–7368.
[20] J. R. Moran, S. Karbach, D. J. Cram, *J. Am. Chem. Soc.,* **1982**, *104*, 5573–5856.
[21] H. W. Tittel, F. K. Smalley, R. E. J. Am, A. S. Lindsey, C. D. Gutsche, B. Dhawan, K. H. No, C. D. Muthukrishnan, B. Gutsche, A. G. S. Hógberg, J. E. Moran, S. Karbach, D. J. Cram, J. L. Ericson, R. C. Helgeson, *J Am Chem Soc* **1988**, *110*, 2353–2698.
[22] C. 0 Dietrich-Buchecker, J. P. Sauvage, J. P. Kintzingi, *Tetrahedron Lett.,* **1983**, *24*, 5095–5098.
[23] P. L. Anelli, S. Organici, I. N. Spencer, J. F. Stoddart, *J. Am. Chem. Soc.,* **1991**, *113*, 5131–5133.
[24] N. Koumura, R. W. J. Zijlstra, R. A. van Delden, N. Harada, B. L. Feringa, *Nature,* **1999**, *401*, 152–155.
[25] J.M. Lehn, *Proc. Natl. Acad. Sci.*, **2002,** *99,* 4763-4768.

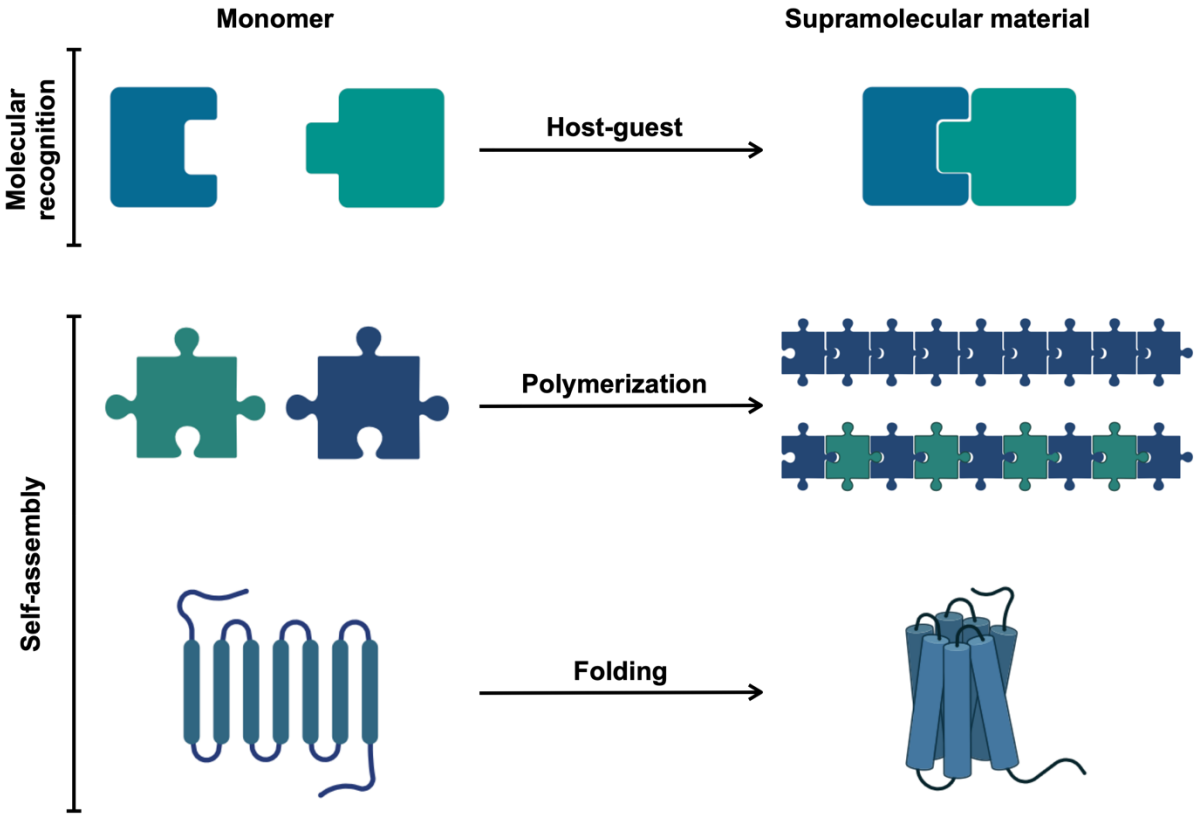

Figure 2. Schematic illustration of different supramolecular processes involving both molecular recognition (top) and self-assembly (bottom). The figure shows monomers and the final supramolecular structures. Created with BioRender.com.

Overall, both mechanisms (molecular recognition and molecular self-assembly) afford "programmed supramolecular systems", as they are built according to molecular design based on different molecular interactions.[26] As Lehn stated in one of his articles: "The program is molecular; its operation is supramolecular".[17]

Over the past sixty years, supramolecular chemistry has evolved into a prominent field, driving advancements at the intersections of biology, chemistry, and physics. The creation of programmed supramolecular systems begins with molecular-level design, where the stored covalent-based information guides the assembly toward specific discrete or extended chemical entities. This concept resembles to the principle of self-organization, a driving force behind the development of complex responsive matter in our universe.[27] Consequently, this emerging science not only studies and understands biological processes but also draws inspiration from them to craft novel, intricate synthetic molecular entities capable of performing diverse functions in several fields. It is worth mentioning that supramolecular chemistry not only contributes to the manufacture of complex

[26] J. M. Lehn, *Science*, **1993**, *260,* 1762-1763.
[27] J. M. Lehn, *Chem. Soc. Rev.,* **2017**, *46*, 2378–2379.

systems but also to the development of different applications such as the catalysis of chemical transformations.[28]

4.1.3. Self-organization in nature

How do complex structures and systems within living organisms control their self-assembly? The phenomenon of biological self-assembly affects to almost all biochemical processes, and even the most basic organisms are the result of a highly cooperative synergy between small and large molecules. This collaborative process begins at the molecular level, where individual molecules are held together to form dynamic cellular nanostructures, which, in turn, self-organize into cells that will end up converging into complete organisms, without falling into thermodynamic wells. The intrinsic ability of biological components to self-assemble with precision and specificity lies in a narrow balance of the diverse range of interactions that biomolecules, monomers of living systems, can establish.[29]

A particularly important example of biomolecular self-assembly are nucleic acids, specifically DNA and RNA, whose building blocks are nucleotides. [8] DNA is a double helix formed by two antiparallel strands wrapped around one another by base pair complementarity (A-T and C-G) in a helical manner. The resulting dimer is a stable structure that not only stores genetic information but also enables its transmission. RNA is usually a single-stranded supramolecule that can also present self-complementary base pairs, normally in a intramolecular manner to fold in specific shapes (e.g., tRNA) but also it can interact with other biomolecules, such as proteins, to form more complex architectures (e.g., ribosomes).[30]

Other biomolecules that stand out for being the main component of cell membranes and cellular compartmentalization are lipids.[31] Their self-organization can give rise to the formation of micelles and lipid bilayers because of their amphipathic character.[32] In micelles formation, the hydrophobic tails clump together, shielded from the surrounding aqueous media, creating spherical structures. Lipid bilayers are formed by aligning the hydrophobic tails between two layers of hydrophilic heads that also end up forming close system, in which a confined aqueous media isolated from the external bulk environment is formed. Moreover, carbohydrates can also assist certain molecular recognition processes on the surface of those lipid bilayers, forming intricate patterns that facilitate

[28] S. J. Cantrill, M. C. T. Fyfe, F. M. Raymo, J. F. Stoddart, *Current challenges on large suprmolecular assemblies. NATO Science Series,* Springer, Dordrecht, **1999**, pp. 17-35-
[29] A. C. Mendes, E. T. Baran, R. L. Reis, H. S. Azevedo, *WIREs Nanomed. Nanobiotechnol.,* **2013**, *5*, 582–612.
[30] H. Li, T. H. LaBean, K. W. Leong, *Interface Focus,* **2011**, *1*, 702–724.
[31] J. H. Collier, P. B. Messersmith, *Annu. Rev. Mater. Res.,* **2001**, *31*, 237–263.
[32] J. N. Israelachvili, D. J. Mitchell, B. W. Ninham, *Biochim. Biophys. Acta.,* **1977**, *470,* 185–201.

cellular communication processes.[33] This molecular recognition is essential for activities such as immune response, cell adhesion or signal transduction, among others.

Finally, it is worth highlighting the remarkable versatility of proteins and shorter peptide fragments for self-assembly.[34] These biomolecules carry out a broad range of functions within living organisms because of their and simple synthesis form available building blocks: the amino acids, which allow a vast array of possible structures and functions. Although the amino acid sequence constitutes the primary structure of the protein, biological functions depend largely on its assembled three-dimensional structure.

Some examples of self-assembled proteins found in nature include long-lived macroscopic architectures such as collagen networks, the main structural protein in connective tissues, which results from the spontaneous assembly of fibrils in the triple collagen helix;[35] the cytoskeleton, a complex and dynamic network formed by protein filaments (e.g. the globular protein actin and dimeric protein tubulin polymerize to form microfilaments and microtubules respectively) that provides structural support to the cells, facilitating both movement and division;[36] or amyloids, which are a type of self-assembled proteins closely associated with various diseases.[37]

Biomolecular machines can also be assembled by the association of proteins with other biomolecules to perform complex functions in living systems. In this group, we can include ribosomes, complex entities composed of RNA and proteins that are generated though a molecular recognition process to be responsible of protein synthesis.[38] Certain enzymes are also supermolecules composed of subunits of different folded proteins that act as catalysts in biochemical reactions by binding to specific substrates (e.g., RNA, DNA polymerase or hemoglobin).[39]

Despite continuous advances and innovative designs, supramolecular chemistry has yet not reached the level of sophistication observed in natural biomolecular self-assembly. However, recent advancements underline the rapid

---

[33] A. Varki, *Glycobiology,* **1993**, *3,* 97–130.
[34] Q. Luo, C. Hou, Y. Bai, R. Wang, J. Liu, *Chem. Rev.,* **2016**, *116*, 13571–13632.
[35] A. Gautieri, S. Vesentini, A. Redaelli, M. J. Buehler, *Nano Lett.,* **2011**, *11*, 757–766.
[36] D. A. Fletcher, R. D. Mullins, *Nature,* **2010**, *463*, 485–492.
[37] A. W. P. Fitzpatrick, G. T. Debelouchina, M. J. Bayro, D. K. Clare, M. A. Caporini, V. S. Bajaj, C. P. Jaroniec, L. Wang, V. Ladizhansky, S. A. Müller, C. E. MacPhee, C. A. Waudby, H. R. Mott, A. De Simone, T. P. J. Knowles, H. R. Saibil, M. Vendruscolo, E. V. Orlova, R. G. Griffin, C. M. Dobson, *Proc. Natl. Acad. Sci. U S A,* **2013**, *110*, 5468–5473.
[38] A. S. Petrov, C. R. Bernier, C. Hsiao, A. M. Norris, N. A. Kovacs, C. C. Waterbury, V. G. Stepanov, S. C. Harvey, G. E. Fox, R. M. Wartell, N. V. Hud, L. D. Williams, *Proc. Natl. Acad. Sci. U S A,* **2014**, *111*, 10251–10256.
[39] S. Gad, S. Ayakar, *Biotechnology Reports,* **2021**, *32.*

translation of principles from biological systems to artificial analogs that mimic life-like structures.[40] These synthetic systems not only help to understand the supramolecular foundations of life, but also to imitate and control cellular responses,[41] which is of great interest in diverse fields, ranging from nanotechnology, advanced materials to biomedicine.

In the following section, we will describe the design principles that allow scientists to control the self-assembly process. For example, how to design monomers at the molecular level considering their future supramolecular interactions (Section 4.2.3.2), or how to use of different external factors (e.g. solvent, pH, ionic strength, etc.) to modulate the assembly conditions (Section 4.2.3.3). Since peptides are the central focus of this doctoral thesis, in the following section we will try to explain these factors in detail, paying special attention to the self-assembly of these biomolecules in particular.

4.1.4. Factors controlling self-assembly

4.2.3.2. Intrinsic factors

4.2.3.2.1. Non-covalent interactions

Self-assembly is governed by non-covalent interactions, forces that, in contrast to covalent bonds (100-400 kJ mol^{-1}), are inherently weaker considering them individually (2-250 kJ mol^{-1}) (Figure 3).[29] Although this difference in individual force strengths, the use of a large number of non-covalent interactions can generate stable supramolecular systems over time maintaining shape and function. Again, this phenomenon is also evident in the supramolecular systems found in nature, as discussed above. These intricate biological architectures exhibit remarkable precision in organization at the nanoscale, a consequence of the specific interactions between monomers driving their assembly. These non-covalent forces will be classified into three main categories depending on their nature, to facilitate the understanding of the thesis: dipoles, Coulombic, and hydrophobic effects. It is important to clarify that this classification is not exclusive, as certain interactions categorized within a specific type, may exhibit characteristics of other interactions, being a hybrid of supramolecular forces.

[40] I. Insua, J. Montenegro, *Chem.,* **2020**, *6*, 1652–1682.
[41] A. Walther, *Adv. Mater.,* **2020**, *32*.

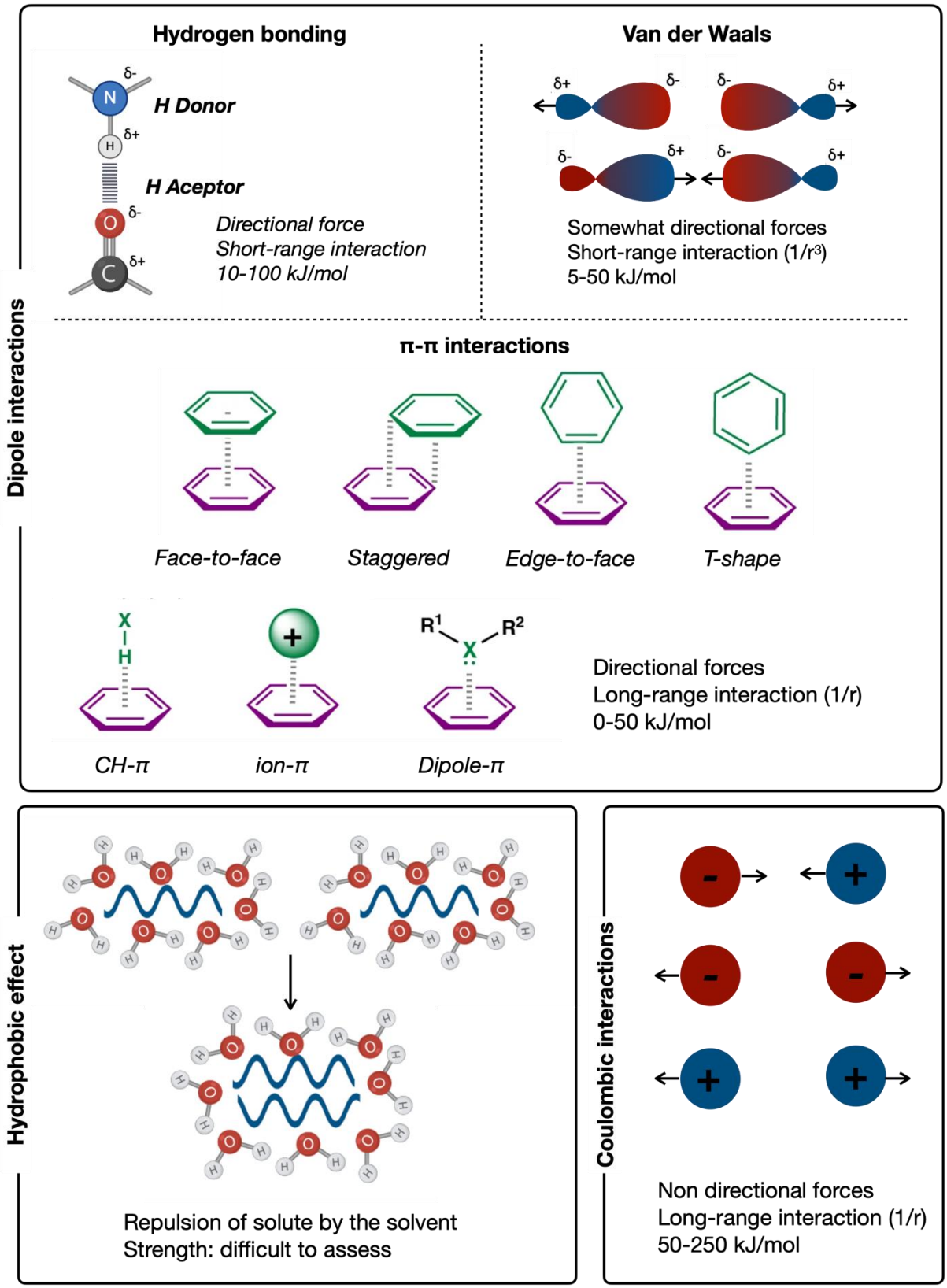

Figure 3. Classification of supramolecular interactions involve in self-assemble systems. Created with BioRender.com.

Dipole interactions

A dipole can be established in a molecule when there is an uneven electron cloud distribution, thus resulting in partial positive and negative charges on the atoms involved in the bond. This typically happens when there is a significant difference in electronegativity between the atoms forming the chemical bond. Within this category of interactions, it is possible to distinguish between hydrogen bonding, π-π stacking, and Van der Waals forces.

Hydrogen bonding is a special type of dipole-dipole attraction that results from the association between an electronegative atom (hydrogen-bond acceptor), usually N, O or F, and a hydrogen atom covalently link to a second electronegative atom (hydrogen-bond donor) (Figure 3, top left). This type of interaction is the strongest of this group, with bond energies between 5-65 $kJmol^{-1}$, and exhibits high selectivity and directionality, which gives stability to complex and robust supramolecular assemblies.[29,42] However, competition with intermolecular interactions with the solvent, especially when it is polar and protic such as water, in many cases significantly reduces its relevance and bond strength. Hydrogen bonds are indeed the main driving force in forming a protein's secondary structure since it's the first non-covalent interaction in their folding process (see section 1.4.1.2).[43] In addition, polar residues and charged amino acids can also provide hydrogen-bond donors and acceptors stabilizing subsequent folding structures (e.g., tertiary and quaternary).[44]

π-π stacking is another attractive interaction, commonly observed in molecules containing aromatic rings, for that reason in this case, a quadrupole, instead of a dipole, is involved. These forces are weaker than hydrogen bonding while still directional, providing a remarkable degree of order in the self-assembly due to geometric restrictions between stacked molecules (Figure 3, middle).[45,46] The strength of this force depends on several factors, including the distance between components (as in the other type of interactions involving also electrostatic forces), their orientation, and the electron density of aromatic moieties involved. Aromatic amino acids (i.e., phenylalanine, tyrosine, and tryptophan) can participate in this type of interaction thank to the aromatic ring in their side chains, which possess a rigid and planar structure with a unique electron distribution in the π orbitals allowing them to interact when nearby.[47] It is possible to distinguish between three types of geometries between aromatic

[42] R. P. Sijbesma, E. W. Meijert, *Curr. Opin. Colloid In. Sci.,* **1999**, *4*, 24–32.
[43] T. P. Knowles, A. W. Fitzpatrick, S. Meehan, H. R. Mott, M. Vendruscolo, C. M. Dobson, M. E. Welland, *Science*, **2007**, *318,* 1900-1903.
[44] M. F. Perutz, T. Johnson, M. Suzuki, J. T. Finch, *Proc. Natl. Acad. Sci. USA,* **1994**, *91,* 5355–5358.
[45] S. Fleming, R. V. Ulijn, *Chem. Soc. Rev.,* **2014**, *43*, 8150–8177.
[46] E. Gazit, *The FASEB Journal,* **2002,** *16,* 77–83.
[47] S. Contorno, R. E. Darienzo, R. Tannenbaum, *Sci. Rep.,* **2021**, *11.*

rings and their strength depends on the complementarity between π-electron clouds:[48]

- Face-to-face or parallel stacked: where aromatic rings are stacked directly on top of each other. If both components are the same, this disposition is unstable because of the repulsion between similarly charged π-electron clouds in addition to the steric hindrance between ring substituents.
- Parallel displaced or staggered: where aromatic rings are stacked but slightly shifted from one another. This arrangement allows more favorable overlap while also helping to decrease the steric hindrance. This shape that, in general, is the most favorable geometry, is the result of the combination of dispersion and Pauli repulsion together with electrostatics.
- Edge-to-face or T-shaped: where one aromatic ring is perpendicular to the other, so the π-electron cloud interacts with the edge of the other ring. This disposition is usually weaker in reference to dispersion forces because of the less overlapping between π-electron clouds, but more favorable from the electrostatic point of view.

Moreover, aromatic moieties can also be involved in other types of π-interactions, depending on the nature of the second component it is possible to include:[47]

- Dipole-π-interaction: when the π-electron cloud interacts with a permanent or induced dipole of another molecule.
- Ion-π interaction: when the π-electron cloud interacts with a cation or anion.
- CH-π interaction: when the π-electron cloud interacts with an electron-deficient hydrogen in a C-H bond.

The important role that π-π interactions play in the self-assembly of peptides can be shown with the assembly behavior of the simple diphenylalanine building block (FF), a minimal fragment derived from the protein responsible for Alzheimer's disease.[49] Its assembly into nanotubes grows perpendicular to the plane of the aromatic rings that interact through π-π stacking. Common aromatic groups used in peptide synthesis (e.g., 9-fluorenylmethyloxy-carbonyl or Fmoc for short) are often used as alternative π-π stacking inducers for self-assembly.[50][51]

[48] R. Chelli, F. L. Gervasio, P. Procacci, V. Schettino, *J. Am. Chem. Soc.,* **2002**, *124*, 6133–6143.
[49] X. Yan, P. Zhu, J. Li, *Chem. Soc. Rev.,* **2010**, *39*, 1877–1
[50] K. Tao, A. Levin, L. Adler-Abramovich, E. Gazit, *Chem. Soc. Rev.,* **2016**, *45*, 3935–3953.
[51] M. Coste, E. Suárez-Picado, S. Ulrich, *Chem. Sci.,* **2022**, *13*, 909–933.

Van der Waals forces are the weakest intermolecular interaction and they involve neutral molecules (polar or apolar) attracted by permanent and/or induced dipoles (Figure 3, top right).[52] On this basis, all molecules and ions exhibit Van der Waals forces to some extent due to temporary fluctuations in electron density. It is possible to differentiate between three main types of Van der Waals forces: interaction between two permanent dipoles, two induced dipoles (also known as London dispersion forces) and mixed induced and permanent dipoles. While not as strong as other non-covalent interactions, these forces are essential for maintaining the structural integrity of large, assembled structures as they become stronger cooperating over large surfaces. Computational studies on peptide conformations have shown their influence on the folding process, demonstrating the requirement of Van der Waals interactions to maintain a compact structure.[53]

Coulombic interactions

Coulombic interactions refer to the electrostatic forces of attraction or repulsion between charged particles, such as ions or charged molecules (Figure 3, bottom right). These interactions are a specific type of electrostatic interactions, which involve a broad range of forces resulting from the interactions of electric fields between particles, as can be observed in the previously described dipole interactions. Coulombic interactions are non-directional and governed by Coulomb's Law, which states that the force between two charged objects is directly proportional to the product of their charges and inversely proportional to the square of the distance between them.[54] In self-assembling peptides, Coulombic interactions primarily involve the negatively (aspartic and glutamic acid) and positively (lysine, arginine and histidine) charged amino acids, in addition, the N- and C-termini of the peptide can also participate if ionized, influencing the assembly process by attractive or repulsive interactions between charged groups.[55] Moreover, the saline content of a solution can affect the strength of these interactions, as salts can shield the ionic groups and hence their binding.[56]

Hydrophobic effect

The hydrophobic effect is a phenomenon in which apolar molecules or regions tend to aggregate in an aqueous environment (Figure 3, bottom left).[57] In this case, the strong water-water association led to the segregation of non-polar molecules into aggregates. For that reason, hydrophobic effects cannot be considered an

[52] F. London, *Transactions of the Faraday Society* **1937**, *33*, 8–26.
[53] S. S. Sung, *Protein Science* **2015**, *24*, 1383–1388.
[54] T. H. Rehm, C. Schmuck, *Chem. Soc. Rev.* **2010**, *39*, 3597–3611.
[55] S. Kumar, R. Nussinov, *Biophys J.,* **2002**, *83,* 1595-1612.
[56] C. Chen, J. Chen, Q. Yu, J. Zhang, X. Niu, L. Hao, L. Yang, Y. Zhao, *Soft Matter,* **2020**, *16*, 9758–9768.
[57] M. N. Rodnikova, *J. Mol. Liq.,* **2007**, *136*, 211–213.

"interaction", as these are not generated by attracting non-polar groups.[58] This effect can be quantified by the free energy associated with the interaction between water and hydrophobic molecules.[5957] While previous supramolecular interactions normally show an enthalpic contribution to the assembly, the contribution of this solvophobic effect is mainly entropic. The enthalpic contribution comes from the rearrangement of hydrogen bonds between water molecules and Van der Waals interactions between water molecules and the surface of the hydrophobic aggregate. However, these overall enthalpic contributions result in a small energy balance while the entropy change is favorable as water molecules tend to reorganize themselves at the surface of hydrophobic molecules, and thus hydrophobic aggregation suppresses those molecules arranged on its surface, leading to increased disorder in the system.

While each of these non-covalent interactions plays a distinct role in driving different stages of peptide self-assembly, from its folding involving intramolecular interactions to their assembly with other monomers, they ultimately work cooperatively to maintain the assembly's integrity. This synergistic effect of these forces is clearly defined both spatially and temporally.[60] Spatially implies that the specific topology of these interactions is well-identified and understood, leading to a precise arrangement in three dimensions. Temporally refers to the kinetic evolution of these cooperative interactions during the assembly process: when they occur, how long they last, and their dynamic changes over time.

4.2.3.2.2. Monomer design

Monomers design is a fundamental step in self-assembly, since they must encode the necessary information to guide the process toward the final supramolecular structure. This molecular design will not only determine the complementarity and affinity between monomers but also the stability and responsiveness of the resulting assembly. Also pivotal is the initial peptide conformation, serving as the foundational step in the assembly process dictating their propensity to stablish the subsequent non-covalent interactions. Because peptide monomers are the focus of this thesis, we will provide a brief explanation of these biomolecules, including their fundamental composition and the conformational structures. This information is essential to tailor monomers and help understanding the self-assembled structures included in next Section 4.1.

[58] D. Chandler, *Nature,* **2002**, *417*, 491.
[59] D. Chandler, *Nature,* **2005**, *437*, 640–647.
[60] J. Li, J. Wang, Y. Zhao, P. Zhou, J. Carter, Z. Li, T. A. Waigh, J. R. Lu, H. Xu, *Coord Chem Rev* **2020**, *421*.

Peptides are relatively short oligomers (M.W. below 6000 Da) made up of covalently linked amino acids.[61] Depending on the number of amino acids that form the peptide chain it is possible to differentiate between: "oligopeptide", if it is formed between 10 and 20 amino acids, or "polypeptide" if it has more than 20 amino acids and up to 50. The general chemical structure of α-L-amino acids has a central α-carbon to which an amino, a carboxyl group and the side chain, which allows the different derivatives to be differentiated, are attached (except Proline, with its side chain directly attached to the backbone) (Figure 4). There are 20 encoded proteinogenic amino acids depending on the side chain and except for glycine, all of them have L configuration.[62] In Figure 4 it is possible to observe their chemical structures as well as the three-letter and one-letter code that identifies them which will be used throughout this dissertation. But beyond these amino acids, there is an extensive library of other non-proteinogenic amino acids that can be used in peptide monomers, including the enantiomeric D-amino acids, β-amino acids, or even completely synthetic amino acids.

Depending on the side chain's polarity, amino acids can be broadly classified into hydrophobic, with aliphatic or aromatic side chains, or polar amino acids. Among this latter category is also possible to distinguish between neutral, acidic or basic amino acids. These diverse molecular structures give them unique physicochemical properties that influence their participation in a variety of supramolecular interactions. For example, hydrophobic residues will tend to aggregate in an aqueous environment through solvophobic effect while aromatic amino acids can engage in π-π interactions. Polar residues, on the other hand, are capable of forming hydrogen bonds, and the ones carrying positive or negative charges can also establish electrostatic interactions. Moreover, the flexibility or rigidity imparted by the side chains can affect the peptide's conformation modulating its ability to interact with other molecules.

Additionally, amino acids can have different charged states due to the presence of charged functional groups in their structures. All of them have at least two ionized states arising from the amino and carboxy-terminal groups, but polar-charged amino acids, as well as cysteine and tyrosine have an additional charged state because of the ionized functional group in their side chain. The different pK_a values assigned for each amino acid in Figure 4 determine the pH at which ionizable groups become protonated or deprotonated.

[61] D. J. Dietzen, in *Principles and Applications of Molecular Diagnostics*, Elsevier, **2018**, pp. 345–380.
[62] F. W. Lichtenthaler, *Angew. Chem – Int. Ed.,* **1992**, *31,* 1541–1556.

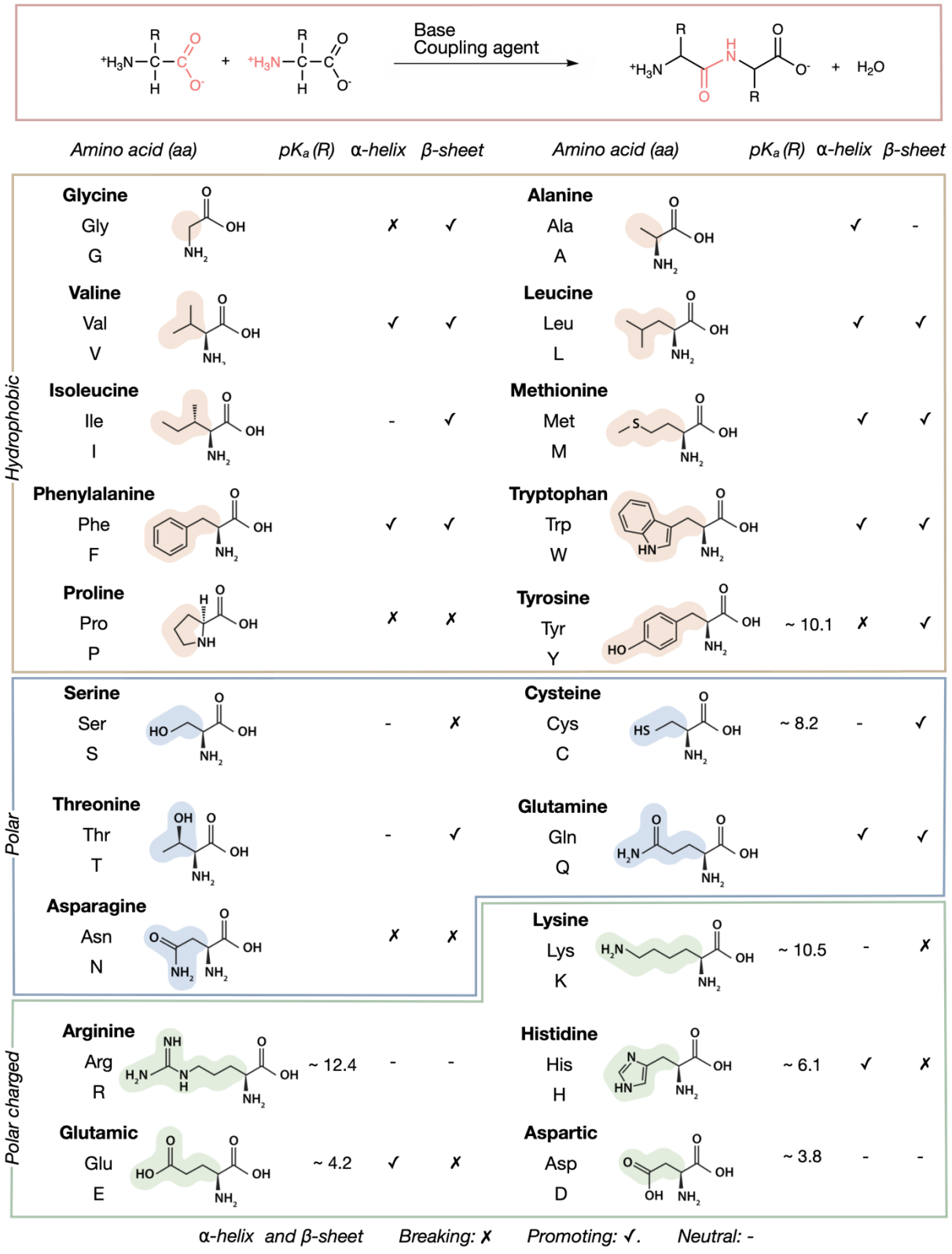

Figure 4. Top: peptide bond formation. Bottom: List of the 20 encoded proteinogenic amino acids with their chemical structure, name and codes (i.e., 1 and 3 letter abbreviations), pK_a of side chain (R) and propensity to forming an α-helix and/or β-sheet. Created with BioRender.com.

Therefore, understanding the relationship between all these properties is crucial in the design of new peptide monomers, since it would enable the strategic positioning of amino acids in a peptide sequence in a programmed supramolecular assembly. For instance, in proteins, the specific arrangement of amino acids along the sequence (primary structure), determines its folding by dictating the successive secondary and tertiary structural conformations but also, its assembly with other proteins (quaternary conformation). In addition, some of these aggregates play specific function to further assembling or interacting with specific molecules. Consequently, researchers have taken inspiration from these natural sequences to design peptide monomers capable of acquiring a specific secondary conformation.[63] The most common secondary structures of natural peptides are the α-helix and the β-sheet,[64] although other motifs such as β-turns[65] or 310 helixes,[66] are also possible.

α-helices are right-handed helical structures when they are formed by L-amino acids, stabilized by intramolecular hydrogen bonds between the carbonyl oxygen and the amide hydrogen of amide bonds separated by four residues in the sequence (i, i+4), leaving 3.6 residues per turn (Figure 5). This arrangement led to a repeated pattern known as "heptad repeat :$(abcdefg)_n$" and defined the repetitive position of seven amino acids on the surface of the helix along its length. This conformation requires chirality to maintain the hydrogen bonding pattern and is generally stabilized by small hydrophobic side chains or functional groups forming salt bridges. Gly and Pro residues are the more destabilizing for this conformation since they lack chirality and have a restrictive backbone, respectively. The helix propensity of each amino acid was studied based on the stability of proteins and it is referred to as promoting or breaking propensity in Figure 4.[67]

β-sheets are flat structures formed by several peptide strands that are held together by a intra- or intermolecular network of hydrogen bonds (Figure 5). This conformation can be either parallel, if strands are positioned in the same sense (i.e., N to C by convention) or antiparallel, with strands are running in opposite directions. While peptide backbone has an extended conformation, the side chains are generally arranged outwards from the plane of the sheet pointing towards either side in an alternating manner. In fact, due to the hybridization of C_α and his angle, β-sheets are more likely to have some "twist" to better accommodate residues, than to be fully extended. As commented for α-helix, certain amino acids have also greater propensity to form β-sheets conformation, for example, amino

[63] C. J. Wilson, A. S. Bommarius, J. A. Champion, Y. O. Chernoff, D. G. Lynn, A. K. Paravastu, C. Liang, M. C. Hsieh, J. M. Heemstra, *Chem. Rev.,* **2018**, *118*, 11519–11574.
[64] Linus Pauling, Robert B. Corey, H. R. Branson, *The Proceedings of the National Academy of Sciences,* **1951**, *37*, 205–211.
[65] E. G. Hutchinson, J. M. Thornton, *Protein Sci.,* **1994**, *3,* 2207–2216.
[66] L. Pal, G. Basu, P. Chakrabarti, *Proteins: Structure, Function and Genetics* **2002**, *48,* 571–579.
[67] C. N. Pace, J. M. Scholtz, *Biophys. J.,* **1998**, *75*, 422–427.

acids with short and bulky side chains (β-branched specially).[68] Although the tendency of amino acids detailed in Figure 4 to promote or break secondary conformation, we need to take into account that the overall stability of the folded state will depend on the collective interactions between all side chains as well as the conditions of the assembly.

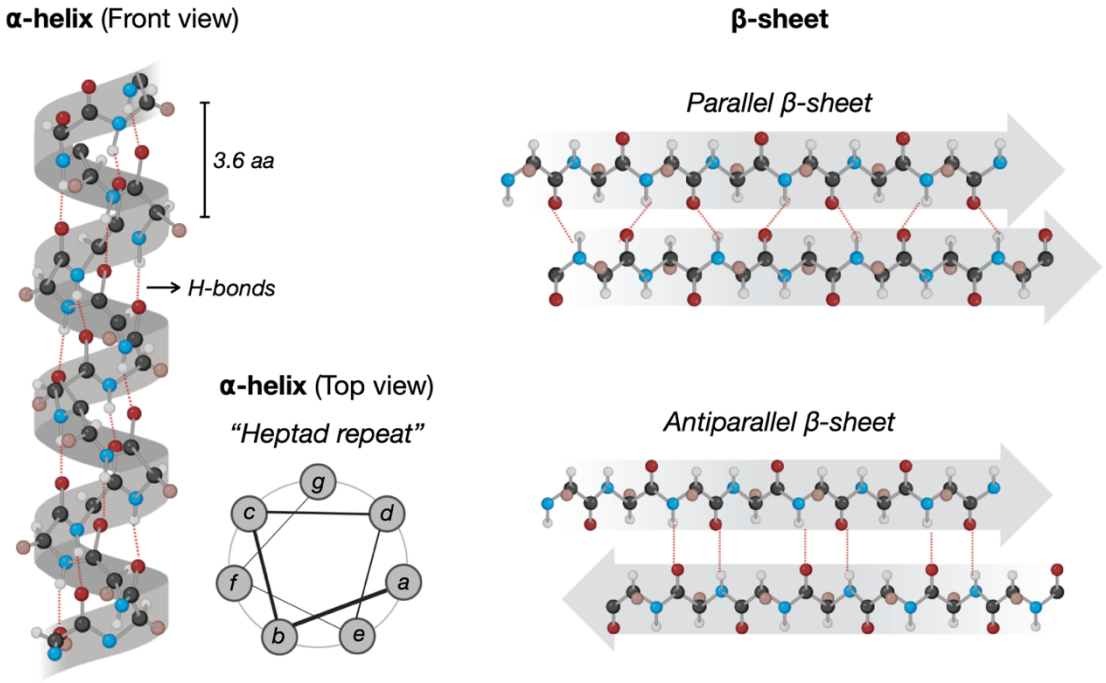

Figure 5. Schematic representation of α-helix conformation with front and top (heptad repeat) view and parallel and antiparallel β-sheets. Created with BioRender.com.

4.2.3.3. External factors

Self-assembly is significantly influenced by environmental factors since they can influence on the supramolecular interactions. For example, variations in temperature, pH, solvents, ionic strength, or even monomer concentrations can be used to modulate the assembly outcome, resulting in nanostructures with different morphologies or even functions.

Temperature has a high impact on non-covalent interactions, influencing their strength and dynamics. An increase in the thermal energy of the systems disrupts and weakens some interactions such as Coulombic and dipole, as the kinetic energy of the molecules also increases.[69][70] The opposite happens with the

[68] K. Fujiwara, H. Toda, M. Ikeguchi, *BMC Struct Biol* **2012**, *12*.
[69] F. Lehmkühler, Y. Forov, M. Elbers, I. Steinke, C. J. Sahle, C. Weis, N. Tsuji, M. Itou, Y. Sakurai, A. Poulain, C. Sternemann, *Phys. Chem. Chem. Phys.*, **2017**, *19*, 28470–28475.
[70] M. R. Tiné, M. Alderighi, C. Duce, L. Ghezzi, R. Solaro, *J. Therm. Anal. Calorim.*, **2011**, *103*, 75–80.

hydrophobic effect, which is enhanced with the increase of temperature due to changes in the entropy and in some cases because of the solubility of the apolar molecules.[71]

Variations in the **pH** of the medium also affect peptide assembly by modifying their ionized state. As explained before, some amino acids present different pKa values determined by the type of functional groups in their side chain, so the overall pKa of the peptide will be determined by the collective influence of individual ionized groups. In general, at a pH below the pKa of a residue, this residue tends to be protonated while at a pH above the pKa, the residue would be deprotonated. However, to precisely calculate the ratio between different charged states at a certain pH value, it is possible to use the Henderson-Hasselbach equation.[72] Moreover, it is important to take into account that the pKa value of an amino acid can be altered in an assembled structure due to the influence of the microenvironment in which the residue is placed (i.e., intrinsic pKa). These alterations in the pH significantly affect electrostatic interactions and hydrogen bonds, leading to transformations in the morphology of peptide assemblies. Researchers have harnessed this pH sensitivity to design stimuli-responsive materials with interesting applications in biomedicine (e.g., drug delivery vehicles).[73,74]

Solvent. The solubility of peptides in a given solvent is a fundamental factor for self-assembly. Most non-covalent interactions are sensitive to solvent conditions playing a central role in solvophobic and amphiphilic association of peptide monomers, determining the clustering or exposure of hydrophobic and hydrophilic domains.[75] In addition to single-solvent systems, the strategic use of co-solvents further extends the toolkit for manipulating peptide self-assembly.[76] By employing co-solvents in varying proportions, researchers can modulate a transition between different structural motifs.

Ionic strength refers to the concentration of ions in a solution and plays a crucial role in shaping the interactions and stability of peptide assemblies. Ionic strength usually influences electrostatic and hydrophobic forces in peptides, as salts may enhance or shield these interactions depending on the ionization

[71] W. Y. Chen, H. M. Huang, C. C. Lin, F. Y. Lin, Y. C. Chan, *Langmuir,* **2003**, *19*, 9395–9403.
[72] Henry N. Po, N. M. Senozan, *J. Chem. Educ.,* **2001**, *78*, 1499.
[73] S. Chagri, D. Y. W. Ng, T. Weil, *Nat. Rev. Chem.,* **2022**, *6*, 320–338.
[74] Z. Li, Y. Zhu, J. B. Matson, *ACS Appl. Bio. Mater.,* **2022**, *5*, 4635–4651.
[75] J. Wang, K. Liu, L. Yan, A. Wang, S. Bai, X. Yan, *ACS Nano,* **2016**, *10*, 2138–2143.
[76] Y. Lin, M. Penna, M. R. Thomas, J. P. Wojciechowski, V. Leonardo, Y. Wang, E. T. Pashuck, I. Yarovsky, M. M. Stevens, *ACS Nano,* **2019**, *13*, 1900–1909.

state.[57,77] Additionally, the Hofmeister effect, is use to explain how different ions exert specific effects on the properties of biomolecules.[78]

Metal ions have also a pronounced effect on peptide self-assembly, as their coordination with some residues can be highly specific contributing to the structure and function of the final assembly. For example, histidine, with its imidazole side chain, can coordinate various transition metals such as copper, nickel, zinc, cobalt, and iron.[79]

Concentration is another crucial external factor that significantly influences self-assembling processes, with the Critical Aggregation Concentration (CAC) as a key parameter in understanding this process.[80] The CAC represents the threshold concentration at which supramolecular building blocks i.e., peptides, start to aggregate and self-assemble into supramolecular polymers, defined (nano) particles or amorphous aggregates. Below the CAC, peptides exist mainly as monomers in a dispersed state. Consequently, the concentration of an assembled system can be also modulated by diluting or aggregating more monomers, leading to the formation of different structures.[81] The concentration is essential to optimize the self-assembly conditions of functional nanomaterials.[82]

In addition to those already mentioned, other external factors can also affect the self-assembly of peptides, such as ultrasound,[83] light,[84] or the application of electric fields.[85]

---

[77] A. Méndez-Ardoy, A. Bayón-Fernández, Z. Yu, C. Abell, J. R. Granja, J. Montenegro. *Angew. Chem., Int. Ed.,* **2020**, *59*, 6902–6908.
[78] P. Lo Nostro, B. W. Ninham, *Chem. Rev.*, **2012**, *112*, 2286-2322.
[79] Y. Chen, K. Tao, W. Ji, V. B. Kumar, S. Rencus-Lazar, E. Gazit. *Mater. Today,* **2022**, *60*, 106–127.
[80] M. Novo, S. Freire, W. Al-Soufi. *Sci. Rep.,* **2018**, *8*.
[81] F. Tantakitti, J. Boekhoven, X. Wang, R. V. Kazantsev, T. Yu, J. Li, E. Zhuang, R. Zandi, J. H. Ortony, C. J. Newcomb, L. C. Palmer, G. S. Shekhawat, M. O. De La Cruz, G. C. Schatz, S. I. Stupp. *Nat. Mater.,* **2016**, *15*, 469–476.
[82] G. Ghosh, R. Barman, A. Mukherjee, U. Ghosh, S. Ghosh, G. Fernández. *Angew. Chem., Int. Ed.,* **2022**, *61*,
[83] C. G. Pappas, T. Mutasa, P. W. J. M. Frederix, S. Fleming, S. Bai, S. Debnath, S. M. Kelly, A. Gachagan, R. V. Ulijn. *Mater. Horiz.,* **2014**, *2*, 198–202.
[84] M. Vilela-Picos, F. Novelli, A. Pazó, A. Méndez-Ardoy, G. Marafon, M. Amorín, A. Moretto, J. R. Granja. *Chem,* **2023**, *9*, 3365–3378.
[85] C. M. Kelly, T. Northey, K. Ryan, B. R. Brooks, A. L. Kholkin, B. J. Rodriguez, N. V. Buchete. *Biophys. Chem.,* **2015**, *196*, 16–24.

4.2.1. Concepts in supramolecular self-assembly

In recent years, the field of self-assembly has experienced exponential growth, both in the complexity of the systems achieved and in the understanding of the processes that govern the supramolecular associations.[86] This complexity has demanded the introduction of new terms intended to characterize and distinguish the new landscape of self-assembled systems. This new terminology will be briefly explained in this section to contextualize discussions in the upcoming chapters.

4.2.3.4. Thermodynamic and kinetic products

Although initially supramolecular process were defined as the thermodynamic more stable system, in the last years, the energy landscape has appeared as a concept to describe an energy map where different conformational states are represented that could drive toward different association processes (**Figure 6**).[87] It is a powerful tool in the study of self-assembled systems since it helps to understand the different energetic states where monomers can be until they form the resulting supramolecular structures. Based on the thermodynamics and kinetics of the system it is possible to distinguish between different products of a supramolecular polymerization:

The **thermodynamic product** represents the most stable and energetically favorable product and thus is positioned as the minimum energetic state (**Figure 6**, red circle).[88] Systems reaching this type of product are usually characterized by predominantly reversible non-covalent interactions, which allow the system to transform into various metastable states.[89] However, it is important to note that while the thermodynamic product has the minimum energy, it does not necessarily have to be in **thermodynamic equilibrium**, as kinetic limitations or other factors can affect the dynamics of the process. In supramolecular assemblies, the equilibrium is reached when a configuration remains unchanged, but monomers can be in constant dynamic exchange with the solution. Additionally, it is worth mentioning that the shape of the energy landscape depends on parameters such as concentration, temperature, and solvent compositions, meaning that thermodynamic products can exhibit different morphologies and energetic states depending on the values of these external conditions (Section 4.2.3.3).[81] However, the different pathways that can be followed to reach these different thermodynamic states with the same monomer do not influence the final morphology, since this is only influenced by the experimental conditions.

---

[86] P. K. Hashim, J. Bergueiro, E. W. Meijer, T. Aida, *Prog. Polym. Sci.,* **2020**, *105.*
[87] J. Matern, Y. Dorca, L. Sánchez, G. Fernández, *Angew. Chem.,* **2019**, *131*, 16884–16895.
[88] T. F. A. De Greef, M. M. J. Smulders, M. Wolffs, A. P. H. J. Schenning, R. P. Sijbesma, E. W. Meijer, *Chem. Rev.,* **2009**, *109*, 5687–5754.
[89] A. Sorrenti, J. Leira-Iglesias, A. J. Markvoort, T. F. A. De Greef, T. M. Hermans, *Chem. Soc. Rev.,* **2017**, *46*, 5476–5490.

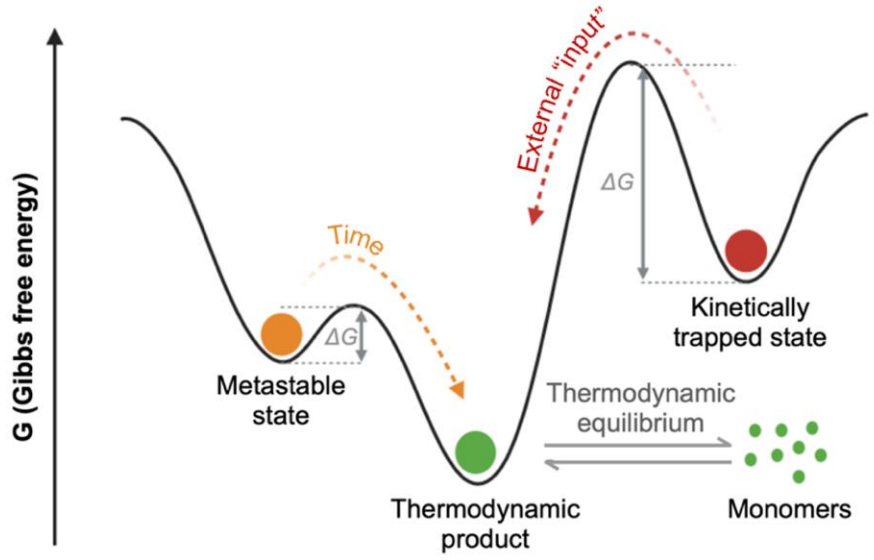

Figure 6. Schematic Gibbs free energy landscape illustrating the possible states in a supramolecular assembly. Created with BioRender.com.

On the other hand, there are processes, that provide **kinetic products** when the non-covalent interactions driving the assembly are strong enough to maintain the formation of metastable intermediates in the evolution toward the thermodynamic product.[89] These intermediate states are usually formed faster (governed by kinetics) and they are found in local energy minima separated by different energy barriers from the other states. Based on the shape of the energy landscape around these intermediates, or in other words, depending on the magnitude of the energy barrier, it is possible to differentiate two types of states:[90]

When the activation energy is small enough so that the system tends to reach the equilibrium state over time, the intermediate states are called **metastable** (**Figure 6**, orange circle).

Alternatively, when the activation barrier is high, the intermediates are retained in the local energy minimum, requiring external energy to evolve towards the thermodynamic state; these are **kinetically trapped states** (**Figure 6**, red circle). In these cases the formation of some of these aggregates depends on the pathway (conditions) followed by the system.

[90] E. Mattia, S. Otto, *Nat. Nanotechnol.,* **2015**, *10*, 111–119.

4.2.3.5. Pathway complexity

The trajectory that monomers follow in self-assembly is not a singular route. As mentioned in the previous section, energy landscapes are the result of the interplay between the thermodynamics and kinetics of the system, therefore, they can include a multitude of diverse pathways leading to various supramolecular products and intermediates. The term **pathway complexity** arises from the recognition that self-assembly is not a simple process and expresses the different and intricate steps that monomers can undergo to achieve the final assembled structures.

In literature, different pathways have been reported based on the routes that interconvert products and intermediates:[87]

Consecutive or on-pathway refers to a process of sequential steps, where monomers are directly transformed into other species following a gradual progression (**Figure 7**, left). Each step leads to the formation of consecutive intermediates and in some cases to the final assembly. This type of pathway can be related to **hierarchical processes**, characterized by successive assembly steps where monomers gradually increase their organization while keeping at each stage the precedent motif.

Competitive or off-pathway process refers to a system where multiple routes or mechanisms compete to form different assembled species that can only be interconverted if they disassemble to the monomeric state (**Figure 7**, middle).

Complex systems involve a combination of both consecutive and competitive pathways (**Figure 7**, right). These landscapes exhibit sequential and ordered steps, but it is possible to also have competition between alternative routes, adding an additional layer of complexity to the assembly dynamics.

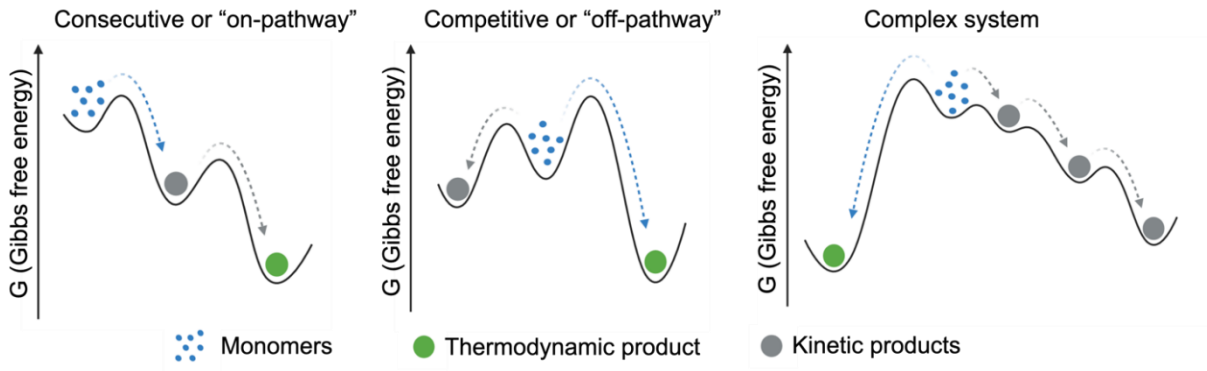

Figure 7. Schematic Gibbs free energy landscapes illustrating the different pathways in supramolecular self-assembly. Created with BioRender.com.

There is a key experiment to distinguish between both pathways that involves the observation of the time-dependent interconversion of the assembled species at varying concentrations.[87] If the transformation accelerates with an increase in concentration, it is a consecutive pathway that needs shorter times to complete the transition. On the other hand, if the time extends with higher concentrations, it suggests the presence of competitive pathways, since in this case species must undergo transformation into monomers before assembling into other structures.

It is common to find a relationship between the terms "on-pathway" and "off-pathway" with thermodynamic and kinetic products in literature, respectively, but these concepts do not always correlate, especially when it comes to more complex processes.[91]

4.2.3.6. Growth mechanism

It is possible to classify self-assembly based on the mechanism that governs the association of monomers, namely cooperative, anticooperative, and isodesmic assembly.[92] These mechanisms are often compared with polymerization events, where isodesmic and cooperative growth resemble step-growth and chain growth polymerization, respectively.[88]

The **isodesmic** mechanism is characterized by a single association constant, which denotes the binding affinity between the monomer and the growing assembly regardless of the extent of polymerization, where each step has the same decrease in free energy (**Figure 8**, top).[89] Thermodynamically, isodesmic assembly reflects balanced and consistent energy profiles, leading to stable and predictable equilibria. From a kinetic perspective, each step of the reaction proceeds at a uniform rate, where no critical concentration or temperature marks the beginning of the supramolecular propagation.

The **cooperative** mechanism is defined by a nonlinear progression involving two distinct stages (**Figure 8**, bottom).[93] The first step: **nucleation** involves the formation of small oligomers (nucleus) that is thermodynamically unfavorable but continuing polymerizing in the second stage, known as **elongation** or **propagation**. This difference between stages results in a critical threshold of concentration or temperature that must be reached to move from the nucleus to the resulting supramolecular assembly.[94] The thermodynamics are characterized by infinite association constants depending on the complexity of the mechanism

[91] T. Fukui, S. Kawai, S. Fujinuma, Y. Matsushita, T. Yasuda, T. Sakurai, S. Seki, M. Takeuchi, K. Sugiyasu, *Nat. Chem.,* **2017**, *9*, 493–499.
[92] M. Hartlieb, E. D. H. Mansfield, S. Perrier, *Polym. Chem.,* **2020**, *11*, 1083–1110.
[93] D. Zhao, J. S. Moore, *Org. Biomol. Chem.,* **2003**, *1*, 3471–3491.
[94] M. M. J. Smulders, M. M. L. Nieuwenhuizen, T. F. A. De Greef, P. Van Der Schoot, A. P. H. J. Schenning, E. W. Meijer, *Chem. Eur J.,* **2010**, *16*, 362–367.

and the number of intermediates involved. Moreover, it is possible to distinguish between cooperative and anticooperative based on the kinetics, if the rate constant for the nucleation step is smaller than the elongation, the mechanism is cooperative, whereas anticooperative has a larger rate constant for the nucleation step.

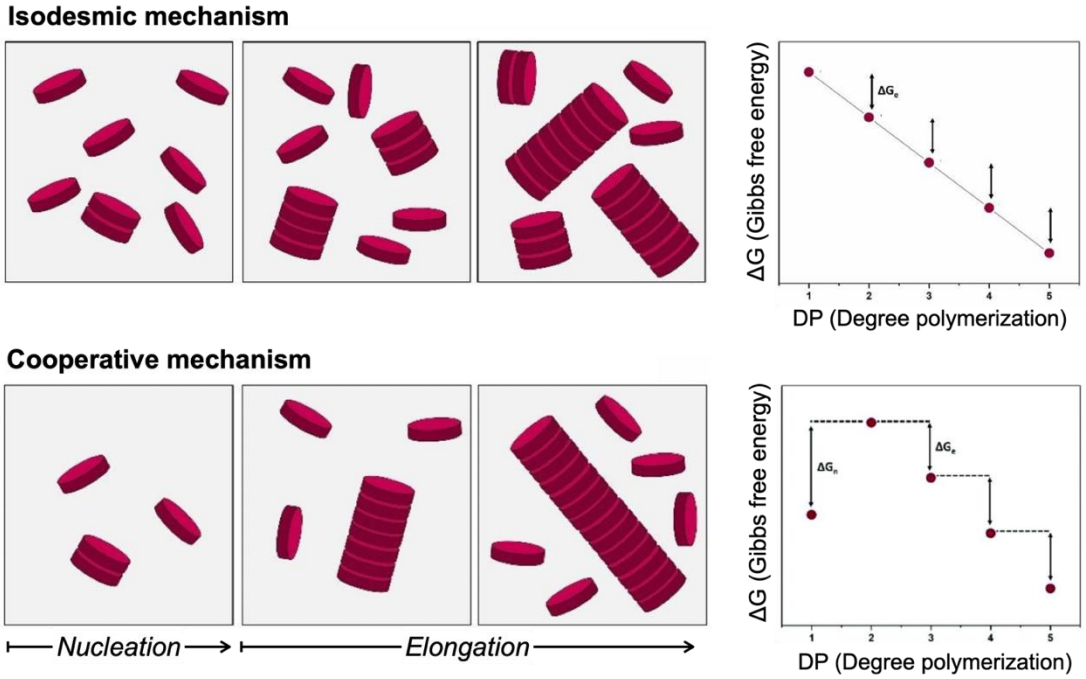

Figure 8. Schematic representation of different polymerization mechanism (left). Thermodynamic diagram of different steps represents as degree of polymerization (DP). Adapted with permission from Ref. 92 Copyright © 2010, Royal Society of Chemistry.

Both mechanisms depend on parameters such as concentration or temperature and this behavior can be used to differentiate them experimentally based on the aggregation fraction (α).[92,94,95] This term refers to the proportion of monomers that have assembled into larger structures compared to the total number of monomers in the system (**Figure 9**a). The signal obtained in the isodesmic mechanisms increases or decreases gradually with concentration or temperature, respectively. The cooperative mechanism exhibits two distinct stage patterns, where the critical concentration and temperature values can be differentiated.

Furthermore, the distinct behaviors exhibited by these mechanisms influence the dispersity and degree of polymerization, which are crucial parameters in the design of these type of materials. Dispersity, represented by the polydispersity index (PDI), characterizes the variety of sizes within the formed aggregates and depends on both the mechanism and the reaction conditions (**Figure 9**b). The degree of polymerization reflects the number of monomer units in a polymer chain

[95] D. Van Der Zwaag, P. A. Pieters, P. A. Korevaar, A. J. Markvoort, A. J. H. Spiering, T. F. A. De Greef, E. W. Meijer, *J. Am. Chem. Soc.*, **2015**, *137*, 12677–12688.

or aggregate. In isodesmic systems, the uniform and gradual increase in the aggregation fraction (α) often leads to a narrower size distribution, resulting in lower dispersity, indicative of a more homogeneous population of assembled structures. In contrast, a cooperative mechanism often leads to a higher dispersity and a more complex pattern in the degree of polymerization due to its two-stage growth, generating a complex array of structures with different lengths. However, this can be controlled by the kinetics of the system by making faster the nucleation process. Overall, the need to fabricate materials with tailored properties and functions has driven researchers to devise methods allowing precise control of self-assembling to obtain monodisperse and uniform structures. Between these methods it is possible to find radical polymerization techniques (e.g, RAFT polymerization) and crystallization or seeded growth mechanisms.

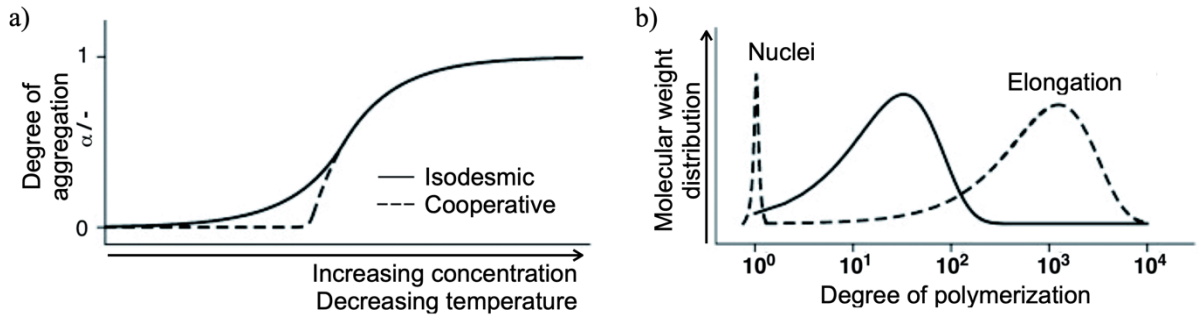

Figure 9. a) Graphic representation of how the degree of aggregation change for each mechanism depending on temperature and concentration. b) Graphic representation of molecular weight distribution versus the degree of polymerization. Adapted with permission from Ref. 94 Copyright © 2010 WILEY-VCH Verlag GmbH & Co. KGaA, Weinheim.

4.2.3.7. Living supramolecular polymerization by seeded growth.

The fundamental idea behind **living polymerization** is that every polymer chain in the process grows uniformly without termination steps (**Figure 10**, left).[96] In supramolecular polymerization, this is usually related to the cooperative mechanism, where monomers can only be add to the active end of the chain. Moreover, in those cases when the initial nucleation step is faster than the elongation (anticooperative) and the subsequent monomer addition is irreversible, a lower dispersity can be obtained.[92] This approach can be achieved by different methods, but in general, they are based on delaying the process of spontaneous formation of thermodynamic species, thus controlling the kinetics of the system.[97] To do this, it is possible to take advantage of metastable or kinetically trapped species by controlling their evolution with external factors or converting them into

[96] R. B. Grubbs, R. H. Grubbs, *Macromolecules,* **2017**, *50*, 6979–6997.
[97] M. Wehner, F. Würthner, *Nat. Rev. Chem.,* **2020**, *4*, 38–53.

reservoirs that are activated in the presence of an initiator.[98] For example, the use of seeds as "preformed nuclei" to control the starting point of elongation has also been exploited as specific stimuli to initiate living polymerization: **seeded living supramolecular polymerization** (**Figure 10**, right).[99] By adding these pre-assembled seeds, the first energetic barrier that limits the nucleation step is quickly overcome.

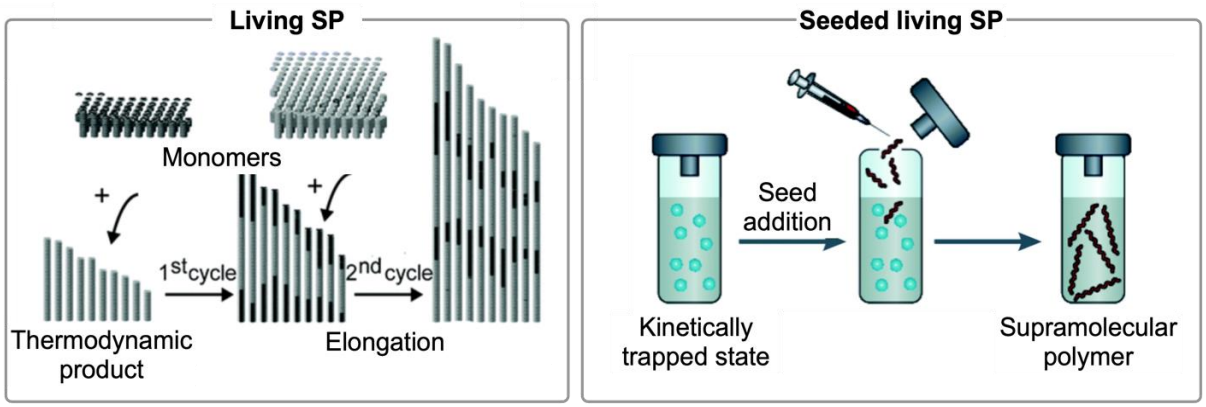

Figure 10. Living supramolecular polymerization (SP) process schematically represented by a thermodynamic product growth with two monomer addition cycles. Adapted with permission from Ref. 96 Copyright © 2016, American Chemical Society. Schematic illustration of the seeded living supramolecular polymerization (SP) process. Adapted with permission from Ref. 51 Copyright © 2022, Royal Society of Chemistry.

One example of how to achieve living polymerization was developed by Ogi et al. by exploiting the competitive off-pathway assembly of zinc complexes since they could aggregate cooperatively both into thermodynamically stable H-aggregates or into kinetically J-aggregates via an isodesmic mechanism (**Figure 11**a).[100] Initially, monomers tend to form J-aggregates, retarding the spontaneous formation of H-aggregates. They demonstrated that a controlled conversion between J- and H-aggregates is possible by adding H-aggregates as seeds to a solution of J-aggregates. These seeds will act as a template to make faster the transition between both states. The sequential addition of kinetic traps to a solution of H-aggregates led to its elongation thus demonstrating the living polymerization and further probing the increase conversion between aggregates.

In another example, Aida and co-workers reported a method based on the use of metastable cage-like structures as monomer reservoir (**Figure 11**b).[101] They designed corannulene-based compounds with a preferential closed and non-

[98] A. J. Markvoort, H. M. M. Ten Eikelder, P. A. J. Hilbers, T. F. A. De Greef, *ACS Cent. Sci.,* **2016**, *2*, 232–241.
[99] E. P. Bruckner, S. I. Stupp, *Polym. Int.,* **2022**, *71*, 590–595.
[100] S. Ogi, K. Sugiyasu, S. Manna, S. Samitsu, M. Takeuchi, *Nat. Chem.,* **2014**, *6*, 188–195.
[101] J. Kang, D. Miyajima, T. Mori, Y. Inoue, Y. Itoh, T. Aida, *Science,* **2015**, *347*, 646–651.

assembling state at lower temperatures due to the formation of intramolecular hydrogen bonds. These structures are in a "dormant" state preventing the spontaneous polymerization, called reservoirs. The addition of a methylated derivative that hinders the intramolecular interactions, serves as an initiator for the elongation since it lowers the energy to promote the reorganization of hydrogen bonds in the reservoirs.

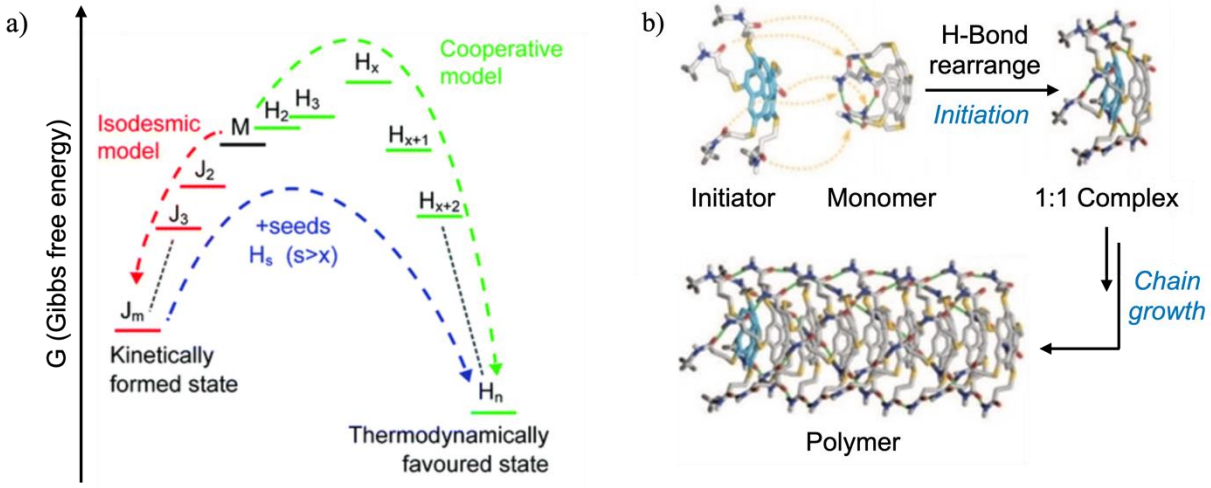

Figure 11. a) Energy landscape of the different assembly pathways for the monomeric zinc complex (M). Adapted with permission from Ref. 98 Copyright © 2014, Springer Nature Limited. b) Schematic representation for the initiation assembly of a monomer reservoir and subsequent chain growth polymerization. Adapted with permission from Ref. 99 Copyright © 2015, The American Association for the Advancement of Science.

Interestingly, Manners, Winnik, and coworkers developed a strategy based on the use of crystallizable monomers as seeds known as crystallization-driven living supramolecular polymerization (Figure 12).102 Crystals are order structures that can impart directionality to the assembly and, moreover, they are stable structures that can maintain the nucleus in a kinetically trapped state, preventing spontaneous assembly. The authors designed semicrystalline block copolymers that are organized into a solvophobic core and a solvophilic corona.103,104 Sonication or heat produces the fragmentation of preformed polydisperse aggregates, giving rise to discrete oligomeric seeds that increase in size through the subsequent addition of free monomer, thus demonstrating the living polymerization process. Subsequently, they discovered that the size of the crystalline seeds is related to the final size of the assemblies so that it is possible

[102] S. Ganda, M. H. Stenzel, *Prog. Polym. Sci.,* **2020**, *101.*
[103] X. Wang, G. Guerin, H. Wang, Y. Wang, I. Manners, M. A. Winnik, *Science,* **2007**, *317,* 644-647.
[104] G. Guérin, H. Wang, I. Manners, M. A. Winnik, *J. Am. Chem. Soc.,* **2008**, *130*, 14763–14771.

to control the dispersion of the final structures.[105,106] Furthermore, hierarchical structures have been achieved through sequential living polymerization steps with different monomers sharing the same crystallizable core, leading to complex systems with spatially distinct functional regions.[107,108,109,110] This new assembly methodology has made possible to manufacture complex systems with controlled shapes and sizes, which would otherwise be extremely difficult to prepare.[111]

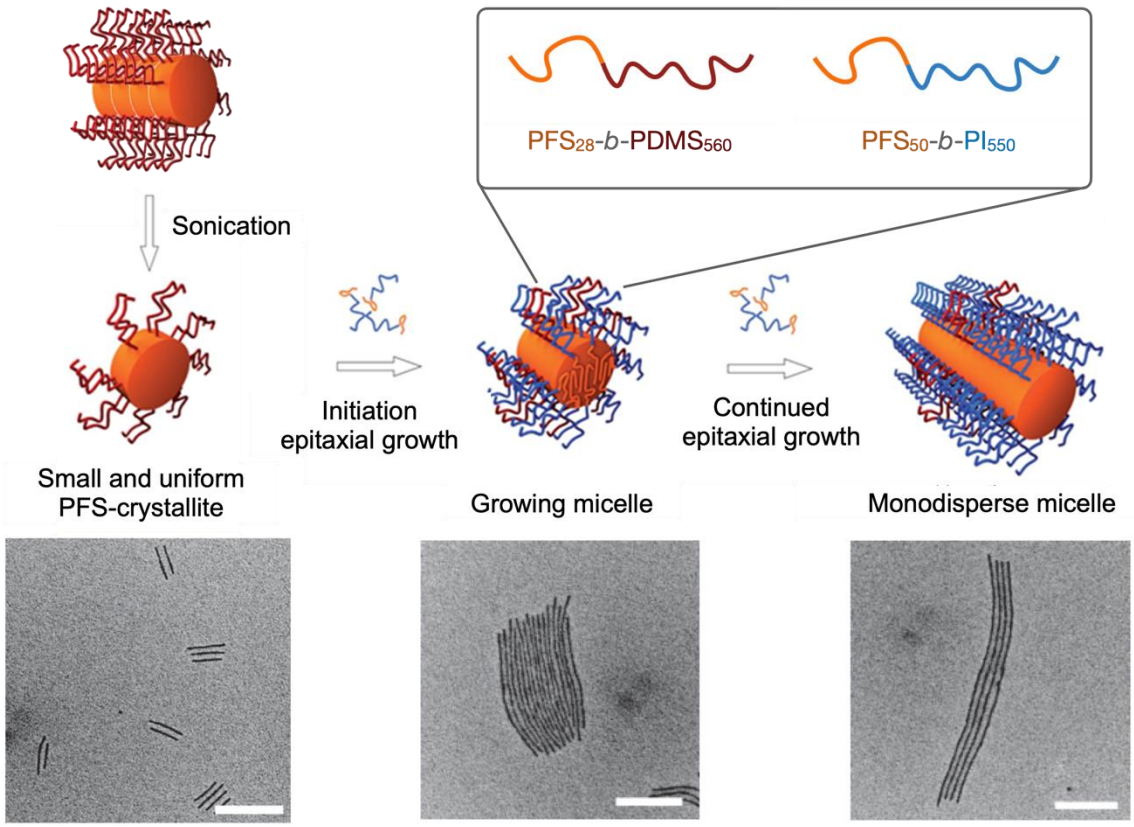

Figure 12. Schematic illustration of a living crystallization-driven self-assembly (CDSA) for two block copolymers as monomers. Arrows indicate the successive steps followed to reach monodisperse supramolecular polymers. Scale bars, 500 nm. Adapted with permission from Ref. 105 Copyright © Springer Nature Limited.

[105] J. B. Gilroy, T. Gädt, G. R. Whittell, L. Chabanne, J. M. Mitchels, R. M. Richardson, M. A. Winnik, I. Manners, *Nat. Chem.,* **2010**, *2*, 566–570.
[106] J. Qian, Y. Lu, A. Chia, M. Zhang, P. A. Rupar, N. Gunari, G. C. Walker, G. Cambridge, F. He, G. Guerin, I. Manners, M. A. Winnik, *ACS Nano,* **2013**, *7*, 3754–3766.
[107] Z. M. Hudson, C. E. Boott, M. E. Robinson, P. A. Rupar, M. A. Winnik, I. Manners, *Nat. Chem.,* **2014**, *6*, 893–898.
[108] R. Deng, X. Mao, S. Pearce, J. Tian, Y. Zhang, I. Manners, *J. Am. Chem. Soc.,* **2022**, *144*, 19051–19059.
[109] X. He, M. S. Hsiao, C. E. Boott, R. L. Harniman, A. Nazemi, X. Li, M. A. Winnik, I. Manners, *Nat. Mater.,* **2017**, *16*, 481–488.
[110] H. Qiu, Z. M. Hudson, M. A. Winnik, I. Manners, *Science,* **2015**, *347*, 1329-1332.
[111] L. MacFarlane, C. Zhao, J. Cai, H. Qiu, I. Manners, *Chem. Sci.,* **2021**, *12*, 4661–4682.

4.1. PEPTIDE-BASED 2D NANOMATERIALS

4.1.1. Introduction to nanomaterials

Nanomaterials are characterized to have dimensions within the range of 1 to 100 nanometers that provide them unique properties compared to their macroscopic analogues. The origin of this field dates back to 1960, when Nobel laureate Richard Feynman said in his talk that: "there's plenty of room at the bottom".[112] Since that moment, research in the field of nanotechnology has experienced a huge expansion, with novel advances leading to breakthroughs in a wide range of fields, ranging from medicine to electronics.

There are two fundamental methodologies to produce nanomaterials: top-down and bottom-up methods (**Figure 13**).[113] The first approach involves the reduction of larger materials to nanoscale dimensions through physical processes like mechanical milling, etching or laser ablation. The second consists of organizing atoms or discrete molecules in a programmed manner, to give rise the desired nanometric structure. This bottom-up approach presents an important advantage, particularly in nanomaterial design, as it allows to tailor the final structural properties precisely from simple and small molecules. Among the methods used, molecular self-assembly stands out, taking advantage of the tendency of molecules to self-organize and associate in an ordered manner by modulating interactions at the molecular level and thus guiding towards the formation of specific nanostructures (**Figure 2**).[114]As we explained in the first section, biomolecules serve as exceptional building blocks for self-assembly (Section 0). They offer specific and programmable interactions, allowing the creation of advanced nanomaterials through complex self-assembly processes. Furthermore, their biocompatibility allows them to be used in a variety of biomedical applications having less tendency to trigger adverse effects in biological systems.

[112] G. A. Ozin, L. Cademartiri, *Small,* **2009**, *5*, 1240–1244.
[113] N. Abid, A. M. Khan, S. Shujait, K. Chaudhary, M. Ikram, M. Imran, J. Haider, M. Khan, Q. Khan, M. Maqbool, *Adv. Colloid. Interface Sci.,* **2022**, *300.*
[114] D. Lombardo, P. Calandra, L. Pasqua, S. Magazù, *Materials,* **2020**, *13.*

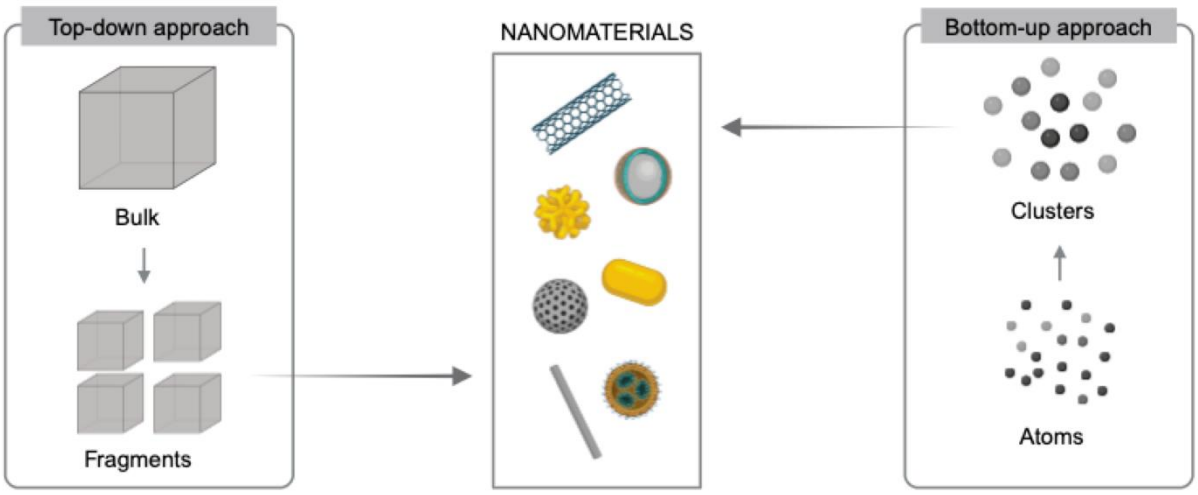

Figure 13. Representation of two synthetic methods for the fabrication of nanomaterials (middle): Top-down approach (left) and bottom-up approach (right). Created with BioRender.com.

Although proteins stand out as functional biomolecules in nature, their utilization in the bottom-up strategy presents significant challenges.[115] The large size and structural variety give rise to numerous interactions, making it difficult to control the self-assembly behavior. However, these characteristics make them excellent monomers for self-assembly due to their great diversity. As a result, the use of peptides, shorter in length but maintaining the fundamental chemical structure of proteins, emerged as an ideal alternative, offering a promising solution for achieving precise self-assembly in nanomaterial design.

4.1.2. Dimensionality in nanomaterials

Nanomaterials can be classified according to the number of dimensions extending beyond the nanoscale (**Figure 14**).[116] Zero-dimensional nanomaterials (0D) have all dimensions within the nanoscale, like nanospheres and nanorods. One-dimensional nanomaterials (1D) have one dimension outside the nanoscale such as nanotubes, nanorods or nanofibers. Two-dimensional (2D) nanomaterials can include nanosheets, nanofilms, and nanobelts. In three-dimensional nanomaterials (3D) all dimensions are propagated, although crystalline materials are usually included in this category, it is possible to find other assembled systems such as Fujita's cages[117] or Woolfson's barrels.[169]

[115] Y. Bai, Q. Luo, J. Liu, *Chem. Soc. Rev.,* **2016**, *45*, 2756–2767.
[116] S. Bayda, M. Adeel, T. Tuccinardi, M. Cordani, F. Rizzolio, *Molecules,* **2020**, *25*.
[117] T. Tateishi, M. Yoshimura, S. Tokuda, F. Matsuda, D. Fujita, S. Furukawa, *Coord. Chem. Rev.,* **2022**, *467*, 214612.

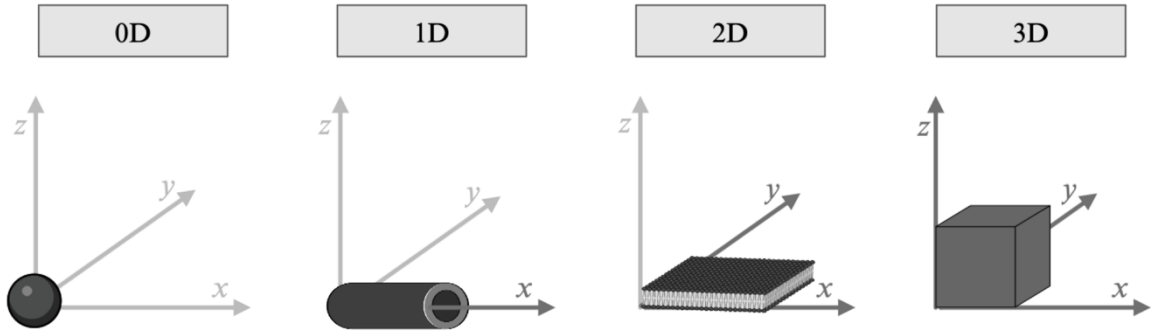

Figure 14. Classification of nanomaterials depending on the propagation axes**.** From left to right: Zero dimensional (0D), one-dimensional (1D), two-dimensional (2D) and three-dimensional (3D) materials exhibiting nanometer-scale size. The growth axis outside nanoscale is represented in darker grey. Created with BioRender.com.

Among them, 2D nanomaterials have emerged as an interesting class with distinctive characteristics due to their unique planar and large surface.[118] Their research journey began with the isolation of graphene, a 2D atomically thin carbon layer obtained from graphite. This discovery marked a revolution in materials chemistry, demonstrating that one-atom-thick films can exhibit remarkable and unique properties without losing their structural strength. After this discovery, the exploration of 2D nanomaterials with different types of monomers has expanded into new materials with potential applications in other disciplines.

The design of monomers for supramolecular self-assembly is a limiting step. There is still a knowledge gap in general design guidelines to predict desired propagation pathways, thus leading to the necessity of optimizing both monomer structure and assembly conditions for each case.[119] However, by strategically placing orthogonal and directional non-covalent binding motifs, it is possible to achieve certain control over the growth along different dimensions (**Figure 15**). Moreover, repulsive forces are also required to maintain the structures and prevent aggregation.

[118] N. Baig, *Compos. Part. A Appl. Sci. Manuf.,* **2023**, *165.*
[119] I. Insua, J. Bergueiro, A. Méndez-Ardoy, I. Lostalé-Seijo, J. Montenegro, *Chem. Sci.,* **2022**, *13*, 3057–3068.

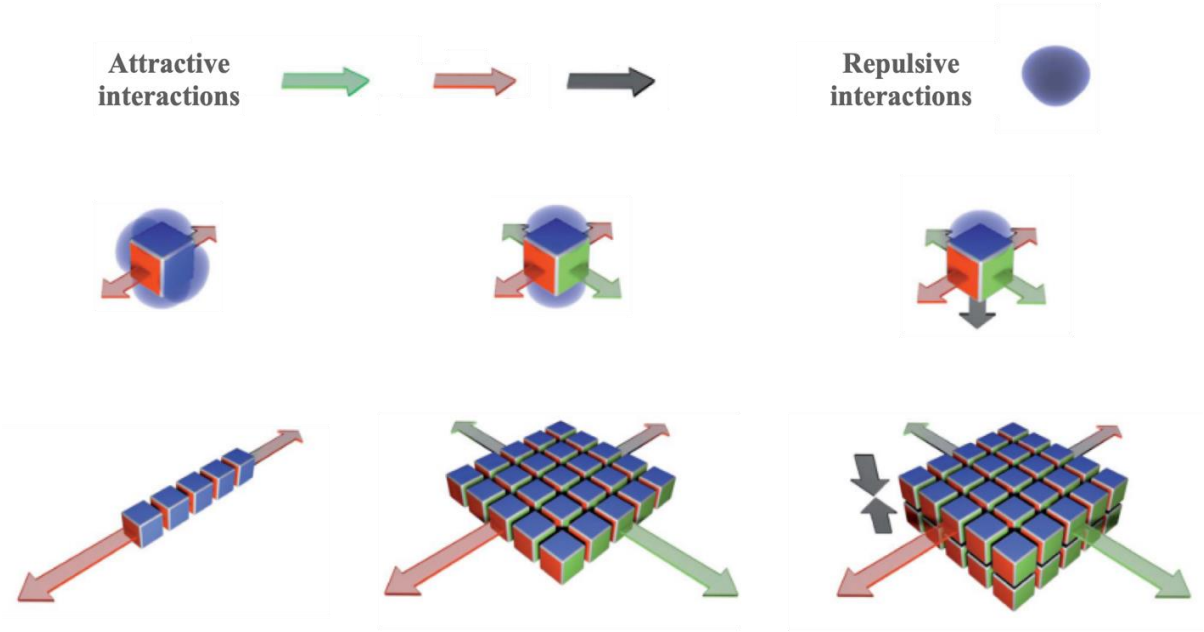

Figure 15. Three monomer design strategy (monomers are represented as cubes in the middle row) for the propagation along different dimensions (the resultant assembled nanostructure for each monomer is represented in the bottom row). Attractive forces are marked as arrows of different colors while repulsive forces are depicted as a blue circle. Adapted from Ref. 116 with permission from the Royal Society of Chemistry.

4.2.3. Peptide monomers for 2D nanomaterials

Peptides offer a multitude of advantages as monomers for nanomaterials as we have already mentioned in previous sections, such as biocompatibility or chemical diversity. Additionally, from a synthetic and design point of view, other benefits stand out. Firstly, peptides can be easily synthesized by solid-phase methods also allowing a precise functionalization at specific residues thanks to orthogonal protecting groups. Secondly, they have an intrinsic ability to self-assemble in hierarchical structures. Based on protein folding, it is possible to design peptide sequences with specific motifs driving the formation of basic conformational units (e.g., β-sheet or α-helix, Section 0). These secondary structures have defined orientations that facilitate the strategic positioning of binding motifs helping to promote the assembly in a predictable way.

In the following sections, we will explain how tailored-made peptides can be used for the self-assembly of different types of nanomaterials. They will be classified according to structural features or whether they are derived from natural protein structures.

4.2.3.8. Amyloid-derived peptides

The term "amyloid" refers to a type of misfolded proteins characterized by their propensity to aggregate into fibrillar structures, generally guided by β-sheet folding (**Figure 16**). The accumulation of these proteins in several tissues and cells is tightly associated with various diseases such as Alzheimer's and type II diabetes among many others.[120] Consequently, a large amount of initial research efforts has been dedicated to elucidate the formation mechanism of amyloid fibrils, aiming to either prevent their formation or design therapies to slow disease progression.[121] These studies have revealed the remarkable diversity of self-assembly pathways that amyloids can follow, resulting in an extensive library of mesoscopic structures ranging from nanospheres to nanofibers and hydrogels. This, in turn, has attracted the attention of supramolecular chemists as amyloids seemed promising building blocks in the fabrication of self-assembled nanostructures.[122]

The large size of amyloid proteins has led researchers to identify minimum peptide fragments able to maintain the amyloid fibril structure, thus facilitating both their synthesis and the study of the assembly mechanisms. This search was aided by X-ray diffraction studies, which revealed the presence of specific regions that direct assembly in repeated patterns throughout the protein's folding structure.[123] By focusing on these fragments, it was possible to identify short oligopeptide sequences that not only retained the ability to assemble into fibrils but also exhibited comparable physicochemical properties like naturally occurring amyloids (i.e., stability and high mechanical stiffness).[124] Inspired by these discoveries, researchers explored how subtle modifications in both the amino acid sequence and assembly conditions could influence the formation of new materials. Although one-dimensional (1D) nanofibrils and nanotubes represent the most predominant morphologies for these peptides,[125] our focus here will specifically delve into those strategies that manage to organize their assembly into two-dimensional (2D) structures.

[120] T. P. J. Knowles, M. Vendruscolo, C. M. Dobson, *Nat. Rev. Mol. Cell. Biol.,* **2014**, *15*, 384–396.
[121] T. Härd, *J.Phys. Chem. Lett.,* **2014**, *5*, 607–614.
[122] I. Cherny, E. Gazit, *Angew. Chem., Int. Ed.,* **2008**, *47*, 4062–4069.
[123] J. D. Sipe, A. S. Cohen, *J. Struct. Biol.,* **2000**, *130*, 88–98.
[124] T. P. J. Knowles, R. Mezzenga, *Adv. Mater.,* **2016**, *28*, 6546–6561.
[125] Y. Lai, F. Li, Z. Zou, M. Saeed, Z. Xu, H. Yu, *Appl. Mater. Today,* **2021**, *22*.

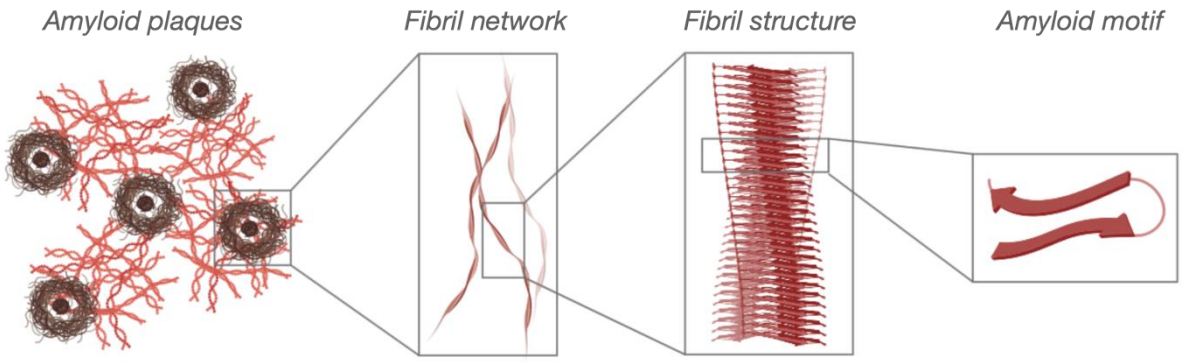

Figure 16. Decreasing structural complexity from an amyloid plaque aggregate to the minimal assembly-forming peptide sequence. Created with BioRender.com.

Zhang's group reported in 1993 a 16-residue peptide (EAK16) capable of forming macroscopic membranes through spontaneous self-assembly upon the addition of salt (**Figure 17**a).[126] The peptide sequence alternates hydrophobic residues of alanine with charged glutamic acid and lysine, allowing the system to adopt a β-sheet conformation with segregated domains on different sides. This structural feature drives the assembly in the formation of membranes through successive staggering of peptides, combining hydrophobic effects and complementary ionic bonds. Scanning electron microscopy reveals an interwoven network of fragments measuring 10-20 nm in diameter, indicating the robust structural integrity of the assembled membranes, which also showed remarkable resistance to dissolution in various conditions, including heat, acidic or alkaline solutions, and several proteolytic enzymes.

Dai and co-workers explored the formation of nanosheets using a mutated form of the amyloid fragments $A\beta_{16-22}$ (KLVFFAK) (**Figure 17**b).[127] Experimental observations and molecular dynamics simulations suggested that peptide monomers are arranged vertically, creating a monolayer with a height value comparable to the peptide's length. The interplay of forces through perpendicular directions allows the formation of well-defined 2D nanosheets. The growth in the fibril axis (a') is driven by β-sheet hydrogen bonds between the peptide backbone while, the growth in the perpendicular axis (b') arises from a distinct mechanism, involving "steric zipper" interactions between the hydrophobic side chains. Notably, authors discovered that through ionic-strength modulation is possible to control the assembly growth, achieving nanosheets with fine-tuned sizes. This work highlighted the relevance of the core motif "LVFFAK" demonstrating that mutations in some of their residues disturb nanosheet assembly, while mutations in the terminal lysines are well tolerated and retain their functional activity. In a later work, infrared spectroscopy was used to study this assembly motif in more

[126] S. Zhang, T. Holmest, C. Lockshin, A. Rich, *Proc. Natl. Acad. Sci. U S A.*, **1993**, *90,* 3334-3338.
[127] B. Dai, D. Li, W. Xi, F. Luo, X. Zhang, M. Zou, M. Cao, J. Hu, W. Wang, G. Wei, Y. Zhang, C. Liua, *Proc. Natl. Acad. Sci. U S A,* **2015**, *112*, 2996–3001.

detail.[128] This aligned stack of β-sheet fibrils through hydrophobic effect was observed in another example, where a Tau-derived peptide fragment ($Tau_{306-327}$) self-assembled in well-ordered 2D laminated flat ribbons with large dimensions (**Figure 17**c).[129]

In contrast to the previous self-assemblies guided by endogenous interactions, ultrathin and uniform 2D biofilms were fabricated via argon glow discharge.[130] In the first step, monomers derived from an amyloidogenic fragment ($A\beta_{16-22}$) are organized into fibres that align perpendicular in the second step after interacting with the added hydrated electrons. Besides this sequence, other peptide derivatives were successfully tested, demonstrating the potential of this new technique to achieve ordered 2D assemblies.

Tyrosine-rich peptides are another important class of self-assembling motifs derived from amyloid proteins.[131] Unlike the other aromatic amino acids, the phenolic group (-OH) can also establish hydrogen bonding interactions, enhancing the stability of the assemblies. Inspired by this property, tyrosine-based peptides have been developed to study their ability to self-assemble. Although most of these peptides were shown to assemble in 1D nanostructures, the sequence YYACAYY presented a different behaviour forming flat nanosheets at the air/water interface that can even be seen with the naked eye (**Figure 18**a).[132] Two main factors are responsible for this 2D assembly. The multiple tyrosine residues along the peptide sequence increase the rigidity of the system establishing π-π interactions and hydrogen bonds. In addition, the incorporation of cysteines in the centre of the sequence was essential for 2D growth by generating dimers through disulfide bridges. Assembly monitoring showed the close relationship between the conformational change from the unfolded monomer to the α-helix dimer and the formation of the 2D peptide films.[133] Note that despite having mentioned that the typical β-sheet is the most repeated conformation in amyloid proteins, it is also possible to have regions with an α-helix conformation.

[128] B. Jia, Y. Sun, L. Yang, Y. Yu, H. Fan, G. Ma, *Phys. Chem. Chem. Phys.,* **2018**, *20*, 27261–27271.
[129] J. Adamcik, A. Sánchez-Ferrer, N. Ait-Bouziad, N. P. Reynolds, H. A. Lashuel, R. Mezzenga, *Angew. Chem.,* **2016**, *128*, 628–632.
[130] Y. X. Pan, C. J. Liu, S. Zhang, Y. Yu, M. Dong, *Chem. Eur. J.,* **2012**, *18*, 14614–14617.
[131] J. Lee, M. Ju, O. H. Cho, Y. Kim, K. T. Nam, *Ad. Sci.,* **2019**, *6*.
[132] H. S. Jang, J. H. Lee, Y. S. Park, Y. O. Kim, J. Park, T. Y. Yang, K. Jin, J. Lee, S. Park, J. M. You, K. W. Jeong, A. Shin, I. S. Oh, M. K. Kwon, Y. Il Kim, H. H. Cho, H. N. Han, Y. Kim, Y. H. Chang, S. R. Paik, K. T. Nam, Y. S. Lee, *Nat. Commun.,* **2014**, *5*.
[133] J. Lee, I. R. Choe, N. K. Kim, W. J. Kim, H. S. Jang, Y. S. Lee, K. T. Nam, *ACS Nano,* **2016**, *10*, 8263–8270.

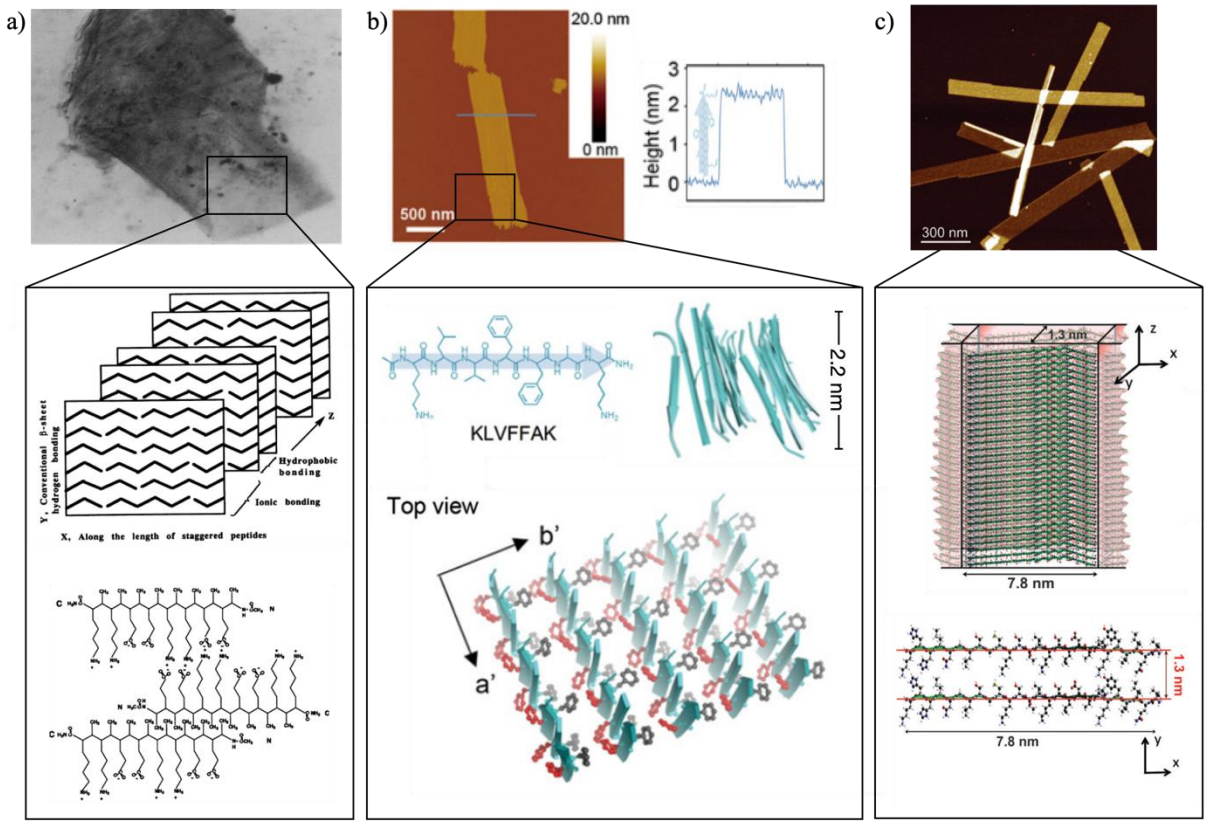

Figure 17. a) Photograph of the membrane formed by EAK16. Magnification: The proposed model for the membrane specifying the non-covalent interactions between residues driving the assembly. Adapted with permission from Ref. 123. Copyright © (1993) National Academy of Science. b) AFM image of the KLVFFAK nanosheet with the height profile. Magnification: the extended peptide sequence and the β-sheet arrangement with the height value estimated. At the bottom: a top view of the proposed assembly model for nanosheets. Adapted with permission from Ref. 124. Copyright © (2015) National Academy of Science. c) AFM image of the assembled $Tau_{306-327}$ peptide. Magnification: The structural model for the 2D laminated flat ribbons observed with coordinates and distance values facilitating its comprehension. Adapted with permission from Ref. 126. Copyright © 2012 WILEY-VCH Verlag GmbH & Co. KGaA, Weinheim.

The significance of aromatic amino acids influencing the process of amyloid formation has led to researchers to have a more reductionist approach. Indeed, some authors have demonstrated that even the simplest diphenylalanine (FF) fragment is able to self-assemble into a diverse range of nanostructures.[49] The stability of these assemblies arises from the directionality offered by repeated hydrogen bonding and phenyl stacking interactions throughout the system. Cong Guo and co-workers investigated the assembly process of FF monomers using coarse-grained molecular dynamics simulations.[134] Their study demonstrated the impact of peptide concentration on the resultant assembled nanostructures. FF nanotubes were observed to initially self-assemble into a bilayer and subsequently, at lower concentrations, the bilayer tended to curve into vesicles or tubes, whereas at higher concentrations, the bilayer structure remained intact in a 2D configuration.

[134] C. Guo, Y. Luo, R. Zhou, G. Wei, *ACS Nano,* **2012**, *6*, 3907–3918.

Gazit and co-workers developed two strategies to vertically align, through axial growth, a multitude of FF nanotubes forming ordered 2D assemblies (**Figure 18**b).[135] One strategy involves an evaporation-initiated technique, where monomers dissolved in HFIP were spread over siliconized glass. This volatile fluorinated solvent allows the existence of monodispersed monomers, and upon rapid evaporation, a thin layer of aligned nanotubes forms on the substrate. Secondly, they assembled FF nanotubes in the presence of magnetite nanoparticles, forming a non-covalent coating layer around it thus making them ferromagnetic. When exposed to an external magnetic field, nanotubes respond and align themselves to the direction of the field. Later studies have demonstrated that FF nanotubes can align without any treatment in the presence of a magnetic field due to the π-electrons delocalized in the aromatic ring.[136]

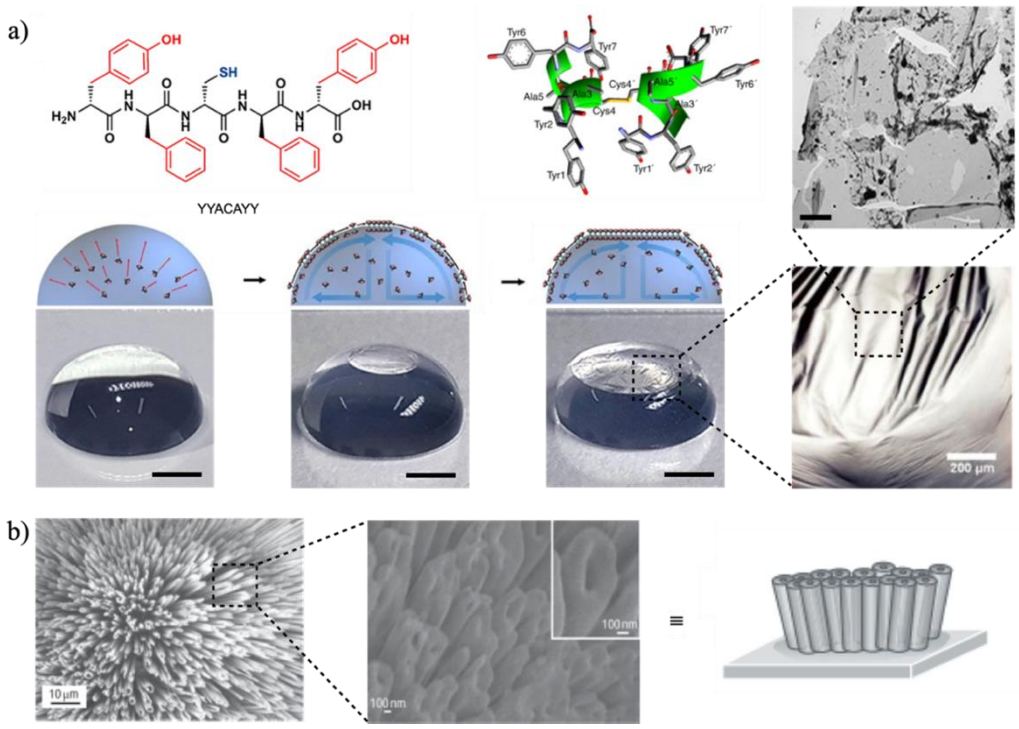

Figure 18. a) Chemical structure of YYACAYY and representation of the lowest energy dimeric structure with the disulfide bridge. At the bottom: schematic representation and optical images of the 2D peptide film formation process at the air-water interface. Right: Microscopy images of the assembled film. Scale bars, 2 mm. Adapted with permission of Ref .129 and 130. Copyright © (2014) Springer Nature Limited. Copyright © (2016) American Chemical Society. b) From left to right: SEM and HRSEM micrographs and model of vertically aligned FF-based nanotubes onto siliconized glass. Adaptes with permission of Ref. 132. Copyright © (2006) Springer Nature Limited.

[135] M. Reches, E. Gazit, *Nat. Nanotechnol.,* **2006**, *1*, 195–200.
[136] R. J. A. Hill, V. L. Sedman, S. Allen, P. M. Williams, M. Paoli, L. Adler-Abramovich, E. Gazit, L. Eaves, S. J. B. Tendler, *Ad. Mater.,* **2007**, *19*, 4474–4479.

4.2.3.9. Peptide amphiphiles (PAs)

In 2001, the Stupp laboratory described a special class of self-assembling short amphiphilic peptides linked to a hydrophobic alkyl chain (**Figure 19**).[137,138] Typically, the peptide sequence comprises two distinct domains. The first domain, situated near to the aliphatic chain, is formed by hydrophobic residues with a strong propensity to adopt a β-sheet conformation. The second domain, situated further away, is composed of polar charged amino acids to promote solubility in water. This distribution facilitates its spontaneous self-assembly into core-shell nano assemblies, such as micelles, fibers, ribbons, and nanosheets.[139] Peptide amphiphiles have garnered considerable attention as functional materials, particularly in the field of regenerative medicine and cancer therapy.[140] By attaching a new domain to the polar region, containing for example bioactive molecules (e.g., epitopes), it is possible to promote interactions with cells and enable other functional properties. For instance, the Stupp laboratory is a pioneer in demonstrating their potential as nano-therapeutics for cancer and cardiovascular diseases.[141,142]

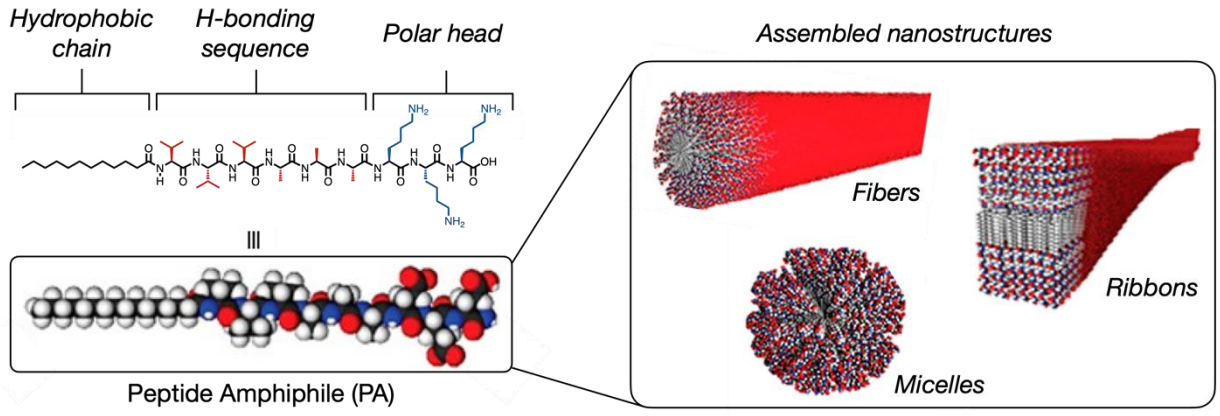

Figure 19. Left: General chemical structure for a peptide amphiphile (PA) with the three different domains marked. Right: Examples of some supramolecular nanostructures that can be achieved by assembling PA. Adapted with permission from Ref. 134. Copyright © (2017) American Chemical Society.

[137] J. D. Hartgerink, E. Beniash, S. I. Stupp, *Science,* **2001**, *294*, 1684–1688.
[138] M. P. Hendricks, K. Sato, L. C. Palmer, S. I. Stupp, *Acc. Chem. Res.,* **2017**, *50*, 2440–2448.
[139] H. Cui, A. G. Cheetham, E. T. Pashuck, S. I. Stupp, *J. Am. Chem. Soc.,* **2014**, *136*, 12461–12468.
[140] A. Dasgupta, D. Das, *Langmuir,* **2019**, *35*, 10704–10724.
[141] M. J. Webber, J. Tongers, C. J. Newcomb, K.-T. Marquardt, J. Bauersachs, D. W. Losordo, S. I. Stupp, Proc. Natl. Acad. Sci. USA, **2011**, *108*, 13438-13443.
[142] D. J. Toft, T. J. Moyer, S. M. Standley, Y. Ruff, A. Ugolkov, S. I. Stupp, V. L. Cryns, *ACS Nano,* **2012**, *6*, 7956–7965.

There are many works on how the molecular structure of peptide amphiphiles influences their self-assembly and resulting morphologies. Although most of them are related to 1D nanostructures, we found a few articles focusing on the lateral growth in the second dimension. One example is the formation of a macroscopic membrane at an aqueous liquid-liquid interface (**Figure 20**a).[143] R. M. Capito et al. reported the rapid formation of a highly ordered membrane after mixing two different solutions, one containing a peptide amphiphile and the other hyaluronic acid. This mixture creates a diffusion barrier where the assembled membrane is maintained by a synergistic effect of the "static" self-assembly of both compounds and the osmotic pressure of ions generated between the two regions.

Stupp's group demonstrated that a single peptide amphiphile can be assembled laterally into ordered and flat nanobelts (**Figure 20**b).[144] This breakthrough was possible thanks to the introduction of glutamic acid alternating between valine residues in the peptide region. Through meticulous pH modulation, they observed a transition from twisted bilayer nanoribbons to the formation of flat nanobelts. This transition is attributed to the deprotonation of glutamic acid residues at lower pH values, effectively neutralizing electrostatic repulsion forces and facilitating the stacking of multiple bilayers. Notably, the study also uncovered a correlation between nanostructure morphology transitions and peptide concentration. As the concentration was gradually decreased, the nanostructures exhibited a propensity to curve. This phenomenon can be attributed to the inherent twisting tendency of the peptide monomers, which becomes more pronounced at lower concentrations. In a later study, researchers further investigated this type of assembly with a systematic study of peptide sequences.[145] A library of compounds varying the number of glutamic acid and valine residues showed that the longer the peptide sequence, the higher the degree of twisting in the β-sheet, thus generating cylindrical structures rather than flat nanobelts. Moreover, they also demonstrated that it is possible to modulate the width and thickness of these assemblies with both peptide length and pH.

[143] R. M. Capito, H. S. Azevedo, Y. S. Velichko, A. Mata, S. I. Stupp, *Science,* **2008**, *319*, 1812–1816.
[144] H. Cui, T. Muraoka, A. G. Cheetham, S. I. Stupp, *Nano Lett.,* **2009**, *9*, 945–951.
[145] T. J. Moyer, H. Cui, S. I. Stupp, *J. Phys. Chem. B,* **2013**, *117*, 4604–4610.

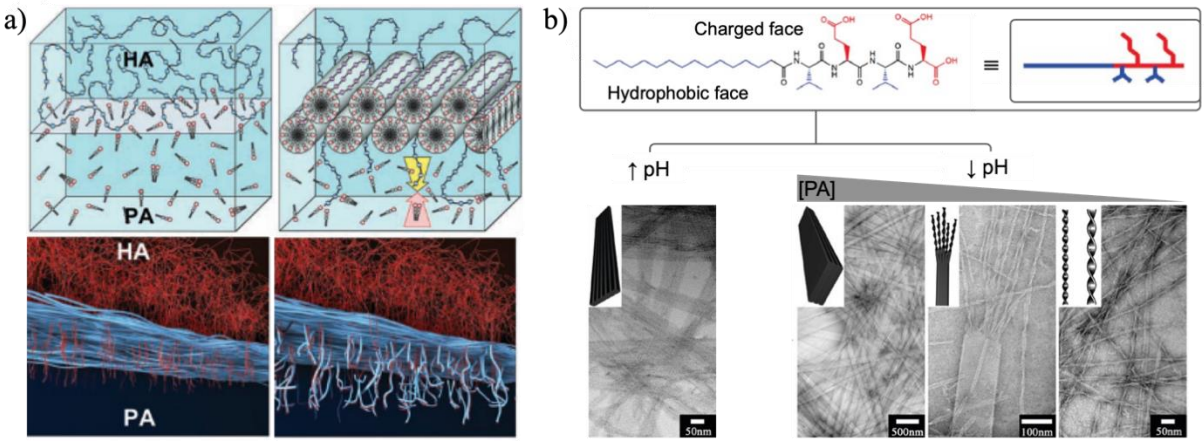

Figure 20. a) From left to right: Schematic representation for the formation of PA-HA membrane at an aqueous liquid-liquid interface (PA: peptide amphiphile; HA: hyaluronic acid). Adapted with permission from Ref. 31. Copyright © (2008) American Association for the Advancement of Science. b) Chemical structure and simplify representation of a PA with segregated charged (red) and hydrophobic (blue) face in the peptide sequence. Bottom: Assembled nanostructures achieved at different pH and concentrations. Adapted with permission from Ref. 32. Copyright © (2009) American Chemical Society.

In another work carried out by the group of Prof. Tong Yen Wah, this pH control also promoted the hierarchical assembly of a peptide amphiphile (**Figure 21**a).[146] In this study, three charged amino acids with different pK_a values were strategically positioned in the sequence. By modulating the pH, it was possible to drive the self-assembly based on the repulsive and attractive electrostatic interactions between residues. Lateral assembly of nanofibers into ordered bundles was achieved in those sequences with complementarily charged residues by increasing the pH to an ionizable state with a zero net charge.

The Stevens laboratory studied the role of the hydrophobic effect in lineal peptide amphiphiles to drive 2D supramolecular growth (**Figure 21**b).[147] The amphiphilic peptide used in this study consists of an alkyl chain attached to a peptide sequence formed by six phenylalanines and two glutamic acids located at the end. The phenylalanine segment promotes the formation of β-sheet along the x-axis through a hydrogen bonding network while driving the stacking of these β-sheet along the y-axis through aromatic interactions. The hydrophobic effect in both directions is enhanced by the alkyl chain and the negatively charged glutamic acids maintains the free-standing nanosheets due to electrostatic repulsion. Overall, the resulting nanosheets have two distinct faces, which allows different functionalization on either face. This has been exploited by the authors to demonstrate its application in improving the catalytic activity of an enzyme retained on its surface. In a later article, the influence of cosolvents on both the

[146] Y. Chen, H. X. Gan, Y. W. Tong, *Macromolecules* **2015**, *48*, 2647–2653.
[147] Y. Lin, M. R. Thomas, A. Gelmi, V. Leonardo, E. T. Pashuck, S. A. Maynard, Y. Wang, M. M. Stevens, *J. Am. Chem. Soc.*, **2017**, *139*, 13592–13595.

thermodynamic and kinetic control of the self-assembly process was studied.[76] They observed two key aspects: Firstly, by modulating the solvent polarity, it becomes possible to control the resulting nanostructure. Secondly, through variations in the sample preparation method, different self-assembly pathways can be followed, ultimately determining whether the system reached the thermodynamic product became kinetically trapped.

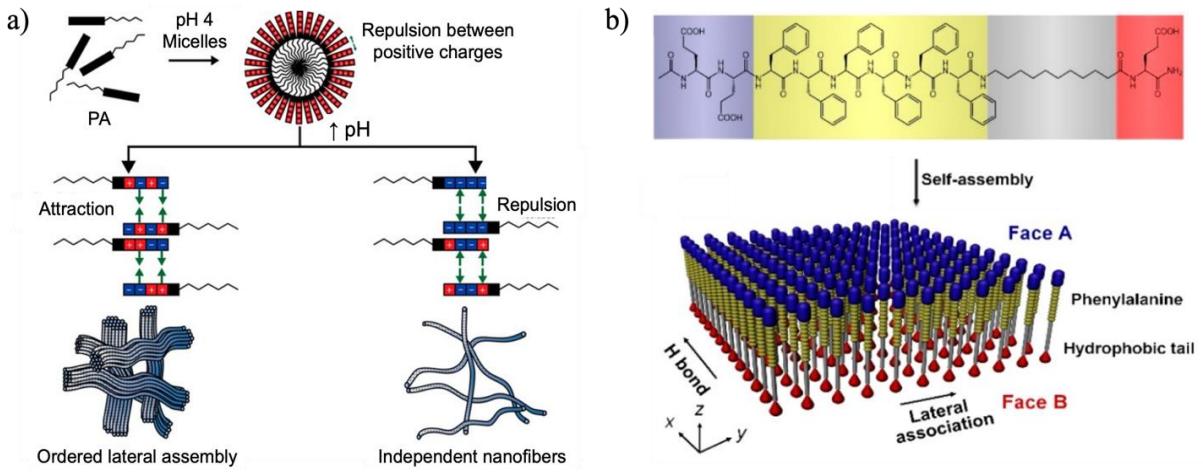

Figure 21. a) Schematic diagram of the self-assembled nanostructures achieved with a PA depending on the pH of the medium. Adapted with permission from Ref. 34. Copyright © (2015) American Chemical Society. b) Chemical structure of PA and proposed model for the 2D Janus nanosheets. Adapted with permission from Ref. 35. Copyright © (2017) American Chemical Society.

4.2.3.10. Surfactant-like peptides (SLP)

The term surfactant-like peptide is used to describe short peptides that contain a region of hydrophobic amino acid residues and a very short hydrophilic head, composed of only one or two polar amino acids (**Figure 22**).[60] Their self-assembly behaviour shares properties with those found in biological systems (e.g., phospholipids), forming a bilayer of hydrophobic tail-to-tail dimeric packing with the polar region exposed to the aqueous environment. Moreover, surfactant-like peptides also establish hydrogen bonding interactions between their backbone chains resembling β-sheet conformations. Their characteristic short sequence, typically comprising fewer than 10 amino acids, is essential for their self-assembly due to its impact on solubility. Excessive presence of charged polar residues could lead to excessive repulsion, while a large size of the hydrophobic chain may generate insolubility and thus disrupt proper packing. Notably, surfactant-like peptides often assemble into cylindrical nanostructures, reflecting their inherent twisting behaviour and the hydrophobic effect-induced instability of their open ends in aqueous environments.[148] This tendency toward curvature leads to the formation of micelles and nanotubes, following pathways of minimum energy.

[148] S. Vauthey, S. Santoso, H. Gong, N. Watson, S. Zhang, *Proc. Natl. Acad. Sci.*, **2002**, *99*, 5355-5360.

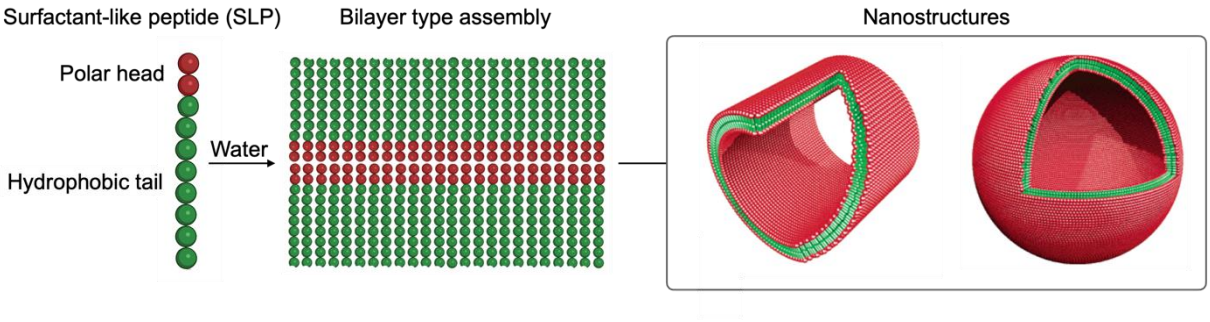

Figure 22. Left: General structure for a surfactant-like peptide (SLP) with a short polar head formed by polar amino acids (red balls) and a tail with hydrophobic amino acids (green balls). Middle: Bilayer structure assemble in water. Right: Examples of some nanostructures (nanotube and nanovesicle). Adapted with permission from Ref. 39. Copyright © (2002) American Chemical Society.

In a seminal study published in 2002, researchers investigated the impact of glycine residues within the hydrophobic chains of SLPs.[149] They observed the unexpected formation of extended flat membranes between adjacent nanotubes, suggesting a deviation from the typical cylindrical nanostructures. However, it was not until subsequent years later that isolated nanosheets were successfully achieved (**Figure 23**a).[150] Researchers found that as the hydrophobic chain length decreased, the propensity for spontaneous curvature also decreased, thus leading to the formation of flat nanosheets. On the other hand, other studies have further demonstrated that the curvature can be influenced also by the composition of the charged head region. In one example, a SLP containing lysine was observed to assemble into stacked parallel sheets at high concentrations.[151] Researchers postulated that the concentration dependence was closely related to the resultant pk_a. Lysine residues can form salt bridges with positively charged N-termini, altering the average peptide charge and thereby influencing the final assembled morphology. Conversely, in another study, the substitution of lysine with arginine led to opposite assembly outcomes.[152] Here, monomers are assembled into bilayers at low concentrations (**Figure 23**b). It was hypothesized that the monomers formed antiparallel dimers, with the guanidinium group stabilizing the planar geometry through electrostatic interactions with the C-terminal carboxylic groups. At high concentrations, however, this stabilization was reduced due to an increase in counterions in the solution, thus screening these interactions and resulting in curved assembled structures. These findings underscore the intricate interplay between the non-covalent interactions of molecular compositions and assembly conditions (Section 0), highlighting the remarkable ability of peptide monomers to modulate them and assemble into diverse nanostructures.

[149] S. Santoso, W. Hwang, H. Hartman, S. Zhang, *Nano Lett.,* **2002**, *2*, 687–691.
[150] H. Xu, J. Wang, S. Han, J. Wang, D. Yu, H. Zhang, D. Xia, X. Zhao, T. A. Waigh, J. R. Lu, *Langmuir,* **2009**, *25*, 4115–4123.
[151] Ç. Cenker, S. Bucak, U. Olsson, *J. Soft Matter,* **2011**, *7*, 4868–4875.
[152] I. W. Hamley, A. Dehsorkhi, V. Castelletto, *Chem. Comm.,* **2013**, *49*, 1850–1852.

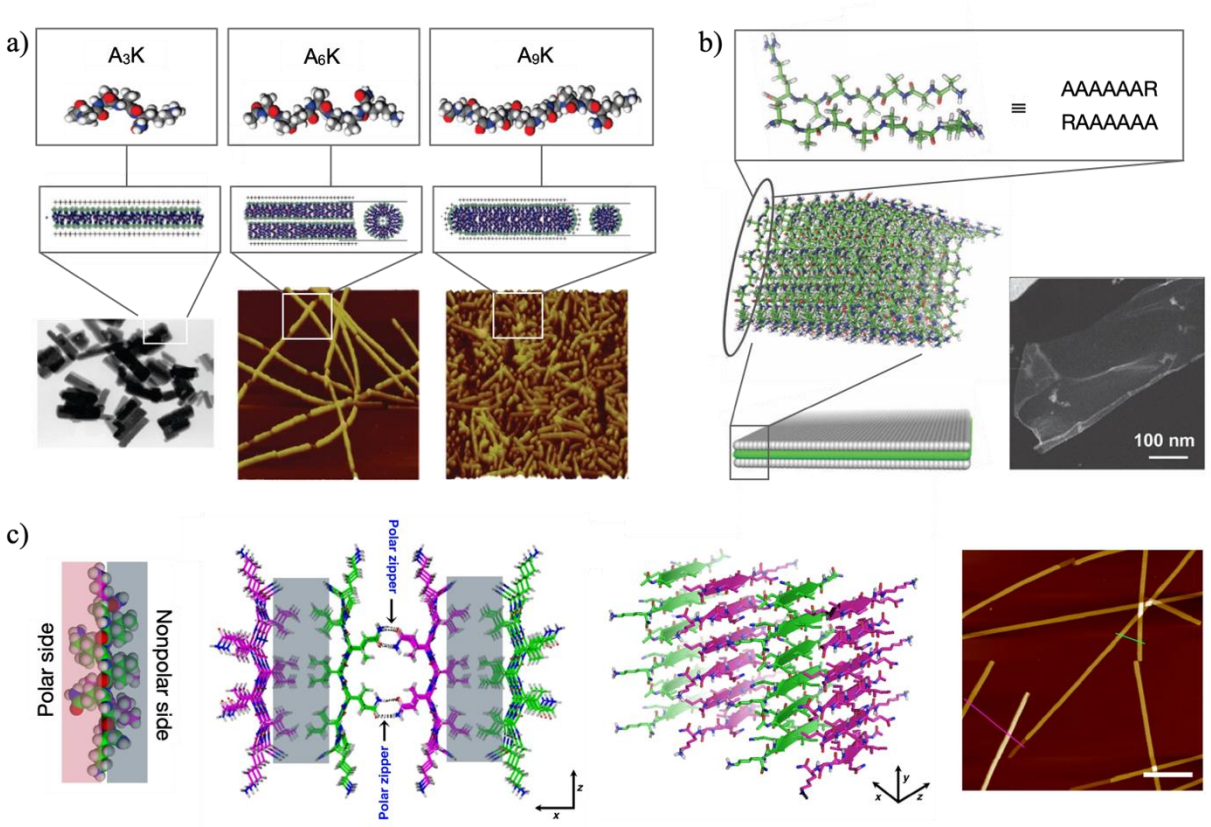

Figure 23. a) Top: Peptide sequences for A_3R, A_6R and A_9R. Middle: Proposed models for the self-assembly in bilayer (A_3R), nanotube (A_6R) and nanorod (A_9R). Bottom: Micrographs of the resultant nanostructures. Adapted with permission from Ref. 147. Copyright © (2008) American Chemical Society. b) Model for the antiparallel stacking of A_6R in single thickness nanosheet and STEM micrograph. Adapted with permission from Ref. 149 Copyright © (2013) Royal Society of Chemistry. c) From left to right: Representation of a peptide structure with a nonpolar side (grey) and a polar side (red). Different views of the proposed assembly model. AFM image of the resultant flat nanoribbons. Scale bars, 500 nm. Adapted with permission from Ref. 150 Copyright © (2018) American Chemical Society. Meng Wang et al.

In another pioneering study about SLPs, Wang et al. introduced a novel assembled motif termed as the "super-secondary structural template", where the 2D growth is directed by "polar zippers" between adjacent β-sheets (**Figure 23**c).[153] This new packing mode was based on the introduction of an uncharged polar residue in the hydrophobic chain, driving the lateral packing perpendicularly to the axial 1D growth. These polar residues (e.g., Gln, Ser, and Asn) enable hydrogen bonding between neighboring β-sheets due to their side chains containing both H-donors and H-acceptors in the amide groups. The directionality of the H-bonding allows the formation of stable flat nanoribbons.

[153] M. Wang, J. Wang, P. Zhou, J. Deng, Y. Zhao, Y. Sun, W. Yang, D. Wang, Z. Li, X. Hu, S. M. King, S. E. Rogers, H. Cox, T. A. Waigh, J. Yang, J. R. Lu, H. Xu, *Nat. Commun.,* **2018**, *9*

Another relevant class of SLP is known as bola-amphiphiles, structurally characterized by two hydrophilic heads connected by a hydrophobic spacer (**Figure 24**a). Bola-amphiphiles assemble in extended conformations but eventually, they also tend to twist into curved structures. Building on the understanding gained from previous SLP assemblies, where the properties of the polar charged residues significantly influenced the final morphology, we will illustrate an example where this has also been exploited with bola-amphiphiles (**Figure 24**b).[154] In this work, while peptides containing arginine's at both ends tend to form nanotubes, histidine variants are assembled into flat multilayered nanoribbons. The different assembled morphologies arise from the varying affinity of polar residues for solvent molecules. Arginine's exhibit a higher propensity to interact with water molecules, resulting in enhanced wetting and preventing the stacking along the z-direction. Consequently, the formation of twisted bilayers leads to the eventual assembly of nanotubes. In contrast, the lower tendency of histidines to be wetted by solvent molecules promotes the formation of His-His pairing between adjacent layers, thus stabilizing the multilayer packing of flat nanoribbons.

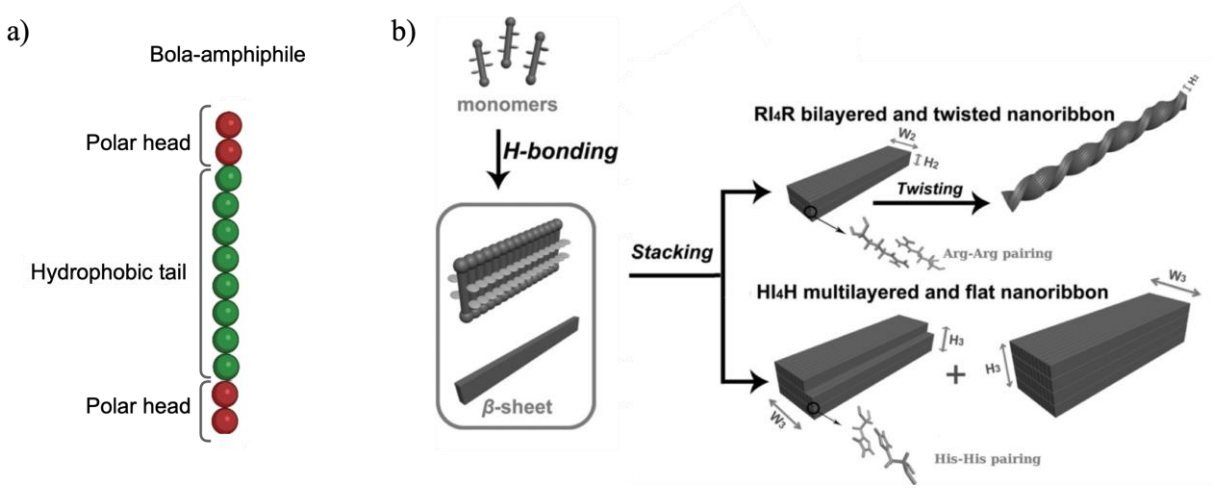

Figure 24. General structure for a bola-like peptide amphiphile with a hydrophobic tail (amino acids as green balls) flanked by two polar heads (amino acids as red balls). b) Schematic illustration of the assembly process for two different monomers: RI_4R (right top) and HI_4H (right bottom). Adapted with permission from Ref. 153. Copyright © (2016) WILEY-VCH Verlag GmbH & Co. KGaA, Weinheim.

[154] Y. Zhao, L. Deng, W. Yang, D. Wang, E. Pambou, Z. Lu, Z. Li, J. Wang, S. King, S. Rogers, H. Xu, J. R. Lu, *Chem. Eur. J.,* **2016**, *22*, 11394–11404.

4.2.3.11. Collagen mimetic peptides (CMP)

Collagen, the most abundant protein in the human body, plays a crucial role in providing structure and support to various tissues.[155] The remarkable properties of these proteins -strength, flexibility, and stability- are attributed to their unique helical structure, composed of three intertwined protein strands (**Figure 25**a). Each strand is formed by repeated motifs characterized by the amino acid pattern: "Xaa-Yaa-Gly" (**Figure 25**b, central motif). Typically, the positions "Xaa" and "Yaa" are occupied by proline (Pro) and (2S, 4R)-4-hydroxyproline (Hyp), respectively. This specific arrangement facilitates tight packing via a hydrogen bonding network between Gly amino group and the Xaa carbonyl, while the unique geometries of Pro and Hyp side chains contribute to the helical stabilization through stereoelectronic effects.[156,157] Crystallographic studies have elucidated a preferential conformation for imino acid residues at both positions, with a C^{γ}-endo conformation for position "Xaa" (Pro) and a C^{γ}-exo conformation for position "Yaa" (Hyp). The inherent complexity of collagen proteins has prompted researchers to design simpler monomers while preserving their properties. Consequently, "collagen mimetic peptides (CMP)" have emerged as new monomers for self-assembly, maintaining the repeated structural motif "Xaa-Yaa-Gly" in their design. However, variations in the peptide sequence, particularly the introduction of charged amino acids, have emerged as a pivotal strategy to modulate their self-assembly through complementary electrostatic interactions (**Figure 25**b).[158,159]

[155] S. A. H. Hulgan, J. D. Hartgerink, *Biomacromolecules,* **2022**, *23*, 1475–1489.
[156] L. E. Bretscher, C. L. Jenkins, K. M. Taylor, M. L. DeRider, R. T. Raines, *J. Am. Chem. Soc.,* **2001**, *123*, 777–778.
[157] S. K. Holmgren, K. M. Taylor, L. E. Bretscher, R. T. Raines, *Nature,* **1998**, *392*, 666–667.
[158] S. Rele, Y. Song, R. P. Apkarian, Z. Qu, V. P. Conticello, E. L. Chaikof, *J. Am. Chem. Soc.,* **2007**, *129*, 14780–14787.
[159] L. E. R. O'Leary, J. A. Fallas, E. L. Bakota, M. K. Kang, J. D. Hartgerink, *Nat. Chem.,* **2011**, *3*, 821–828.

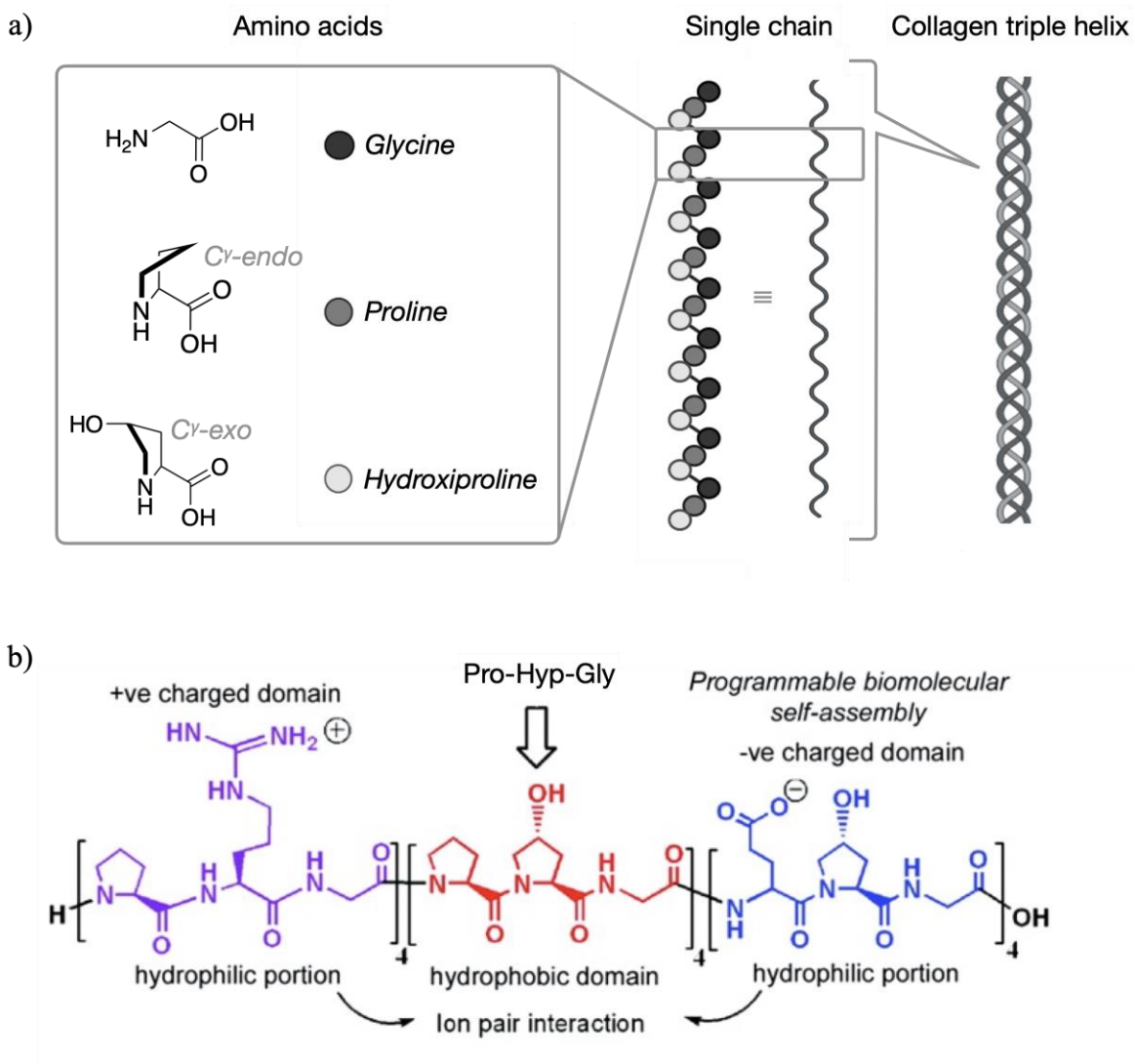

Figure 25. a) Schematic illustration of the collagen structure: Chemical structure of amino acids forming the tripeptide (Pro-Hyp-Gly) with its most stable spatial orientation. Helical structure of a single chain formed by successive tripeptides with amino acids marked as color circles. Triple helix formation of the collagen. Created with BioRender.com. b) Collagen mimetic peptide sequence modified with charged amino acids in the tripeptide motifs at the ends. Adapted with permission from Ref. 156. Copyright © (2007) American Chemical Society.

The Conticello group has exploited these complementary monomers to design collagen mimetic peptides capable of not only self-assembling into ordered 2D nanostructures, but also with precise control in their shape and size. They achieved this hierarchical assembly through the strategic incorporation of non-canonical imino acids at key positions within the peptide sequence, namely (2S, 4R)-4-aminoproline (Amp) and (2S, 4S)-4-aminoproline (amp) (**Figure 26a**). These residues were chosen to fine-tune Coulombic interactions as well as for their ability to mimic the stereoelectronic properties of Pro and Hyp, pivotal for the triple helix stability.[160,161] Specifically, Amp was strategically introduced to

[160] I. R. Babu, K. N. Ganesh, *J. Am. Chem. Soc.,* **2001**, *123*, 2079–2080.
[161] M. Umashankara, I. Ramesh Babu, K. N. Ganesh, *Chem. Comm.,* **2003**, *3*, 2606–2607.

replace the Hyp position while amp replaced Pro, given their preferential adoption of C^{γ}-exo and C^{γ}-endo conformations, respectively. Initially, a peptide sequence was designed based on the previously mentioned triblock pattern (**NSI**).[162] They maintained the tripeptide Pro-Hyp-Gly for the central motif and incorporated a positive and a negative triblock on both sides (**Figure 26b**). The positively charged tripeptide contained the non-canonical Amp residue while in the negatively charged they incorporated a Glu residue. The triple helix was assembled by segregating both domains at each end which subsequently arranged vertically through complementary electrostatic interactions (**Figure 26a**). They observed the formation of 2D nanosheets with a height value similar to the length of the peptide sequence, confirming the single-layered structure (**Figure 26b**). Besides the high polydispersity achieved in lateral dimensions, nanosheets were formed independently and with defined edges, suggesting an organized packing of triple helices. They hypothesized that the introduction of the imino derivative Amp residue played a key role in guiding this internal order during the 2D growth since it destabilizes the initially formed 1D assembled triple helix. Although Amp residue has the preferred spatial conformation (C^{γ}-exo) for that position in the formation of a triple helix, the additional amino group can generate elastic distortion, thus decreasing the thermodynamic stability.

In a subsequent investigation, they designed a new peptide sequence NSIII with the aim to refine the assembly behaviour and minimize polydispersity (**Figure 26c**).[163] The main difference with the previous CMPs was the introduction of the imino derivative "amp" residue in the positively charged motif replacing the Pro, while maintaining the successive Hyp and Gly (amp-Hyp-Gly). The authors hypothesized that the co-localization of both substituted pyrrolidine rings within the positively charged block is sterically unfavourable. Thereby, the presence of amp residues necessitated elastic deformation to accommodate coulombic interactions, resulting in structural distortion and suffering an associated energy penalty. This gives as a result a uniform population of assembled nanosheets with a narrow size distribution (**Figure 26c**). The energy penalty emerged as a limiting factor in hierarchical assembly growth, ultimately resulting in the formation of homogeneous nanostructures. This phenomenon in the assembly process was termed **geometrical frustration** and is based on how minor conformational distortions can exert significant control in growth propagation.[164]

[162] T. Jiang, C. Xu, Y. Liu, Z. Liu, J. S. Wall, X. Zuo, T. Lian, K. Salaita, C. Ni, D. Pochan, V. P. Conticello, *J. Am. Chem. Soc.,* **2014**, *136*, 4300–4308.
[163] T. Jiang, C. Xu, X. Zuo, V. P. Conticello, *Angew. Chem., Int. Ed.,* **2014**, *53*, 8367–8371.
[164] T. Jiang, E. L. Magnotti, V. P. Conticello, *Interface Focus*. **2017**, *7*.

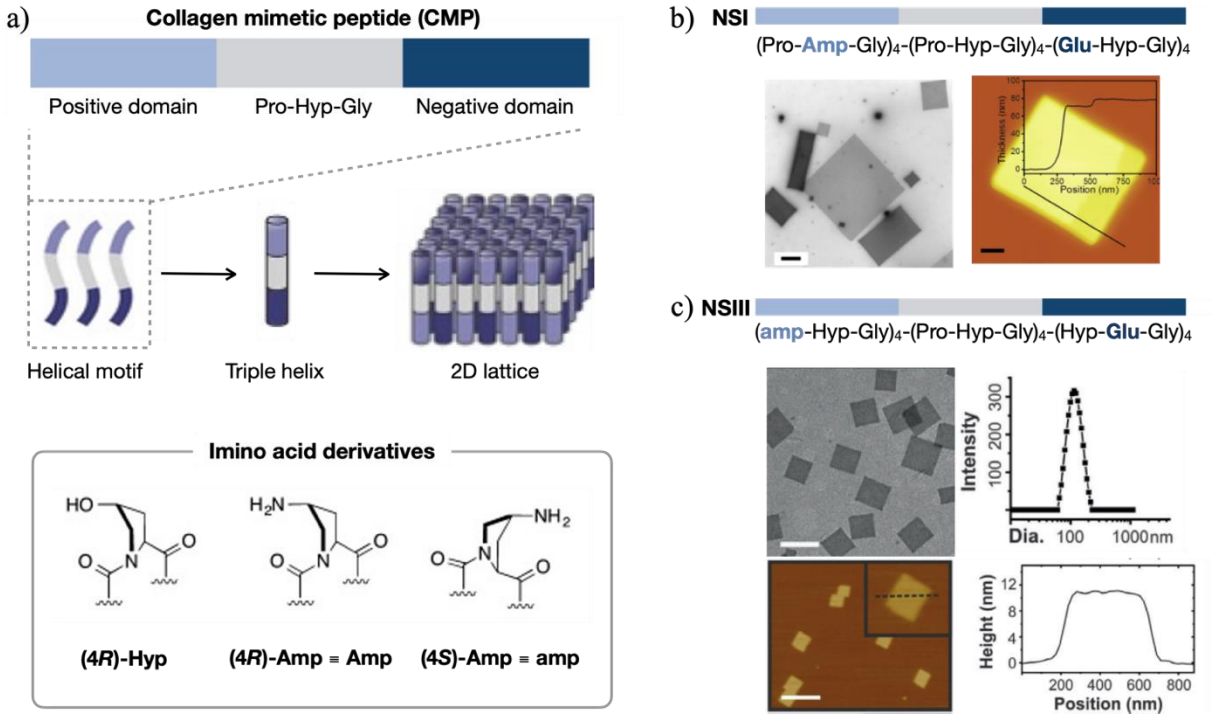

Figure 26. a) General structure for collagen mimetic peptides designed with three domains: positive (light blue) neutral (grey) and negative (dark blue). Their folding in helical motifs give rise to the triple helix and the subsequent arrangement in 2D nanosheets. At the bottom, the chemical structure for the imino acid derivatives used in the CMP sequences. Adapted with permission from Ref. 162. Copyright © (2019) WILEY-VCH Verlag GmbH & Co. KGaA, Weinheim. b) Peptide sequence of **NSI** and STEM and AFM image of the assembled nanosheets. Scale bars, 1 μm and 200 nm, respectively. Adapted with permission from Ref. 159. Copyright © (2014) American Chemical Society. c) Peptide sequence of **NSIII** with STEM and AFM image and DLS showing the homogeneous size distribution. Scale bars, 500 nm and 1 μm, respectively. Adapted with permission from Ref. 162. Copyright © (2019) WILEY-VCH Verlag GmbH & Co. KGaA, Weinheim.

Further work has discovered that by increasing the number of the central motif Pro-Hyp-Gly in NSIII, is possible to decrease the size of the resultant nanosheets and control polydispersity.[165] This effect, elucidated with X-ray diffraction analysis, stems from distortion and contraction within the resultant lattice, and since the assembly process is nucleation-dependent, this will affect the final nanosheet's size. Interestingly, within these results, they hypothesized that the assembly process resembles crystallization-driving living polymerization, and they demonstrated it by adding more monomers marked with a fluorophore to preassemble nanosheets, observing homoepitaxial growth and affirming the potential for controlled expansion of the nanosheets (**Figure 27**a). Expanding on these insights, another study explored living polymerization using two different monomers distinguished by their melting temperatures (**Figure 27**b).[166] This

[165] A. D. Merg, G. Touponse, E. van Genderen, X. Zuo, A. Bazrafshan, T. Blum, S. Hughes, K. Salaita, J. P. Abrahams, V. P. Conticello, *Angew. Chem.*, **2019**, *131*, 13641–13646.
[166] A. D. Merg, E. Van Genderen, A. Bazrafshan, H. Su, X. Zuo, G. Touponse, T. B. Blum, K. Salaita, J. P. Abrahams, V. P. Conticello, *J. Am. Chem. Soc.*, **2019**, *141*, 20107–20117.

approach enables the sequential assembly of 2D multicomponent structures through thermally controlled heteroepitaxial growth.

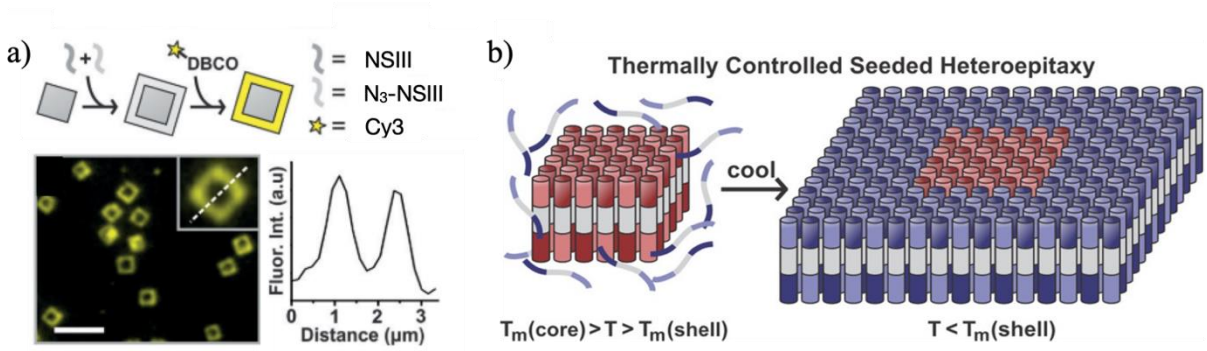

Figure 27. a) Top: Schematic illustration of the epitaxial growth followed by the attachment of the fluorescence Cy3. Bottom: Fluorescence micrograph of nanosheets and fluorescence scan. Scale bar, 5 μm. Adapted with permission from Ref. 162. Copyright © (2019) WILEY-VCH Verlag GmbH & Co. KGaA, Weinheim. b) Schematic representation of the living polymerization. Adapted with permission from Ref. 163. Copyright © (2019) American Chemical Society.

4.2.3.12. α-helical peptides

α-helical peptides possess a remarkable well-defined geometry that makes them valuable monomers for self-assembly. This precise geometry arises from the characteristic arrangement of amino acid residues within the helix, where approximately 3.6 residues are accommodated per helical turn (**Figure 5**; Section 0). This specific value is due to the optimal alignment of hydrogen bonds along the peptide backbone, stabilizing the helical conformation and imparting rigidity to the structure. Importantly, the consistent spacing between residues ensures uniformity in the pitch (vertical distance) and diameter of the helix, resulting in a regular arrangement that gives rise to the heptad repeat often designated abcdefg (**Figure 5**; Section 0).[167] This characteristic repeated motif serves to strategically position side chains along the outside of the helix, generating, for example, amphiphilicity with segregated hydrophobic and hydrophilic domains. This segregation has been used by researchers to modulate the assembly of multiple helices into hierarchical supramolecular architectures.

The most representative example of hierarchical assembly is the formation of coiled coil structures, where multiple α-helices come together and intertwine around each other (**Figure 28**a).[168] This assembly is mainly governed by hydrophobic effects, which promote the burial of hydrophobic residues in the interior of the coiled coil. However, the precise arrangement of amino acids in the heptad motif also defines important structural features. Notably, side chains of

[167] W. Zhang, S. Mo, M. Liu, L. Liu, L. Yu, C. Wang, *Front. Chem.,* **2020**, *8.*
[168] D. N. Woolfson, *J. Biol. Chem.,* **2023**, *299*

adjacent helices do not simply interact with each other, they are spatially interlocked in a specific and complementary way defined as "knob-into-hole" packing (**Figure 28**a).[169] The details of this packing determine the number of the helices and the core-packing angles of the final assembled structure. To date, there are many possible combinations of helices, including parallel or antiparallel arrangement and homo- or hetero-oligomerization states. The group of Woolfson has demonstrated the formation of stable assemblies with up to nine helices, defined as α-helical barrels (**Figure 28**b).[170,171,172]

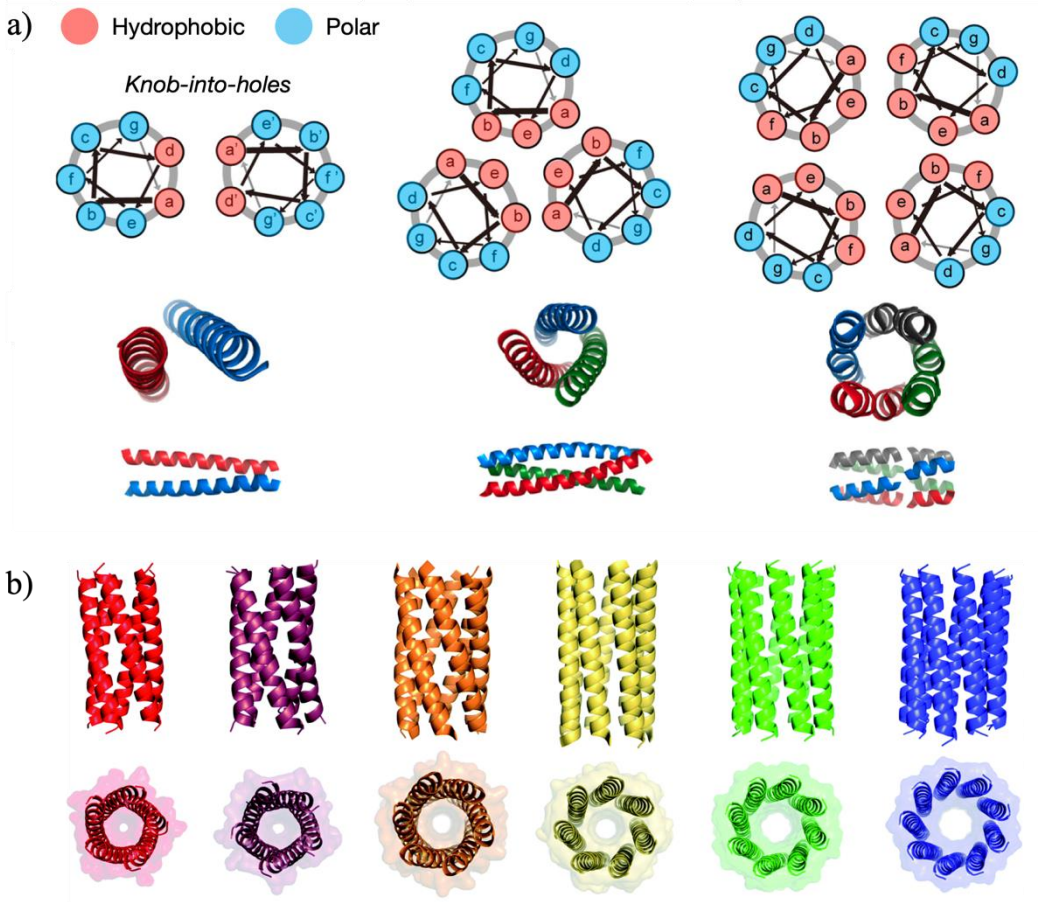

Figure 28. a) Schematic illustration of coiled coil assemblies formed by two, three and four helices (from left to right). Hydrophobic residues are represented as pink and polar as blue circles. Adapted with permission from Ref. 165 Copyright © 2020 Zhang, Mo, Liu, Liu, Yu and Wang b) X-ray crystal structures of coiled coil assemblies from five to nine helices. At the top side view and at the bottom top view. Adapted with permission from Ref. 167 Copyright © (2021) Royal Society of Chemistry.

[169] D. N. Woolfson, G. J. Bartlett, M. Bruning, A. R. Thomson, *Curr. Opin. Struct. Biol.,* **2012**, *22*, 432–441.
[170] W. M. Dawson, F. J. O. Martin, G. G. Rhys, K. L. Shelley, R. L. Brady, D. N. Woolfson, *Chem. Sci.,* **2021**, *12*, 6923–6928.
[171] P. Kumar, N. G. Paterson, J. Clayden, D. N. Woolfson, *Nature,* **2022**, *607*, 387–392.
[172] A. R. Thomson, C. W. Wood, A. J. Burton, G. J. Bartlett, R. B. Sessions, R. L. Brady, D. N. Woolfson, *Science,* **2014**, *346*, 485–488.

The longer the peptide sequence, the more difficult predicting self-assembly becomes. However, a study conducted by the research groups of Pochan and Saven tackled this challenge with the use of computational methods (**Figure 29**a).[173] They deciphered 29-residue peptides capable of forming homotetrameric bundles that subsequently packed into 2D lattices. Remarkably, subtle variations in the peptide sequences resulted in the formation of distinct lattices characterized by rectangular, squared, or hexagonal local symmetries. Experimental characterization provided further evidence of the formation of 2D lattices supporting the computational predictions. In a later research they showed precise control over peptide self-assembly, demonstrating the potential to engineer a diverse array of structures by modulating solution conditions (**Figure 29**b).[174,175] While the hydrophobic core is robust enough, the polar charged residues in the exterior of the bundle led to fine-tuning assembly kinetics by varying the pH of the medium. Moreover, elevating the temperature facilitates a faster assembly process as peptide bundles are packed into 2D nanosheets. In a more recent approach, Chen and co-workers utilized a peptide capable of oligomerizing into trimers, with isoleucines strategically included at positions a and d forming the knob-into-hole hydrophobic packing (**Figure 29**c).[176] Subsequently, these trimers laterally pack into 2D nanosheets due to the peptide sequence encoding complementary electrostatic interactions. By introducing positively and negatively charged residues at opposite ends of the sequence, trimeric bundles are assembled in antiparallel conformation. Furthermore, the authors demonstrated effective molecular functionalization without disrupting the integrity of the 2D assemblies, highlighting the versatility and potential applications of such precisely engineered nanostructures.

With a different approach, Woolfson and collaborators engineered coiled coil structures by combining homodimeric and homotrimeric blocks linked by a flexible linker, which were then pinned back-to-back with a disulfide bond (**Figure 30a**).[177] Interestingly, the authors observed that the position of the disulfide pin played a pivotal role in determining the final assembly morphology. When the disulfide pin was located proximal to the flexible loop linker, nanoparticles were formed. In contrast, when the disulfide pin was distal, the assemblies transformed into nanosheets with the coiled coil blocks arranged into hexagonal arrays.

---

[173] H. V. Zhang, F. Polzer, M. J. Haider, Y. Tian, J. A. Villegas, K. L. Kiick, D. J. Pochan, J. G. Saven, *Sci. Adv.,* **2016**, *2*.

[174] Y. Tian, H. V. Zhang, K. L. Kiick, J. G. Saven, D. J. Pochan, *Org. Biomol. Chem.,* **2017**, *15*, 6109–6118.

[175] Y. Tian, F. B. Polzer, H. V. Zhang, K. L. Kiick, J. G. Saven, D. J. Pochan, *Biomacromol.,* **2018**, *19*, 4286–4298.

[176] X. Chen, C. Xia, P. Guo, C. Wang, X. Zuo, Y. B. Jiang, T. Jiang, *Angew. Chem. Int. Ed.,* **2023**, *63*.

[177] J. M. Galloway, H. E. V. Bray, D. K. Shoemark, L. R. Hodgson, J. Coombs, J. M. Mantell, R. S. Rose, J. F. Ross, C. Morris, R. L. Harniman, C. W. Wood, C. Arthur, P. Verkade, D. N. Woolfson, *Small,* **2021**, *17*.

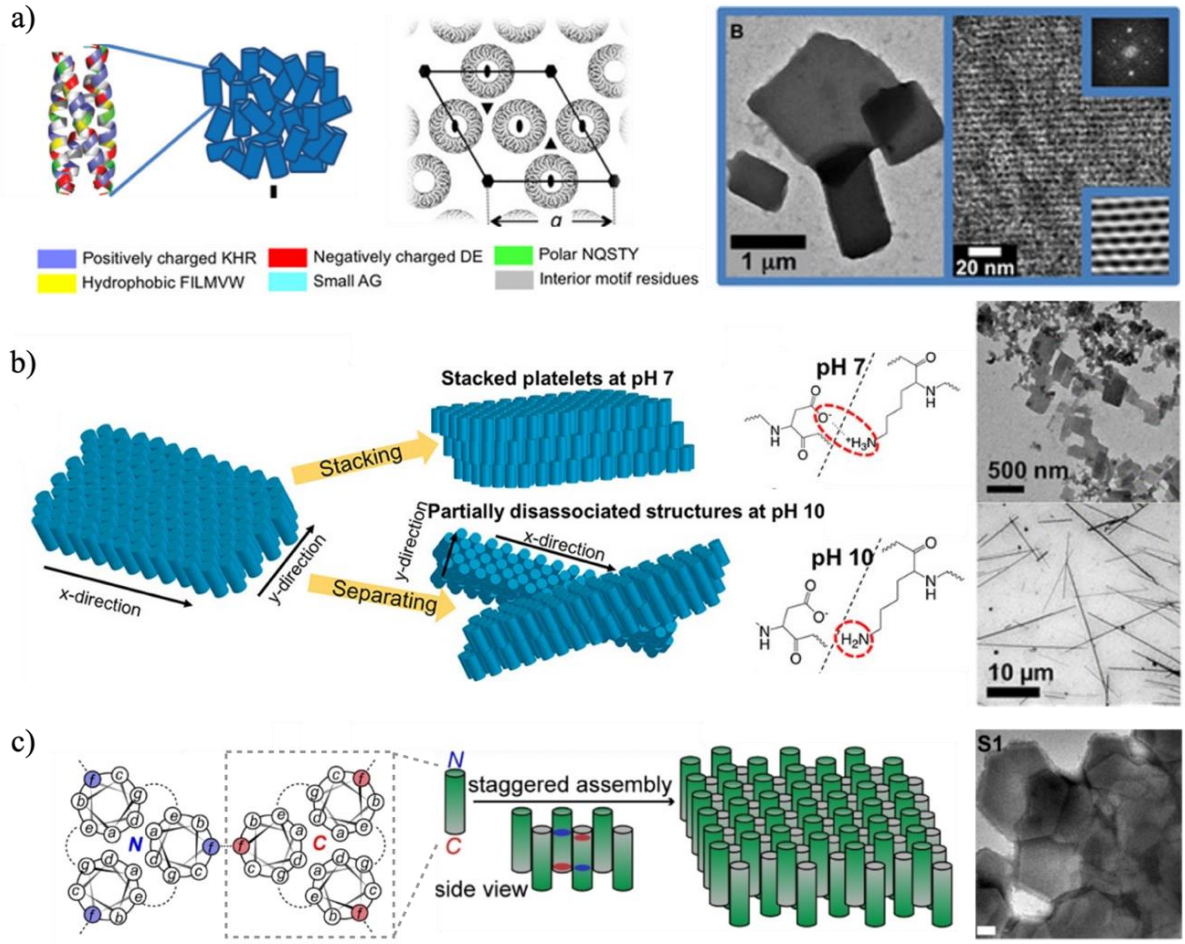

Figure 29. a) On the left: Model for homotetramer coiled coil and the unit cell. On the right: TEM image and high-magnification with Fast Fourier Transform analysis inset. Adapted with permission from Ref. 170 Copyright © 2016 Huixi Violet Zhang et al. b) Coiled-coil bundle assemblies At pH 7 (top) and pH 10 (bottom) and TEM image of stacked platelets (top) and needle-like structures (bottom). Adapted with permission from Ref. 172 Copyright © 2018, American Chemical Society. c) Schematic representation of the heptad repeats forming trimeric assemblies (green bundles) that subsequently staggered forming 2D nanosheets. On the right: TEM image. Scale bar, 200 nm. Adapted with permission from Ref. 173 Copyright © 2023, WILEY-VCH Verlag GmbH & Co. KGaA, Weinheim.

In addition to the assembly of coiled coil structures, researchers have also achieved remarkable success in the self-assembly of individual α-helices into 2D lattices, challenging considering the inherent instability of individual peptide helices. Conticello et col. have demonstrated a design and assembly strategy for helical peptides into 2D nanostructures (**Figure 30**b).[178] In their study, they designed a novel peptide consisting of two repeats of an 18-amino acid sequence. This peptide sequence was engineered to promote the formation of straight α-helices with three orthogonal interfaces with the same amino acids, adopting a 3-

[178] E. L. Magnotti, S. A. Hughes, R. S. Dillard, S. Wang, L. Hough, A. Karumbamkandathil, T. Lian, J. S. Wall, X. Zuo, E. R. Wright, V. P. Conticello, *J. Am. Chem. Soc.,* **2016**, *138*, 16274–16282.

fold symmetric monomer configuration. This structural design resulted in a minimal superhelical twist, effectively suppressing coiled coil formation and stabilizing individual helical strands. Consequently, the peptides exhibited lateral assembly through a combination of hydrophobic effect and electrostatic interactions, resulting in a hexagonal array resembling a nanoporous 2D structure.

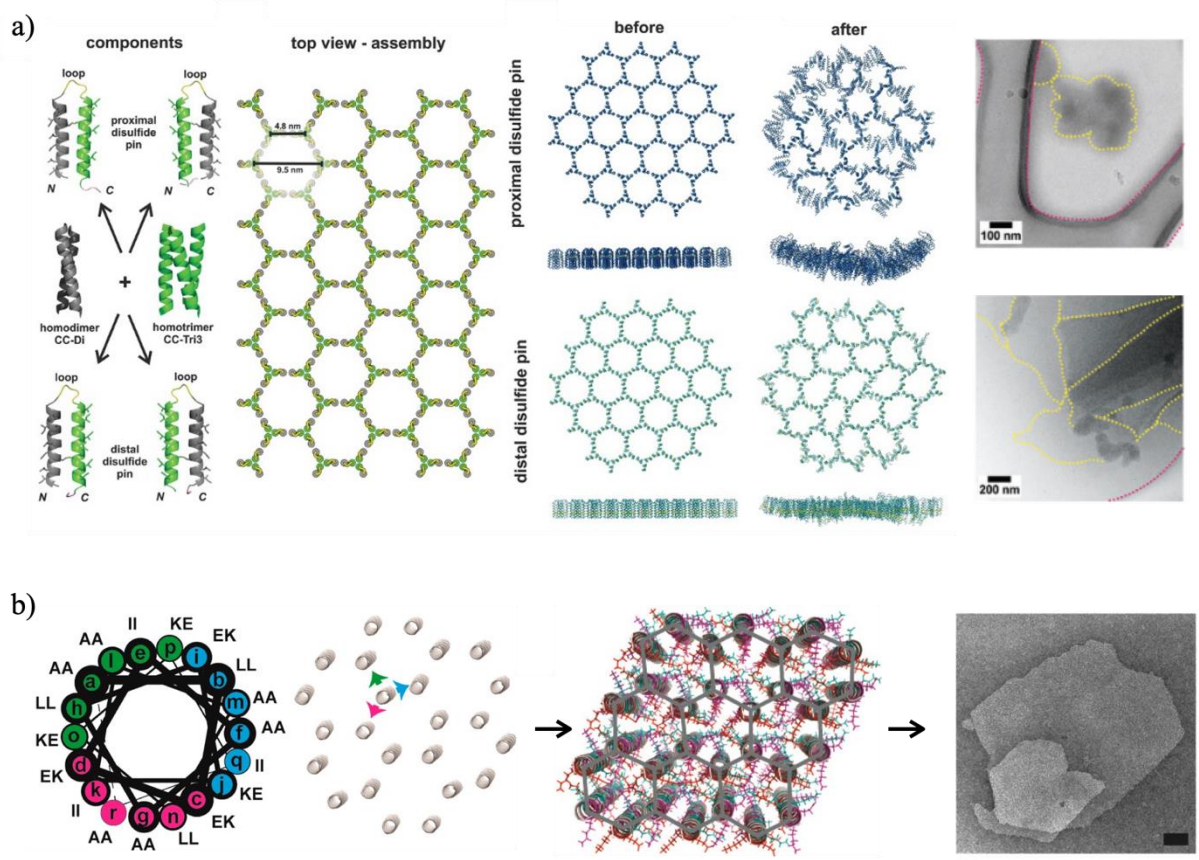

Figure 30. a) From left to right: Schematic representation of both coiled coil components with loops and disulfide pins. Top view of the assembly lattice. Snapshots from molecular dynamics simulations of assembled structures. Cryo-TEM images with peptide assemblies marked with yellow dotted line. Adapted with permission from Ref. 174 Copyright © 2021 Derek N. Woolfson, Paul Verkade, Christopher Arthur, et al. Small published by Wiley-VCH GmbH B) From left to right: Peptide sequence in an helical representation indicating the three repeated motifs as green, blue and pink. Proposed assembled packing in hexagonal lattice. TEM image of nanosheets. Scale bar, 200 nm. Adapted with permission from Ref. 175 Copyright © 2016, American Chemical Society.

4.2.4. Cyclic peptides as monomers for self-assembly

In a theoretical analysis published in 1974, De Santis et al. postulated that cyclic polypeptides comprising an even number of amino acids with alternating chirality could assemble into nanotubes.[179] They demonstrated that the rotation angles in enantiomeric amino acids within the cyclic peptide led to the formation of a planar structure. In this conformation, the amide groups of the peptide backbone would be perpendicular to the plane of the ring, with the carbonyl and amine pointing toward opposite directions. This disposition allows the formation of hydrogen bonds like those observed in β-sheet conformation, with the oxygen of the carbonyl acting as a acceptor for the hydrogen of the amide. This gives as a result cylindrical structures where cyclic peptides are stacked and maintained through a network of hydrogen bonds and van der Waals interactions. However, these tubular structures were not experimentally demonstrated until 1993, when the group of Ghadiri characterized the nanotube assembled from an octapeptide (**Figure 31**).[180] They strategically designed a sequence: cyclic-[(L-Gln-D-Ala-L-Glu-D-Ala)$_2$] to be completely soluble at basic conditions thanks to the negative charge of glutamic acids, which prevents aggregation. By progressively acidifying the solution, needle-type microcrystalline aggregates were found, and a full characterization confirmed the presence of tubular structures formed by stacked cyclic peptides.

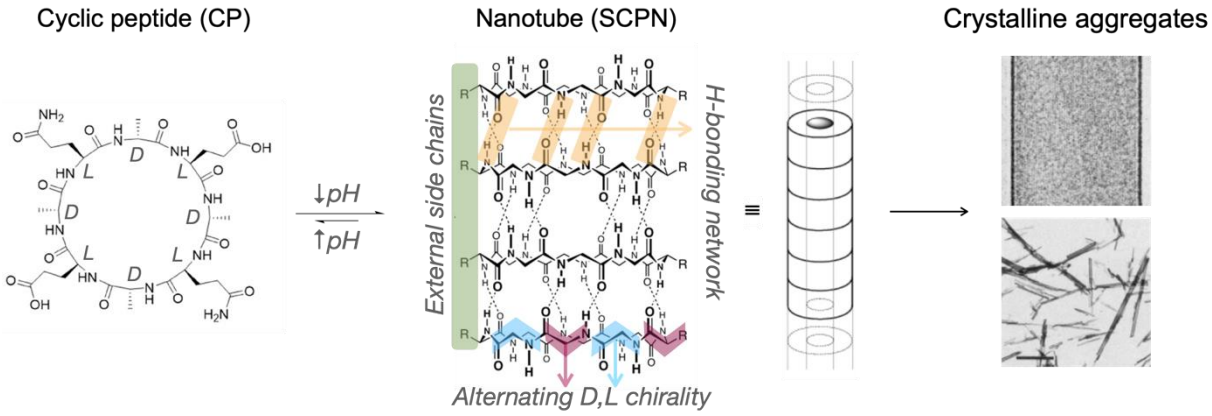

Figure 31. From left to right: Chemical structure of cyclic-[(L-Gln-D-Ala-L-Glu-D-Ala)$_2$], self-assembling cyclic peptide nanotube at acidic conditions and electron microscopy images of crystalline aggregates showing longitudinal striations (top) and tubular structures (bottom). Scale bar, 1 μm. Adapted with permission from Ref. 177 Copyright © 1993, Sprinter Nature Limited.

[179] P. De Santis, S. Morosetti, R. Rizzo, *Macromolecules*, **1974**, *7*, 52-58.
[180] M. R. Ghadiri, J. R. Granja, R. A. Milligan, D. E. McRee, N. Khazanovich, *Nature,* **1993**, *366*, 324–327.

These monomers were arranged in a β-sheet-like structure, with intermolecular hydrogen bonds between peptide backbones resulting in a spacing of 4.7 Å and with the side chains pointing outward the nanotube in a perpendicular position. Molecular dynamics simulation showed the hydrophilic character of the cavity with water molecules inside however, they do not compete for hydrogen bonds, making nanotubes highly stable in an aqueous environment.[181]

These discoveries paved the way for subsequent studies on the self-assembly of cyclic peptides, as they resulted in an innovative strategy to construct tubular structures highly attractive for nanotechnology. Despite the potential electronic and mechanical properties of carbon nanotubes, they presented certain limitations such as solubility and controlled synthetic methods that could be solved with these new supramolecular cyclic peptide nanotubes (SCPNs).[182,183] Furthermore, as their research progressed, new characteristics and properties were discovered that positioned cyclic peptides as promising monomers for molecular self-assembly and revealed potential applications in multiple fields.[184]

New cyclic peptide sequences were studied to evaluate their structure-assembly relationships. Larger cyclic peptides demonstrated the possibility of modulating the internal diameter of the nanotube, achieving values of 10 and 13 Å for deca- and dodecapeptide respectively, higher than the value of 7.5 Å for the octapeptide (**Figure 32**).[185] However, the larger the diameter, the higher the flexibility of the cyclic structure, weakening the preorganization required for the hydrogen bond formation, resulting in a less stable structure.[186] Additionally, a study evaluated the influence of different sequences in the tubular assembly, as different amino acids are expected to contribute differently to non-covalent interactions.[187] The resulting crystalline structures demonstrated that cyclic peptides stacked in a similar way forming nanotubes but with a different lateral packing. Therefore, these results showed that side chains do not interfere with the hydrogen-bonding network stabilizing the nanotube, but rather influence the subsequent tubular bundling through lateral contacts. They postulated that this behaviour could be exploited to rationally decorate the surface of the nanotubes.

---

[181] M. Engels, D. Bashford, M. R. Ghadiri, *J. Am. Chem. Soc.,* **1995**, *117*, 9151-9158.
[182] R. H. Baughman, A. A. Zakhidov, W. A. De Heer, *Science,* **2002**, *297*, 787–792.
[183] S. Iijima, *Nature* **1991**, *354*, 56–58.
[184] Q. Song, Z. Cheng, M. Kariuki, S. C. L. Hall, S. K. Hill, J. Y. Rho, S. Perrier, *Chem. Rev.,* **2021**, *121*, 13936–13995.
[185] N. Khazanovich, J. R. Granja, D. E. McRee, R. A. Milligan, M. Reza Ghadiri, A. P. Sloan, *J. Am. Chem. Soc.,* **1994**, *116*, 6011-6012.
[186] T. D. Clark, J. M. Buriak, K. Kobayashi, M. P. Isler, D. E. Mcree, M. R. Ghadiri, *J. Am. Chem. Soc.,* **1998**, *120*, 8949-8962.
[187] J. D. Hartgerink, J. R. Granja, R. A. Milligan, M. R. Ghadiri, *J. Am. Chem. Soc.,* **1996**, *118*, 43-50.

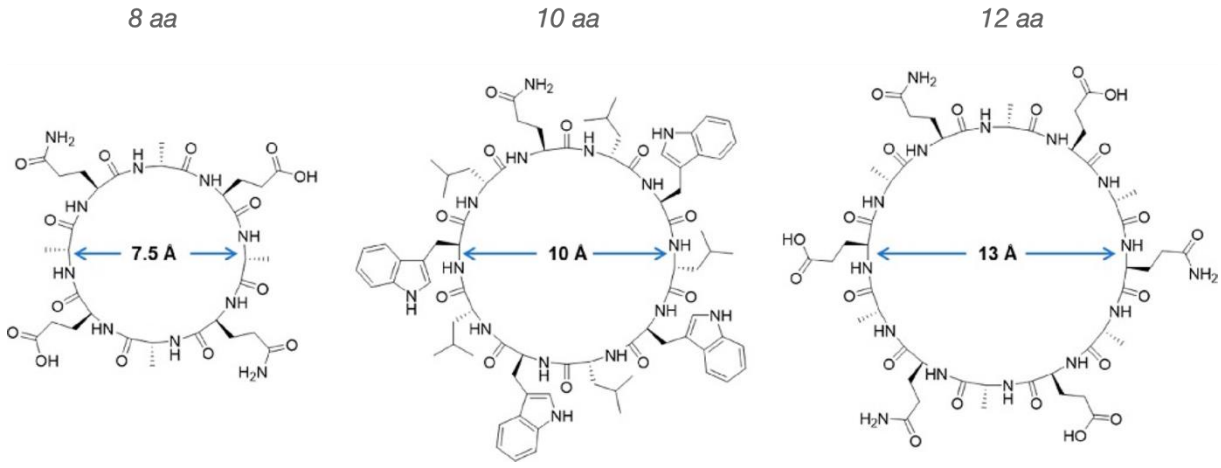

Figure 32. Chemical structures for cyclic peptides with increased number of residues. The calculated internal diameter is represented inside. Adapted with permission from Ref. 182 Copyright © 2021, American Chemical Society.

The study at the atomic level of the stacking interactions within the nanotubes as well as their thermodynamic properties was hindered by the length of the assemblies and their tendency to aggregate. To solve this problem, dimeric structures were synthesized by capping the growth of the nanotube (**Figure 33**.[188] This was achieved by selectively alkylating the backbone amine of amino acids with the same chirality. These homochiral residues are exposed toward the same face of the macrocycle, thus preventing hydrogen bonding interactions and ultimately, nanotube propagation. Single-crystal X-ray analysis of these cyclic peptide dimers confirmed the same distances between monomers found in tubular ensembles. Moreover, thermodynamic parameters were calculated from NMR investigations and revealed a large enthalpic contribution from the hydrogen bonding between cyclic peptides while a small entropic contribution. This entropic penalty would be increased with each monomer added in nanotube formation, however, as the interactions would also be amplified, the resultant structure would be very stable..[189,190] Indeed, it was demonstrated that fibrillar structures formed by cross-linked nanotubes were found to be as strong as natural fibres (e.g., collagen and enamel) and could be employed to fabricate hydrogels in different solvents.[191]

[188] K. Kobayashi, J. R. Granja, Ghadiri M. R., *Angew. Chem. Int. Ed.,* **1995**, *34*, 95–98.
[189] D. J. Rubin, S. Amini, F. Zhou, H. Su, A. Miserez, N. S. Joshi, *ACS Nano,* **2015**, *9*, 3360–3368.
[190] D. J. Rubin, H. T. Nia, T. Desire, P. Q. Nguyen, M. Gevelber, C. Ortiz, N. S. Joshi, *Biomacromolecules,* **2013**, *14*, 3370–3375.
[191] H. Shaikh, J. Y. Rho, L. J. Macdougall, P. Gurnani, A. M. Lunn, J. Yang, S. Huband, E. D. H. Mansfield, R. Peltier, S. Perrier, *Chem. Eur. J.,* **2018**, *24*, 19066–19074.

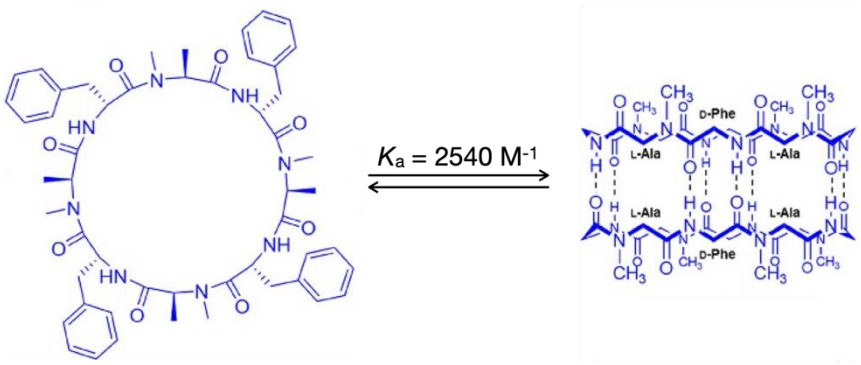

Figure 33. Chemical structure of a cyclic peptide with N-methylated residues and the resulting dimeric structure. The association constant calculated from NMR experiments is shown above the arrow. Adapted with permission from Ref .185 Copyright © 1995 by VCH Verlagsgesellschaft mbH, Germany.

Like β-sheet motifs in proteins, cyclic peptides can also stack in a parallel or antiparallel conformation, with the only requirement that the residues in axial alignment must be homochiral (**Figure 34**).[192] The antiparallel conformation was the most recognized in literature and the most thermodynamically stable for dimeric species studied. However, a recent study with similar peptide sequences revealed crystal structures with both conformations, which suggested that both parallel and antiparallel stacking are possible and the most stable conformation would be biased according to the specific amino acid sequence, being steric hindrance between the side chains a critical factor.[193]

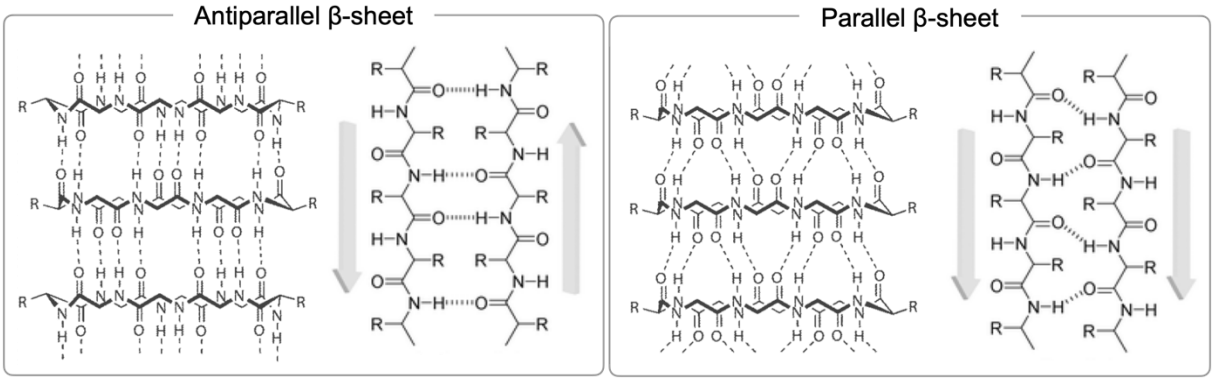

Figure 34. Representation of both possible conformations in self-assembling cyclic peptide nanotubes: parallel (left) and antiparallel (right). Adapted with permission from Ref. 189 and 190 Copyright © 1991 Royal Society of Chemistry. Copyright © 2017 Royal Society of Chemistry.

[192] Y. B. Lim, M. Lee, *J. Mater. Chem.*, **2008**, *18*, 723–727.
[193] M. R. Silk, J. Newman, J. C. Ratcliffe, J. F. White, T. Caradoc-Davies, J. R. Price, S. Perrier, P. E. Thompson, D. K. Chalmers, *Chem. Comm.*, **2017**, *53*, 6613–6616.

While the chemical structure of the above-mentioned cyclic peptides comprises alternating D,L-α-amino acids, subsequent studies demonstrated that other variants can be assembled into nanotubes. Therefore, it has been shown that cyclic peptide nanotubes can be assembled from β-peptides,[194] α, γ-peptides[195] and cyclic peptides with δ-[196] or ε-[197,198] amino acids (**Figure 35**). The difference between these artificial residues is the number of carbons separating the amino and carbonyl groups. These residues present a certain conformational equivalence with α-amino acids and therefore, by choosing the correct chirality, the rings will acquire the planar conformation required for the stacking and hydrogen bond interactions. The advantages that these new residues present are a higher resistance toward enzymatic degradation and greater freedom in the spatial arrangement as they have fewer conformational restrictions in the case of cyclic residues. Furthermore, and more importantly, the methylene groups pointing towards the cavity of the nanotubes allow modulation of their internal properties, ranging from variable polarity to chemical modification incorporating new functional groups.

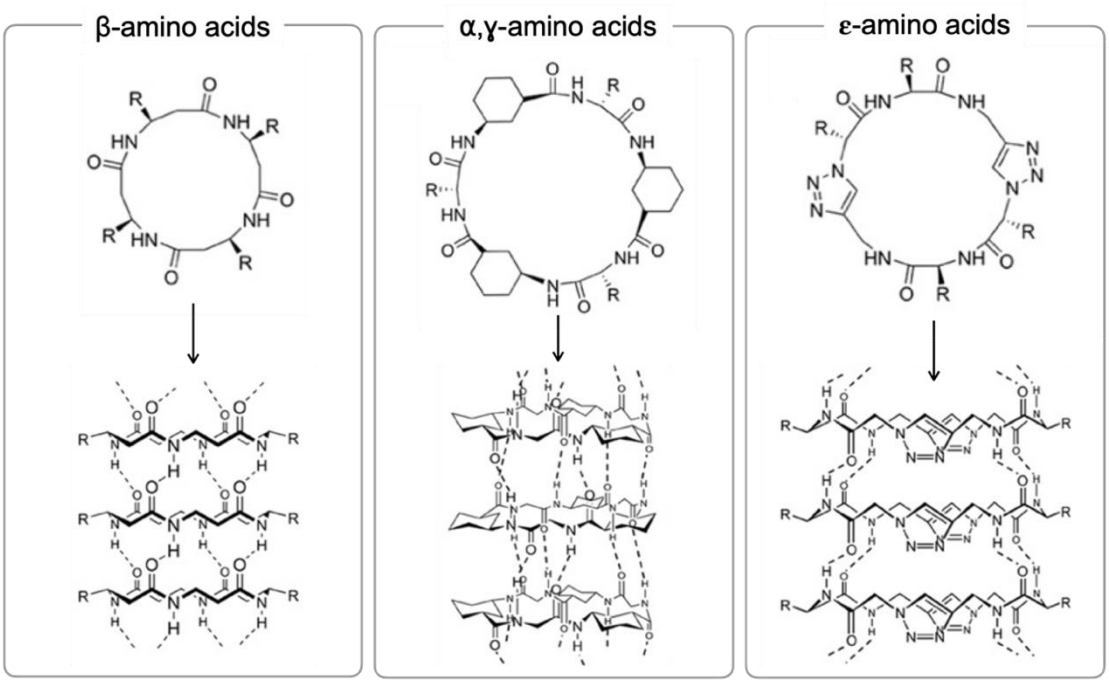

Figure 35. Chemical structure of cyclic peptides and resulting self-assembling nanotubes with β-amino acids (left), α, γ-amino acids (middle) and ε-amino acids (right)**.** Adapted with permission from Ref 181. Copyright © 2021, American Chemical Society.

[194] D. Seebacb, J. L. Matthewsl, A. Meden2, T. Wessels, C. Baerlocher, L. B. Mccusker, *Helv. Chim. Acta*, **1997**, *80.*

[195] M. Amorín, L. Castedo, J. R. Granja, *J Am Chem Soc* **2003**, *125*, 2844–2845.

[196] D. Gauthier, P. Baillargeon, M. Drouin, Y. L. Dory, *Angew. Chem. Int. Ed.,* **2001**, *40*, 4635–4638.

[197] W. S. Horne, C. D. Stout, M. R. Ghadiri, *J. Am. Chem. Soc.,* **2003**, *125*, 9372–9376.

[198] J. H. Van Maarseveen, W. S. Horne, M. R. Ghadiri, *Org. Lett.* **2005**, *7*, 4503-4506.

All these characteristics around cyclic peptides make them interesting monomers in the fabrication of assembled nanostructures. The possibility of modifying both internal and external properties drives the interest of researchers in finding new applications for a wide range of fields.

4.2.4.1. Internal properties

The internal cavity of these supramolecular nanotubes can be modified by varying the number of residues within the sequence or the type of amino acids employed. These variations can lead to different diameters ranging from the smallest 1 Å value, achieved with a cyclic-α,γ-tetrapeptide, to the highest values obtained by using α,δ-amino acids.[199,200] The variability in the inner diameter was exploited to encapsulate and transport different types of molecules. This characteristic, together with their capacity to insert into membranes, allows the transport of molecules across lipid bilayers artificially, mimicking the structure and function of cellular ion channels.[201] Studies in the rate transport of ions such as K^+ and Na^+ across membranes demonstrated to be faster than rates exhibited by the natural gramicidin A and moreover, selective for other larger cations.[202] In fact, this transport capacity has been exploited for antiviral activity, where nanotubes embedded in endosome membranes modulated the pH, thus impeding virus escape and reducing infection, as discovered by Horne et al (**Figure 36**a).[203] Furthermore, the simplest dimeric motifs, achieved by N-methylation, were also demonstrated as useful molecular capsules acting as a host for different guest molecules.

The use of unnatural amino acids made it possible to modulate inner polarity allowing the encapsulation of nonpolar compounds as large as fullerene (C_{60}) (**Figure 36**b).[204] Moreover, the use of these artificial amino acids also allows chemical modification, incorporating new functional groups without interfering with nanotube stability. For example, the attachment of a pyridine moiety allowed the encapsulation of different guests such as metal ions,[205] carboxylic acids allowed the encapsulation of platinum complexes,[205] and ionizable nitrogen units endowed the cavity with pH responsiveness.[206]

---

[199] M. Calvelo, A. Lamas, A. Guerra, M. Amorín, R. Garcia-Fandino, J. R. Granja, *Chem. Eur. J.* **2020**, *26*, 5846–5858.
[200] R. J. Brea, L. Castedo, J. R. Granja, *Chem. Comm.***2007**, 3267–3269.
[201] M. Reza Ghadiri, J. R. Granja, L. K. Buehler, *Nature* **1994**, *369*, 301–304.
[202] R. García-Fandiño, M. Amorín, L. Castedo, J. R. Granja, *Chem Sci* **2012**, *3*, 3280–3285.
[203] W. S. Horne, C. M. Wiethoff, C. Cui, K. M. Wilcoxen, M. Amorin, M. R. Ghadiri, G. R. Nemerow, *Bioorg Med Chem* **2005**, *13*, 5145–5153.
[204] A. Lamas, A. Guerra, M. Amorín, J. R. Granja, *Chem Sci* **2018**, *9*, 8228–8233.
[205] N. Rodríguez-Vázquez, R. García-Fandiño, M. J. Aldegunde, J. Brea, M. I. Loza, M. Amorín, J. R. Granja, *Org Lett* **2017**, *19*, 2560–2563.
[206] S. M. Darnall, C. Li, M. Dunbar, M. Alsina, S. Keten, B. A. Helms, T. Xu, *J. Am. Chem. Soc.,* **2019**, *141*, 10953–10957.

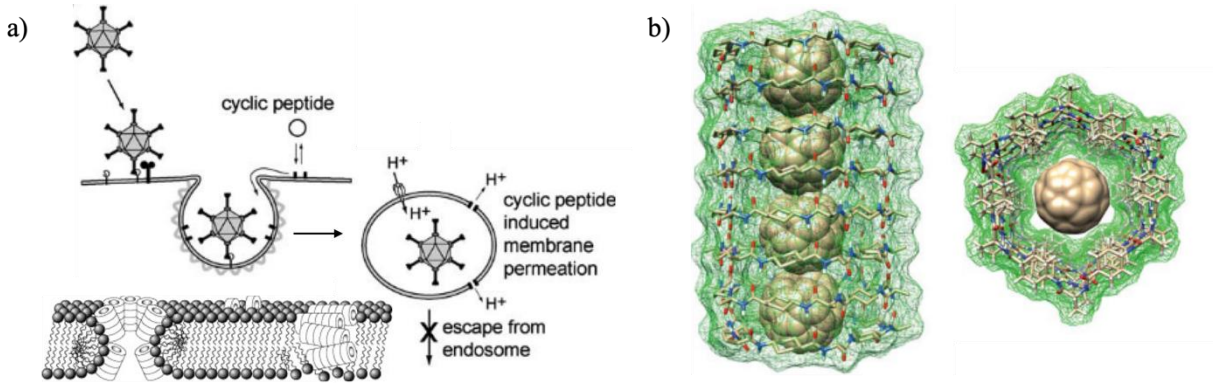

Figure 36. Schematic illustration of the association of cyclic peptides to membranes inhibiting the endosomal escape. Adapted with permission from Ref. 200 Copyright © 2005 Elsevier Ltd. b) Computational model for de encapsulation of C_{60} in the cavity of a self-assembling cyclic peptide nanotube. Adapted with permission from Ref 201. Copyright © 2018, Royal Society of Chemistry.

4.2.4.2. External properties

In cyclic peptide nanotubes, the lateral side chains of the amino acids point outwards of the tubular longitudinal axis, which allows for surface chemistry modulation. This feature influences the assembly process in different directions as sequence variations affect both cyclic peptide stacking (i.e., axial nanotube growth) and the lateral contacts between nanotubes (i.e., lateral nanotube bundling). By peptide sequence modulation, it is possible to rationally design multidimensional structures beyond one-dimensional nanotubes, which is the main focus of this dissertation. This property also serves as a platform to decorate the surface with useful reactive groups, for example, as an anchoring point for other compounds or as recognition sites. This functionalization has been widely exploited to expand the applications and properties of nanotubes.

One of the strategies to functionalize nanotubular structures is based on the conjugation of aromatic moieties. As cyclic peptides stack forming nanotubes, aromatic pendants can enhance and direct molecular alignment through π-π stacking and partial charge transfer. In a work carried out by Ghadiri's group, a cyclic peptide-bearing naphthalenediimide (NDI) was capable of self-assembly into nanotubes triggered by a redox reaction.[207] The resulting system exhibited electronic active states, representing a great approach for the construction of optical or electronic devices. Another example showed the fabrication of hybrid nanomaterials, with pyrene-modified cyclic peptides capable of interacting with carbon nanotubes and metal clusters (**Figure 37**a).[208,209] Moreover, the

[207] W. S. Horne, N. Ashkenasy, M. R. Ghadiri, *Chem. Eur. J.,* **2005**, *11*, 1137-1144.
[208] J. Montenegro, C. Vázquez-Vázquez, A. Kalinin, K. E. Geckeler, J. R. Granja, *J. Am. Chem. Soc.,* **2014**, *136*, 2484–2491.
[209] M. Cuerva, R. García-Fandiño, C. Vázquez-Vázquez, M. A. López-Quintela, J. Montenegro, J. R. Granja, *ACS Nano,* **2015**, *9*, 10834–10843.

conjugation of π-systems also provides an approach to control the assembly of higher structures. Méndez-Ardoy et al. designed a cyclic peptide combining charged amino acids with a pyrene moiety capable of polymerizing under external stimuli (e.g., pH or ionic strength) forming viscoelastic hydrogels.[210] More interestingly, the authors further demonstrated the spatially controlled formation of these assemblies in water droplets, triggering the assembly process in a microfluidics setup (**Figure 37**b).[77]

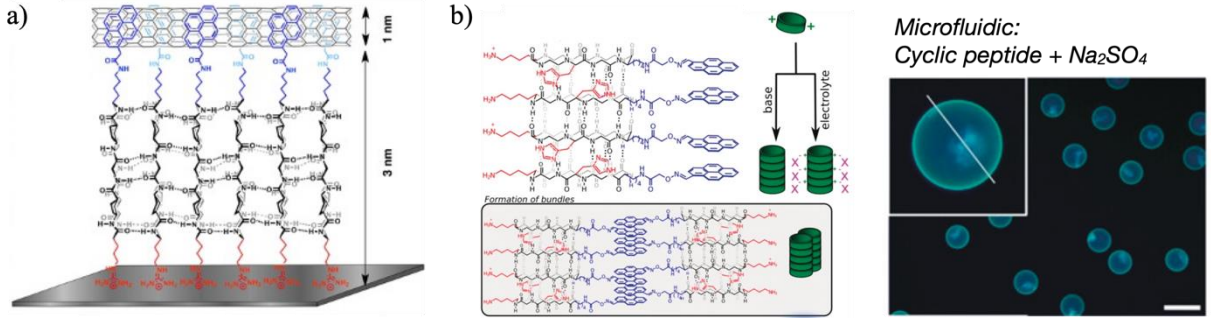

Figure 37. a) Proposed model for the interaction between cyclic peptide and carbon nanotubes. Adapted with permission from Ref 205. Copyright © 2014 American Chemical Society. b) Schematic illustration of the self-assembly based on pH or ionic strength (left) and fluorescence micrograph of droplets formed by microfluidics. Scale bars, 100 μm. Adapted with permission from Ref. 76 Copyright © 2020, WILEY-VCH Verlag GmbH & Co. KGaA, Weinheim.

Another interesting functionalization strategy is the attachment of polymer chains to cyclic peptides. This conjugation helps enhance the solubility of the nanotube, preventing aggregation and enabling a new level of control in the assembly process. It was found that the dimensions of the resulting nanotube bundles, both in diameter and length, could be controlled depending on the nature of the polymer, showing an inverse correlation between the chain size and the final length of the nanotube.[211,212] In addition, varying the chemical nature of polymer chains can expand the functionalities and applications of these systems. For example, stimuli-responsiveness can be achieved by incorporating polymers sensitive to temperature,[213] pH,[214] or light,[215] thus creating dynamic materials with great potential for advancing biomedical technologies. In general, cyclic peptide-polymer conjugates can be designed bearing one or two polymer

[210] A. Méndez-Ardoy, J. R. Granja, J. Montenegro, *Nanoscale Horiz.,* **2018**, *3*, 391–396.
[211] J. Couet, M. Biesalski, *Small,* **2008**, *4*, 1008–1016.
[212] R. Chapman, K. A. Jolliffe, S. Perrier, *Polym. Chem.,* **2011**, *2*, 1956–1963.
[213] R. Chapman, P. J. M. Bouten, R. Hoogenboom, K. A. Jolliffe, S. Perrier, *Chem. Comm.,* **2013**, *49*, 6522–6524.
[214] R. Chapman, G. G. Warr, S. Perrier, K. A. Jolliffe, *Chem. Eur. J.,* **2013**, *19*, 1955–1961.
[215] J. Yang, J. I. Song, Q. Song, J. Y. Rho, E. D. H. Mansfield, S. C. L. Hall, M. Sambrook, F. Huang, S. Perrier, *Angew. Chem. Int. Ed.,* **2020**, *59*, 8860–8863.

chains.[216,217,218] One example are tubisomes, assembled structures that typically consist of a cyclic peptide with a hydrophobic polymer forming the core, and an orthogonal hydrophilic polymer forming the shell (**Figure 38**a).[219] They have been used in anticancer treatment as delivery vehicles for drugs. By encapsulating doxorubicin in the core and adding a UV-responsive group, it was possible to disassemble the system when exposed to UV light, thus controlling the release of the doxorubicin (**Figure 38**b).[215]

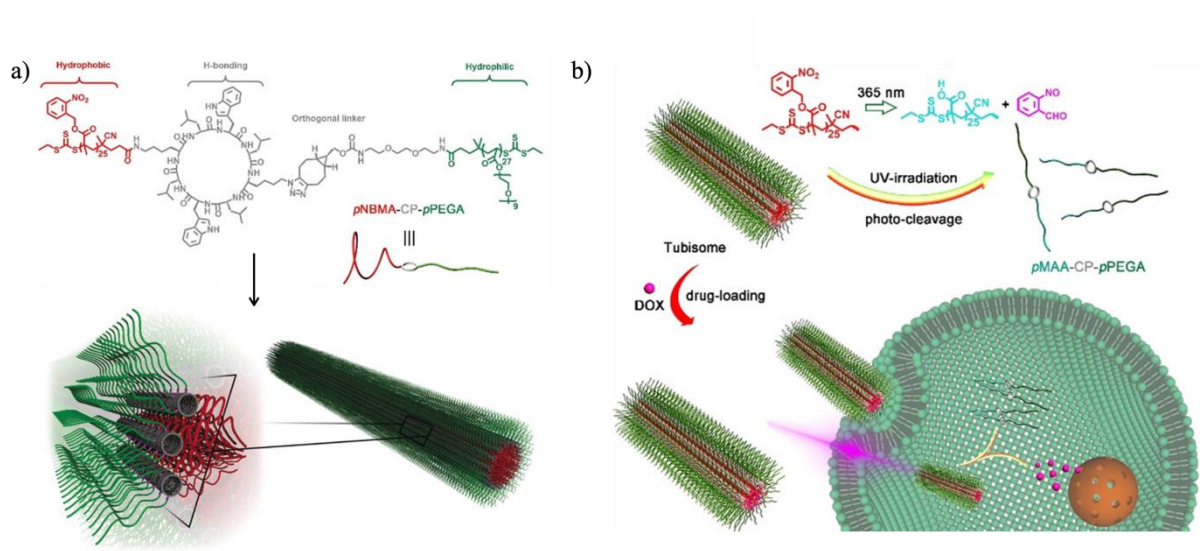

Figure 38. a) Chemical structure of a cyclic peptide conjugated with two different polymer chains and schematic representation of the self-assembled tubisome. b) Schematic illustration of cellular uptake mediated by light of a doxorubicin-loaded tubisome. Adapted with permission from Ref. 216 Copyright © 2018 WILEY-VCH Verlag GmbH & Co. KGaA, Weinheim and Ref. 214 Copyright © 2020 WILEY-VCH Verlag GmbH & Co. KGaA, Weinheim.

In addition to the properties achieved by conjugating other compounds, nanotubes formed solely by amino acids have also shown diverse applications, for example, antibacterial activity.[220] A wide variety of D,L-α-cyclic peptides have been tested as antimicrobials, exhibiting superior activity against positive-Gram bacteria. Overall, it has been observed that octapeptides with a higher number of basic residues increase antibacterial activity.[221] As mentioned before, their membrane-binding capability has been also exploited as transmembrane

[216] J. Y. Rho, H. Cox, E. D. H. Mansfield, S. H. Ellacott, R. Peltier, J. C. Brendel, M. Hartlieb, T. A. Waigh, S. Perrier, *Nat. Commun.,* **2019**, *10.*
[217] E. D. H. Mansfield, M. Hartlieb, S. Catrouillet, J. Y. Rho, S. C. Larnaudie, S. E. Rogers, J. Sanchis, J. C. Brendel, S. Perrier, *Soft Matter.,* **2018**, *14*, 6320–6326.
[218] M. Danial, C. My-Nhi Tran, P. G. Young, S. Perrier, K. A. Jolliffe, *Nat. Commun.,* **2013**, *4*,
[219] J. C. Brendel, J. Sanchis, S. Catrouillet, E. Czuba, M. Z. Chen, B. M. Long, C. Nowell, A. Johnston, K. A. Jolliffe, S. Perrier, *Angew. Chem. Int. Ed.,* **2018**, *57*, 16678–16682.
[220] S. Fernandez-Lopez, H. S. Kim, E. C. Choi, M. Delgado, J. R. Granja, A. Khasanov, K. Kraehenbuehl, G. Long, D. A. Weinberger, K. M. Wilcoxen, M. R. Ghadiri, *Nature*, **2001**, *412*, 452-455.
[221] V. Dartois, J. Sanchez-Quesada, E. Cabezas, E. Chi, C. Dubbelde, C. Dunn, J. Granja, C. Gritzen, D. Weinberger, M. R. Ghadiri, T. R. Parr, *Antimicrob Agents Chemother* **2005**, *49*, 3302–3310.

channels.[222] Moreover, this ability was extended to the intracellular delivery of drugs. For example, it has been demonstrated that nanotubes, can enhance the antitumoral activity of 5-FU (5-fluoracile) in different cell lines.[223]

4.2.4.3. Hierarchical 1D-to 2D self-assembly

Based on previous findings suggesting that side chains mainly affect lateral packing between nanotubes rather than the stacking of cyclic peptides, our group designed a new monomer capable of sequentially self-assembling from 1D-to-2D forming nanosheets (**Figure 39**).[224] This work pioneered showed that higher-ordered structures can be achieved through strategically positioned side chains within the peptide sequence.

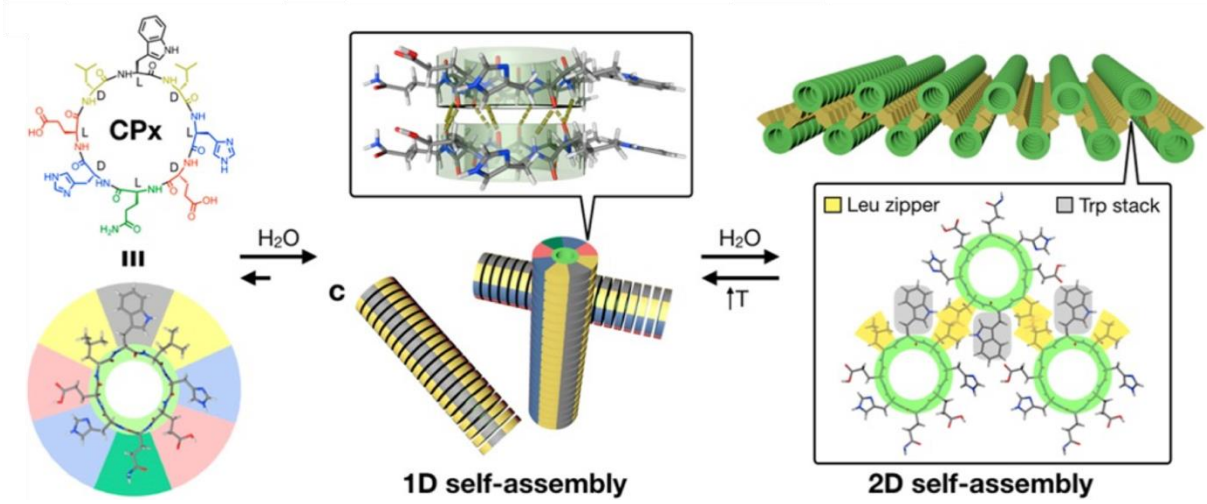

Figure 39. Schematic representation of the sequential 1D-to-2D self-assembly of CPx into 1D nanotubes and subsequent 2D nanosheets. Adapted with permission from Ref 221. Copyright © 2020 American Chemical Society.

The newly designed cyclic peptide monomer **CPx**, has an asymmetric structure with eight alternating D/L amino acids distributed in two different domains. The hydrophobic region is formed by a tripeptide with two leucines flanking a tryptophan, and the polar region has two charged histidine and glutamic acid residues on either side of a central glutamine. In solution, a one-dimensional nanotube is expected to form with both domains aligned in segregating faces, which subsequently tend to pack laterally in an ordered bilayer (**Figure 39**). This growth in the second dimension is driven by hydrophobic effects with directionality imparted by leucines zippers. These interactions place nanotubes staggered in a zig-zag configuration along the bilayer. AFM analysis revealed a

[222] J. Montenegro, M. R. Ghadiri, J. R. Granja, *Acc Chem Res* **2013**, *46*, 2955–2965.
[223] J. Chen, B. Zhang, F. Xia, Y. Xie, S. Jiang, R. Su, Y. Lu, W. Wu, *Nanoscale* **2016**, *8*, 7127–7136.
[224] I. Insua, J. Montenegro, *J Am Chem Soc* **2020**, *142*, 300–307.

thickness of 3.2 nm for the 2D nanosheets, confirming the bilayer packing as nanotubes alone reached a value of 1.5 nm in diameter. Additionally, nanosheets remain extended because of an overall superficial electrostatic repulsion. At physiological pH, the total charge in the system has a negative value because of the deprotonation of glutamic acid and neutralization of histidine. This generates a strongly anionic surface that prevents aggregation and thus maintains flat and extended supramolecular nanosheets.

The reversibility of the system between 1D nanotubes and 2D nanosheets was also demonstrated under the effect of pH and temperature. Upon heating, an assembled nanosheet sample was reverted into a nanotubular state, which after cooling returned to the nanosheet assembly (**Figure 40**a). Moreover, the importance of having an optimal ionizable state was demonstrated through pH experiments (**Figure 40**b). The system collapsed upon acidification close to the pKa of the histidine (6.0). At this acidic state, the protonation of histidine induced electrostatic attraction of anionic glucamic acids, generating amorphous peptide aggregates. Recovery of the system from this aggregated state was achieved by reverting pH back to a physiological value. Interestingly, nanosheets were also observed in their opposite ionizable state, with a fully cationic surface at pH 2.0, due to protonation of histidine and neutralization of glutamic acid.

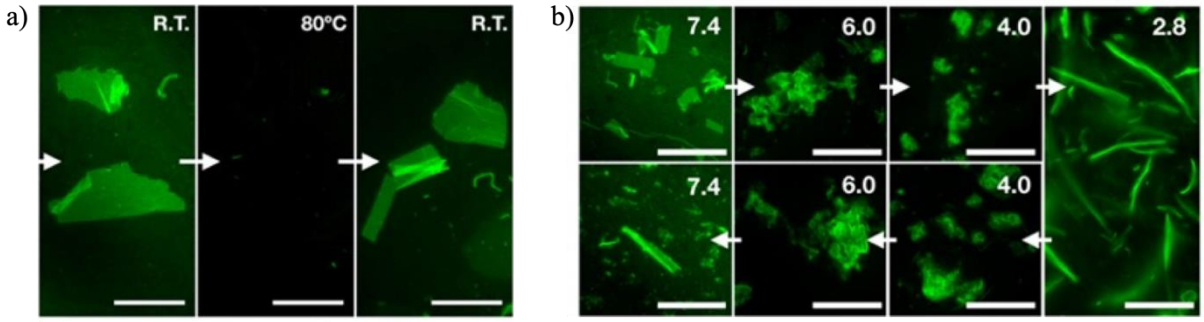

Figure 40. Reversibility between 1D and 2D supramolecular assemblies with a) temperature and b) pH. Scale bars, 50 μm. Adapted with permission from Ref 223. Copyright © 2020 American Chemical Society.

This work has shown that a rationally designed cyclic peptide can drive the lateral growth of nanotubes in an ordered way. These formed nanosheets reached dimensions in the high micron range, one of the largest supramolecular 2D materials ever assembled. Overall, this work postulates an innovative strategy to expand the library of hierarchical supramolecular structures accessible by rational monomer design. In this dissertation, we have been inspired by this latest investigation to further study the general rules around the design of cyclic peptides to direct the subsequent arrangement of nanotubes in different higher-order nanostructures.

5. GENERAL OBJECTIVES

Nature perfectly realized the bottom-up approach of small molecules creating complex functional nanostructures and thus showing the potential of self-assembly to create architectures with remarkable precision and efficiency. This natural sophistication has inspired scientists to use biomolecules as monomers in the fabrication of multidimensional nanomaterials since they can offer specific and programmable interactions. Among all biomolecules, we decided to focus on peptides because of their great chemical diversity and their intrinsic ability to self-assemble hierarchically.

As explored in the introduction, significant progress has been made in the fabrication of 2D nanostructures using various peptide monomers. However, several approaches still rely on trial-and-error methods, while others are limited to natural sequences, hindering the exploration of novel structural variations. Consequently, there is still a knowledge gap in how to rationally predict multidimensional assemblies at the molecular design stage.

Recently, our research group has discovered the potential of cyclic peptides to hierarchically assemble into ordered 2D nanosheets. This behaviour is thanks to their planar and rigid conformation along 1D nanotubes that allows the segregation of orthogonal binding motifs. Therefore, we postulated that these features could be used advantageously to tailor supramolecular architectures by controlling the growth along different directions.

For that reason, the main objective of this thesis is to explore the use of cyclic peptide monomers in the fabrication of highly ordered nanostructures beyond the widely explored 1D nanotubes, and thus contributing to overcoming the gap between molecular design and the predictable assembly into different multidimensional architectures.

In the first chapter, we will study the structure-assembly relationships that determine the formation of 2D bilayers. We will systematically design cyclic peptide monomers with structural modifications tp the original sequence with the aim of determining key positions and understanding their impact on the intermolecular forces that drive the assembly.

In the second chapter, we will focus on designing a new cyclic peptide monomer capable of assembling novel monolayer nanosheet structures. By placing binding motifs in different angle-defined positions we will control the direction of elongation in the second dimension.

In the third and final chapter, our objective was to go one step further and add one more direction of propagation, overcoming the limits of 2D assembly and growing the system into ordered multilayer nanosheets.

6. METHODOLOGIES

6.1. SEQUENCE DECODING OF 1D-TO-2D SELF-ASSEMBLING CYCLIC PEPTIDES

6.1.1. Materials

Chemical reagents were adquired from Acros Organics, Aldrich, Fisher Scientific, Iris Biotech and Novabiochem. Dichloromethane was dried under reflux over calcium hydride. D_2O was purchased from EMD Millipore. Glass slides for fluorescence microscopy were obtained from Ibidi (Cat# 80827). TEM grids (Cu carbon type-B, 300 mesh) and PELCO® mica discs for AFM were acquired from Ted Pella.

6.1.2. Synthesis of CPx variants

Cyclic peptides were prepared manually on solid phase as depicted in **Scheme 1**.1 and following these four steps:[225,226,227]

- Coupling of amino acids. Rink Amide resin (167 mg, 0.1 mmol) was swollen in DMF for 30 min and then treated with piperidine in DMF (20% v/v, 3 mL) to remove the Fmoc protecting group. The resin was washed with DMF (3 x 3 mL) and a solution of Fmoc-L-Glu(OH)-OAll (163.6 mg, 0.4 mmol), *N*-HBTU (132.5 mg, 0.35 mmol) and DIPEA (95 µL, 0.6 mmol) in DMF (3 mL) was added over the resin and shaken for 1 h. Then the mixture was filtered and washed with DMF (3 x 3 mL) and DCM (3 x 3 mL). Cycles of Fmoc protecting group removal with piperidine in DMF (20% v/v, 2 mL) for 15 min and amino acid coupling (0.4 mmol for each Fmoc-protected amino acid (**Table 1**.1), 0.35 mmol N-HBTU and 0.6 mmol DIEA in DMF for 30 min) with their respective washes (DMF 3 x 3 mL) were followed to complete the uncycled peptide sequence. After the coupling of the last amino acid, the resin was washed with DMF (3 x 3 mL) and DCM (3 x 3 mL)

- To **remove OAll** group, the resin was treated with a solution of PPh_3 (39.3 mg, 0.15 mmol), N-methylmorpholine (110 µL, 0.01 mmol), phenylsilane (123 µL, 1.0 mmol) and $Pd(OAc)_2$ (6.7 mg, 0.03 mmol) in dry DCM (4 mL) overnight (16-20 h). The resin was then washed with DCM (3 x 3 mL) and DIEA in DMF (2% v/v, 3 x 3 mL) and soaked in a solution of sodium diethyldithiocarbamate in DMF (0.5% w/v, 2 x 3 mL) for 30 min to remove all traces of Pd. Finally, the resin was stirred with piperidine/DMF (20% v/v, 3 mL) for 30 min for removal of Fmoc group at N-terminous.

- Cyclization was carried out by shaking the resin with a solution of PyAOP (208.6 mg, 0.4 mmol) and DIEA (95.1 mL, 0.6 mmol) in DMF (3 mL) for 2 h. After

[225] A. El-Faham, F. Albericio, *Chem. Rev.,* **2011**, *111*, 6557–6602.
[226] J. M. Palomo, *RSC Adv.,* **2014**, *4*, 32658–32672.
[227] M. B. Coppock, A. J., *Methods in Molecular Biology: Peptide Macrocycles Methods and Protocols,* Vol. 2371, Winton Editors, **2022,** pp. 467-469.

washing with DMF (3 x 3 mL) and DCM (3 x 3 mL), the cyclization was repeated two more times under the same conditions.

- Peptide cleavage. The peptide was deprotected and cleaved from the resin by addition of a freshly prepared TFA cocktail (4 mL, TFA:DCM:H_2O:TIPS, 0.9:0.05:0.025:0.025), this mixture was shaken for 2 h and then filtered. The resin was washed with TFA (0.5 mL) twice and concentrated under nitrogen. The resulting reaction mixture was precipitated by dropwise onto cold diethyl ether (40 mL) under stirring. The resulting suspension was centrifuged for 10 min at 3000 rpm and the sediment was dried with a stream of air and dissolved in MilliQ H_2O. The sample was purified by semipreparative HPLC using a Phenomenex Luna C18 100Å column [gradient of H_2O+0.1%TFA : ACN+0.1%TFA→100:0 (0 min) to 25:75 (30 min)]. Peptide fractions were concentrated in vacuo to remove ACN and TFA and the remaining solution was freeze dried.

Table 1.1. Representation of the amino acid sequences in all the cyclic peptides arranged according to their coupling to the resin (from R_1 to R_8). Amino acid mutations respect the original $\mathbf{CP_x}$ are highlighted.

	$\mathbf{R_1}$	$\mathbf{R_2}$	$\mathbf{R_3}$	$\mathbf{R_4}$	$\mathbf{R_5}$	$\mathbf{R_6}$	$\mathbf{R_7}$	$\mathbf{R_8}$
$\mathbf{CP_x}$	H	E	L	W	L	H	E	Q
$\mathbf{CP_A}$	H	E	L	A	L	H	E	Q
$\mathbf{CP_L}$	H	E	L	L	L	H	E	Q
$\mathbf{CP_F}$	H	E	L	F	L	H	E	Q
$\mathbf{CP_{2F}}$	H	E	F	W	F	H	E	Q
$\mathbf{CP_{3F}}$	H	E	F	F	F	H	E	Q
$\mathbf{CP_{oE}}$	E	H	L	W	L	H	E	Q
$\mathbf{CP_{2E2H}}$	E	E	L	W	L	H	H	Q
$\mathbf{CP_K}$	K	E	L	W	L	K	E	Q
$\mathbf{CP_{4E}}$	E	E	L	W	L	E	E	Q

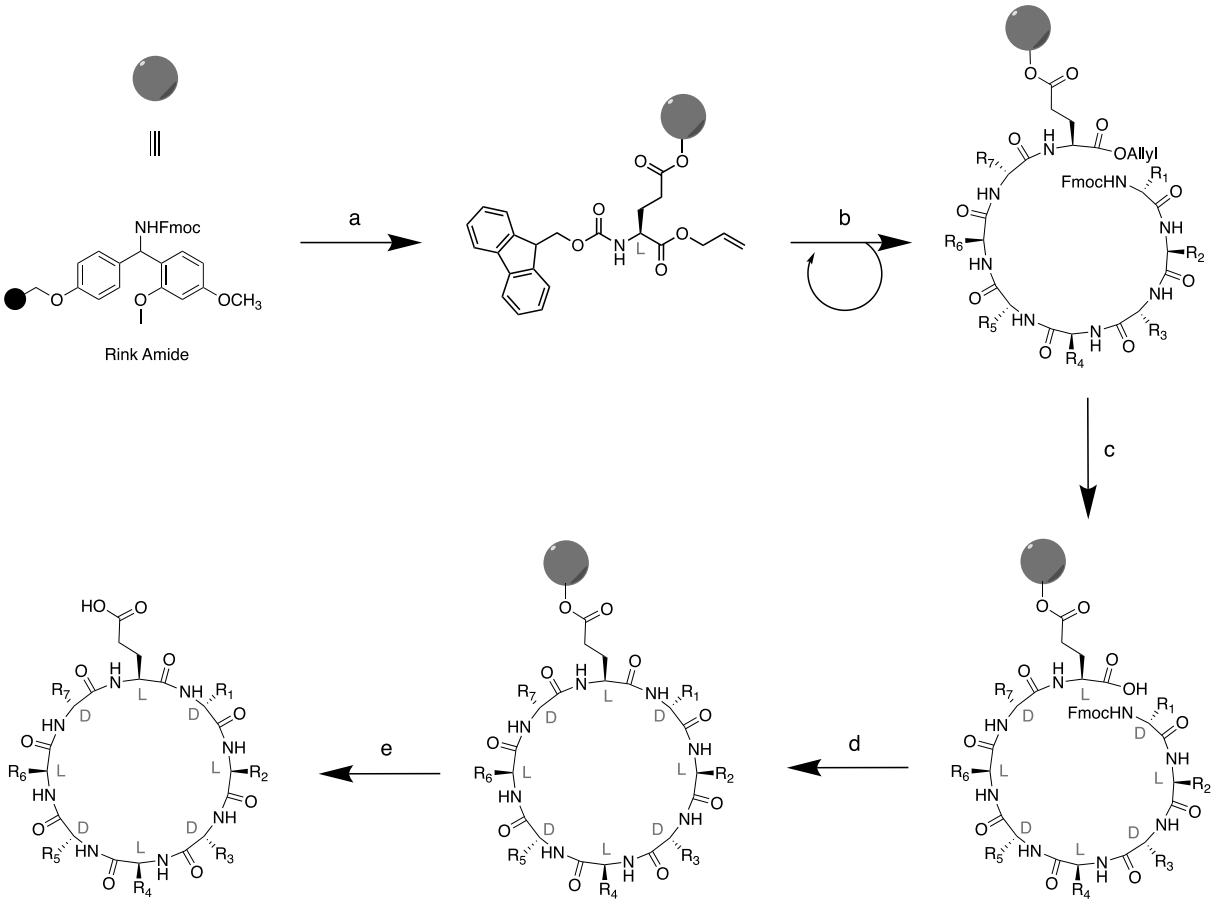

Scheme 1.1. Synthetic protocol for the synthesis of all CPx variants. a) Rink Amide resin functionalization with the first amino acid attached by its side chain: i. Piperidine in DMF (20% v/v), 30 min; ii. Fmoc-L-Glu-OAll, *N*-HBTU, DIEA, DMF, 1 h. Note that in this case, glutamic acid is the first coupled amino acid, since after reacting its side chain with the Rink Amide resin, its acid group transforms into an amide group that, after step e, leaves a glutamine residue in the sequence. b) Peptide elongation: i. Piperidine in DMF (20% v/v), 15 min; ii. Fmoc-amino acid, *N*-HBTU, DIEA, DMF, 30 min. This process was repeated 7 times to couple all the amino acids in the sequence in the order shown in Table 1. The last amino acid will maintain the Fmoc protecting group in the amine end. c) Allyl removal: Pd(OAc)2, PPh3, phenylsilane, 4-methylmorpholine, DCM, overnight (16-20 h). The final product was washed with a solution of sodium diethyldithiocarbamate in DFM (0.5% w/v). d) Cyclization: i. Fmoc removal: piperidine in DMF (20% v/v), 30 min; ii. Peptide cyclization: PyAOP, DIEA, DMF, 2 h (repeat twice to ensure the yield of cyclization). d) Peptide cleavage: TFA, DCM, H2O, TIS (0.9:0.05:0.025:0.025), 2 h.

6.1.3. Self-assembly protocol

Cyclic peptides were dissolved to a concentration of 100 μM in sodium phosphate buffer (20 mM, pH 7.4) in glass vials. Samples were sonicated for 5 min and then incubated without shaking at 80°C for 1.5 h. Next, peptide solutions were stored at room temperature for 1 h, where 2D elongation takes place. For nanosheet formation at different concentrations, cyclic peptide solutions at 100 μM were diluted to the desired final concentration in sodium phosphate buffer (20 mM, pH 7.4). To study the assembly behavior at different pH, cyclic peptide

solutions prepared likewise were adjusted with HCl or NaOH 1M and then annealed (i.e. 1. 80ºC/1.5 h; 2.R.T./1 h). To study the effect of salts in the assembly, samples were prepared likewise but adding the desired amount of salt to the buffer prior to the annealing. For fluorescence microscopy samples, thioflavin-T (vide infra) was initially added to the cyclic peptide solution and then annealed as indicated above.[228,229]

- The preparation of a thioflavin-T staining solution involves dissolving ~5 mg of thioflavin-T in 2 mL H_2O, followed by sonication for 60 min and filtration through a 0.22 μm filter. Subsequently, the absorbance of a diluted solution in both H_2O and EtOH is measured, and the concentration is determined by comparing it for both solvents. The extinction coefficients employed for H_2O and EtOH are 36,000[230] and 26,620[231] $M^{-1}cm^{-1}$ at 412 nm, respectively.

6.1.4. Fluorescence microscopy

10 μL of cyclic peptide samples annealed in the presence of 10 μM thioflavin-T were deposited on glass slides and left to dry completely overnight in the dark at room temperature before imaging. Epifluorescence micrographs were taken at room temperature with a Nikon Eclipse Ti (60x immersion objective, Excitation=475/35 nm; Emission=530/43 nm). All images were analyzed using ImageJ.[232,233]

6.1.5. Scanning transmission electron microscopy

Annealed nanosheet samples (without thioflavin-T) were diluted 10-fold with water and gently homogenized by vial inversion to then drop-cast 5 μL on Cu Grids. Once dry, samples were imaged without washing nor staining. STEM images were acquired on a FESEM Ultra plus (Zeiss) operating at 20 kV.

[228] L. S. Wolfe, M. F. Calabrese, A. Nath, D. V Blaho, A. D. Miranker, Y. Xiong, *Proc. Natl. Acad. Sci. U.S.A,* **2010**, *107*, 16863–16868.
[229] P. K. Singh, A. K. Mora, S. Nath, *Chem. Comm.,* **2015**, *51*, 14042–14045.
[230] M. Groenning, *J. Chem. Biol.,* **2010**, *3*, 1–18.
[231] R. Khurana, C. Coleman, C. Ionescu-Zanetti, S. A. Carter, V. Krishna, R. K. Grover, R. Roy, S. Singh, *J. Struct. Biol.,* **2005**, *151*, 229–238.
[232] C. A. Schneider, W. S. Rasband, K. W. Eliceiri, *Nat. Methods,* **2012**, *9*, 671–675.
[233] J. Schindelin, I. Arganda-Carreras, E. Frise, V. Kaynig, M. Longair, T. Pietzsch, S. Preibisch, C. Rueden, S. Saalfeld, B. Schmid, J. Y. Tinevez, D. J. White, V. Hartenstein, K. Eliceiri, P. Tomancak, A. Cardona, *Nat. Methods,* **2012**, *9*, 676–682.

6.1.6. Atomic force microscopy

Annealed nanosheets samples (without thioflavin-T) were concentrated by centrifugation (10 Krcf/10 min), resuspending the pellet in water by gently pipetting using a tenth of its original volume. 5 μL of this 10-fold concentrated sample were spotted on mica, left to completely dry and imaged. AFM analysis was carried out on a NX-10 microscope (Park Systems) in non-contact mode and using ACTA cantilevers (silicon tips, nominal values: spring constant = 40 N m^{-1}, frequency = 300 kHz, ROC less than 10 nm). Image analysis was carried out using Gwyddion.[234]

6.1.7. Fluorescence measurement

To determine the critical aggregation concentration (CAC), the cyclic peptides were dissolved in sodium phosphate buffer (20 mM, pH 7.4) containing thioflavin-T (10 μM), and then serially diluted across a range of 0.1 μM to 50 μM. These solutions underwent a thermal cycle, as previously described (see 1.3.), before measuring their fluorescence. A FluoroMax-3 Horiba Jobin Yvon and a Cary Eclipse Fluorescence Spectrophotometer (Agilent) equipped with a temperature-controlled cell chamber and a Hellma® fluorescence quartz cell (10 x 2 mm) were utilized for spectroscopic analysis. Spectra were recorded between 440 to 600, with an excitation wavelength of 420 nm, using slits set at 2.5 nm, and a scan rate of 1200 nm/min. All measurements were conducted at a temperature of 20°C.

To analyze the kinetics of the system, an unheated sample dissolved in sodium phosphate buffer (20 mM, pH 7.4) containing thioflavin-T (10 μM) was heated from 20 to 80°C with a rate of 10°C/10 min, fluorescence was recorded at each temperature point. After the measurement at 80°C, cell chamber was set to 20°C and fluorescence was recorded every 60 sec at 480 nm for 60 min as the sample cooled down. Data was normalized to the maximum emission observed in all cases to facilitate the comparison.

6.1.8. Fourier transform infrared spectroscopy

FT-IR measurements were performed by directly placing a solid sample of the cyclic peptide on the diamond plate (ATR) after measuring the background.

[234] D. Nečas, P. Klapetek, *Cent. Eur. J. Phys.,* **2012**, *10*, 181–188.

6.1.9. Nuclear magnetic resonance spectroscopy

A portion of solid peptide (ca. 5 mg) was dissolved in D_2O. ^1H-NMR spectra were recorded on a Varian 300 MHz spectrometer. Chemical shifts are reported in ppm (δ) referenced to D_2O's residual signal (δ = 4.79).

6.1.10. High-performance liquid chromatography-mass spectrometry

HPLC-MS analysis of peptide solutions in MilliQ water was carried out on an Agilent 1260 Infinity II fitted with an Agilent SB-C18 column connected to a 6120 Quadrupole MS detector. Samples were filtered through a 0.22 μm syringe filter before injection. HR-MS was acquired on a Bruker MicroTOF.

6.2. SELF-ASSEMBLY OF CYCLIC PEPTIDE MONOLAYERS BY HYDROPHOBIC SUPRAMOLECULAR HINGES

6.2.1. Materials

Chemical reagents were acquired from Acros Organics, Aldrich, Carbolution, Fisher Scientific, Iris Biotech, and Novabiochem without additional purification unless otherwise specified. All solvents employed were HPLC grade or synthesis grade, except dry CH_2Cl_2 which was dried under reflux over CaH_2. D_2O was purchased from EMD Millipore. Glass slides for fluorescence microscopy were obtained from Ibidi (Cat# 80827). TEM grids (Cu carbon type-B, 300 mesh) and PELCO® mica discs for AFM were acquired from Ted Pella.

6.2.2. Synthesis of CP10 and variants

All peptides were synthesized manually as shown in Scheme 2.1 following the standard Fmoc solid phase peptide protocol described by our group.[225,226,227]

- Attachment of amino acids. Wang resin (100 mg; loading 1.0 mmol/g) was soaked in dry DMF (4 mL) for 30 min. The solvent was filtered off, and a solution of Fmoc-D-Glu-OAll (163.7 mg, 0.4 mmol) in dry DMF (2 mL) was stirred at rt for 5 min, then a solution of HOBt (54 mg, 0.4 mmol) and DIC (62 mL, 0.4 mmol) in dry THF (2 mL) and a solution of DMAP (12.2 mg, 0.1 mmol) in dry THF (2 mL) were successively added. The suspension was mechanically shaken (3-4h) and then, the resin was washed with DMF (3 x 4 mL x 1 min) and DCM (3 x 4 mL x 1 min) under a nitrogen stream. A mixture of acetic anhydride and pyridine (1:1, 4mL) was added to the reaction vessel and left to react for 30 min under a nitrogen stream to end cap any unreacted hydroxyl groups on the resin. Finally, was washed with DCM (3 x 4mL x 1 min) and vacuum dried to obtain the desired Fmoc-D-Glu-(Wang Resin)-OAll. The loading of the resin after the first coupled amino acid was calculated using the Fmoc test to get mmol/g.[235][235] For this, a small portion of the resin (ca 5 mg) was treated with a solution of piperidine in DMF (20% v/v, 4 mL) for 30 min. After this time, the concentration of dibenzofulvene-piperidine adduct from the Fmoc removal was measured by averaging its absorbance at 290 and 301 nm of a small aliquot (20 mL).

All reagent amounts were calculated based on the new loading calculated above. Subsequent coupling cycles consisted of Fmoc removal upon treatment with piperidine in DMF (20% v/v, 4 mL) for 15 min and coupling protocol using a solution of (D or L)-α-amino acids (4 equiv), *N*-HBTU (3.8 equiv), DIPEA (6 equiv) in DMF (4 mL) under a nitrogen stream for 30 min. Washings with DMF (3 x 4 mL x 1 min) were performed after each step. Having coupled the last amino acid (Table 2.1), the resin was washed with DCM (4 mL x 1 min) and filtered.

[235] C. Kay, O. E. Lorthioir, N. J. Parr, M. Congreve, S. C. Mckeown, J. J. Scicinski, S. V Ley, *Biotechnol. Bioeng.,* **2000**, *71*, 110-118.

- To deprotect the C-terminal group (allyl), a solution of PPh_3 (34.4 mg, 0.13 mmol), N-methylmorpholine (95 µL, 0.87 mmol), phenylsilane (107 µL, 0.87 mmol), and $Pd(OAc)_2$ (5.8 mg, 0.026 mmol) in dry DCM (4 mL) was added to the resin and mechanically shaken for 3 h. The resin was washed with DCM (3 x 4 mL x 1 min) and then filtered with a solution of DIPEA in DMF (2% v/v, 4 mL). Finally, was soaked in a solution of sodium diethyldithiocarbamate (0.5% w/v in DMF, 2 x 4 mL x 30 min) to remove all traces of Pd.

- To deprotect the N-terminal group (Fmoc), the resin was treated with a solution of piperidine in DMF (20% v/v, 4 mL) for 30 min. After filtration, the resin was washed with DMF (3 x 4 mL x 1 min), a solution of DIPEA in DMF (2 % v/v, 4 mL) was passed through the resin filtering it and finally it was washed with a solution of LiCl in DMF (0.5% v/v, 4 mL, 15 min).

- Cyclization was carried out by shaking the resin with a solution of PyAOP (177.3 mg, 0.34 mmol) and DIPEA (90 mL, 0.36 mmol) in DMF (4 mL) for 2 h by mechanical stirrer. After washing with DMF (3 x 4 mL x 1 min) and DCM (3 x 4 mL x 1 min), the cyclization was repeated two more times under the same conditions.

- Peptide cleavage. The peptide was deprotected and cleaved from the resin by the addition of a freshly prepared TFA cocktail (4 mL, TFA:DCM:H_2O:TIPS, 90:5:2.5:2.5), this mixture was shaken for 2 h and then filtered. The resin was washed with TFA (0.5 mL) twice and concentrated under nitrogen. The concentrated reaction crude was precipitated dropwise into 40 mL of cold diethyl ether. The resulting suspension was centrifuged and the pellet was then dissolved in a 1:1 mixture of MilliQ H_2O:ACN and purified by semipreparative HPLC using a Phenomenex Luna C18 100Å column. Solvents used were H_2O + 0.1%v/v TFA (solvent A) and CH_3CN + 0.1%v/v TFA (solvent B) and the method used a gradient of H_2O + 0.1% TFA: CH_3CN + 0.1% TFA → 95:5 (0 min) to 25:75 (30 min). Peptide fractions were concentrated in vacuo to remove ACN and TFA and the remaining solution was freeze-dried. A white powder was obtained for all cyclic peptides. **CP10** (26 mg, 19 %); **3L** (18 mg, 15 %); **LW** (22 mg, 16 %); **2W** (18 mg, 11.7 %); **2L** (28 mg, 22.4 %); **EHEH** (22 mg, 16.2 %); **2E2H** (15 mg, 11.1 %)

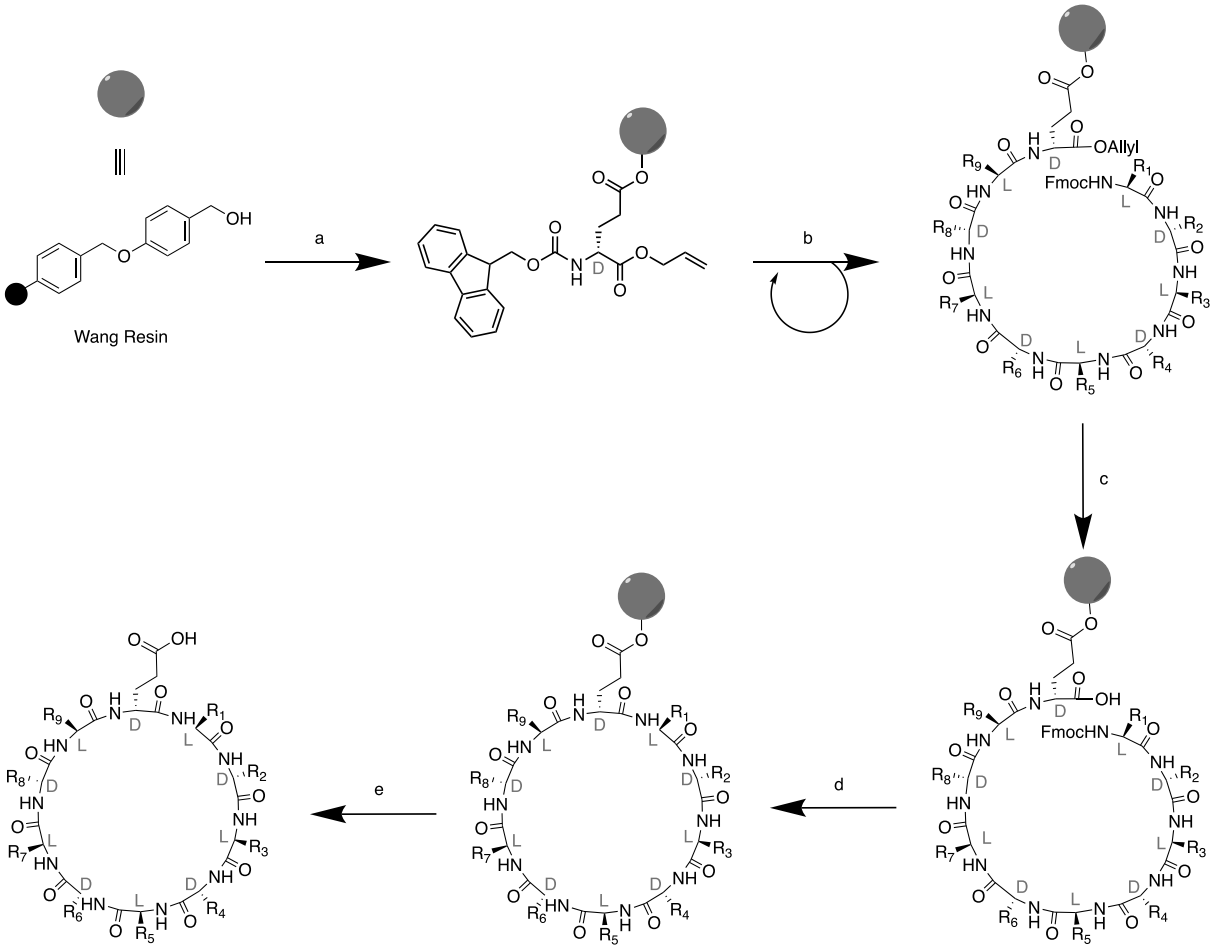

Scheme 2.1. Synthetic protocol for the synthesis of **CP10** and variants. a) Wang resin functionalisation: Fmoc-D-Glu-OAll in DMF, HOBt, DIC, DMAP in THF, 3h. b) Peptide elongation: i) Piperidine in DMF (20% v/v), 15 min; ii) Fmoc-amino acid, *N*-HBTU, DIPEA, DMF, 30 min. This process was repeated 9 times to couple all the amino acids in the sequence in the order shown in Table 1 for each cyclic peptide. The last amino acid will maintain the Fmoc protecting group in the amine end. c) Allyl removal: Palladium (II) acetate, triphenylphosphine, phenylsilane, 4-methylmorpholine, DCM, 3h. The final product was washed with a solution of sodium diethyldithiocarbamate in DFM (0.5% w/v). d) i. Fmoc removal: piperidine in DMF (20% v/v), 30 min; ii) Peptide cyclization: PyAOP, DIPEA, DMF, 2h (step repeat two times to ensure the yield of cyclization). e) Peptide cleavage: TFA-DCM-H_2O-TIPS (90:5:2.5:2.5), 2h.

Table 2.1. Representation of the amino acid sequences in all the cyclic peptides arranged according to their coupling to the resin (from R_1 to R_{10}).

	R_1	R_2	R_3	R_4	R_5	R_6	R_7	R_8	R_9	R_{10}
CP10	H	L	W	L	E	H	L	W	L	E
3L	H	L	L	L	E	H	L	L	L	E
LW	H	W	L	E	H	E	W	L	H	E
2W	H	W	W	E	H	E	W	W	H	E
2L	H	L	L	E	H	E	L	L	H	E
EHEH	H	L	W	L	H	E	L	W	L	E
2E2H	H	L	W	L	E	H	L	W	L	E

6.2.3. Self-assembly protocol

Cyclic peptides were dissolved to a concentration of 100 μM in sodium phosphate buffer (20 mM, pH 7.4) in glass vials. Samples were sonicated for 5 min and then incubated without shaking at 80°C for 1.5 h. Next, peptide solutions were stored at room temperature for 1 h, where 2D elongation takes place. For nanosheet formation at different concentrations, cyclic peptide solutions at 100 μM were diluted to the desired final concentration in sodium phosphate buffer (20 mM, pH 7.4). For study the assembly behavior at different pH, cyclic peptide solutions prepared likewise were adjusted with HCl or NaOH 1M and then annealed. For fluorescence samples (vide infra), thioflavin-T was initially added to the cyclic peptide solution and then annealed as indicated above.

- The preparation of the thioflavin-T solution was described in the previous Chapter I (see methodologies, Section 6.1.3).[228,229]

6.2.4. Fluorescence microscopy

10 μL of cyclic peptide samples annealed in presence of 10 μM thioflavin-T were deposited on glass slides and left to dry completely overnight in the dark at room temperature before imaging. Epifluorescence micrographs were taken at room temperature with a Nikon Eclipse Ti (60x immersion objective, Excitation=475/35 nm; Emission=530/43 nm). All images were analysed using ImageJ.[232,233]

6.2.5. Scanning-transmission electron microscopy

Assembled monolayers (without thioflavin-T) were diluted 10-fold with water and after gently homogenizing by shaking manually, 10 μL of samples were casted on Cu Grids. After adsorption for 10 min, the excess solution was removed with kimwipes and the samples were stained with phosphotungstic acid (1 mg·mL^{-1} in MilliQ water) for 1 min. Grids were then washed twice with MilliQ water (5 μL/1 min) and then, samples were imaged without washing nor staining. STEM images were acquired on a FESEM Ultra plus (Zeiss) operating at an extra high tension of 20 kV.

6.2.6. High-resolution transmission electron microscopy

Assembled samples were diluted 10-fold with MilliQ water and 10 μL of the diluted sample were cast on TEM grids. After adsorption for 10 min, the excess solution was removed, and grids were washed twice with MilliQ water (5 μL for 1 min).

6.2.7. Atomic force microscopy

Assembled peptide monolayers were diluted 10-fold with MilliQ water and 10 μL of the diluted sample was cast on mica. After adsorption for 10 min, the excess solution was removed, and the mica surface was washed twice with MilliQ water. Image analysis was carried out using Gwyddion.[234]

6.2.8. Fluorescence measurement

To determine the critical aggregation concentration (CAC), cyclic peptides were dissolved in sodium phosphate buffer (20 mM, pH 7.4) and then serially diluted across a range of 0.75 μM to 100 μM. These solutions underwent a thermal cycle, as previously described (vide supra), before measuring their fluorescence. A FluoroMax-3 Horiba Jobin Yvon Fluorescence Spectrophotometer equipped with a temperature-controlled cell chamber and a Hellma® fluorescence quartz cell (10 x 2 mm) was utilized for spectroscopic analysis. Spectra were recorded from 300 to 450 nm, with an excitation wavelength of 280 nm, using slits set at 2.5 nm, and a scan rate of 1200 nm/min. All measurements were conducted at a temperature of 20°C.

To analyze the kinetics of the system, an unheated sample dissolved in sodium phosphate buffer (20 mM, pH 7.4) was heated from 20 to 80°C at a rate of 10°C/10min, and fluorescence was recorded at each temperature point. After the measurement at 80°C, the cell chamber was set to 20°C and fluorescence was recorded every 60 sec at 350 nm for 60 min as the sample cooled down. These measurements were made in a Cary Eclipse Fluorescence Spectrophotometer (Agilent) equipped with a temperature-controlled cell chamber.

6.2.9. Fourier transform infrared spectroscopy

A portion of the solid peptide was directly placed on the diamond plate (ATR), and the FT-IR spectrum was recorded at room temperature with subtracted background. The measurements were performed on a Perkin Elmer Spectrum Two.

6.2.10. Circular dichroism

Spectra were acquired at 25°C from a 2 mm-light path quartz cuvette, recording 60 accumulations between 390-190 nm at 200 nm·min^{-1}, 2 s response time, 1 nm bandwidth, 0.2 nm data pitch. Data was collected at a concentration of 100 μM for each peptide at pH 7.4 in phosphate buffer. Subtraction of the solvent background was done in all cases. CD spectra were acquired on a Jasco J-1100 CD spectrometer equipped with temperature control.

6.2.11. Nuclear magnetic resonance spectroscopy

A portion of solid peptide (approx. 5 mg) was dissolved in D_2O. ^1H NMR spectra were recorded on a Varian 300 MHz spectrometer. Chemical shifts are reported in ppm (δ) referenced to D_2O's residual signal (δ = 4.79).

6.2.12. High-performance liquid chromatography-mass spectrometry

HPLC-MS analysis of a peptide sample in MilliQ water was carried out on an Agilent 1260 Infinity II fitted with an Agilent SB-C18 column and connected to a 6120 Quadrupole MS detector. Samples were filtered through a 0.22 μm syringe filter before measuring.

6.3. 3D SELF-ASSEMBLY OF CYCLIC PEPTIDES INTO MULTILAYERED NANOSHEETS

6.3.1. Materials

Chemical reagents were adquired from Acros Organics, Aldrich, Fisher Scientific, Iris Biotech, and Novabiochem. Dichloromethane was dried under reflux over calcium hydride. D_2O was purchased from EMD Millipore. Glass slides for fluorescence microscopy were obtained from Ibidi (Cat# 80827). TEM grids (Cu carbon type-B, 300 mesh) and PELCO® mica discs for AFM were acquired from Ted Pella.

6.3.2. Synthesis of CP6 and variants

CP6 was prepared manually in solid phase as depicted in Scheme 3. and following these four steps:[225,226,227]

- Attachment of the first amino acid. 2-Chlorotrytil chloride resin (2CTC, 312.5 mg, 1.6 mmol chloride per g resin) was soaked for 30 min in freshly distilled DCM (5 mL). The resin was filtered and a solution of Fmoc-L-Glu(OH)-OAll (614.1 mg, 1.5 mmol) and DIPEA (425 µL, 3 mmol) in dry DMF (5 mL) was added over the resin and shaken for 1 h. Then the mixture was filtered and washed with DCM (3 x 3 mL). The free reactive groups of the resin were capped with a solution of DCM:MeOH:DIPEA (8.5:1.0:0.5, 5 mL) that was added and shaken for 30 min. Finally, the resin was filtered off, washed with DMC (3 x 3 mL), and dried under a high vacuum to determine the new loading by Fmoc quantification.[235] A small fraction of dried resin was reacted with a solution of piperidine in DMF (20% v/v, 5 mL) for 30 min. After this time, the new loading was calculated by measuring the absorbance of the adduct after Fmoc removal.

- Linear peptide growth. The rest of the amino acids were coupled considering the new loading. Cycles of Fmoc removal, piperidine in DMF (20% v/v, 2 mL) for 15 min, and amino acid coupling, Fmoc-protected amino acid (0.4 mmol), N-HBTU (0.35 mmol) and DIEA (0.6 mmol) in DMF (x mL) for 30 min, with their respective washes (DMF 3 x 3 mL) were followed. After the coupling of the last amino acid (Table 3.1), the resin was washed with DMF (3 x 3 mL), DCM (3 x 3 mL) and dried under vacuum.

- For **OAll removal** the resin was reacted with a solution of PPh_3 (39.3 mg, 0.15 mmol), N-methylmorpholine (110 µL, 0.01 mmol) and phenylsilane (123 µL, 1.0 mmol) and Pd(OAc)2 (6.7 mg, 0.03 mmol) in dry DCM (4 mL) overnight (16-20 h). The resin was then washed with DCM (3 x 3 mL) and DIEA in DMF (2% v/v, 3 x 3 mL) and soaked in a solution of sodium diethyldithiocarbamate (0.5% w/v in DMF, 2 x 3 mL) for 30 min to remove all traces of Pd. Finally, the resin was stirred with piperidine/DMF (20% v/v, 3 mL) for 30 min for removal of the Fmoc group at the N-terminus.

- Cyclization was carried out by shaking the resin with a solution of PyAOP (208.6 mg, 0.4 mmol) and DIEA (95.1 mL, 0.6 mmol) in DMF (3 mL) for 2 h. After washing with DMF (3 x 3 mL) and DCM (3 x 3 mL), the cyclization was repeated two more times under the same conditions.

- Peptide cleavage. The peptide was deprotected and cleaved from the resin by addition of a freshly prepared TFA cocktail (4 mL, TFA:DCM:H_2O:TIS, 0.9:0.05:0.025:0.025), this mixture was shaken for 2 h and then filtered. The resin was washed with TFA (0.5 mL) twice and concentrated under nitrogen. The resulting reaction mixture was precipitated by dropwise addition onto cold diethyl ether (40 ml) under stirring. The resulting suspension was centrifuged for 10 min at 3000 rpm and the pellet was dried with a stream of air and dissolved in MilliQ:ACN (80:20). The sample was purified by semipreparative HPLC using a Phenomenex Luna C18 100Å column [gradient of H_2O+0.1% TFA:ACN+0.1% TFA→80:20 (0 min) to 25:75 (30 min)]. Peptide fractions were concentrated in vacuo to remove ACN and TFA and the remaining solution was freeze-dried.

The structural variants of CP6 with glutamine residues in the sequence were prepared manually following the protocol already described in Methodologies of Chapter I for Rink Amide Resin.

Table 3.1. Amino acid sequences for all the cyclic peptides according to their coupling to the resin (from R_1 to R_6).

	R_1	R_2	R_3	R_4	R_5	R_6
CP6	L	L	H	E	H	E
2W	W	W	H	E	H	E
EQEQ	L	L	Q	E	Q	E
EQQH	L	L	Q	E	Q	H
LWL	H	L	W	L	E	Q
LAL	H	L	A	L	E	Q

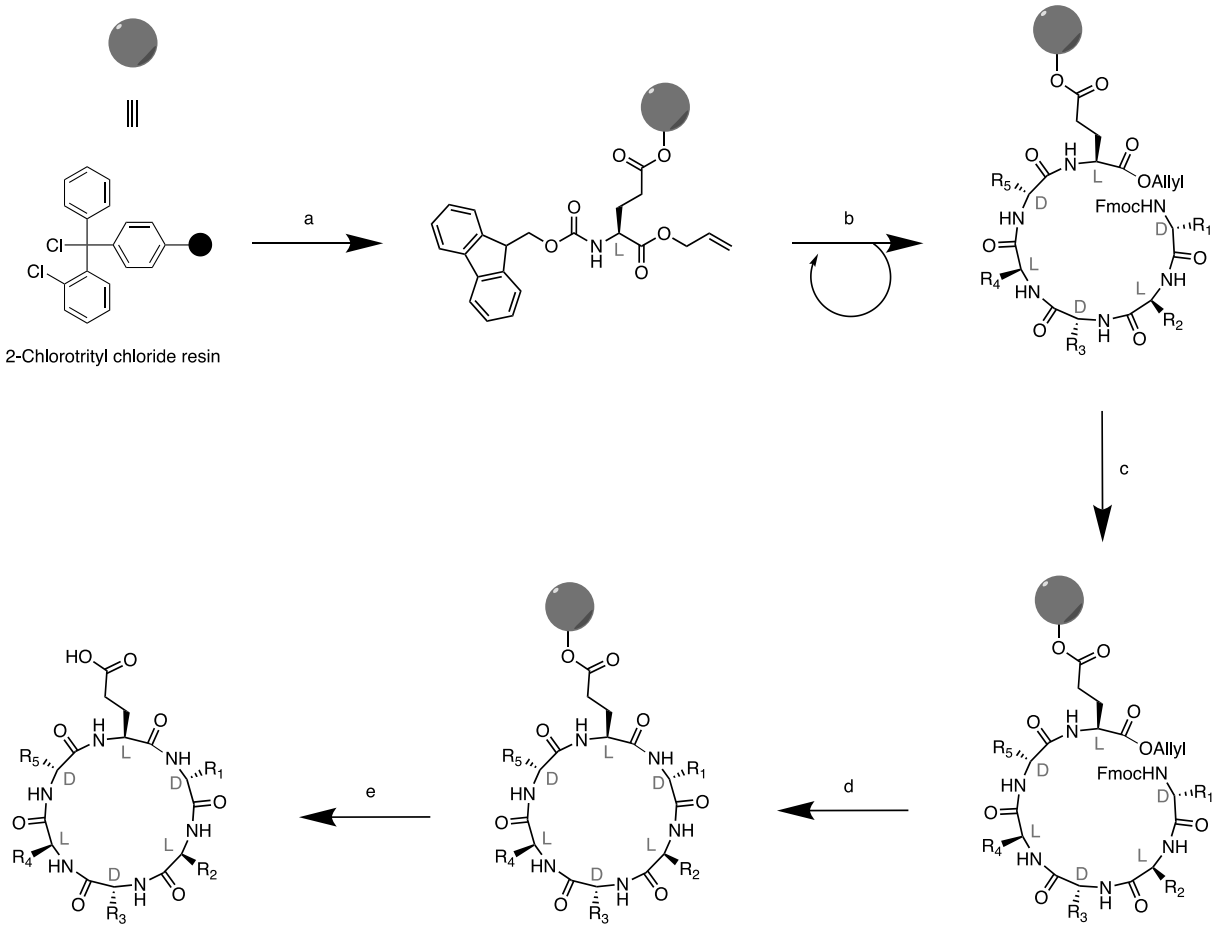

Scheme 3.*1.* Synthetic protocol for the synthesis of **CP6** and some of the variants. a) 2-Chlorotrityl chloride resin functionalization with the first amino acid coupled by its side chain: i. Fmoc-L-Glu-OAll, DIEA, distilled DCM, 1 h. ii) Resin capping: DCM:MeOH:DIPEA (8.5:1.0:0.5) b) Peptide elongation: i. Piperidine in DMF (20% v/v), 15 min; ii. Fmoc-amino acid, *N*-HBTU, DIEA, DMF, 30 min. This process was repeated 5 times to couple all the amino acids in the sequence in the order shown in Table 1. The last amino acid will maintain the Fmoc protecting group in the amine end. c) Allyl removal: $Pd(OAc)_2$, PPh_3, phenylsilane, 4-methylmorpholine, DCM, overnight (16-20 h). The final product was washed with a solution of sodium diethyldithiocarbamate in DFM (0.5% w/v). d) Cyclization: i. Fmoc removal: piperidine in DMF (20% v/v), 30 min; ii. Peptide cyclization: PyAOP, DIEA, DMF, 2 h (step repeated two times to ensure the yield of cyclization). d) Peptide cleavage: TFA:DCM:H_2O:TIS (90:5:2.5:2.5), 2h.

6.3.3. Self-assembly protocol

Cyclic peptides were dissolved to a concentration of 100 μM in sodium phosphate buffer (20 mM, pH 6.5) in glass vials. Samples were sonicated for 5 min and then incubated without shaking at 80°C for 1.5 h. Next, peptide solutions were stored at room temperature for 1 h to promote an ordered assembly. For nanosheet formation at different concentrations, cyclic peptide solutions at 100 μM were diluted to the desired final concentration in sodium phosphate buffer (20 mM, pH 6.5). To study the assembly behavior at different pH, cyclic peptide solutions prepared likewise were adjusted with HCl or NaOH 1M and then annealed. For

fluorescence sample preparation, thioflavin-T was initially added to the cyclic peptide solution and then annealed as indicated above.

- The preparation of the thioflavin-T solution was described in the previous Chapter 1 (see methodologies, section 6.1.3).[228,229]

6.3.4. Fluorescence microscopy

10 μL of cyclic peptide samples annealed in the presence of 10 μM thioflavin-T were deposited on glass slides and left to dry completely overnight in the dark at room temperature before imaging. Epifluorescence micrographs were taken at room temperature with a Nikon Eclipse Ti (60x immersion objective, Excitation=475/35 nm; Emission=530/43 nm). All images were analyzed using ImageJ.[232,232]

6.3.5. Scanning transmission electron microscopy

Annealed nanosheet samples (5 μL; without thioflavin-T) were deposited on Cu Grids. Once dry, samples were washed twice with water (10 μL) for 1 min and stained with 5 μL of phosphotungtic acid (2% v/v in water) for 1 min, then the rest was removed. STEM images were acquired on a FESEM Ultra plus (Zeiss) operating at an extra high tension of 20 kV.

6.3.6. Atomic force microscopy

Annealed nanosheet samples (5 μL, without thioflavin-T) were spotted on mica, left to completely dry, gently washed with water, and imaged. AFM analysis was carried out on a NX-10 microscope (Park Systems) in non-contact mode and using ACTA cantilevers (silicon tips, nominal values: spring constant = 40 $N \cdot m^{-1}$, frequency = 300 kHz, ROC less than 10 nm). Image analysis was carried out using Gwyddion.[234]

6.3.7. Fluorescence measurement

A Cary Eclipse Fluorescence Spectrophotometer (Agilent) equipped with a temperature-controlled cell chamber and a Hellma® fluorescence quartz cell (10 x 2 mm) was utilized for spectroscopic analysis. Spectra were recorded between 440 to 600, with an excitation wavelength of 420 nm, using slits set at 2.5 nm, and a scan rate of 1200 nm/min. All measurements were conducted at a temperature of 20°C.

6.3.9. Nuclear magnetic resonance spectroscopy

FT-IR measurements were performed by directly placing a solid sample of the cyclic peptide on the diamond plate (ATR) after measuring the background.

6.3.9. Nuclear magnetic resonance spectroscopy

A portion of solid peptide (approx. 5 mg) was dissolved in D_2O. ^{1}H-NMR spectra were recorded on a Varian 300 MHz spectrometer. Chemical shifts are reported in ppm (δ) referenced to D_2O's residual signal (δ = 4.79).

7. RESULTS

7.1. SEQUENCE DECODING OF 1D-TO-2D SELF-ASSEMBLING CYCLIC PEPTIDES

***Some of the results from this chapter have already been published:**

Sandra Díaz[a,b], Dr. Ignacio Insua[a,b], Dr. Ghibom Bhak[a,c], Dr. Javier Montenegro[a,b,c]. Sequence decoding of 1D to 2D self-assembling cyclic peptides. *Chemistry A European Journal,* **2020**, *26*, 14765.

DOI: 10.1002/chem.202003265

Affiliations

[a] Departamento de Química Orgánica e Centro Singular de Investigación en Química Biolóxica e Materiais Moleculares (CiQUS), Universidade de Santiago de Compostela, Santiago de Compostela, Spain.

[b] These authors contributed equally

[c] e-mail: javier.montenegro@usc.es

7.1.1. Objectives

The fundamental challenge of this chapter is to study how the primary sequence of cyclic peptides influences their hierarchical self-assembly from 1D nanotubes into 2D nanosheets. The fabrication of 2D nanostructures is often based on trial-and-error strategies, which requires the use of natural peptide sequences with predetermined folding patterns, restricting the potential of non-natural peptide analogues and limiting the range of structural possibilities. Therefore, the main challenge is to establish general design principles that can be applied to a wide range of building blocks, thereby enabling the rational engineering of new nanostructures.

As mentioned in the introduction (section 4.2.4.3), our group has reported the self-assembly of a cyclic peptide through a sequential 1D-to-2D process forming nanosheets with defined thickness (**Figure 39**).[224] The key features of the design that direct this hierarchical assembly are encoded in the primary sequence of the cyclic peptide (**CP$_x$**): amino acids arranged with alternating D/L-chirality are segregated by polarity to generate an amphiphilic surface. Furthermore, different charged residues are incorporated to modulate the surface charge of the cyclic peptide. Together, these characteristics allow a delicate balance between attractive (H-bonding and hydrophobic effects) and repulsive (Coulombic) forces to direct the sequential 1D-to-2D self-assembly. After this successful design, we decided to expand the study and address the structure-assembly relationships to unlock the full potential of this process.

Our goal in this chapter is to perform a structural exploration of the previously studied cyclic peptide, **CPX**,[224] seeking to decipher the key positions and amino acids within the sequence that drive and regulate the hierarchical assembly process. Our plan is to systematically modify the peptide sequence and observe the impact of these mutations on the final assembled nanostructure to better understand the relationship between molecular design and the intermolecular interactions that direct the assembly (**Figure 1.1**). We postulate that this study will contribute to overcome the challenge of establishing general design rules for the creation of new materials. To achieve this main goal, we propose the following successive objectives:

- Design, synthesize and characterize a library of peptides derived from the original 1D to 2D cyclic peptide example (**CPX**),[224] by systematically varying the key positions of the primary sequence to assess their effect on 2D nanosheets assembly.
- Evaluate their ability to form nanosheets under the conditions defined by **CPX** by microscopy.
- Study the influence of pH and ionic strength on self-assembly.

- Characterize their self-assembly behavior using spectroscopic techniques.

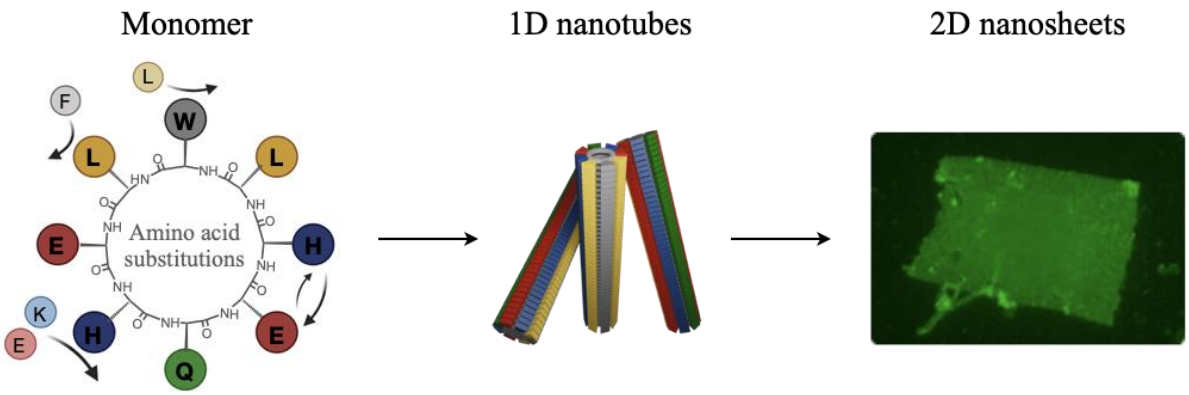

Figure 1.1. Schematic representation of the sequential 1D-to-2D self-assembly of cyclic peptides, where amino acid permutations in the cyclic peptide scaffold (left) are represented as coloured balls with arrows pointing out the exchange positions.

7.1.2. Results and discussion

7.1.2.1. Design of CPx variants

A library of peptides structurally derived from the original nanosheet-forming **CPx** sequence was designed (Scheme 1.2). Each sequence was meticulously selected with systematic modifications in the two key domains of the original peptide, thus allowing the obtaining of structure-assembly relationships. The importance of these domains in 1D to 2D assembly behavior was detailed in the introduction (Section 4.2.4.3, **Figure 39**). Briefly, the arrangement of amino acids within the cyclic peptide segregates two distinct domains: one hydrophobic and another hydrophilic (**Figure 1.2**). The former region, comprising the tripeptide Leu-Trp-Leu, drives the bilayer packing of nanotubes in an aqueous environment through hydrophobic effects. The latter region is constituted by charged and polar amino acids, which, under optimal pH conditions (7.4), maintain anionic nanosheets in an extended colloidally stable state due to repulsive forces. This previous research has underscored the critical importance of amphiphilicity and a delicate balance between attractive (hydrogen bonds and hydrophobic effect) and repulsive (Coulombic) non-covalent interactions as pivotal design motifs for the sequential 1D-to-2D assembly.[224] The key modifications we propose have been specifically designed to question the role that each amino acid has in the assembly process.

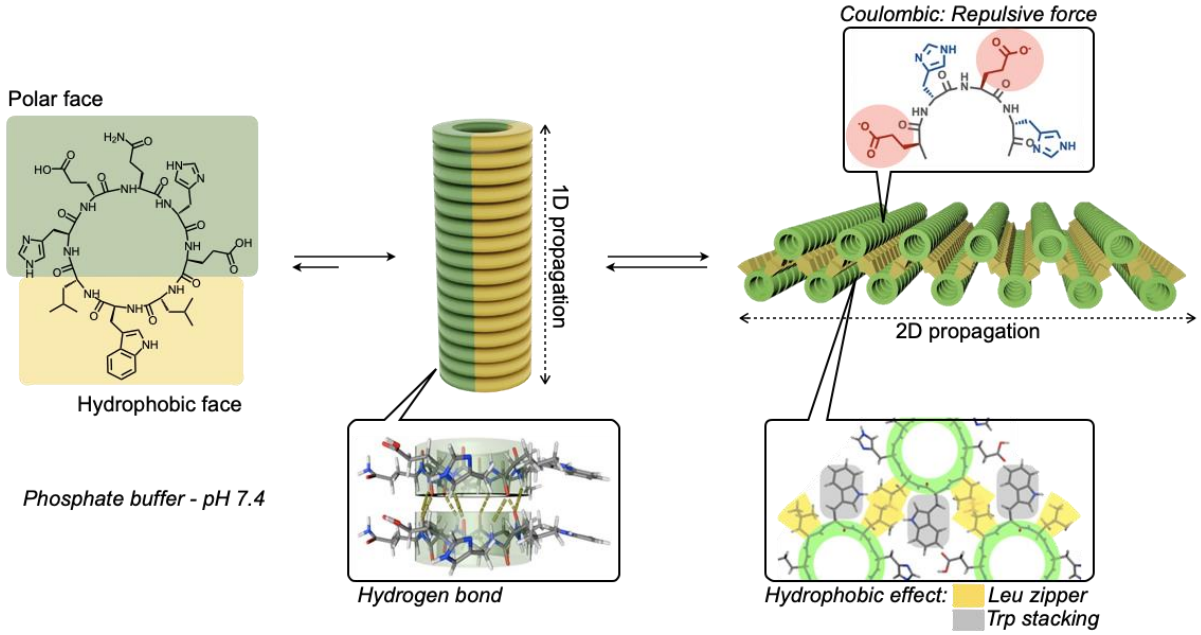

Figure 1.2. Schematic representation of the sequential 1D-to-2D self-assembly of **CPx**. Left: Cyclic peptide sequence with two segregated domains colour as yellow (hydrophobic region) and green (polar region). Middle: Formation of 1D nanotubes through hydrogen bonding network between stacked monomers. Right: 2D nanosheets stabilized by hydrophobic effect and repulsive Coulombic forces.

Initially, we targeted modifications in the central hydrophobic domain (Scheme 1.2, bottom). In this region, the formation of a leucine zipper-type packing provides directionality to the 2D elongation, organizing nanotubes in a staggered zig-zag bilayer configuration. Moreover, the hydrophobic packing is further strengthened and directed by π-π stacking interactions between the indole groups of adjacent tryptophan within the nanotube. To study the contribution of these residues to the final assembly, we first designed sequences where the tryptophan of the central hydrophobic core was replaced by other non-polar amino acids, spanning from non-aromatic (alanine, **CP$_A$**, and leucine, **CP$_L$**) to smaller aromatic residues (phenylalanine, **CP$_F$**). Secondly, the hydrophobic leucines that mediate the lateral association, were replaced for aromatic phenylalanines (**CP$_{2F}$**), and we also explored the substitution of all three hydrophobic residues (i.e., leucine and tryptophan) for phenylalanines (**CP$_{3F}$**) to obtain an homogenous hydrophobic domain.

We then evaluated mutations in the polar region (Scheme 1.2, top), where alternated glutamic acids and histidines distribute negative charges on both sides, creating a buffering effect within the molecular structure and thus reducing the anionic repulsion between adjacent residues. To assess the role of this motif, we designed two peptides varying the position of both amino acids: **CP$_{oE}$**, is designed with the same number of glutamic acid and histidine residues but permuting the positions occupied by one of the His/Glu pairs (Scheme 1.2). In contrast to this peptide, in the **CP$_{2E2H}$** scaffold, residues with identical chemical properties are arranged together on the same side of the macrocycle (Scheme 1.2). Expanding our exploration within the polar region, we sought to evaluate the influence of the negative corona on self-assembly, which motivated the design of two additional peptides with different net charges: **CP$_K$**, where histidines were replaced for more basic lysines, and **CP$_{4E}$**, a fully anionic variant that incorporates four glutamic acids.

It is worth mentioning that glutamine was remained constant in the library of CPs analyzed because it is the common anchoring point of the peptides to their solid support during their synthesis. This, being a neutral and hydrophilic residue, should not interfere with the structure-assembly study of the peptide. However, we believe that this position, since it is not crucial in the assembly and it is exposed on the surface of the bilayer, could serve as functionalization point to derivatize the resulting nanosheets.

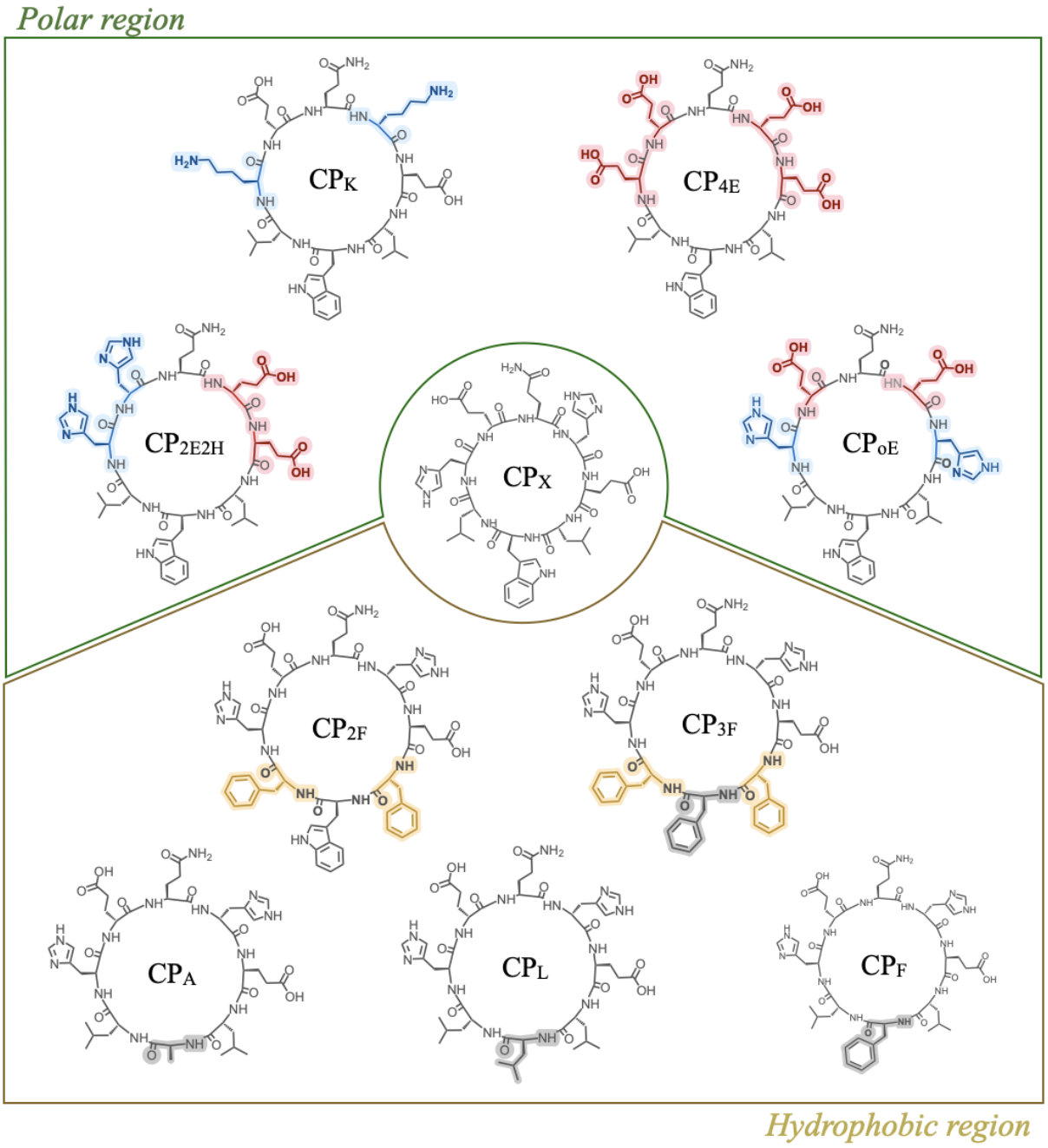

Scheme 1.2. Representation of the amino acid sequence of the cyclic peptide variants derived from **CPX** (inside the circle). Each amino acid mutation in comparison with **CPX** is highlighted. The scheme is divided in two areas, the one above with the four mutations in the polar region (**CPoE**, **CP2E2H**, **CPK**, **CP4E**) and the one below with the five mutations in the hydrophobic region (**CPA**, **CPL**, **CPF**, **CP2F**, **CP3F**).

7.1.2.2. Determination of critical aggregation concentration

To explore the dynamics of the assembly of cyclic peptides, our initial investigation focused on determining the critical aggregation concentration (CAC) of all derivatives. This parameter represents the concentration at which the transition from monomeric to assembled structures occurs, offering insights into the peptide's self-assembly behavior. This value was assessed by measuring changes in the emission intensity of an external dye (i.e., Thioflavin-T, or ThT) in response to increasing monomer concentrations. ThT was chosen as a fluorescence strain-sensitive probe as it gives enhanced green fluorescence upon planarization within hydrophobic pockets, which will also allow visualization of the morphology under the microscope.[236,80]

In the experimental procedure, individual samples were prepared with different concentrations of cyclic peptides, keeping the ThT concentration constant at 10 μM in phosphate buffer at pH 7.4. The different solutions were subjected to an annealing process, following two steps protocol: i) heating at 80°C for 1.5 h; ii) cooling down to room temperature allow to equilibrate during 1h. This protocol ensures thermodynamic control over the sequential transition from 1D to 2D assembly of cyclic peptides. The reason is that, by heating to 80°C, the only supramolecular ensemble that remains in solution are the 1D nanotubes, something that was confirmed by its isolation. Therefore, once the samples are cooled to room temperature, these small nanotubes are organized in an order manner to give rise to the 2D bilayer previously described.[224] Once assembled, the samples were analyzed in the fluorometer as described in the methodology section and the results indicated a clear difference in the emission intensities among various derivatives (Figure S1.19, Experimental Section 10.1.2). The maximum emission values against the concentration were plotted to better identify the critical aggregation concentration.

Notably, certain peptides exhibited a CAC point with an exponential emission increase at concentrations below 10 μM while other derivatives (**CP$_{2E2H}$**, **CP$_{K}$** and **CP$_{4E}$**) did not show such a pronounced change at any concentration, suggesting a different assembly behaviour (**Figure 1.3**, CAC: 4 μM for **CP$_{A}$**, b) 6 μM for **CP$_{L}$**, c) 6 μM for **CP$_{F}$**, d) 8 μM for **CP$_{2F}$**, e) 8 μM for **CP$_{3F}$**, f) **CP$_{oE}$**, g) N.D. for **CP$_{2E2H}$**, h) N.D. for **CP$_{K}$**, i) N.D. for **CP$_{4E}$**). To sum up, this feature could indicate that six of the nine new monomer designs are assembling into higher-order structures or aggregates beyond monomers.

[236] C. Xue, T. Y. Lin, D. Chang, Z. Guo, *R. Soc. Open Sci.,* **2017**, *4.*

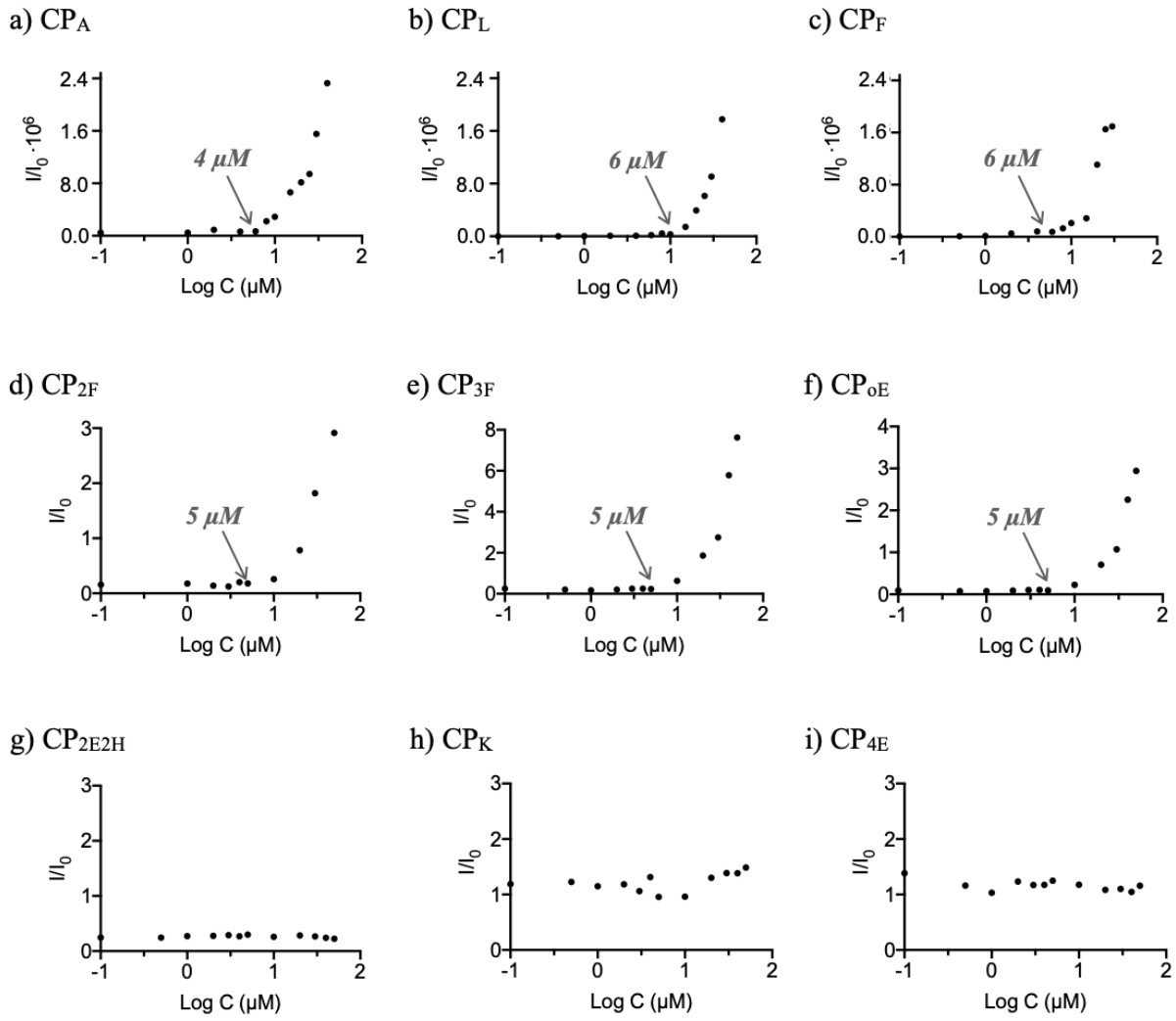

Figure 1.3. Comparison of critical aggregation concentration (cac) for the different cyclic peptide variants. The graphs illustrate changes in ThT emission intensity relative to varying concentrations of cyclic peptide monomers: a) **CP$_A$**, b) **CP$_L$**, c) **CP$_F$**, d) **CP$_{2F}$**, e) **CP$_{3F}$**, f) **CP$_{oE}$**, g) **CP$_{2E2H}$**, h) **CP$_K$**, i) **CP$_{4E}$** in sodium phosphate buffer (20 mM, pH 7,4) with ThT (10 μM) after annealed treatment. I is the ThT fluorescence emission intensity at 480 nm for cyclic peptide samples and I0 is the ThT fluorescence emission intensity of a sample containing ThT (10 μM) alone in sodium phosphate buffer (20 mM, pH 7,4).

As hypothesized, if these new derivatives assembled in a bilayer of nanotubes as **CP$_x$**, the enhanced emission can be attribute to the planarization of ThT in the hydrophobic core within the nanosheets. To determine the morphological characteristics of these assembled samples, we employed epifluorescence microscopy. This method involved depositing a droplet of each cyclic peptide sample onto a glass surface, allowing it to dry completely. Based on these results, we decided to analyze the behavior of the assembly at three different concentrations: 10, 50 and 100 μM (Figures S1.20, S1.21; Experimental Section 10.1.2). Subsequent microscopic inspection revealed the formation of 2D nanosheets in six of the nine peptide designs explored that match with those with the observed exponential growth of CAC.

7.1.2.3. Microscopic analysis of self-assembly

Mutation of the central hydrophobic residue tryptophan in the original peptide was surprisingly well tolerated. In this position, a much smaller alanine residue (**CP$_A$**) and non-aromatic leucine (**CP$_L$**) led to the formation of large micrometric nanosheets (**Figure 1.4**a,b). Even the analogue **CP$_F$**, bearing an aromatic phenylalanine residue instead of tryptophan, assembled in 2D (**Figure 1.4**c). Regarding mutations of the two original leucine residues in positions R_4 and R_6 (**Table 1**, Methodologies section 6.1.2), it was previously demonstrated that an analogue (**CP$_{2A}$**) bearing smaller and less hydrophobic alanine residues instead of leucine lost most of its 2D assembling capacity, forming fibrillar structures with a few small sheets (Figure S1.24a, Experimental Section 10.1.2).[224] Based on this result, an aromatic and more hydrophobic residue was explored, phenylalanine, which should establish alternative phenylalanine stacks to drive the 2D arrangement of the tubes (**CP$_{2F}$**). Microscopic analysis of **CP$_{2F}$** showed well-defined and extended nanosheets, demonstrating the tolerance of this key position for 2D assembly to be replaced for other hydrophobic residues (**Figure 1.4**d). Motivated by the positive results obtained with both **CP$_{2F}$** and **CP$_F$**, a variant with all three hydrophobic positions incorporating phenylalanine residues was investigated, **CP$_{3F}$**. Despite assembling into large nanosheets (ca. 500 μm), reaching even longer values than the original **CP$_X$** (ca. 260 μm), amorphous aggregates were found in the background of the sample, suggesting a certain degree of disordered hydrophobic packing (**Figure 1.4**e). Like **CP$_L$**, with all three hydrophobic positions filled with the same isobutyl group of leucine residue, **CP$_{3F}$** also does not segregate different amino acids in the hydrophobic tripeptide domain. This lack of hydrophobic mismatch between side and central non-polar residues might compromise the lateral association of tubes via leucine or phenylalanine zippers specifically between residues R_4 and R_6. Therefore, the high degree of wrinkling of **CP$_L$** and **CP$_{3F}$** nanosheets, together with the background aggregation of the latter, may result from the interference of the central hydrophobic residue in the 2D elongation, mainly driven by positions R4 and R6 (**Table 1**.1, Methodologies section 6.1.2).

While the hydrophobic region of the cyclic peptides showed some structural flexibility, variations in the polar ionic region of the parent peptide **CP$_X$**, which consists of alternating glutamic acid and histidine residues (i.e., positions $R_{2\text{-}3}$ and $R_{7\text{-}8}$, **Table 1**.1, Methodologies section 6.1.2), presented important design limitations its assembly into nanosheets. **CP$_{oE}$**, which stands for the **CP$_X$** with outer glutamic acids, has symmetrically distributed ionic domains, unlike the original mismatched design. **CP$_{oE}$** formed well-defined nanosheets regardless of this sequence alteration (**Figure 1.4**f). However, segregation of glutamic acid and histidine residues on two opposite sides of the peptide **CP$_{2E2H}$**, completely inhibited nanosheet formation (**Figure 1.4**g). These results indicate that, despite allowing order variations, glutamic acid and basic histidine residues must be

placed together in the peptide sequence. This requirement is probably due to the weakening of like-charge repulsions from glutamic carboxylates by partially protonated histidines (pKa~6.0).

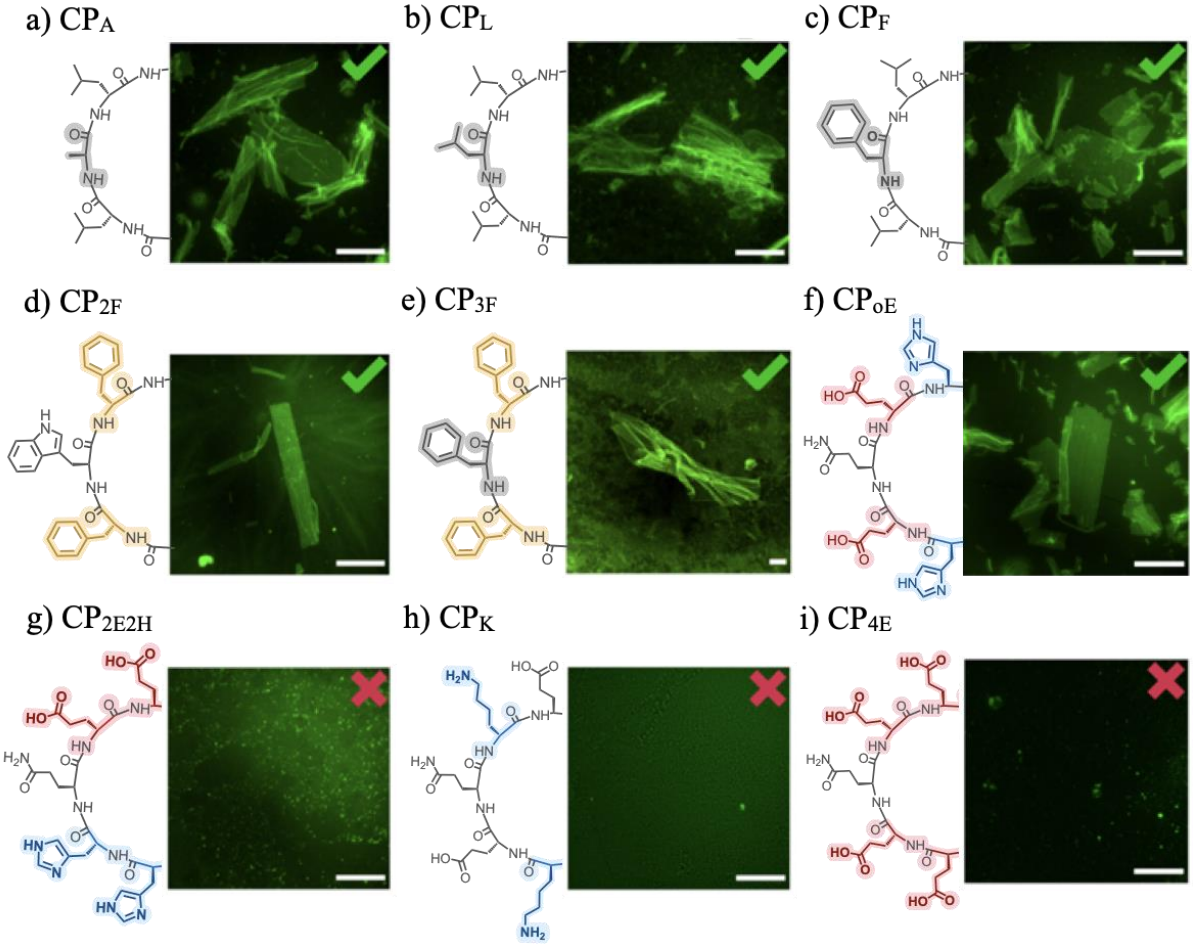

Figure 1.4. Epifluorescence micrographs (right) with the structural mutations of all cyclic peptide variants coloured highlighted (left). Images were taken after annealed samples (50 μM) for 2D assembly, (i. 80°C/1.5 h; ii. RT/1 h) in sodium phosphate buffer (20 mM; pH 7,4) with ThT (10 μM). Green ticks indicate the formation of nanosheets while red crosses indicate the inability to self-assembly in 2D. Scale bars = 50 μm.

Substitution of histidines in the parent peptide for more basic lysine residues (pKa~10.6) was also explored to assess the ability of a fully ionized peptide with zero net charge to assemble into nanosheets. Unfortunately, **CP_K** did not form nanosheets (**Figure 1.4**h), indicating that a certain repulsive character is required for cyclic peptides to assemble 2D. Being charge repulsions necessary for self-assembly, a derivative with four anionic glutamic acids was evaluated. However, **CP_{4E}** was also unable to form nanosheets (**Figure 1.4**i), probably because of very high energy barriers derived from this more self-repulsive and strongly anionic structure. Moreover, it is worth mentioning that two additional modifications had been previously explored in the polar region, which consisted of replacing the two glutamic acids and histidines with neutral glutamine residues (**$CP_{E->Q}$** and **$CP_{H->Q}$**). Neither of them showed nanosheet formation (Figure

S1.24b,c, Experimental Section 10.1.2), which further confirmed the importance of having both imidazole and carboxylate groups in this region.

To confirm that the presence of the fluorescence dye does not influence the assembly behavior, assembled samples prepared without ThT were then studied via scanning transmission electron microscopy (STEM). The micrographs obtained corroborate the previous epifluorescence results (Figure S1.22, Experimental Section 10.1.2), showing 2D nanosheets for **CP$_A$**, **CP$_L$**, **CP$_F$**, **CP$_{2F}$**, **CP$_{3F}$** and **CP$_{oE}$**, while only 1D nanotubes or amorphous aggregates were observed in the case of **CP$_{2E2H}$**, **CP$_K$** and **CP$_{4E}$**. In some micrographs, such as in the case of **CP$_A$**, it is possible to observe how the surface of the nanosheets presents areas with localized signs of tearing, which, when observed at higher magnification, were formed by laterally associated nanotubes (**Figure 1.5**). This continuous transition confirms the coexistence of both 1D and 2D states in the same supramolecular structure as in the original **CP$_x$** work.[224] The backward 2D-to-1D disassembly of the nanosheets could be induced by sonication of the 2D state, proving that both the intermediate 1D and the final 2D assemblies can be isolated (Figure S1.23, Experimental Section 10.1.2).

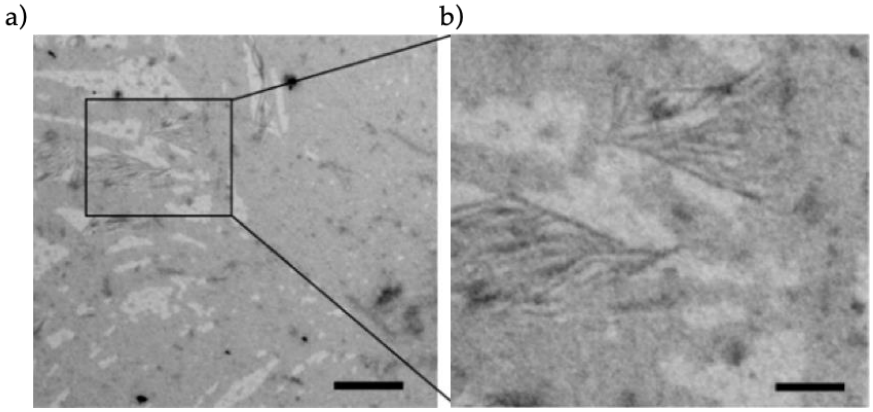

Figure 1.5. STEM micrographs of a) pre-assembled **CP$_A$** sample (50 μM) in 20 mM sodium phosphate buffer pH 7.4 diluted 10-fold in MilliQ (10 μM) without ThT and without any treatment. b) Magnification 3x of the area marked with a rectangle. Scale bars = 300 nm (a) and 100 nm (b).

Finally, the topography of the assembled nanosheets was analyzed by atomic force microscopy (AFM). **CP$_A$** and **CP$_{oE}$** were selected as representative variants, each belonging to distinct domains. The analysis of cross-sectional profiles derived from their respective AFM images revealed consistent height across CP derivatives, averaging 3.2±1 nm for both peptides (**Figure 1.6**). These AFM profiles matched with the height previously observed in the original **CPx** nanosheets (3.2 nm),[224] confirming the same nanotubular bilayer architecture of the assembled nanosheets regardless of the CP sequence.

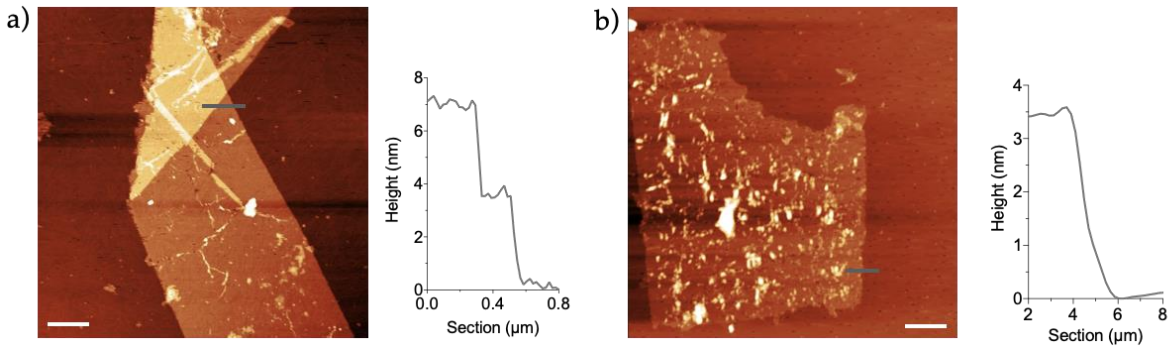

Figure 1.6. AFM images of a) **CP$_A$** and b) **CP$_{oE}$** with their respective Z-height profile of the section label with a grey line. Scale bars = 2 μm.

7.1.2.4. Spectroscopic characterization

Fourier Transform Infrared (FTIR) spectroscopy was carried out to gain further insight in the internal arrangement of cyclic peptides within nanotubes, as it has the capability to reveal the presence of stacked β-sheet structures.[237] Specific vibrational modes are attribute to the presence of a robust network of aligned hydrogen bonds: the stretching of C=O bonds (amide I) and the bending of N-H bonds (amide II) are indicative of an elongated, flat backbone conformation while the stretching of N-H bonds (amide A) indicates tightly packed hydrogen bonding interactions.[181] Numerous studies on self-assembling nanotubes have reported values for these bands of approximately 1540 and 3277 cm^{-1} for amide II and a respectively and, values in the 1600 cm^{-1} range for amide I.[238,239,240,241] In the former region, it was observed that the appearance of bands at low or low and high frequency can be indicative of parallel or antiparallel stackings, respectively.[242] However, these findings should be considered as suggestive rather than conclusive since the conformation adopted will largely depend on the peptide sequence.[194] Density functional theory (DFT) calculations demonstrated that **CPx** dimers favor a parallel conformation (**Figure 39**), with corresponding values of 1540 cm^{-1} for Amide II, 1627 and 1674 cm^{-1} for amide I, and 3267 cm^{-1} for amide A.[224] FTIR analysis of new **CPx** derivatives revealed values close to those described for **CPx** (**Figure 1.7**), suggesting the same parallel structure.

[237] R. Sarroukh, E. Goormaghtigh, J. M. Ruysschaert, V. Raussens, *Biochim. Biophys. Acta Biomembr.,* **2013**, *1828*, 2328–2338.
[238] M. Reza Ghadiri, K. Kobayashi, J. R. Granja, D. E. McRee, *Angew. Chem. Int. Ed. Ingl.*, **1995**, *34,* 93-95.
[239] M. Amorín, L. Castedo, J. R. Granja, *Chem. Eur. J.,* **2008**, *14*, 2100–2111.
[240] E. González-Freire, F. Novelli, A. Pérez-Estévez, R. Seoane, M. Amorín, J. R. Granja, *Chem. Eur. J.*, **2021**, *27*, 3029–3038.
[241] Y. Zou, Y. Li, W. Hao, X. Hu, G. Ma, *J. Phys. Chem. B,* **2013**, *117,* 4003–4013.
[242] T. D. Clark, J. M. Buriak, K. Kobayashi, M. P. Isler, D. E. Mcree, M. R. Ghadiri, *J. Am. Chem. Soc.,* **1998**, *120*, 8949-8962.

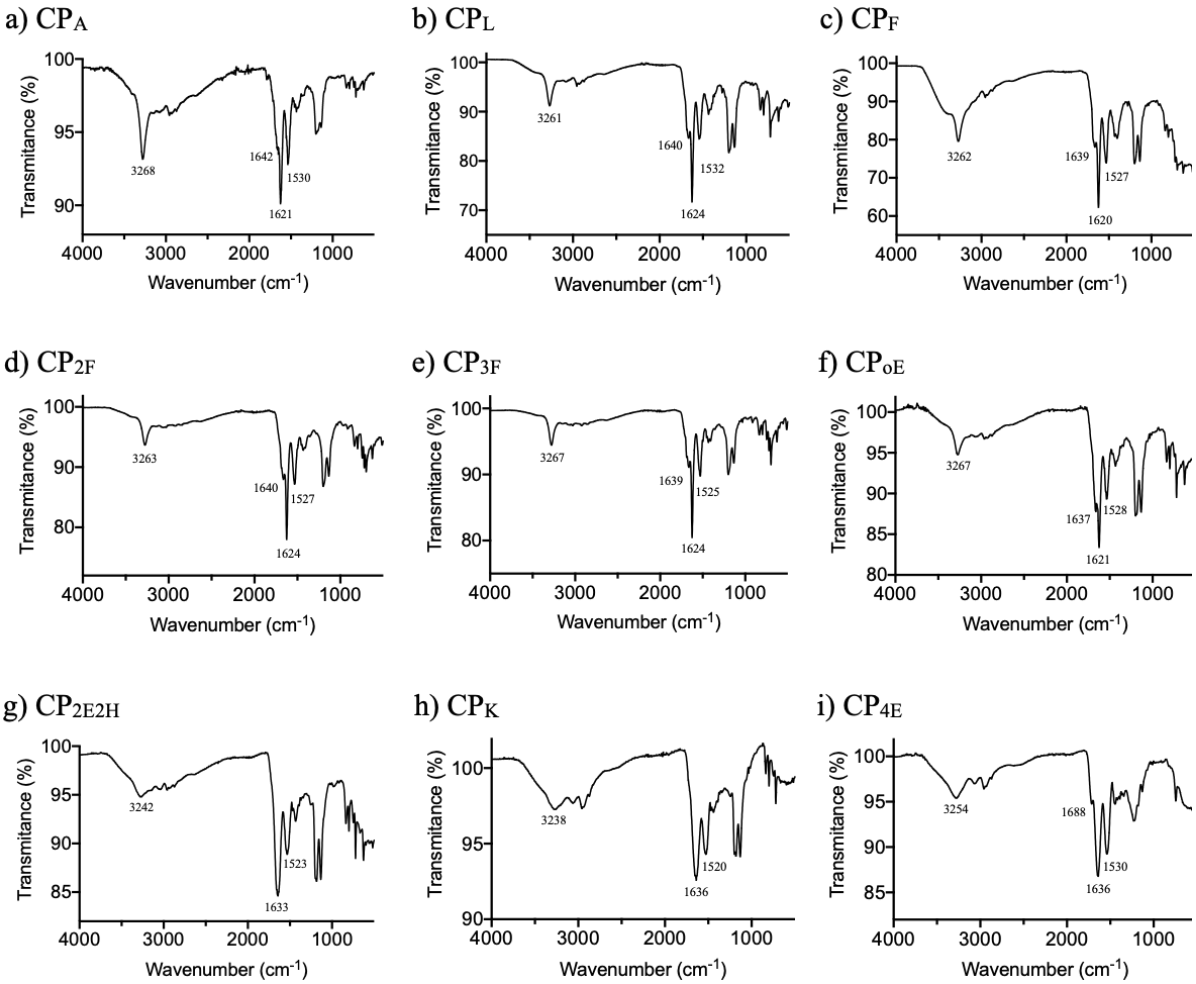

Figure 1.7. ATR-FTIR spectra for freeze-dried cyclic peptide samples. Values of wavenumber (cm-1) are indicated close to their corresponding amide peak.

The self-assembly process was studied by measuring changes in ThT emission with temperature. As previously mentioned, heat supply induces the 2D-to-1D backward isolation of nanotubes that subsequently, upon cooling, can orderly return to the final 2D nanosheet structure.[224] The coexistence of 1D and 2D supramolecular assemblies was initially observed by electron microscopy (STEM) (**Figure 1.5**) and could be confirmed with fluorescence spectroscopy (**Figure 1.8**). Firstly, we measured the changes in the intensity of emissions during the heating step, observing that they progressively decreased as the temperature increases up to 80°C (**Figure 1.8**a). Secondly, we fix the temperatura of the sample at 20°C and intensities at the maximum emission wavelength were recorded with time, observing that the system reaches a plateau at 60 min suggesting that supramolecular process is finished forming the final 2D nanostructures (**Figure 1.8**b).

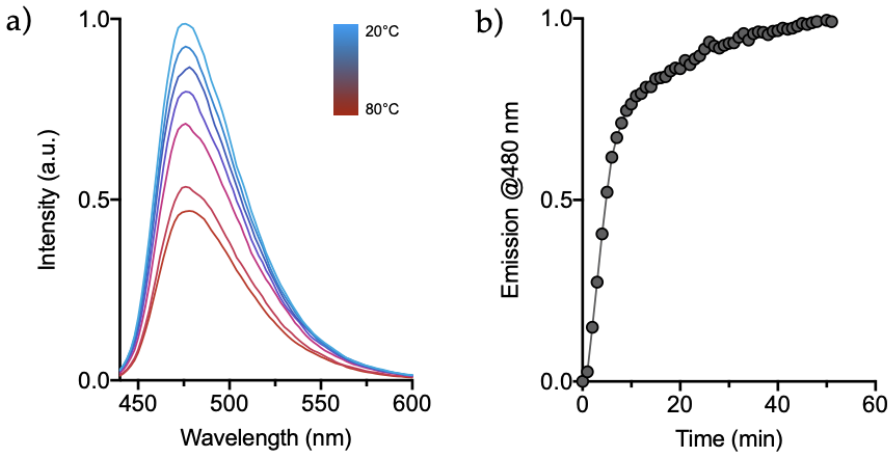

Figure 1.8. Overlay of the fluorescence emission spectra of ThT (10 μM) for a **CP$_A$** sample (50 μM in 20 mM sodium phosphate buffer at pH 7.4) heated from 20 to 80°C. Spectra were recorded with intervals of 10°C (20, 30, 40, 50, 60, 70 and 80°C) with 15 min of equilibration at each temperature. The total heating time was 90 minutes, following the self-assembly protocol. b) Representation of the fluorescence emission intensity at 480 nm of ThT (10 μM) in the previous **CP$_A$** sample over time, cooled from 80 to 20°C with emission recorded every minute. Both data were normalized to their respective maxima.

7.1.2.5. pH and ionic strength modulation

It has been shown that changes in pH or ionic strength can be employed to trigger the self-assembly of cyclic peptides thanks to the consequent modifications of the electrostatic balance between monomers.[243,244] Hence, we decided to test the formation of nanosheets with cyclic peptide variants that were unable to assemble in 2D nanosheets under the conditions previously described (i.e., 20 mM sodium phosphate buffer at pH 7.4) by adjusting pH and through the addition of NaCl.

As previously mentioned, a balance between attractive and repulsive supramolecular forces drives the hierarchical assembly and stabilizes the final nanosheet bilayer (**Figure 1.2**). Both **CP$_{2E2H}$** and **CP$_{4E}$** were not able to follow this assembly pathway due to the lack of correct supramolecular balance in their structure. Despite 2D assembly requires the repulsive contribution of negative charges of glutamic acids, it seems that these charges must be positioned apart and equilibrated with neighboring histidines. Therefore, we postulated that despite not having this requirement in the monomeric structure, it could be possible to achieve the desired assembly by changing external factors, such as pH and ionic strength.

Firstly, the self-assembly of **CP$_{2E2H}$** and **CP$_{4E}$** was studied by modulating the pH of sodium phosphate buffer from pH 7.4 to pH 2.0. Having a theoretical pk$_a$ of

[243] A. Méndez-Ardoy, A. Bayón-Fernández, Z. Yu, C. Abell, J. R. Granja, J. Montenegro, *Angew. Chem.Int. Ed.,* **2020**, *59*, 6902–6908.
[244] A. Méndez-Ardoy, J. R. Granja, J. Montenegro, *Nanoscale Horiz.,* **2018**, *3*, 391–396.

6.0 and 4.0 for histidine and glutamic acids respectively, they could change the monomeric charged state in the studied range. For **CP_{2E2H}**, the system will transition from a negatively charged state (-2) at pH 7.4 to the opposite situation at pH 2 with a positive charge (+2) passing through an intermediate state at pH 4.0 where glutamic acids are partially deprotonated and, therefore, the monomer has a net charge close to zero (**Figure 1.9**a). Neither of these conditions showed assembled structures, most likely, due to the excessive electrostatic repulsion between adjacent charged residues. Contrary, **CP_{4E}** presents a higher charged state at pH 7.4 (-4) due to the increased number of glutamic acids in the polar face which results in a more repulsive system preventing the order 2D arrangement (**Figure 1.9**b). At pH 2, the monomer will be fully protonated, lacking the balanced repulsion needed to maintain the nanosheet formation. Interestingly, **CP_{4E}** showed very small platelets (3.7±0.4 μm; n=20) at pH 4.0, which matches glutamic acid's pk_a, that could arise from a 1:1 equilibrium between repulsive anionic and attractive neutral ionization states (i.e., H-bonding), thus generating a certain tendency to assembly, but not enough to be arranged macroscopically in large nanosheets.

Secondly, with respect to ionic strength, the addition of NaCl to the solution could drive assembly by effectively shielding the negative charges, thus facilitating the formation of assemblies by overcoming the electrostatic barrier. However, micrographs of annealed samples with concentrations of NaCl ranging from 1 to 100 mM did not show any evidence of nanosheets or any other supramolecular structure (**Figure 1.10**). These findings suggest that the alternating position of charged amino acids is crucial to properly assemble, so both changes: **CP_{2E2H}** and **CP_{4E}** disrupt the delicate electrostatic balance required making the system less responsive to the addition of salts.

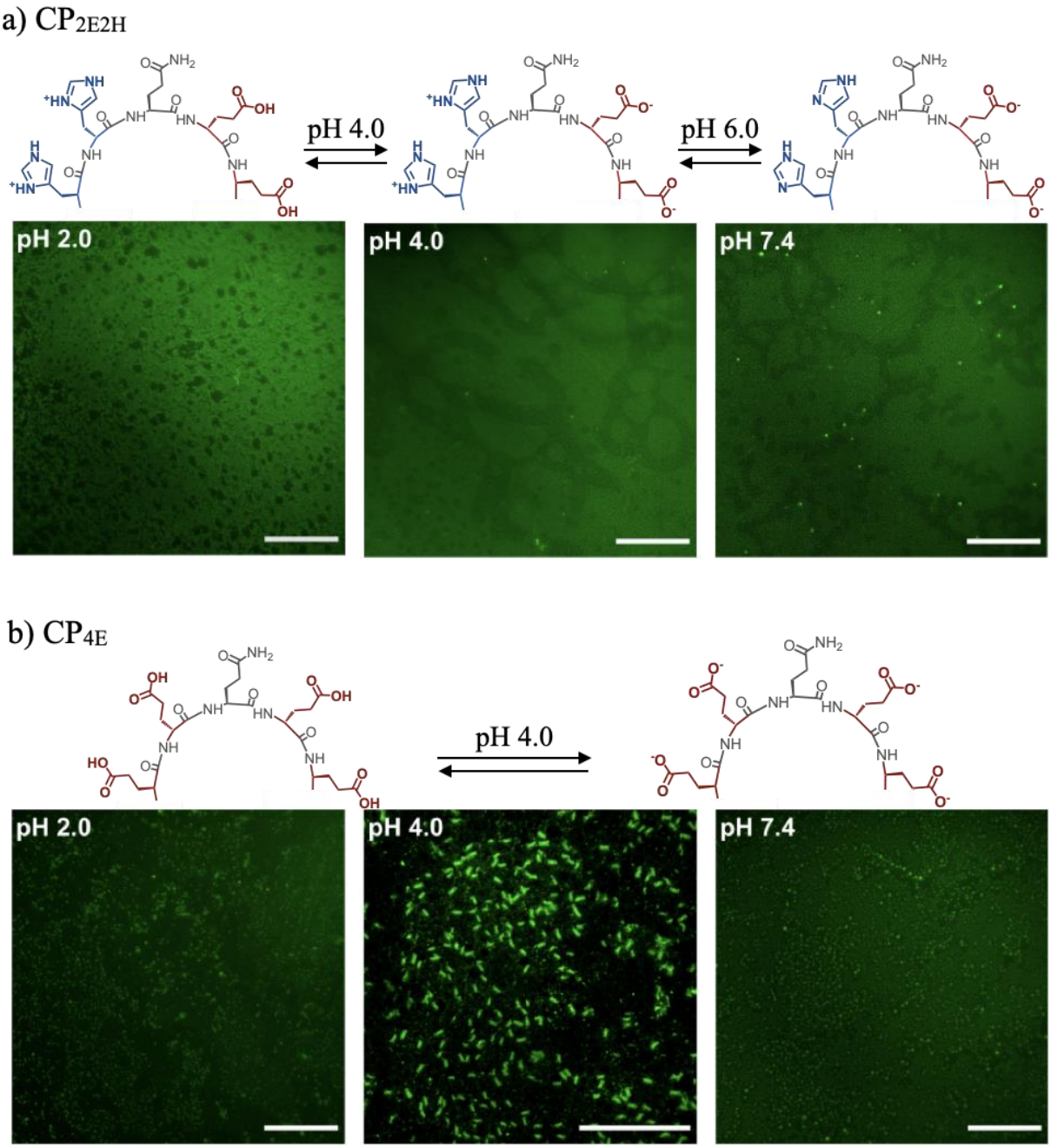

Figure 1.9. Epifluorescence micrographs of a) **CP$_{2E2H}$** and b) **CP$_{4E}$** at 50 μM in 20 mM sodium phosphate buffer adjusted at pH 7.4, 4.0 and 2.0 (from left to right, see insets) in presence of ThT (10 μM). Note that pH modulation was changed before the annealed protocol for 2D assembly (i. 80°C/1.5 h; ii. RT/1 h. Scale bar = 50 μm.

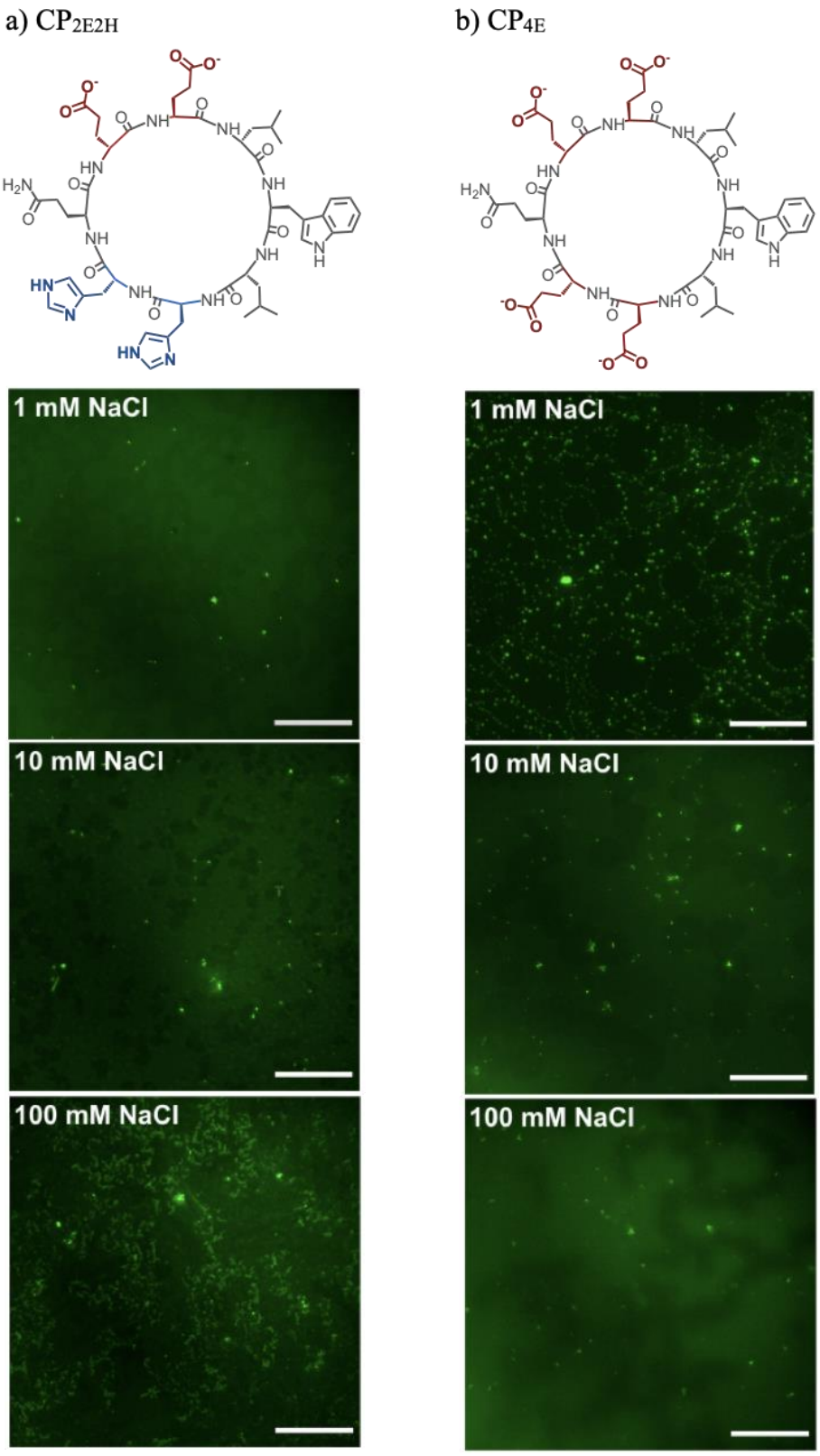

Figure 1.10. Epifluorescence micrographs of a) **CP$_{2E2H}$** and b) **CP$_{4E}$** at 50 μM in sodium phosphate buffer (20 mM, pH 7.4) with increasing concentrations of NaCl from 1 to 100 mM (from left to right, see insets) in presence of ThT (10 μM). NaCl solution was added before the annealed protocol for 2D assembly (i. 80°C/1.5 h; ii. RT/1 h). Scale bar = 50 μm.

7.1.3. Conclusions

In this chapter, we have described the systematic exploration of the relationship between the structure of **CP_x**, an octameric D/L-alternating cyclic peptide capable of sequential self-assembly in aqueous medium in 1D and 2D materials, and the formation of supramolecular aggregates. Firstly, we have designed a library of monomers with modifications in key positions in both hydrophobic and polar region (Scheme 1.2). From the nine new designed cyclic peptide, six of them could form 2D nanosheets (**Figure 1.4**). The conclusions that can be drawn from the results presented here are:

Modifications in the hydrophobic domain were well tolerated in general: the substitution of the central tryptophan residue for alanine (**CP_A**), leucine (**CP_L**) and phenylalanine (**CP_F**) showed the formation of nanosheets (**Figure 1.4**). The Leucine residues were more sensitive to modifications. For example, a certain degree of hydrophobicity is needed for the two flaking leucines, as substitution for the less hydrophobic alanine inhibits 2D assembly. However, it was also observed that **CP_L**, with a trileucine sequence, has a greater tendency towards disordered aggregation. Thus, we postulated that the hydrophobic tripeptide domain requires different lateral and central amino acids with a certain balance in the degree of hydrophobicity for efficient 2D packing. We probed this theory with a peptide with all hydrophobic amino acids replaced for phenylalanines (**CP_{3F}**), also showing nanosheets but with a highly wrinkled appearance and with many aggregates in the background. On the contrary, the substitution of the two leucines for phenylalanines (**CP_{2F}**), which maintains the mismatch between central and lateral positions, formed extended 2D nanosheets.

Modifications in the polar domain were more sensitive with a greater dependence of the 2D assembly on the ionized state of the monomer. It seems necessary to have a certain charge repulsion to maintain the formation of the 2D nanosheets (**Figure 1.2**). The replacement of both histidines for glutamic acids (**CP_{4E}**) increases the negative charge and hence the high electrostatic repulsion generated hinders self-assembly. On the other hand, a peptide without electrostatic repulsion (**CP_K**), is not capable of self-organizing into nanosheets. Moreover, the positioning of charged amino acids (i.e., anionic glutamic acid and buffering histidine) is critical, requiring adjacent positions for 2D assembly regardless of their order, as shown in **CP_{oE}** and **CP_x**, but never segregated in domains as observed for the 2D assembly inhibition of **CP_{2E2H}**.

These findings not only provide important design rules for the rational design of self-assembling cyclic (octa)-peptides, but also underpin supramolecular concepts and requirements (e.g., attractive-repulsive balance, non-covalent connector disposition, etc.) applicable to other peptide scaffolds and self-assembling monomers.

Table 1.2. Top: Depiction of cyclic peptide sequence for all variants and chemical structure of **CP$_x$**. Bottom: Summary of CP monomers tested specifying their differentiating characteristic from **CP$_x$** and the resulting 2D assembly.

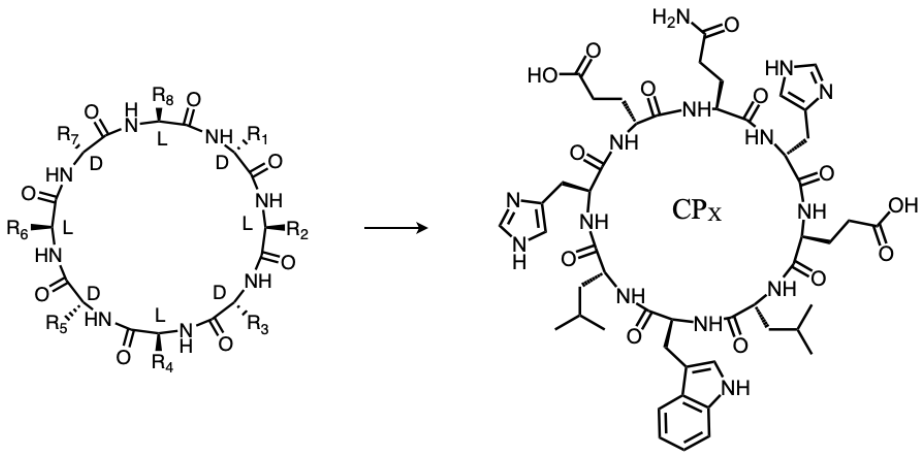

Hydrophobic domain		
Monomer	**Characteristics**	**2D assembly**
CP$_A$	R$_4$: W→A	Yes
CP$_L$	R$_4$: W→L	Yes
CP$_F$	R$_4$: W→F	Yes
CP$_{2F}$	R$_3$, R$_5$: L→F	Yes
CP$_{3F}$	R$_3$, R$_5$: L→F + R$_4$: W→3F	Yes

Polar domain		
Monomer	**Characteristics**	**2D assembly**
CP$_{2E2H}$	R$_2$, R$_6$ exchange: E↔H	No
CP$_{oE}$	R$_1$, R$_2$ exchange: H↔E	Yes
CP$_K$	R$_1$, R$_6$: H→K	No
CP$_{4E}$	R$_1$, R$_6$: H→E	No

7.2. SELF-ASSEMBLY OF CYCLIC PEPTIDE MONOLAYERS BY HYDROPHOBIC SUPRAMOLECULAR HINGES*

***Some of the results from this chapter have been done and published in collaboration with the group of Prof. Giovanni M. Pavan:**

Ignacio Insua,[a,b,] Annalisa Cardellini,[c,d,] Sandra Díaz,[a] Julian Bergueiro,[a] Riccardo Capelli,[e] Giovanni M. Pavan[c,d] and Javier Montenegro[a]. Self-assembly of cyclic peptide monolayers by hydrophobic supramolecular hinges. *Chemical Science*, **2023**, 14, 14074-14081.

DOI: 10.1039/D3SC03930G

Affiliations

[a] Departamento de Química Orgánica e Centro Singular de Investigación en Química Biolóxica e Materiais Moleculares (CiQUS), Universidade de Santiago de Compostela, Santiago de Compostela, Spain.

[b] Departamento de Farmacoloxía, Farmacia e Tecnoloxía Farmacéutica. Facultade de Farmacia, Universidade de Santiago de Compostela, 15782, Spain.

[c] Department of Applied Science and Technology, Politecnico di Torino, 10129 Torino, Italy.

[d] Department of Innovative Technologies, University of Applied Sciences and Arts of Southern Switzerland, Polo Universitario Lugano, 6962 Lugano-Viganello, Switzerland.

[e] Department of Biosciences, University of Milan, 20133 Milano, Italy.

7.2.1. Objectives

In the previous chapter, the sequence-assembly relationships of a 1D-to-2D self-assembling cyclic peptide were described, demonstrating the potential of these monomers in the construction of ordered nanostructures (**Figure 39**, **Figure 1.2**).[224,245] It has been shown that two-dimensional materials are achieved by controlling the propagation forces across different directions of growth.[119] This control can be achieved by designing monomers with non-covalent binding motifs strategically positioned. To this end, we proposed cyclic peptides as suitable monomers in hierarchical assemblies due to their unique structural properties: their rigid and planar conformation not only leads to the spontaneous formation of one-dimensional nanotubes, but it can also direct the axial self-sorting of orthogonal side chains around the nanotube. We have demonstrated that this spontaneous segregation of amphiphilic domains drives lateral contacts toward supramolecular elongation in a second dimension.

Based on this knowledge, we here propose to explore new design motifs in a cyclic peptide structure that allow modifying the direction of the propagation, thereby controlling the propagation directions and, ultimately, controlling the supramolecular polymerization towards the formation of newly assembled monolayer nanostructures.

Moreover, due to the lack of mechanistic understanding of these hierarchical assemblies at the molecular level, we rely on computational simulations to study in detail the different supramolecular stages along the polymerization process. We postulate that this investigation will help in implementing key general rules in the rational design of monomers for higher-order assemblies, thus shifting fundamental empirical work toward predictable designs.

To achieve the proposed objectives, we therefore established the following objectives:

- Design and synthesize a cyclic peptide monomer (**CP10**) with orthogonal non-covalent binding motifs within the sequence capable of guiding the self-assembly process toward a novel monolayer supramolecular architecture (**Figure 2.1**). Based on the previous CPx design, we would introduce two confronted hydrophobic faces to direct lateral contacts at an angle of 180°.

- Characterize, by microscopy and diffraction techniques, the self-assembly behaviour to study the potential assembly of the monolayered structure. Study the hierarchical process spectroscopically demonstrating the transition from 1D nanotubes to 2D nanostructures.
- Investigate the self-assembly mechanism of **CP10** monomers across different propagation stages by molecular dynamics simulations in order to study the system by all-atoms simulations and to a more collective behaviour by coarse-grained models. Additionally, we will question the impact that the new design motifs have on directing the self-assembly process.
- Design and synthesize **CP10** variants with specific mutations in the hydrophobic domain to experimentally validate computational studies.

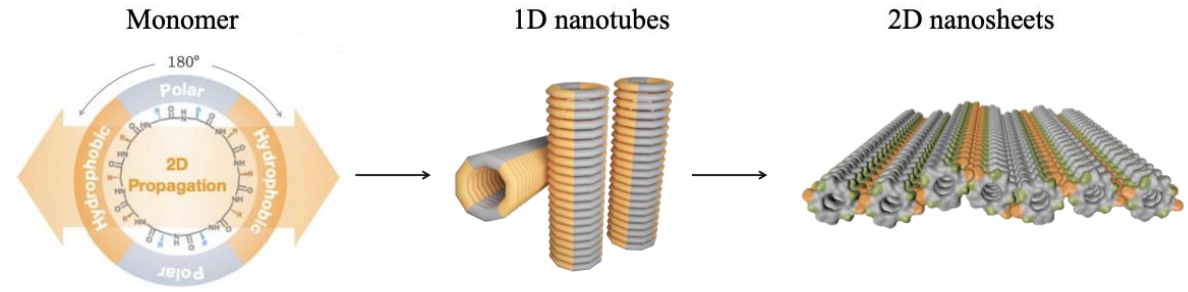

Figure 2.1. Schematic representation of the sequential self-assembly of a new cyclic peptide monomer. The cyclic peptide design has two orthogonal hydrophobic regions (orange) that drive the 2D propagation toward the formation of a monolayer within nanotubes laterally packed. Polar regions are exposed to the surface and are represented in grey.

7.2.2. Results and discussion

7.2.2.1. Design

Previous research has elucidated that the inherent rigidity of cyclic peptide monomers makes them suitable for assembling new hierarchical architectures.[224,245] This rigidity not only facilitates monomer fixation along 1D polymerization via inter-backbone hydrogen bonding but also leads to axial self-sorting tendency.[246] Consequently, we hypothesized that this self-sorting behaviour effectively constrains the rotational freedom of cyclic peptides within the nanotube, leading to the orthogonal segregation of different domains. Under this assumption, we hypothesized that by tailoring cyclic peptide scaffolds with complementary binding motifs in angle-defined positions, it is possible to predictably direct the elongation in 2D, generating new supramolecular architectures.

Drawing inspiration from the structural characteristics of **CPx**, particularly its hydrophobic domain responsible for directing nanotube elongation as a bilayer, we now incorporate two confronted hydrophobic faces strategically positioned to induce 2D elongation as nanotube monolayers (**Figure 2.1**). To this end, we designed a cyclic peptide composed of 10 amino acids alternating their D/L chirality **CP10**: cyclo-(L-Trp-D-Leu-L-Glu-D-His-L-Leu-D-Trp-L-Leu-D-Glu-L-His-D-Leu) as represented in **Figure 2.2**. The size of the monomer was increased from eight to ten amino acids with the aim to incorporate the same hydrophobic tripeptide, previously found to be optimal in two bilayer assemblies, while preserving both polar charged amino acids used in octameric **CPx**. As depicted in **Figure 2.2**, while **CPx** self-assembles in a bilayer with nanotubes staggered in a zig-zag configuration, the new **CP10** design self-assembles in a monolayer driven by lateral contacts between interfacing hydrophobic domains. In addition to the hydrogen bonding and hydrophobic effect, electrostatic interactions also play a crucial role in stabilizing assembled nanosheets. As discussed in detail in previous sections, these nanosheets remain extended thanks to a delicate balance between these supramolecular forces (**Figure 1.2**). At physiological pH 7.4, histidines become neutralized while glutamic acids are negatively charged, thus generating negative surfaces on both sides of the monolayer (**Figure 2.2**, grey square). As a result, this electrostatic repulsion maintains the nanosheets completely flat and prevents them from folding or aggregating with themselves or with neighbouring nanosheets.

[245] S. Díaz, I. Insua, G. Bhak, J. Montenegro, *Chem. Eur. J.,* **2020**, *26*, 14765–14770.
[246] M. Panciera, E. Gonzalez-Freire, M. Calvelo, M. Amorín, J. R. Granja, *J. Pept. Sci.,* **2020**, *112*.

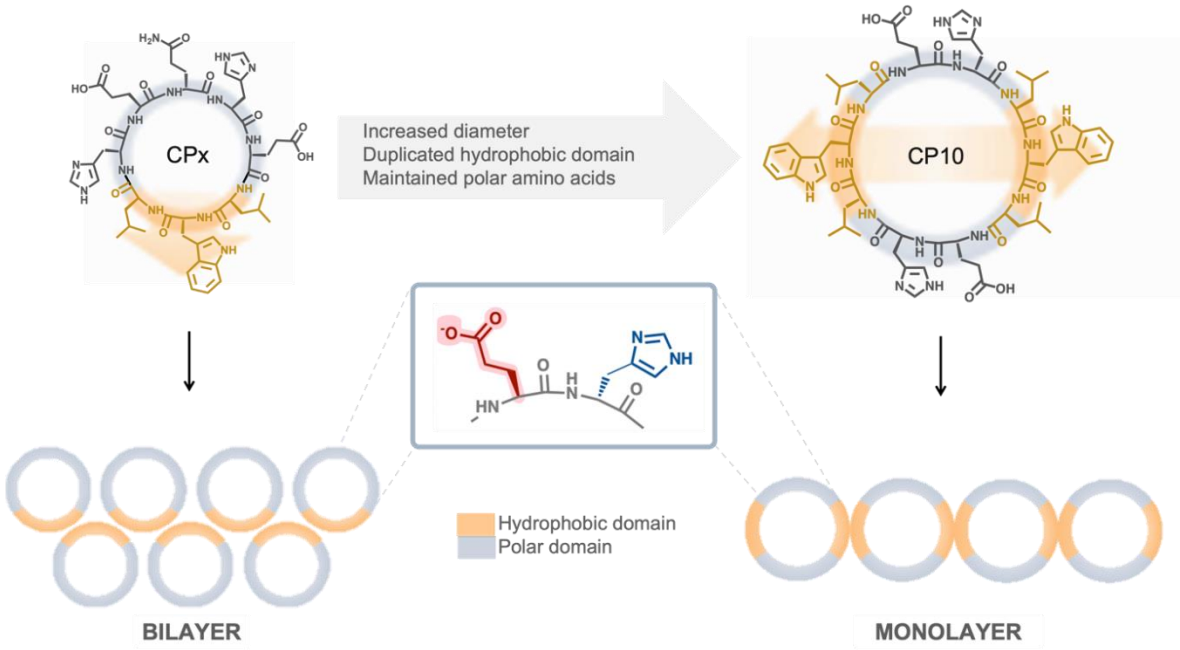

Figure 2.2. Rational design and structural scheme of self-assembled cyclic peptides. (Left) Primary amino acid sequence of the previous **CPx** and the new **CP10** monomers with color coding of the hydrophobic (orange) and polar (grey) regions. (Right) Schematic representation of 2D nanotubular assemblies achieved with each monomer. In the grey square in the middle the ionization state of polar residues is represented, highlighting the negative glutamic acids in red.

7.2.2.2. Microscopic analysis of self-assembly

To experimentally test our supramolecular design, the synthesized **CP10** (**Scheme 2**, Methodologies section 2.2) was dissolved in 20 mM sodium phosphate buffer at pH 7.4. The samples were subjected to a heating-cooling cycle to gradually anneal the monomers (see self-assembly protocol in methodologies). This process can help dissociate any kinetically trapped aggregates, thus starting the self-assembly process at maximum monomer solubility for a more ordered assembly. Firstly, we evaluated the assembled structures by epifluorescence microscopy. For this, we prepared **CP10** samples at different concentrations (10, 50, 100 μM) following the annealing protocol above with the addition of thioflavin-T (ThT).[236] Nanosheets were observed at all concentrations, reaching over 100 μm in lateral dimensions for the highest value (**Figure 2.3**a). It must be noted that micrographs were acquired from dry samples (see section 6.2.4 in methodologies), demonstrating the structural robustness of the supramolecular 2D ensemble even out of solution. The laminar 2D morphology was further confirmed by scanning-transmission electron microscopy (STEM). In this case, a sample at 100 μM was annealed without ThT, and similar rectangular nanosheets were observed (**Figure 2.3**b). Notably, the edges of the sheets seem very straight, suggesting ordered lateral packing of the nanotubes. In both cases, certain folds and wrinkles appeared, probably due to a drying effect on the surface.

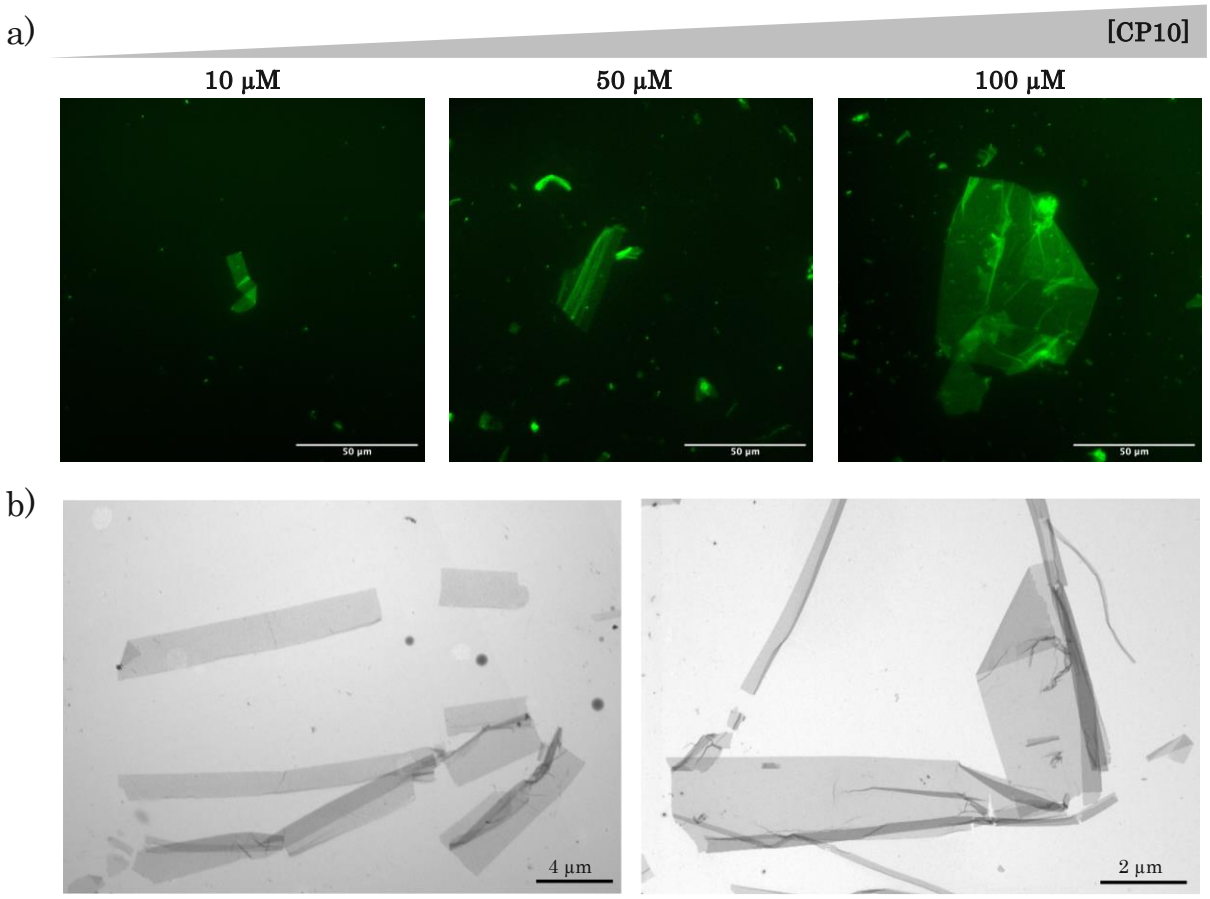

Figure 2.3. a) Epifluorescence micrographs of assembled samples of **CP10** at different concentrations. b) STEM images of an assembled sample **CP10** at 100 μM diluted at 10-fold in MilliQ. Images were taken after annealed samples (50 μM) for 2D assembly, (i. 80°C/1.5 h; ii. RT/1 h) in sodium phosphate buffer (20 mM; pH 7,4). ThT (10 μM) was added to the samples after annealing protocol. STEM samples (without ThT) were stained with phosphotungstic acid.

Atomic force microscopy (AFM) revealed a thickness of approximately 2.6 nm for nanosheets (**Figure 2.4**a). We hypothesized that this value could correspond to a monolayer arrangement based on the previous investigations from **CP$_x$**. Drawing parallelisms between both systems, if a bilayer of **CP$_x$**, with only 8 amino acids, exhibited a thickness of 3.2 nm and isolated nanotubes 1.6 nm wide, we could expect an intermediate thickness for **CP10** nanotube monolayers between these two values: larger than **CP$_x$** nanotubes (1.6 nm) and smaller than a **CP$_x$** bilayer (3.2 nm), because of the larger size with 10 amino acids. Furthermore, we could not isolate any nanotubular assemblies from **CP10** samples. We attribute this difficulty to the higher hydrophobicity of **CP10** compared to **CPx** (**Figure 2.4**a), which could potentially hinder the visualization of isolated nanotubes, as they are prone to aggregate in solution. However, high-resolution TEM revealed two perpendicular diffraction spacings, providing details about the arrangement of nanotubes within the monolayer (**Figure 2.4**b). The first spacing at 4.7 Å, corresponds to the reported distance between 1D stacked cyclic peptides, corroborating the presence of aligned nanotubes forming the nanosheets.[180] The second spacing at 2.8 Å, could be assigned to the lateral contact between the

aromatic residues of the nanotubes, indicative of their 2D elongation within the assembly.

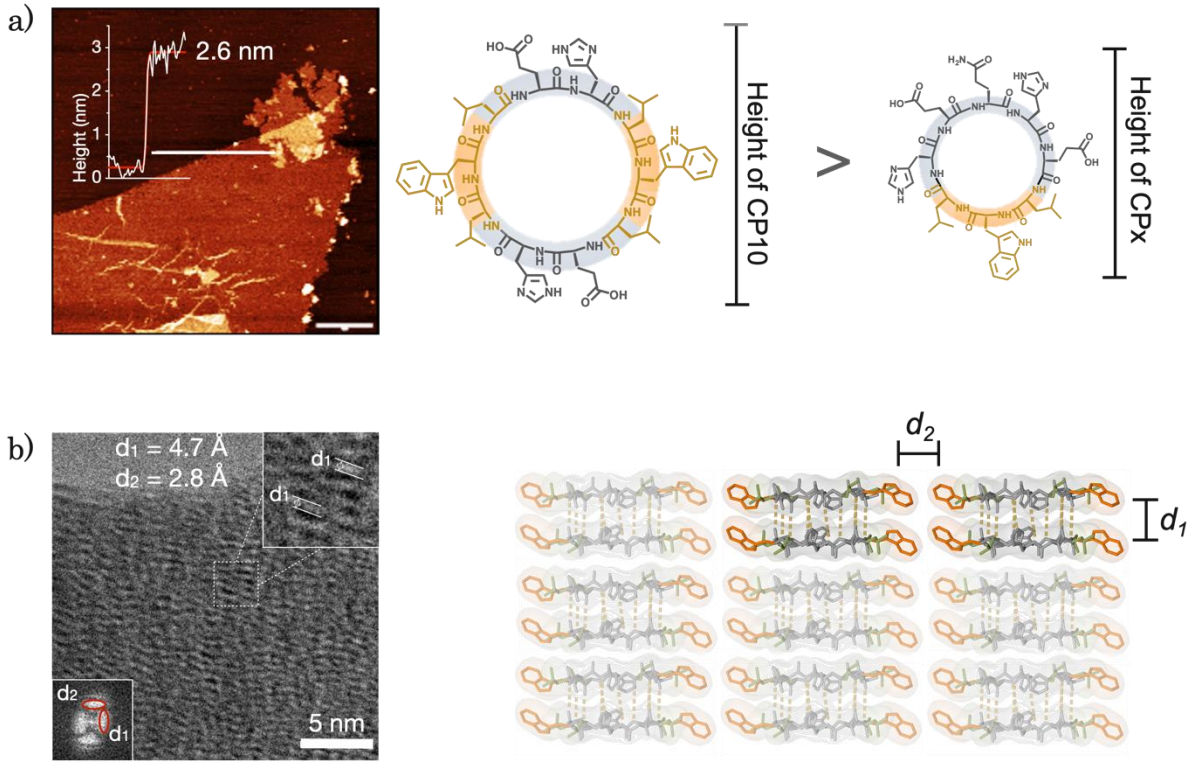

Figure 2.4. a) Left: AFM image of an assembled monolayer with the height profile corresponding to the white line intersecting the nanosheet. Right: Comparison between the expected heights for **CP10** and **CPx** monomers. b) Left: Electron diffraction pattern by HR-TEM and its Fourier transform (inset) revealing two predominant distances. Right: schematic representation of both distances in the nanotubular structure where d_1 correspond to the axial spacing of stacked **CP10** and d_2 to the lateral contact between closed nanotubes.

7.2.2.3. Spectroscopic characterization

Having confirmed the formation of **CP10** monolayers, we decided to study the internal arrangement of monomers within the ensemble. Fourier transform infrared spectroscopy (FTIR) exhibited characteristic bands corresponding to key amide vibrations (**Figure 2.5**a). Specifically, peaks were observed at 1525 cm^{-1} for Amide II (N-H bending), 1637 and 1700 cm^{-1} for Amide I (C=O stretching), and 3277 cm^{-1} for Amide A (N-H stretching). Relating these observations with previous studies reported on peptide conformation, we hypothesized that **CP10** monomers could be adopting an antiparallel β-sheet conformation along the nanotube axis (**Figure 2.5**b).[241] This configuration typically displays a lower frequency band below 1640 cm^{-1} and a higher frequency band above 1680 cm^{-1}. In contrast, the parallel conformation lacks the higher frequency band and exhibits two components between 1640 and 1670 cm^{-1}. Since the peak at a higher frequency is not sharp and well-defined in the spectrum, it is possible to observe a clear shoulder at 1700 cm^{-1}, supporting the antiparallel configuration.

Circular dichroism (CD) provides further insights into the internal organization, particularly concerning the interaction between indole groups of tryptophan residues.[247] The CD spectrum (**Figure 2.5**c) revealed exciton-coupling bands at 210 and 226 nm, indicative of spatially ordered interactions between proximal tryptophan residues, consistent with previous findings. Moreover, an increased signal in the near UV CD region, around 280 nm, suggests that the indole side chains are in a well-defined chiral environment within the assembled nanosheets.

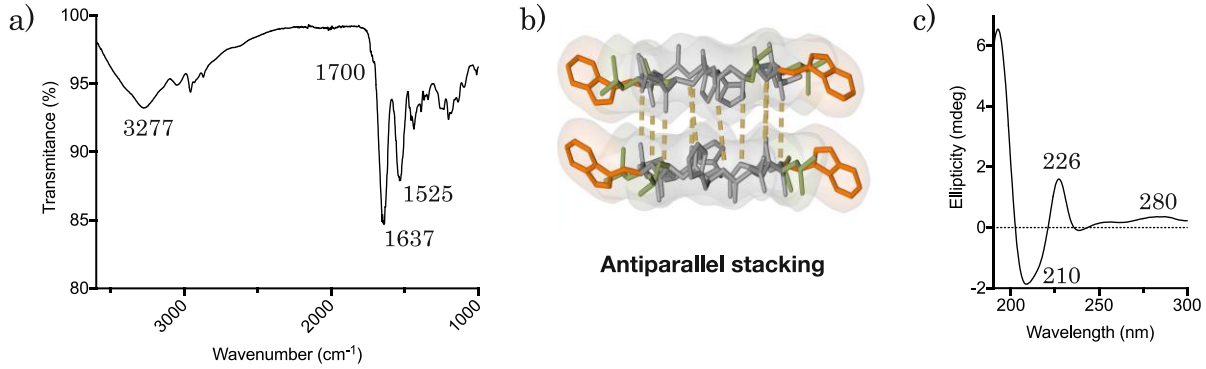

Figure 2.5. a) FTIR of freeze-dried **CP10**. Values of frequency (cm^{-1}) are indicated close to their corresponding Amide peak. b) Antiparallel stacking of two cyclic peptide monomers, dashed lines represent the hydrogen bonding between peptide backbones. c) Circular dichroism of an assembled **CP10** sample at 100 μM. Values for minimum and maximums are indicated.

The self-assembly process was evaluated by fluorescence titrations. Firstly, we determined the critical aggregation concentration (CAC) by tracking the changes in tryptophan emission with increasing concentrations of **CP10** (**Figure 2.6**a). The results indicated a clear change at 5 μM, indicating that nanosheet formation begins at this value. This observation was in agreement with previous epifluorescence micrographs, which probed the formation of nanosheets at 10 μM. Secondly, to further elucidate the assembly mechanism, we conducted temperature-dependent fluorescence studies. Building upon the previously explained **CPx**, we hypothesize a similar 1D-to-2D transition, where nanotubes first form and subsequently pack laterally to create the monolayers. Notably, the self-assembly protocol involved heating samples to ensure maximal monomer solubility and a cooling step where nanotubes can be arranged orderly. To validate this hypothesis, we initially monitored changes in the emission intensity of tryptophan while incrementally heating the sample, registering the spectrum every 10°C. The observed changes in the spectrum (**Figure 2.6**b) may be attributed to a solvation effect of Trp indoles with solvent molecules, resulting in solvatochromic alterations. Specifically, the decreased tendency as temperature increases can arise from a higher molecular motion due to the solvent interacting with them, disrupting the packing arrangements. The resulting spectrum

[247] A. G. Cochran, N. J. Skelton, M. A. Starovasnik, *Proc. Natl. Acad. Sci.,* **2001**, *8*, 5578-5583.

(**Figure 2.6**b) exhibited a decrease in intensity, which may be attributed to enhanced molecular motion and disrupted packing arrangements at elevated temperatures. Afterward, we cooled the heated sample to 20 °C and we monitored fluorescence emission over time (**Figure 2.6**c). Results revealed a rapid increase in emission intensity within 5 min, followed by a plateau extending up to 60 min. We postulate that this observation can explain the difficulty in isolating nanotubes in previous AFM analyses. The hydrophobicity of **CP10** makes nanotubes very unstable in solution, thus exhibiting a rapid tendency to pack via solvophobic effects once the temperature starts to decrease. Therefore, we evaluated this behavior by taking aliquots and depositing them at the initial point (Figure 6c (i) t=0 min; 80°C) and final point (Figure 6c (ii) t=60 min; 20°C) of the measurement. The resulting micrographs showed nanosheets in both cases, confirming their rapid assembly.

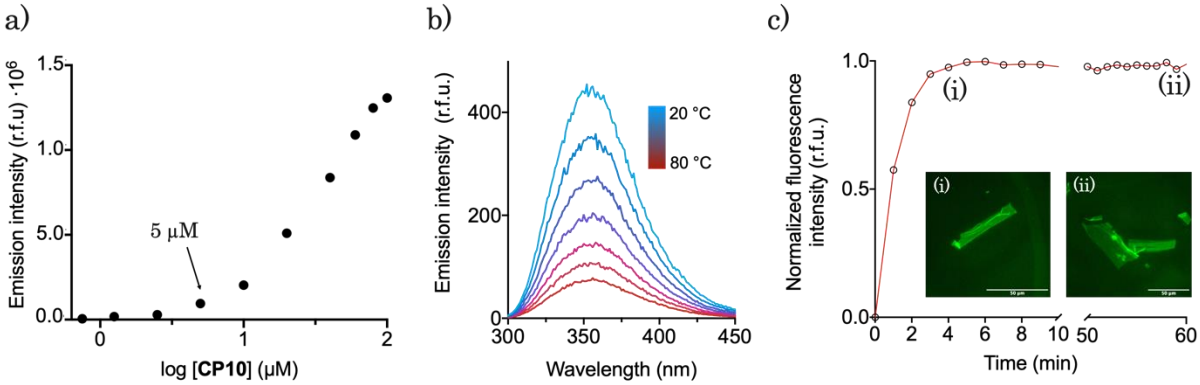

Figure 2.6. a) Critical aggregation concentration of **CP10**. The graph represents the variation in the Trp emission with respect to **CP10** concentration. Samples at different concentrations were annealed as described in the self-assembly protocol. b) Overlay of the emission spectra of Trp gradually decreasing temperature for a sample of **CP10** at 100 µM. c) Representation of the cooling step for the previous heated sample. Emission intensity at 350 nm is represented over time.

7.2.2.4. Assembly behavior with pH

As previously found for the bilayer-forming peptides (*Chapter* 7.1), the assembly behavior of CPs can be influenced by variations in pH. The formation of stable supramolecular ensembles relies on maintaining a negatively charged surface to balance hydrophobic effects with electrostatic repulsion, preventing uncontrolled aggregation. **CP10** was designed based on the structural characteristics of **CPx**, maintaining both polar charged amino acids (glutamic acid and histidine) in between the hydrophobic faces. With this arrangement in the sequence, the resultant monolayer structure should leave these polar residues exposed. Therefore, we postulate that it should have a similar behavior with pH. To prove it, samples of **CP10** were prepared at a concentration of 100 µM across a pH range from 5.6 to 7.4. These pH values were strategically chosen to explore the influence of different ionization states on assembly dynamics (**Figure 2.7**a). Epifluorescence micrographs confirmed our expectations, revealing a

disappearance of nanosheets with progressive acidification below the pk_a value of histidine (**Figure 2.7**a b). This observation underlines the necessity of maintaining a negative net charge within the monomers, with histidines neutralized and contributing to the stabilization of the 2D monolayer through salt bridges with nearby glutamic acids.

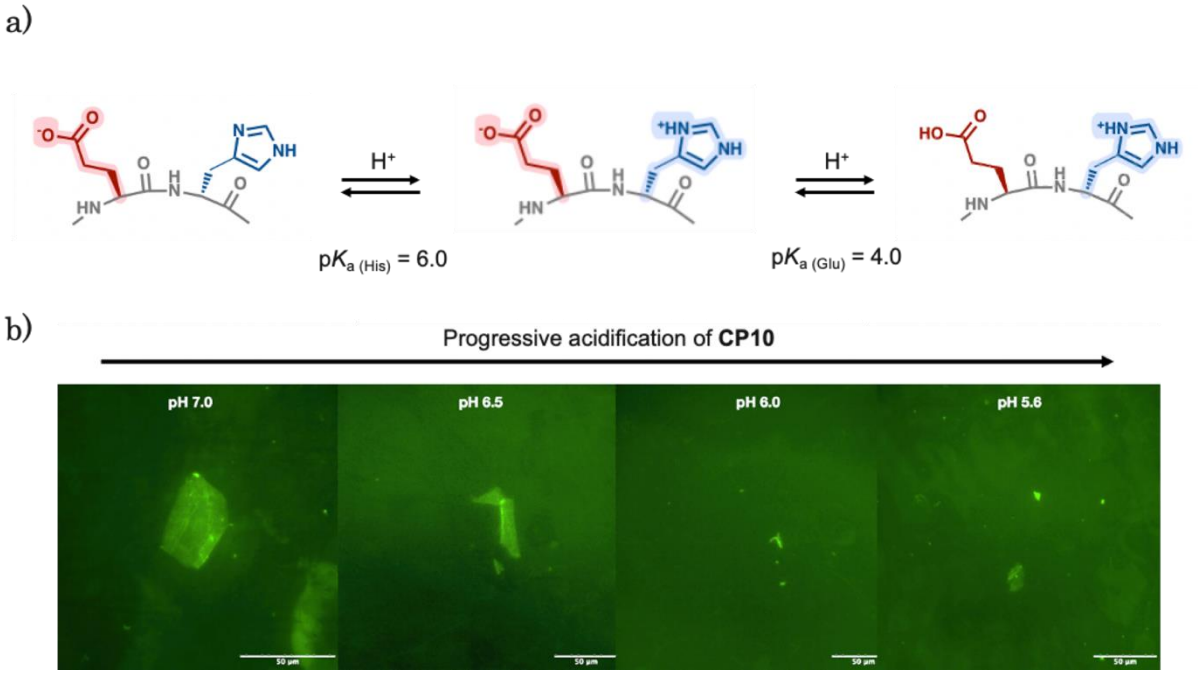

Figure 2.7. a) Ionization states of polar charged amino acids. b) epifluorescence micrographs of assembled **CP10** samples prepared at different pH values. Images were taken after annealed samples (50 µM) for 2D assembly, (i. 80°C/1.5 h; ii. RT/1 h) in sodium phosphate buffer (20 mM) at a pH adjusted with HCl 1M. ThT (10 µM) was added to the samples after annealing protocol.

7.2.2.5. Computational approaches for studying self-assembly behavior

We next hypothesized that the self-assembly process occurs hierarchically, progressing from the initial formation of 1D nanotubes to the final 2D nanosheets. Therefore, computational simulations were also explored to delve into this hypothesis and help unravel the underlying mechanism governing **CP10** self-assembly. In collaboration with the group of Prof. Giovanni Pavan, we gradually progressed from fundamental systems (all-atoms simulations) to more complex molecular populations (coarse-grained models), aiming to elucidate the underlying mechanism that dictates the possible supramolecular stages along the polymerization process.

All-atoms molecular dynamic simulations: Parallel vs. Antiparallel

All-atoms (AA) molecular dynamics (MD) simulation is a computational technique employed to study the behavior of molecules, providing a detailed understanding of their interactions and motion at the molecular level. In this study, we investigated the most stable conformation of **CP10** monomers within nanotubes by comparing the parallel and antiparallel configurations (**Figure 2.8**; left). Each atom in the system is explicitly represented, along with its covalent and non-covalent interactions. To evaluate the stability of both conformations, the energy kinetic profile of the system was recorded over time (100 ns). Simulations were performed in water and the energy profile represented in the graph corresponds to the top two **CP10** monomers within the nanotubes, represented with a darker color (**Figure 2.8**). The results revealed that the most stable conformation is the antiparallel, as previously postulated based on the FTIR experiment. In the MD simulations is possible to observe how the potential energy of the parallel conformation increased after 60 ns while the antiparallel value remained constant over time. As depicted in Figure 8b, this is related to the disassembly of the system in the parallel conformation, suggesting the antiparallel as the energetically favorable state.

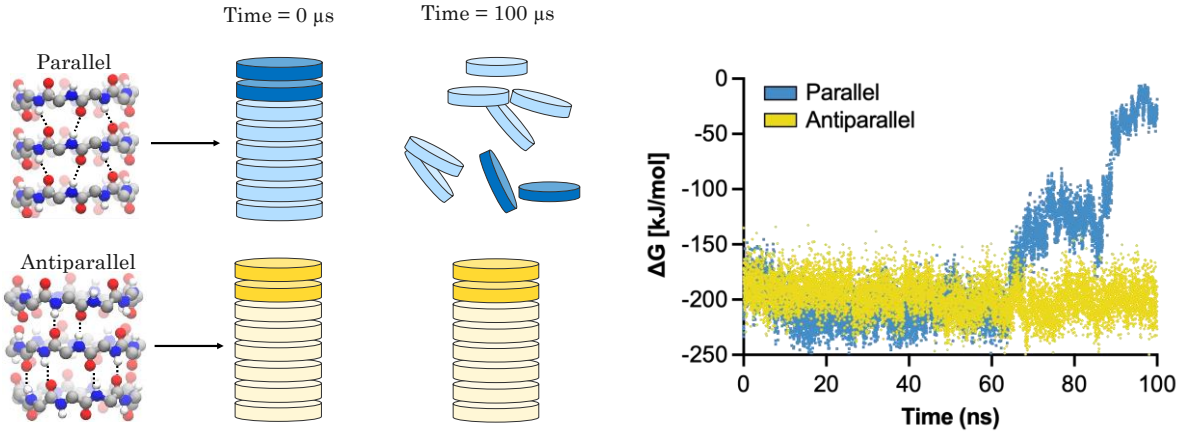

Figure 2.8. Left: Atomistic representation of **CP10** in parallel (top) and antiparallel (bottom) configurations. Middle: MD simulations of one single nanotube made of eight **CP10** units stacked in either parallel (blue) or anti-parallel (yellow) configuration at the initial and final time of the simulation. Right: Potential energy of both configuration over time. The data show the total interaction energy, including both Lennard-Jones and Coulomb potentials, between the top two **CP10** units of the nanotubes (in darker colour) simulated for 100 ns in aqueous solution.

In silico modeling of self-assembly mechanism: <u>Dimerization energies</u>

Once we confirmed the antiparallel conformation was more stable, we then used in silico modeling to study the self-assembly process of **CP10** oligomers. Specifically, we calculated the dimerization energies of **CP10** oligomers, both in axial and lateral directions, as a function of their degree of oligomerization. By comparing these energies, we aimed to identify any supramolecular bias

promoting either axial or lateral propagation as polymerization progresses. Axial growth is represented in red and denotes 1D elongation (nanotube formation) and lateral growth is represented in green and indicates 2D elongation (lateral packing of nanotubes) (**Figure 2.9**). It is important to note that oligomers of **CP10** are named as 'xCP10-NT', "x" being the number of **CP10** monomers forming the nanotube (NT).

Utilizing umbrella sampling (US), we obtained the potential of mean force (PMF) profile of two approaching xCP10-NTs with fixed orientation (preventing rotational movement), from a non-interacting distance (ΔG=0 in **Figure 2.9**a,b) to the assembled state (ΔG minima in **Figure 2.9**a,b), either in axial (red) or lateral (green) directions. PMF was calculated for the axial and lateral dimerization for oligomers from 1 to 8 cyclic peptides. As an example, we showed the axial dimerization of 3CP10-NT (**Figure 2.9**a) and the lateral dimerization of 8CP10-NT (**Figure 2.9**b). This allowed us to obtain the global minimum of Gibbs free energy for each case, which is correlated with the binding strength between the oligomers under study. By representing the global free energies as a function of the oligomerization state, it is possible to observe different tendencies for axial and lateral dimerization (**Figure 2.9**c). Short oligomers, particularly those ranging from 3-5mers (3CP10-NT and 5CP10-NT), exhibited significantly higher axial association energies compared to larger and shorter ones. We attributed this phenomenon to their increased backbone rigidity compared to shorter oligomers, as their larger H-bonding network imparts directionality and stability. This situation stabilizes terminal faces in the nanotubes (i.e., CPs in the ends) since the more rigid and stronger the bond, the more favorable the addition of more monomers. Indeed, we performed an estimation of the interfacial matching to compare the dimerization of 1CP10-NT and 3CP10-NT based on the packing angle and deviation from a reference cyclic peptide (**Figure 2.10**). The results showed that the shorter nanotube exhibits greater deviation and reduced propensity for interfacial matching, thus leading to weaker axial dimerization energies. Moreover, we postulate that the cooperative axial elongation drops from pentamers onwards because of the more defects that can be generated and amplified along the nanotube, which decreases the tendency for a perfect alignment.[248,249]

Regarding lateral 2D association, dimerization energies could only be extracted from 4mer blocks onwards, showing a gradual increase in association energy up to a 7mer state (**Figure 2.9**c). These phenomena can be rationalized by the enhanced hydrophobicity of longer oligomers, that enhances their solvophobic 2D packing and limits the lateral association of small oligomers to a negligible energy value.

[248] D. Bochicchio, S. Kwangmettatam, T. Kudernac, G. M. Pavan, *ACS Nano,* **2019**, *13*, 4322–4334.
[249] A. L. de Marco, D. Bochicchio, A. Gardin, G. Doni, G. M. Pavan, *ACS Nano,* **2021**, *15*, 14229–14241.

Overall, whereas axial elongation seems favored in short oligomers, the lateral association is enhanced by larger ones, suggesting an inversion of the preferential dimension of growth in favor of 2D propagation as nanotubes propagate. Therefore, these results are consistent with a hierarchical assembly mechanism, where **CP10** monomers grow axially until a certain hydrophobicity threshold, which then favors the lateral association of tubular oligomers.

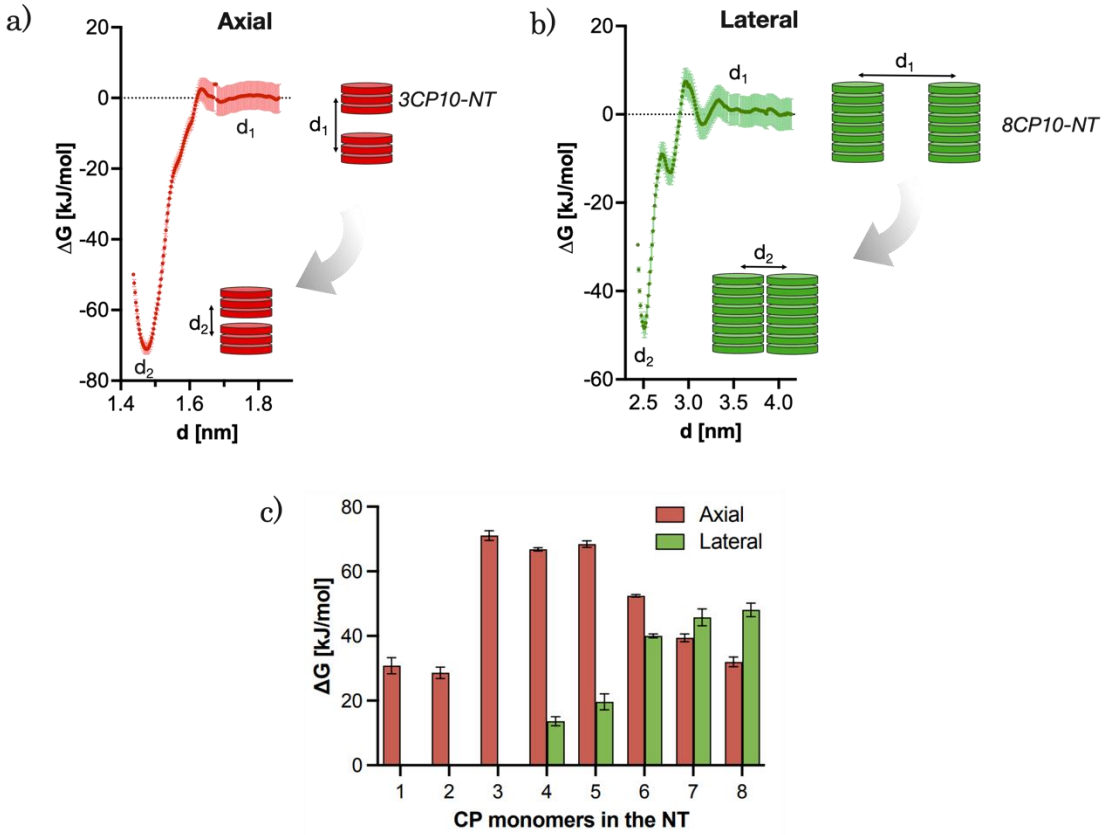

Figure 2.9. a) Potential of Mean Force (PMF) profile of two **3CP10-NTs** in axial assembly and antiparallel configuration. 'd' indicates the distance between the centre of mass of the nanotubes. b) PMF profile of two **8CP10-NTs** in lateral assembly and antiparallel configuration. c) Global free energy (ΔG) minima, i.e. dimerisation free energy, for **CP10** nanotubes in axial (red) and radial (green) association (see B-C) as a function of their oligomerisation degree in antiparallel configuration. Error bars were obtained from the PMF calculation. Because of their low probability to laterally assemble, **1CP10-NT**, **2CP10-NT** and **3CP10-NT** have a negligible lateral (green) dimerisation ΔG.

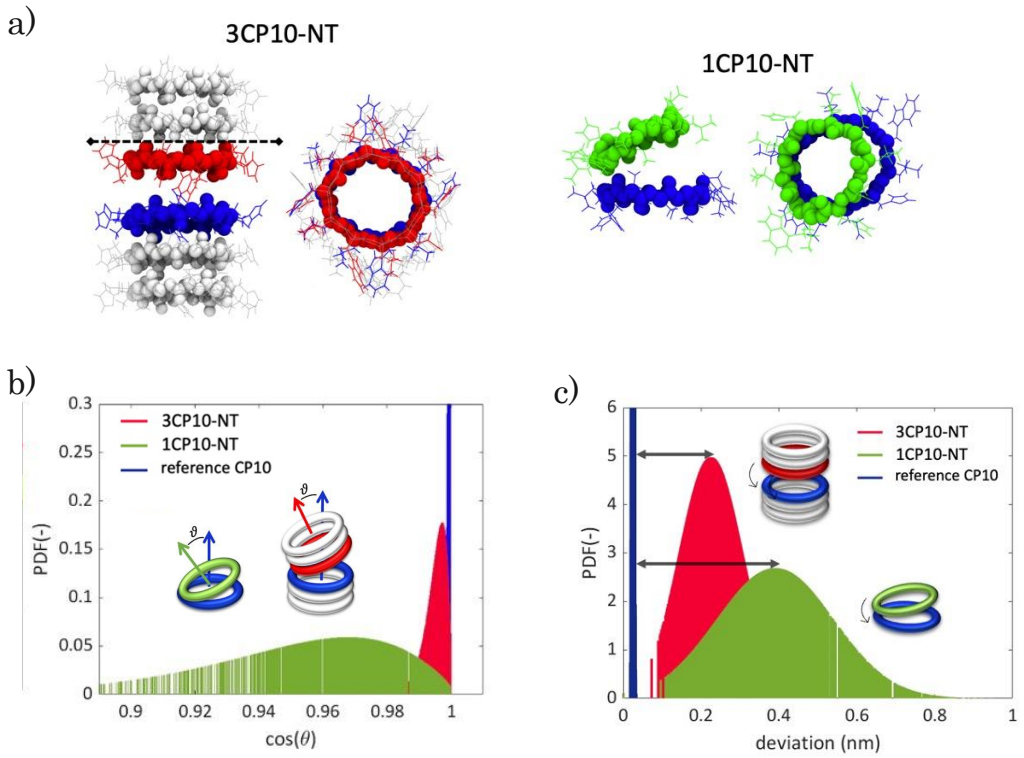

Figure 2.10. a) Side and front view of 3mer (**3CP10-NT**) and monomer (**1CP10-NT**) PMF snapshots at 0.7 nm distance during dimerisation. Blue cyclic peptides function as reference for red and green ones, which are selected to quantitatively estimate the angle and deviation of interfacial matching. b) The interfacial matching of the NTs during the oligomerisation process is calculated from the angle (ϑ) between the plane of approaching NTs (green/red versus blue). The time distribution of cos(ϑ) and the probability distribution function (PDF) of cos(ϑ) show that the shorter **1CP10-NT** interface deviates more from the ideal oligomerisation interface value of cos(ϑ) = 1. c) The probability distribution function (PDF) of the deviation shows that the shorter **1CP10-NT** deviates more from its reference while the oligomerisation takes place (PMF).

Well-tempered metadynamics simulations: Tryptophan lateral contacts

Well-tempered metadynamics simulations are a computational tool that allows the exploration of more complex transitions compared to AA-MD during the assembly process.[250] By applying bias potentials, these simulations allow the investigation of the energy landscape of a system across specific variables. Specifically, we employed this technique to investigate the lateral packing of two contacting nanotubes, composed of 8 monomers (8CP10-NT). The specific variables chosen for this study were: (i) the number of contacting tryptophan residues between two nanotubes (y axis, the higher the value, the more contact points between tryptophans) and (ii) the sum of distances between the center of mass of the two cyclic peptides at the top and bottom of two laterally interfacing nanotubes (x axis). For the latter, long distances ($d_1+d_2 > 5$ nm; **Figure 2.11** left) represent axially mismatched nanotubes that cannot fully connect their hydrophobic

[250] . Barducci, G. Bussi, M. Parrinello, *Phys. Rev. Lett.,* **2008**, *100.*

domains, and short distances (d_1+d_2 ~ 4 nm; **Figure 2.11** right) correspond to NTs in parallel and aligned orientation, favorable for 2D elongation.

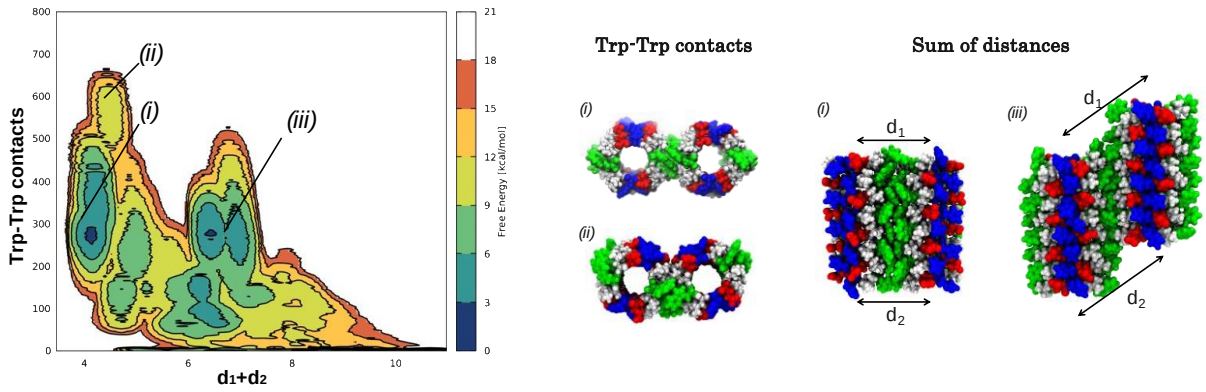

Figure 2.11. Free energy surface (FES) metadynamics simulation of the spatial evolution of two 8CP10-NTs shown as free energy surface mapping as a function of Trp-Trp contacts and sum of d_1+d_2 distance. Structural snapshots at different states.

Free energy landscapes of the spatial evolution of two 8CP10-NT were projected along these two geometrical parameters (**Figure 2.11**). At first glance, it was possible to observe different thermodynamic states, being the blue ones the most stable. Analyzing in detail the energy profile we selected three energy minima for detailed analysis, two in the region at short distances and other at long distances, referred to as (i), (ii) and (iii) in the figure, to analyze the structural disposition of the nanotubes. The snapshots in **Figure 2.11** (Trp-Trp contacts and sum of distances), represent the different states with a dual Trp-Trp and Leu-Leu interface for the most stable and less thermodynamically favored direct Trp-Trp contact. Notably, both configurations can spontaneously exchange during the simulation. Given the symmetry and complementarity of the **CP10** structure, with His and Glu residues on opposite sides, both directions of rotation are possible (**Figure 2.12**). These findings suggested the necessity for flexibility within the hydrophobic interface to facilitate the formation of 2D monolayers. We therefore hypothesized that the tryptophan contacts could serve as the supramolecular motif to impart this required flexibility, thereby promoting efficient lateral packing of the nanotubes. This adaptable motif, which we coined as the "tryptophan hinge", facilitates the effective rotation of nanotubular interfaces, crucial for the assembly of stable 2D nanosheets.

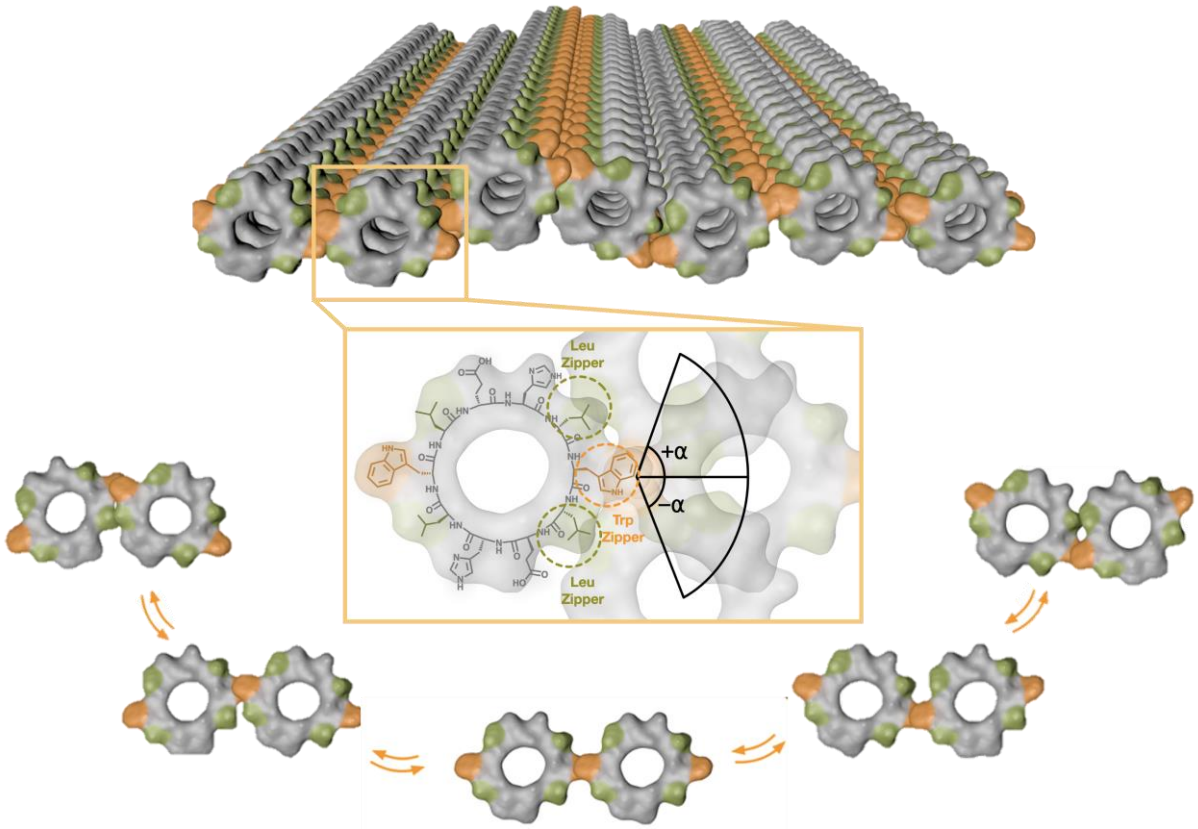

Figure 2.12. Supramolecular structure of a two-dimensional monolayer assembled from nanotubes through lateral hydrophobic contacts between aligned Trp (orange) and Leu (green) residues of **CP10**. In the bottom the lateral contact model: 'Trp hinge' with the aromatic residue pivoting between the two possible Leu zippers is represented.

Coarse-grained modeling of nanotube assembly

To further interrogate the assembly of multiple CP10-NTs, a coarse-grained (CG) model was constructed to simulate the system beyond the calculation limits of atomistic molecular dynamic simulations. This model allows the evaluation of the self-assembly behavior of complex systems by simplifying their computational representation. The simplification consists of grouping atoms into beads, reducing the level of detail of all-atom studies while maintaining their chemical and physical properties. In our study, the CG model for **CP10** monomers was built by adopting the protein Martini force-field philosophy, with beads differentiating both backbones and side chain atoms (**Figure 2.13**a).[251] The bond interactions between the beads were optimized with Swarm-CG software to reproduce the equilibrium arrangement of one single monomer within a nanotube.[252] Additionally, virtual dipole sites (depicted in blue and red) were added to simulate intermolecular forces and improve the directional orientation of **CP10** packing in

[251] S. J. Marrink, H. J. Risselada, S. Yefimov, D. P. Tieleman, A. H. De Vries, *J. Phys. Chem. B,* **2007**, *111*, 7812–7824.
[252] C. Empereur-Mot, L. Pesce, G. Doni, D. Bochicchio, R. Capelli, C. Perego, G. M. Pavan, *ACS Omega,* **2020**, *5*, 32823–32843.

the resultant CP10-NT. It is worth noting that, while the Martini CG force field is very well suited to treat the hydrophobic interactions between the NTs during the self-assembly (e.g., 2D-growth due to lateral Trp-Trp interactions), the treatment of directional hydrogen bonding is not trivial in CG models. As recently performed for other supramolecular polymers where hydrogen-bonding plays a major role, the addition of rigid virtual site dipoles in this CG model allows to approximate well (via dipole-dipole interactions) the effect of H-bonds in keeping these NTs as stacked and rigid as in the previous AA models.[253,254,255]

The first simulation carried out consisted of analyzing the dynamic evolution of different xCP10-NTs over time (**Figure 2.13**). The spatial evolution of NTs during this simulation was analysed based on their relative orientation and represented as cos(θ) versus time; "θ" being the average angle created by the longitudinal axes of all possible NT pairs, leading to cos(θ) values of 0 for all perpendicular and 1 for all parallel NT axes, as represented in **Figure 2.13**b. Three different oligomers were studied (3CP10-NT, 4CP10-NT and 6CP10-NT) and simulations showed that the oligomerization degree significantly influences the NT alignment and hence 2D self-assembly. While the value of cos(θ) for the 3CP10-NT remains constant at 0.5 (i.e., random alignment) during the whole simulation, larger oligomers showed a gradual increase to 1 with time, thus meaning a parallel alignment between NTs required for 2D elongation. As shown in the snapshots (**Figure 2.13**c), a cluster with random orientation of NTs is achieved over time for 3CP10-NTs. In contrast, larger oligomers induce an all-parallel cluster, showing that a minimum of 4 cyclic peptides within a nanotube is enough to act as a nucleus for lateral growth (i.e., 4CP10-NT). If we compare these results with previous ΔG values found in all-atoms MD simulations, is possible to observe the same tendency, as values found for lateral contact of shorter oligomers were negligible. Overall, CG modelling did not show a significant improvement in 2D association dynamics for a longer 6C10P-NT oligomer, suggesting 4CP10-NT is suitably balanced in hydrophobic strength and diffusion/rotation freedom for 2D propagation.

[253] D. Bochicchio, M. Salvalaglio, G. M. Pavan, *Nat. Commun.,* **2017**, *8*.
[254] D. Bochicchio, G. M. Pavan, *ACS Nano,* **2017**, *11*, 1000–1011.
[255] D. Bochicchio, G. M. Pavan, *J. Phys. Chem. Lett.,* **2017**, *8*, 3813–3819.

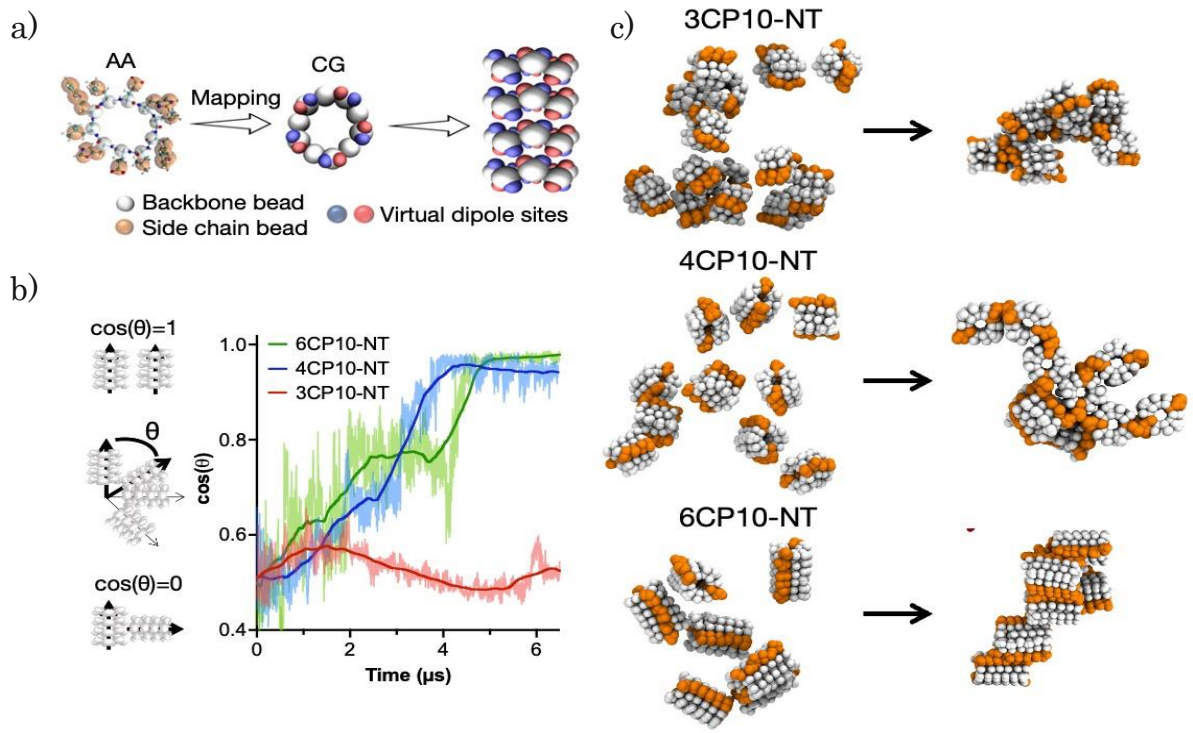

Figure 2.13. a) Coarse-grained (CG) mapping of all-atoms (AA) **CP10** structure and nanotube (NT) assembly. b) Time evolution of the average cos(θ) between the tube central axes of all possible NT pairs. Randomly oriented NTs generate a cos(θ) = 0.5 at the beginning of the simulation, which can evolve over time to an all-parallel configuration (i.e. cos(θ) = 1). c) Examples of CG-MD snapshots of **CP10-NTs** of different 1D oligomerisation states (3, 4 and 6) in aqueous solution. The snapshots show the **CP10-NT** configurations at the initial state (left) and after 5 μs of CG-MD simulations (right). Orange beads indicate hydrophobic tryptophan residues working as 2D propagation interfaces.

CG-MD simulations were then performed with variations in the hydrophobic strength (Δ_{hpho}) of Trp to study the contribution of this central amino acid to the 2D-driving Trp hinge motif. As a model, the self-assembly of ten 4CP10-NTs was assessed by their ability to aggregate into one single cluster of aligned nanotubes (i.e. cos(θ) = 1) as a function of Δ_{hpho} (**Figure 2.14**a). In these experiments, a Δ_{hpho} value of 0 corresponds to the native hydrophobicity of Trp —used in all previous calculations. The system was tested with an initial 50% reduction of Δ_{hpho}, showing dispersed and randomly aligned NT clusters unable to elongate in 2D. A milder 30% reduction of Δ_{hpho} led to a single NT cluster with aligned 1D axes, hence successfully assembling in 2D despite taking longer to reach the 2D state than the native Trp (**Figure 2.14**b,c). Regarding the hierarchical 1D-to-2D assembly pathway, a comparison between 2D cluster size and cos(θ) shows that NTs first come together into a single cluster, which then reorganizes cooperatively to align all 1D axes (Figure 14d). It is also clear that the reduction of Trp's Δ_{hpho} compromises NT clustering and axial alignment. Together with the energy mapping of Trp-Trp contacts, these experiments confirmed the central role of the Trp residue in driving the second hierarchy of self-assembly in 2D based on the geometrical flexibility of this interface. Importantly, Trp Δ_{hpho} reductions could not

be compensated by adjacent Leu residues –unmodified across all simulations–, reinforcing the need for a hinging Trp-Trp interface for lateral elongation.

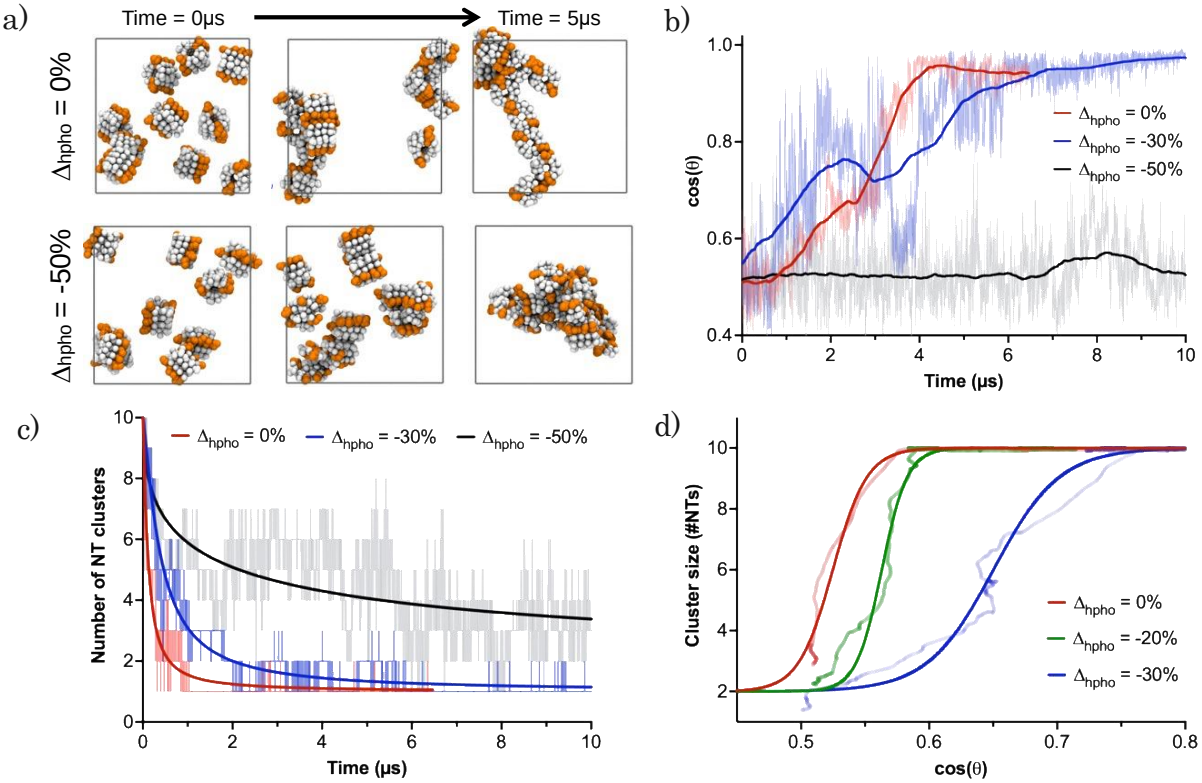

Figure 2.14. CG-MD simulations of ten **4CP10-NTs** in aqueous solution with variations in the hydrophobic strength of Trp residues (Δ_{hpho}; see methods). a) Snapshots of the native **4CP10-NT** model (Δ_{hpho} = 0) and a customised analogue with Trp beads displaying a 50% reduction of their original hydrophobic strength (Δ_{hpho} = -50%). Orange beads indicate tryptophan residues. b) Time evolution of the average cos(ϑ) between the longitudinal axes of all possible NT couples. c) Time evolution of the number of **4CP10-NT** clusters versus Δ_{hpho}. d) Self-assembly pathway as function of Δ_{hpho} comparing solvophobic **4CP10-NT** clustering versus relative orientation based on Trp's hydrophobic character

7.2.2.6. Sequence variations of CP10

To assess the importance of the tryptophan hinge (i.e., Leu-Trp-Leu) for the solvophobic stabilization of the tubular monolayers, four **CP10** variants with modified hydrophobic domains were synthesized: **3L**, bearing a Leu triad with no steric mismatch between residues; **LW**, **2W** and **2L** only possessing two hydrophobic residues (**Figure 2.15**). The hydrophobic amino acids removed from these structures were replaced by histidine and glutamic acid in confronted positions to maintain alternating charge neutrality with polar residues. By design, neither variation should be capable of establishing pivotal Trp hinges (**Figure 2.12**) due to the lack of Trp or additional Leu contacts. Microscopic analysis of samples did not show any 2D nanosheets, only high-aspect ratio assemblies that may result from nanotubular bundles associated through less ordered hydrophobic packing (**Figure 2.15**). These results suggest that the structural flexibility of the

Trp hinge allows tubular interfaces to adjust their orientation and compensate for local misalignments during the lateral elongation of 2D monolayers.

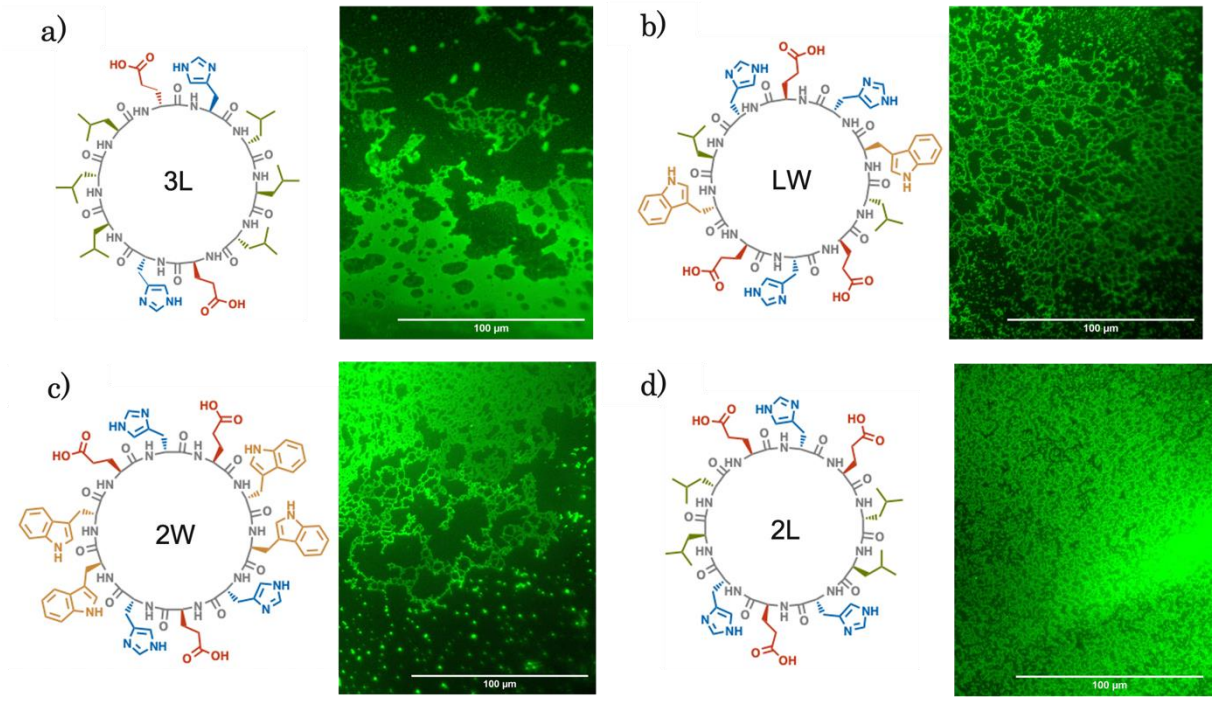

Figure 2.15. Structures and epifluorescence micrographs of **CP10** variants: a) **3L**, b) **LW**, c) **2W** and d) **2L**. Images were taken after annealed samples (50 µM) for 2D assembly, (i. 80°C/1.5 h; ii. RT/1 h) in sodium phosphate buffer (20 mM; pH 7,4). ThT (10 µM) was added to the samples after annealing protocol.

Moreover, we also evaluated the influence of the polar region on the assembled state. We designed two variants by placing both histidine and glutamic acid at different positions within the sequence: **EHEH** and **2E2H** (**Figure 2.16**). We have shown in the previous chapter that these residues must be placed together to form bilayer nanosheets (**Figure 1.4**). We hypothesized that if they were segregated on the same side, the repulsion generated along the nanotube would cause instability in the assembly. It should be noted a main difference between previous structures of $\mathbf{CP_x}$ and variants and the newly designed **CP10** monomer: while $\mathbf{CP_x}$ is stacked in parallel conformation within the nanotube, **CP10** prefers an antiparallel conformation. Therefore, we postulate that **CP10** could maintain the assembled monolayer even with the **2E2H** variation. The reason is that with the antiparallel conformation, the domains with the same residue will be alternated along the nanotube, therefore stabilizing the assembly (Figure S2.11, Experimental section 10.2.2). As expected, the microscopic analysis of these mutations confirmed the formation of nanosheets in both cases (**Figure 2.16**).

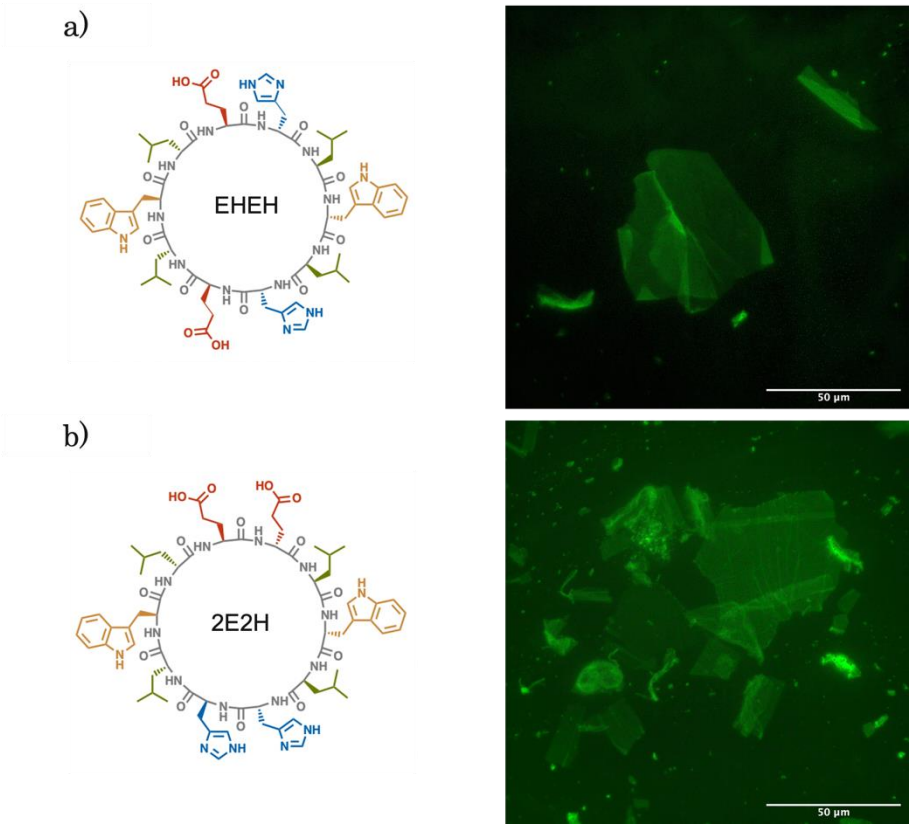

Figure 2.16. Structure and epifluorescence micrograph of **CP10** variants: a) **EHEH** and b) **2E2H.** Images were taken after annealed samples (50 µM) for 2D assembly, (i. 80°C/1.5 h; ii. RT/1 h) in sodium phosphate buffer (20 mM; pH 7,4). ThT (10 µM) was added to the samples after annealing protocol.

7.2.3. Conclusions

In this chapter, we have studied the hierarchical supramolecular polymerization of a new cyclic peptide monomer forming monolayered structures. We have extensively studied the assembly process with both experimental and computational techniques.

Firstly, we engineered a hierarchically self-assembled architecture by incorporating two hydrophobic domains into a CP monomer with increased diameter: **CP10**, *cyclo*-(L-Trp-D-Leu-L-Glu-D-His-L-Leu-D-Trp-L-Leu-D-Glu-L-His-D-Leu). Nanotubes from **CP10** self-sorted their amphiphilic domains and generated confronted hydrophobic faces. As a result, two-dimensional elongation was induced at a 180° angle, forming a monolayered structure from peptide nanotubes in lateral association. We have characterized the formation of this new architecture by microscopy and diffraction techniques, demonstrating the lateral packing of nanotubes along a single monolayer in aqueous conditions (20 mM sodium phosphate buffer pH 7.4; CAC: 5 μM). Moreover, we have studied the self-assembly process through spectroscopic techniques, demonstrating the transition toward the assembled state.

Secondly, we have used atomistic and coarse-grained models to simulate the self-assembly of **CP10** monomers and mechanistically elucidate the polymerization process. A set of molecular dynamics (MD) simulations revealed a bias towards two-dimensional propagation based on the degree of polymerization of pre-formed nanotubular assemblies. **CP10** monomers preferentially undergo one-dimensional elongation at short oligomerization states (*i.e.* 3CP10-NT and 4CP10-NT), while longer oligomers prefer 2D propagation as their hydrophobic character is amplified along the tubular axis. Additionally, CG-MD modelling has shown that polymerization is a stepwise process consisting of the hydrophobic clustering of nanotubes, initially in random orientation, to be then realigned in parallel for lateral extension. Interestingly, metadynamics simulations have demonstrated that the formation of monolayers is maintained due to the flexibility imparted by the hydrophobic tripeptide: Leu-Trp-Leu. Since tryptophan residues play a key role in maintaining this pivoting non-polar interface, we call this new design motif a “tryptophan hinge”.

Finally, we have demonstrated the relevance of the “tryptophan hinge” motif by designing a library of cyclic peptide monomers with selected mutations in the hydrophobic region. Control experiments by epifluorescence microscopy confirmed the incapability of monomers lacking either the central tryptophan residue or lateral leucines to self-assemble in 2D. These results further confirmed the importance of the Leu-Trp-Leu triad to allow flexible contact between nanotubes with the freedom to exchange Leu zippers in either direction.

These findings demonstrated the supramolecular versatility of cyclic peptides of alternating chirality for the rational design of hierarchical self-assembled systems across different dimensions of space. Moreover, we postulated that the new mechanistic concepts introduced in this chapter pave the way for the rational design and assembly of complex architectures from custom peptide monomers.

7.3. 3D SELF-ASSEMBLY OF CYCLIC PEPTIDES INTO MULTILAYERED NANOSHEETS

7.3.1. Objectives

As discussed in the previous chapters, the key feature for designing monomers capable of self-assembling into different morphologies lies in an appropiated arrangement of non-covalent binding motifs throughout the monomer structure. The rational disposition of confronted domains can bias the supramolecular propagation towards different directions, thus controlling the dimensionality of the resultant architecture.[245,256] It is possible to find many examples describing 1D and 2D peptide-based nanomaterials (Introduction, section 0), but very few have achieved a higher level of complexity (3D) as the controlled interplay between non-covalent forces also becomes more difficult. Therefore, there is still a challenge in the design of simple monomers capable of directing their self-assembly into ordered three-dimensional structures.

Indeed, the fabrication of 3D systems with monomers aligned in a controlled way could facilitate the final achievement of crystallinity, an interesting property from the point of view of materials science.[257] Crystallinity enhances materials' properties such as mechanical strength or chemical stability, while also offering precise control over important features like anisotropy or aspect ratio. This control can extend also to the size and shape of the resultant structure as well as the internal arrangement. However, a significant challenge in the fabrication of 3D materials through self-assembly lies in achieving those uniformity and reproducibility.

As opposed to the classical crystallization based on a diffusion-controlled growth process, where crystals growth in a supersaturated medium by the successive incorporation of components migrating from smaller crystals, the hierarchically oriented organization is a new concept for the final fabrication of self-assembling crystals.[257] This process involves a particle-mediated growth mechanism where the spontaneously oriented organization of primary assembled structures acts as a nucleus to drive the successive arrangement of monomers yielding higher-order assemblies. Therefore, these oriented assemblies required the formation of long-range directional interactions to stabilize their successive growth alogn different directions of propagation

Based on this information and in successful results of the previous chapters, we hypothesized that cyclic peptide monomers could also be tailored to direct their self-assembly toward the third dimension. As cyclic peptides stack into 1D nanotubes through a directional hydrogen bonding network, this stable arrangement could behave as nucleus promoting the orientation of additional nanotubes. We have previously observed that these nanotubes are orderly packed

[256] I. Insua, A. Cardellini, S. Díaz, J. Bergueiro, R. Capelli, G. M. Pavan, J. Montenegro, *Chem Sci* **2023**, *14*, 14074–14081.
[257] C. Yuan, W. Ji, R. Xing, J. Li, E. Gazit, X. Yan, *Nat Rev Chem* **2019**, *3*, 567–588.

into bilayers (Chapter 7.1) or monolayers (Chapter 7.2) through solvophobic effects depending on confronted domains. We here propose that this hierarchical assembly can also grow in 3D dimension introducing an additional attractive force that specifically propagates the system in an extra direction forming a multilayered packing (**Figure 3.1**).

To this end, we proposed the following objectives:

- To design a new cyclic peptide monomer capable of directing the self-assembly towards 3D nanostructures. In addition to hydrogen bonding and hydrophobic effects, electrostatic interactions will be used to direct growth along the third dimension.
- To study the self-assembly of the new monomer by testing different conditions and then analyze the resulting nanostructures through microscopy and diffraction techniques.
- Design a library of new monomers to decipher structure-assembly relationships.

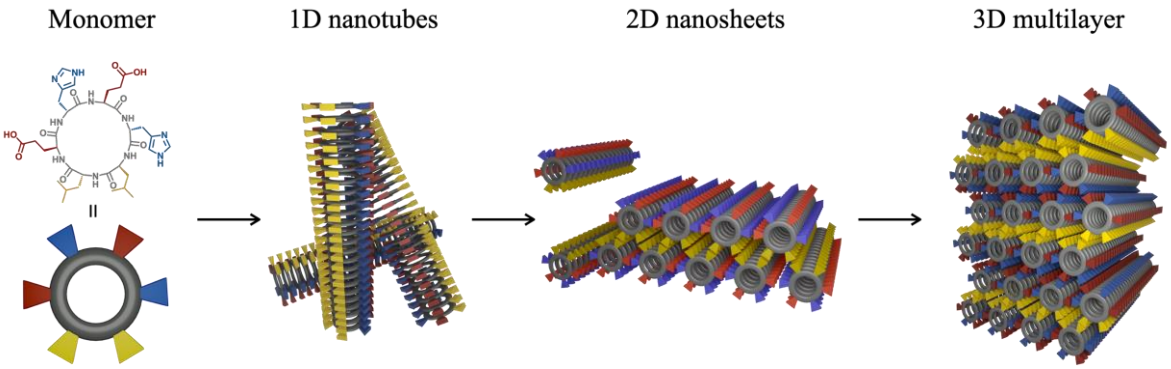

Figure 3.1. Proposed assembly model for a cyclic peptide formed by six amino acids. Left: Hydrophobic residues are represented in yellow while negatively and positively charged residues are represented in red and blues, respectively.

7.3.2. Results and discussion

7.3.2.1. Cyclic peptide design

As demonstrated in previous chapters, an amphiphilic cyclic peptide equipped with a hydrophobic domain can promote the sequential self-assembly from 1D nanotubes into higher-ordered 2D structures.[224,256] While hydrogen bonds direct the stacking of cyclic peptide monomers along nanotubes (1D growth), solvophobic effects drive their ordered lateral packing into nanosheets. This ordering is modulated by the different dispositions of hydrophobic residues within the sequence, guiding the 2D propagation at different angles and thus allowing different two-dimensional assemblies (**CP$_x$**: bilayer and **CP10**: monolayer, **Figure 1.2**, **Figure 2.12**). Additionally, polar domains also contributed to the stabilization of the final structure by electrostatic coating of the nanosheet surface. These 2D assemblies require a total negative ionizable state at physiological pH (7.4) since histidine protonation and hence charge neutralization leads to aggregation (**Figure 1.2**).

We hypothesized that electrostatic interactions could also be used as an additional orthogonal binding motif to direct self-assembly of cyclic peptides in a third dimension. In addition to the hydrogen bonding network directing growth along the y-axis and hydrophobic effects along the x-axis, complementary electrostatic surfaces could drive the assembly along the z-axis, generating a multilayered packing of nanotubes (**Figure 3.3**). However, as **CP$_x$** leads to a disordered state by lowering the pH, we also speculated that the new monomer should be tailored imposing certain geometrical constraints. To maintain an ordered three-dimensional assembly without aggregating, monomers should be restricted in a matched lattice (**Figure 3.2**).

For the design of the new cyclic hexapeptide **CP6** (**Figure 3.2**a, left), we maintained two segregated domains: the hydrophobic including two consecutive leucines and the hydrophilic (or polar) consisting in four residues of alternating histidine and glutamic acid. This reduction in size compared to the previously studied octapeptide **CP$_x$** (**Figure 3.2**b, left)[223] affords a more rigid cyclic peptide backbone.[224] Thus, we postulated that this higher rigidity could lead to more crystalline and tightly packed assemblies. As simplified in **Figure 3.2**, there is a clear difference between the proposed 3D lattices for both cyclic peptides: **CP6** gives rise to a lattice resembling a hexagonal closed packed structure (hcp) where monomers are in perfect matching, leaving hydrophobic and polar domains separated with complementarity between all residues (**Figure 3.2**a, right).[178] In contrast, **CP$_x$**'s 3D lattice exhibits imperfections that would result in unstable multilayering with mismatched residues, thus generating empty pockets with confronted polar and hydrophobic residues (**Figure 3.2b**, right).

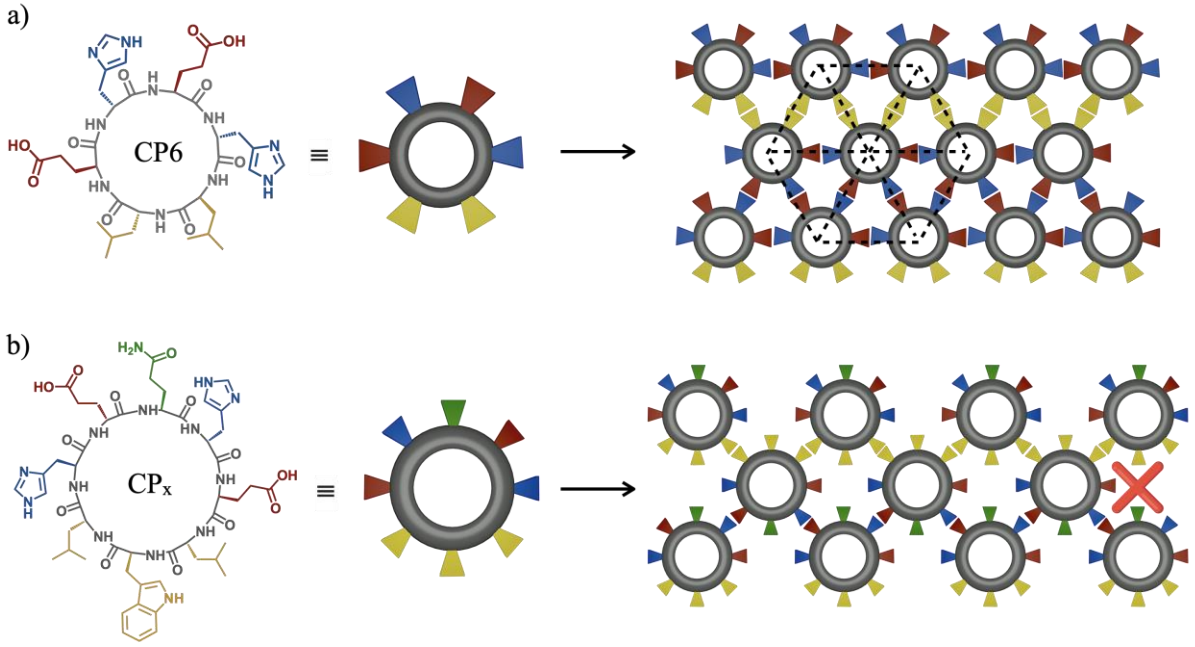

Figure 3.2. Comparison of the three-dimensional networks obtained with a) the new monomer designed **CP6** and b) the previous cyclic peptide **CPx**. Left: peptide sequence. Middle: Simplify representation for both cyclic peptide with the following color coding for each residue: In yellow, the hydrophobic leucine and tryptophan; in blue, histidine; in red, glutamic acid and in green, glutamine. Right: Schematic representation of how a three-dimensional network would be for each monomer. The dotted lines (above) mark the hexagonal lattice proposed for the packing and the red cross (below) the unstable gap with hydrophobic and polar resides.

We hypothesized that the geometrical disposition in **CP6** could be suitable for the growth of nanosheets in an additional third dimension (i.e., multilayering). Once nanotubes are packed in the bilayer (solvophobic effect), the system can propagate along the z-axis through pH regulation (**Figure 3.3**). At a slightly acidic pH (6.5), glutamic acid remains deprotonated, while histidine, close to its pka (6.0), will be partially in its protonated form. This ionizable state would allow the formation of electrostatic interactions between opposite charges leading to the attraction of nanotubes at exposed polar faces. Thus, the sequential 1D-to-2D self-assembly of bilayered nanosheets can be continued toward 3D growth, where bilayers can stack together into multilayers. It is also possible that nanotube clusters hiding their hydrophobic domains into an inner pocket can rearrange over preformed bilayers, thus contributing to the 3D multilayering of nanotubes with alternating biphasic layers..

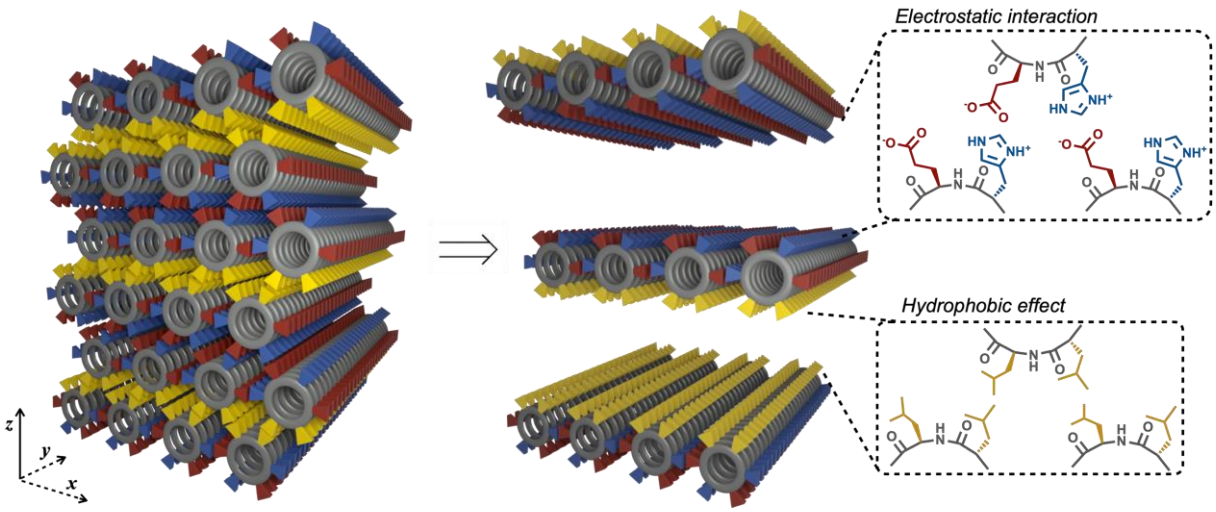

Figure 3.3. Schematic representation of the assembly propagation through the z-axis.

7.3.2.2. Assembly characterization

To probe our design principles, **CP6** was synthesized and assembled following the procedure previously reported (Scheme 3.1). For an initial screening, we tested a range of concentrations (10, 50, and 100 μM) at pH values in which the system went from full negative charge due to glutamic acid deprotonation, to slightly acidic by gradually protonating the histidines (7.4, 7.0, 6.5). Unlike for previous cyclic peptides (Chapters 1, 2), no evidence of nanosheets was found in epifluorescence micrographs at physiological pH 7.4 (**Figure 3.4**). However, at lower pH values, rectangular structures appeared, being most abundant at pH 6.5. At high magnification, multiple sheet-like structures were revealed with a different, more regular, morphology than in the previous chapters (**CP$_x$**, **CP10**). These new nanosheets seemed more homogeneous, having more defined edges, free from wrinkles or irregularities, but reaching shorter dimensions. We decided to continue studying in more detail the structures obtained at pH 6.5, as this pH is the best condition identified for self-assembly in this initial screening.

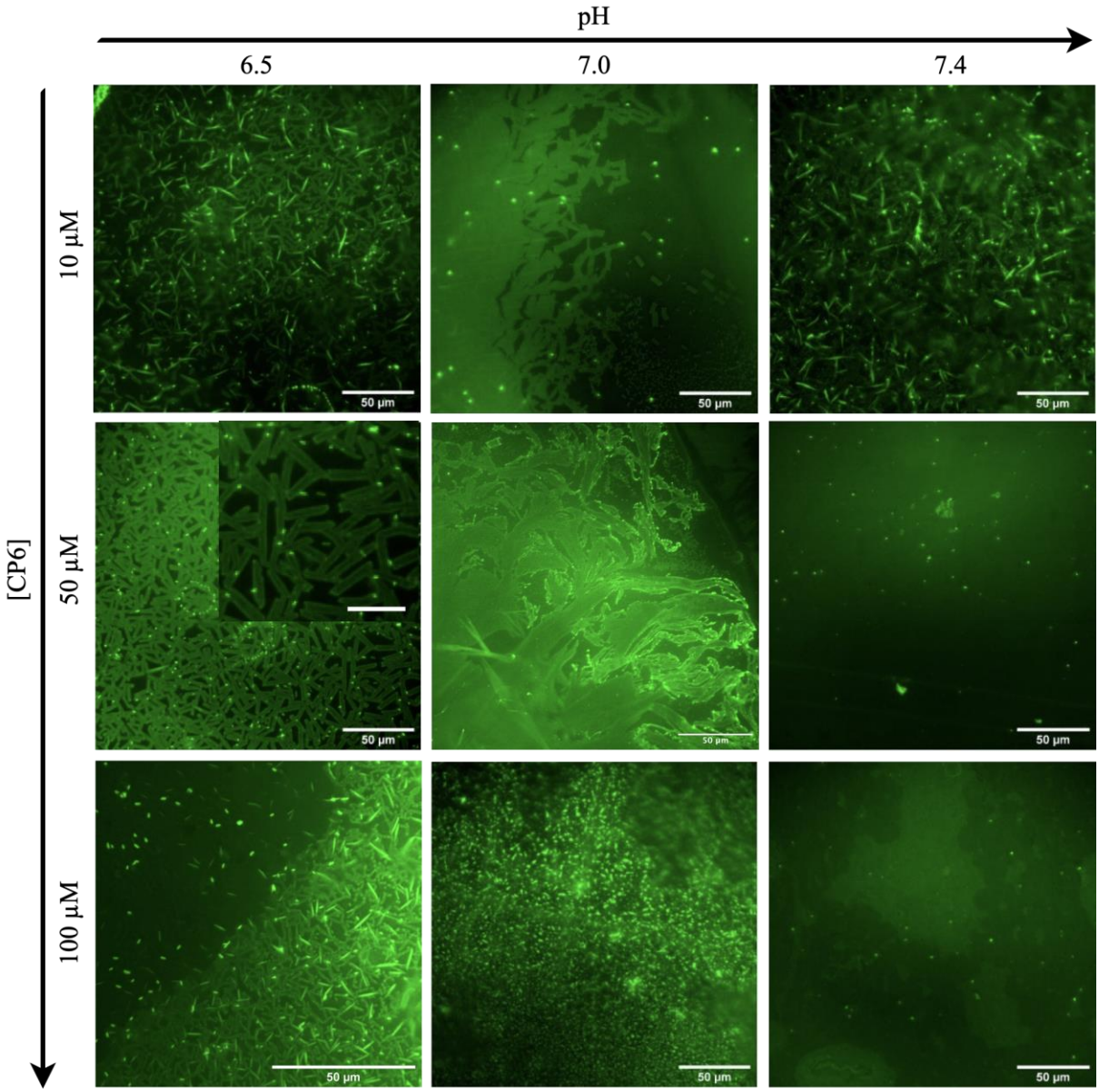

Figure 3.4. Epifluorescence micrographs of an assembled **CP6** sample at different pH and concentrations. Samples at each condition were subjected to the assembly protocol (i. 80°C/1.5 h; ii. RT/1h) in sodium phosphate buffer (20 mM) adjusted to the pH and with ThT (10 µM). The inset image at 50 µM, pH 6.5 is an amplification of the one below with scale bar = 10 µm.

As discussed above, the equilibrium of ionized states is crucial for growing multilayered nanosheets (**Figure 3.3**). To further study the effect of electrostatic interactions between charged amino acids, we decided to evaluate the self-assembly properties over a range of pH. For this purpose, samples were prepared by gradually decreasing the pH of the medium to 3.5 in addition to those previously tested at 7.0 and 7.5. In this range, the system can go from a state with a net negative charge (7.5) with glutamic acids deprotonated and histidines neutralized, to the opposite one with a net positive charge, where glutamic acids and histidines become protonated ($pk_{a(Glu)}$=4.0 and $pk_{a(His)}$=6.0). Epifluorescence micrographs showed nanostructures with a sheet-type morphology in all cases except at the

lowest value of 3.5 (**Figure 3.5**). Within the range of pHs corresponding to the pk_a values of the polar amino acids, between 4.0 and 6.0, the system is at zwitterionic state, observing irregular nanosheets and more aggregation. On the contrary, at pH values slightly exceeding the pk_a of histidine, with one amino acid fully charged (Glu) and the other only partially charged (His), homogeneous nanosheets with straight edges were formed. These findings suggest that a net charge of 0 in the system does not allow an ordered arrangement into nanosheets, but it is once again necessary to have a balance between attractive and repulsive forces. This complementarity between charged ionic groups is widely employed in assembled nanostructures by tuning the pH of the medium (Introduction, Section 0).

CP6 samples were observed to have a homogeneous shape thoughout the epifluorescence sample so we measured the aspect ratio in some regions containing these uniformly shaped structures. Interestingly, we found that nanosheets in each population maintained similar aspect ratio values with certain inter-batch variability (Figure S3.8, Experimental section 10.3.2). The consistency of aspect ratios found in these samples suggests a new level of control in assembly kinetics not accessible from larger monomers (i.e., octa- and decapeptides in Chapters I and II, respectively). This structural homogeneity observed with **CP6** could arise by favoring specific packing arrangements, which exhibit a high degree of structural order and periodicity, similar to crystalline materials. It is possible that once the first assembled nuclei are formed, the successive addition of monomers towards specific growth orientations occurs due to the well-defined orthogonal interactions.[257] We hypothesize that the smaller the size of the cyclic peptide, the higher its rigidity, and therefore the balance between flat and distorted macrocyclic conformations could affect the elongation kinetics and, hence, its polydispersity. Moreover, as commented in the introduction, geometrical frustration could be another phenomenon that controll the assembly endings by tuning the balance between attractive and repulsive forces.[164] This repulsive character could derived from the repetitive structural distortions throughout the assembly, reaching a threshold that stops the elongation. Both mechanisms could explain the constant aspect ratio and height homogeneity that is observed in the AFM pictures.

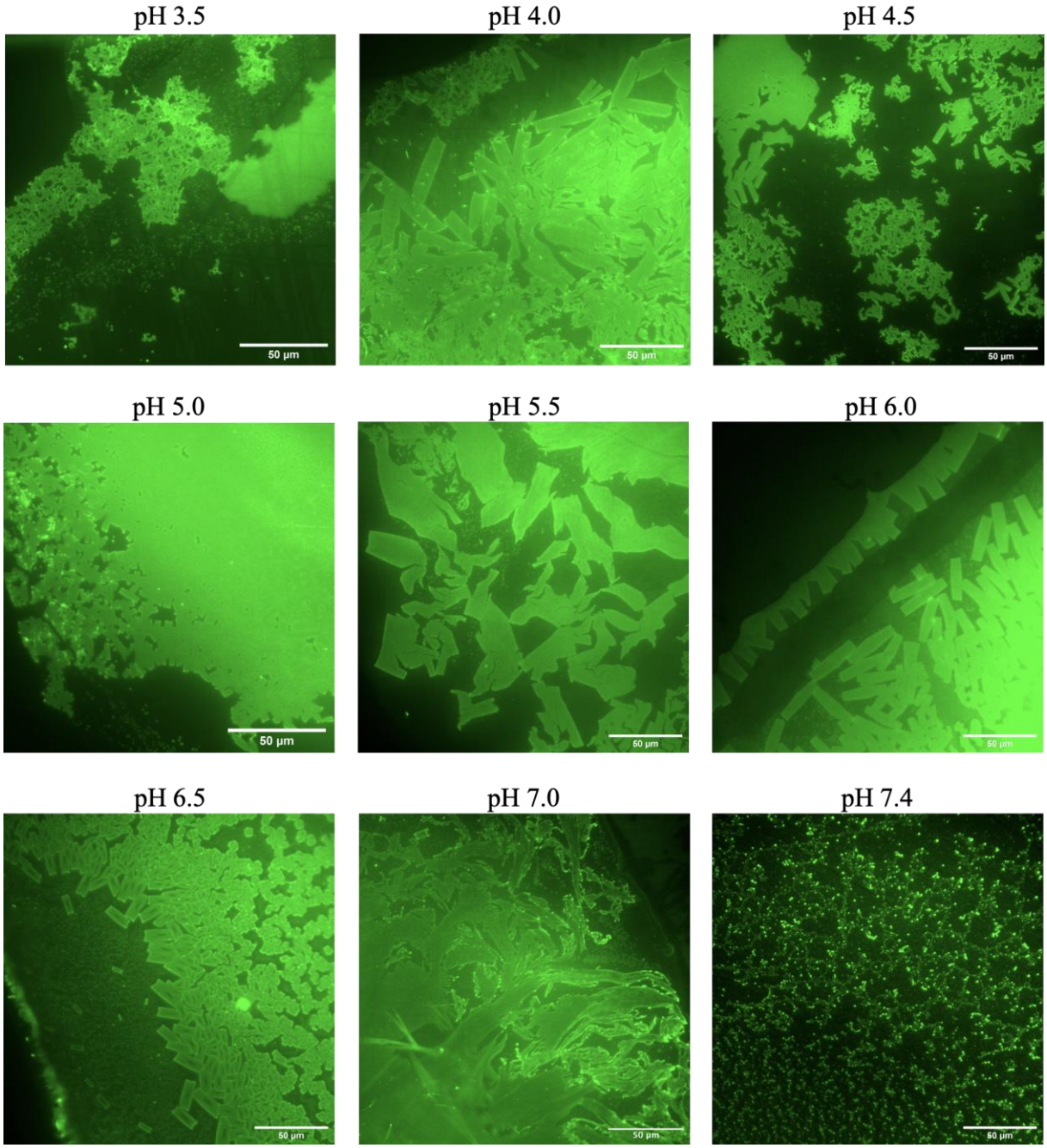

Figure 3.5. Epifluorescence micrographs of assembled **CP6** samples at different pH at 50 µM. Samples at each condition were subjected to the assembly protocol (i. 80°C/1.5 h; ii. RT/1h) in sodium phosphate buffer (20 mM) adjusted to the pH and with ThT (10 µM).

STEM micrographs revealed the presence of nanosheets although with a slightly different morphology compared to the epifluorescence ones (**Figure 3.6**a). This could be due to the drying effect on the different surfaces on which they are deposited. In fact, AFM images further confirmed these differences, as samples are deposited on a different surface than TEM grids. The AFM revealed discrete height values of 10 and 20 nm for the nanosheets (**Figure 3.6**b,c). Moreover, it was possible to observe tubular aggregates in the same sample (**Figure 3.6**d). The size distribution of these nanotubes showed heights ranging from 0.7 to 1.1 nm, averaging 0.90±0.12 nm (mean±SD). Based on previous results from Chapters I and II, where both bilayer and monolayer presented heights of up to 3.2 nm for larger monomers (**Figure 1.6** and **Figure 2.4**[a]), it is possible to correlate these findings with a multilayer packing of nanotubes, confirming growth along the third dimension.

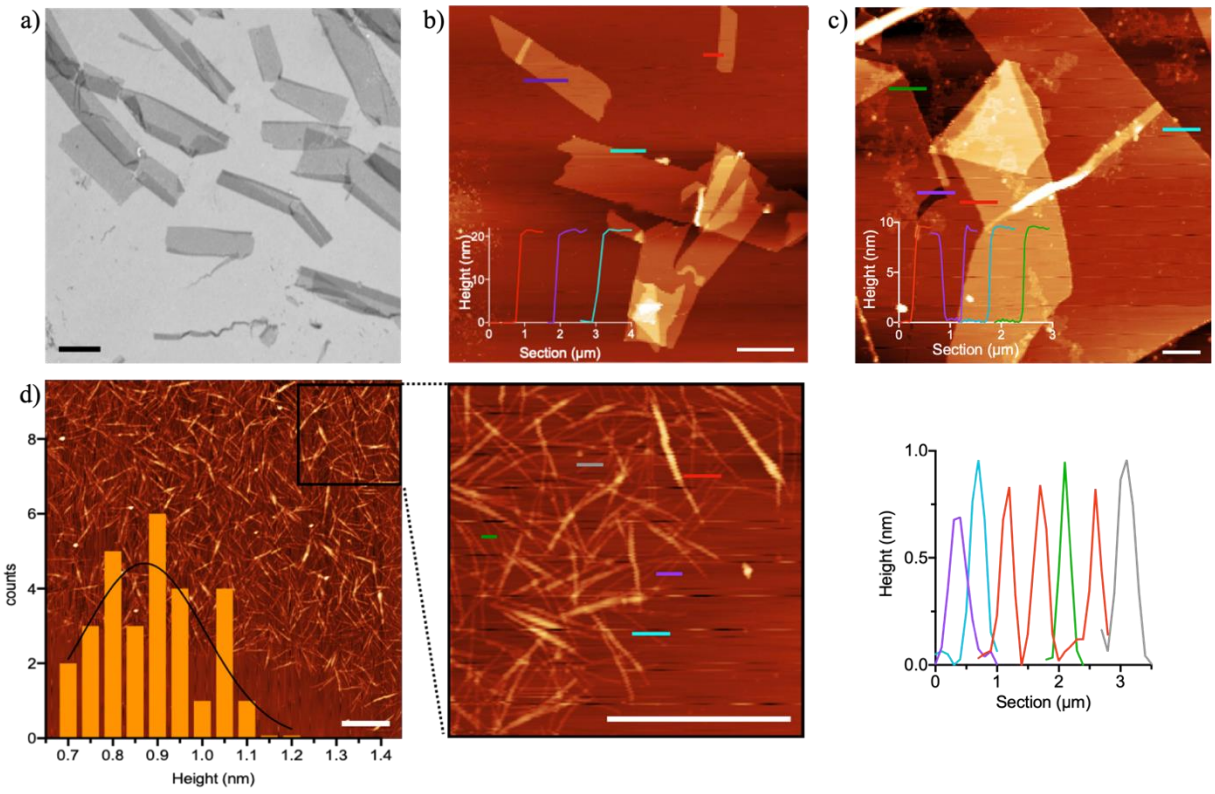

Figure 3.6. a) STEM micrograph of an assembled sample of **CP6** at 100 µM stained with phosphotungsting acid (scale bar 1 µm). b,c) AFM micrographs of nanosheets with the height profile of the regions marked inset (scale bar 5 µm (b) and 1 µm (c)) d) Left: AFM micrograph of tubular aggregates (scale bar 1 µm) with an histogram of the heights inset (30 nanotubes measured). Middle: expansion of the framed region (scale bar 1 µm). Right: Height profile of the nanotubes marked.

Small angle X-ray scattering (SAXS) experiments provided additional insights into the assembled structures in solution. A plot depicting intensity against momentum transfer (q) exhibited a curve characterized by two different scattering intensities at low and high q regions. This variation indicates the presence of two different objects coexisting in solution with well-defined shapes, as they followed

the power law with distinct values (**Figure 3.7**, left). At high q values (>0.3 nm^{-1}), a characteristic -1 Porod slope suggested the presence of one-dimensional (1D) objects, while at low q values (<0.3 nm^{-1}), the slope shifts to -2.2, indicating the presence of 2D assemblies. After applying a model-based analysis, it was possible to obtain size information for both assemblies.[258] A value of 1.2±0.5 nm was calculated for the 1D objects in the high q region while a thickness of 19.7±0.5 nm was calculated for 2D objects at low q values. These data match the values found in AFM and confirmed the coexistence of both 1D nanotubes and 2D nanosheets in solution.

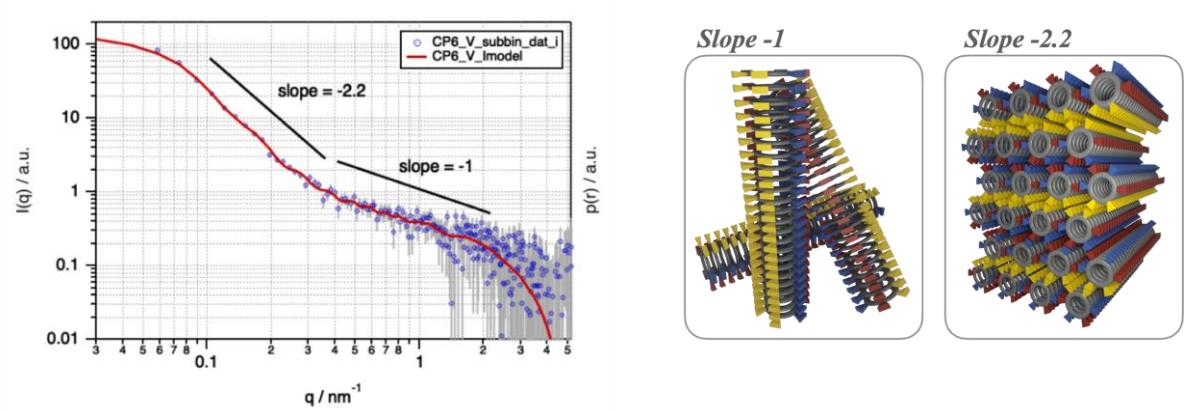

Figure 3.7. Left*:* SAXS data from a **CP6** sample at 100 μM in phosphate buffer (20mM, pH 6.5). The graph shows the plot of the log intensity of the scattering against the scattering vector. Two different slopes were estimated. Right: Representation of the structures related with both slopes.

7.3.2.3. Spectroscopic characterization

To gain insight into the internal arrangement of the assembled state, we studied the organization of **CP6** within the nanosheets. Fourier-transform infrared (FTIR) analysis showed an N-H stretching band at 3256 cm^{-1}, one band at 1528 cm^{-1} in the Amide II region, and one sharp and narrow band at 1655 cm^{-1} corresponding to Amide II, attributed to the β-sheet stacking of cyclic peptides (Figure S3.9, Experimental Section 10.3.2). In this system, the parallel sheet of stacked CP monomers is the only one possible since heterochiral stacking should be sterically prohibited as demonstrated by Ghadiri et col.[187]

To further evaluate this tubular assembly, we performed wide-angle X-ray scattering (WAXS) measurements. As shown in **Figure 3.8**a, the scattering pattern reveals three main diffraction peaks. The peak at 4.5 Å is attributed to the d-spacing value reported for the distance between two stacked monomers, confirming the formation of nanotubes (**Figure 3.8**b).[180] The peak at 9.5 Å corresponds to the distance between the centers of two adjacent cyclic peptides in the multilayer (**Figure 3.8**c). This value would also correspond to the monomer's

[258] J. S. Pedersen, *Analysis of Small-Angle Scattering Data from Colloids and Polymer Solutions: Modeling and Least-Squares Fitting I*, ELSEVIER, **1997**.

diameter, estimated to be ca. 0.8 nm by AFM. Finally, we postulate the peak at 2.1 Å relate to the distance between residues of contiguous monomers. We have observed a slightly higher value (2.8 Å) for the monolayer formed by CP10 that we assigned to the lateral contacts between the aromatic residues (**Figure 2.4**). This new value observed for CP6 can be due to the smaller size of their residues compare to the tryptophan in **CP10**. Overall, these structural parameters are consistent with the proposed model for a multilayered nanosheet (

Figure 3.2a), reinforcing the predicted assembly mode accessible from rigid CP monomers through rational design.

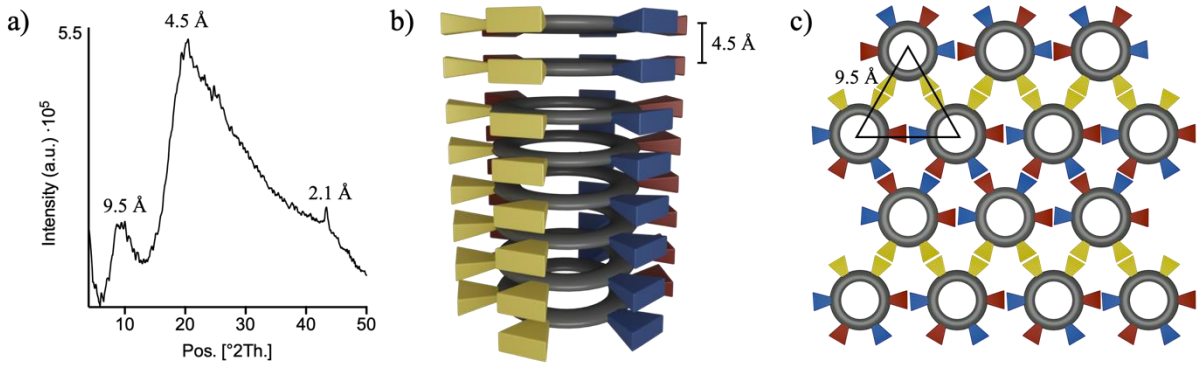

Figure 3.8. a) WAXS profile of **CP6** with two differentiated signals. Schematic representation of the distances found in WAXS: b) distance between stacked cyclic peptides in the nanotube and c) distance between the centers of adjacent monomers.

Once the formation of multilayered assemblies composed of nanotubes was confirmed, we aimed to study the assembly behavior to decipher a possible sequential 1D-to-2D-to-3D growth. For this purpose, we decided to follow the assembly process using the dye Thioflavin-T by fluorescence spectroscopy. Unexpectedly, Thioflavin-T (ThT) did not show an increase in emission intensity with peptide assembly, suggesting that this probe might not be efficiently inserted between stacked cyclic peptides (Figure S3.10, Experimental Section 10.3.2). This external dye is intercalated in β-sheet-type structures and, being a molecular rotor, when planarized it becomes increasingly fluorescent. As already reported and previously observed (**Figure 1.8** and **Figure 2.6**), ThT is used to evaluate cyclic peptide assembly by changes in emission intensity.[224] However, its binding mechanism is not clear and may differ between systems. Several studies have revealed some features that can hamper its binding, for example, the type of hydrophobic residues, being aromatic ones better than aliphatic.[259] Moreover, as ThT is a cationic molecule, its insertion could be prevented in systems with negative charges on the surface, remaining sequestered on the surface as a non-fluorescent complex instead of inserted.[260] **CP6** has a hydrophobic core only formed by two leucine residues, without any aromatic moiety, which might not be

[259] M. Biancalana, K. Makabe, A. Koide, S. Koide, *J. Mol. Biol.,* **2009**, *385*, 1052–1063.
[260] V. Babenko, W. Dzwolak, *Chem. Comm.,* **2011**, *47*, 10686–10688.

well suited for ThT intercalation. Additionally, **CP6** nanosheets seem to present a greater ordering of monomers than previously studied CPs, leading to a more rigid structure that could complicate the insertion and diffusion of an external dye. As demonstrated in other studies, ThT is not able to enter solid aggregates of strongly associated monomers.[261] Although this external dye does not appear to efficiently intercalate between **CP6** monomers, nanosheets could be observed by epifluorescence microscopy - hence labeled with ThT. We hypothesized that this might be possible because of the drying process for microscopy, where ThT can be trapped and planarized over the surface of the deposited nanosheets.

7.3.2.4. Structural derivatives

Considering the importance of the charged state for assembly, we decided to design new cyclic peptides by modifying specific residues of **CP6** (Figure 9). First, we replaced both histidines for glutamines to block complementary electrostatic contacts (**Figure 3.9**: **EQEQ**) Glutamine, as His can also form hydrogen bonds and help drive propagation, H-bonds are not as strong as ionic interactions, making difficult the stabilization of the system.[29] We also places two Gln at the central hydrophilic part, replacing one glutamic acid and one histidine (**Figure 3.9**: **EQQH**), to maintain lateral electrostatic interactions between nanotubes while preventing growth in the z-axis (i.e., multilayering). Epifluorescence screening revealed the presence of some assemblies (pH 6.5, 6.0) but mainly aggregates were observed (Figure S3.11, Experimental Section 10.3.2). Moreover, we studied the assembly behavior by STEM and, although some assembled nanostructures also appeared at different pH for both derivatives (**EQEQ**, **EQQH**), their morphology was quite irregular and does not resemble the sheet-type structure, presenting a lot of aggregation all over the sample (Figure S3.12, Experimental Section 10.3.2). These results suggest that these modified monomers can assemble beyond 1D nanotubes but without the order observed with **CP6**, confirming that having both charged residues in the central polar domain is needed for the controlled assembly.

[261] M. Abbas, W. P. Lipiński, K. K. Nakashima, W. T. S. Huck, E. Spruijt, *Nat. Chem.*, **2021**, *13*, 1046–1054.

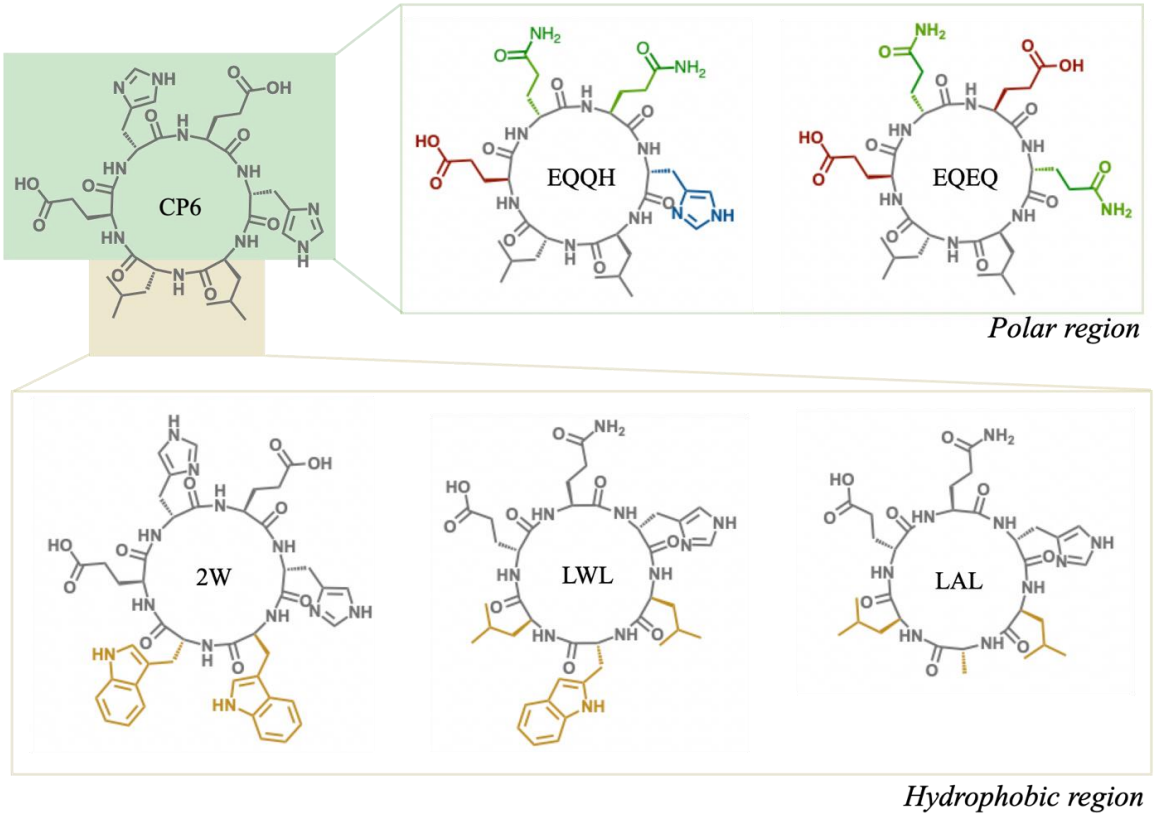

Figure 3.9. Chemical structures of cyclic peptide variants designed. At the top (green), modifications in the polar region: **EQQE** and **EQEQ**. At the bottom (yellow), modifications in the hydrophobic region: **2W**, **LWL**, **LAL**.

We also tested some modifications in the hydrophobic region by replacing both leucines for tryptophans (**Figure 3.9**: **2W**). This change led to the formation of large anisotropic nanosheets, as observed by both epifluorescence and AFM (**Figure 3.10**). A height of 8 nm was observed, which suggested also a potential multilayered assembly. The obtained nanosheets were less flat and not regular, which was similar to the previously published 2D assemblies. These findings suggest that the hydrophobic region of **CP6** could be more tolerant to potential modifications. However, the more irregular shape of the nanosheets confirmed the importance of the leucine residues and the potential leucine interdigitation (zipping) for the more regular assembly observed in the epifluorescence micrographs of **CP6**.

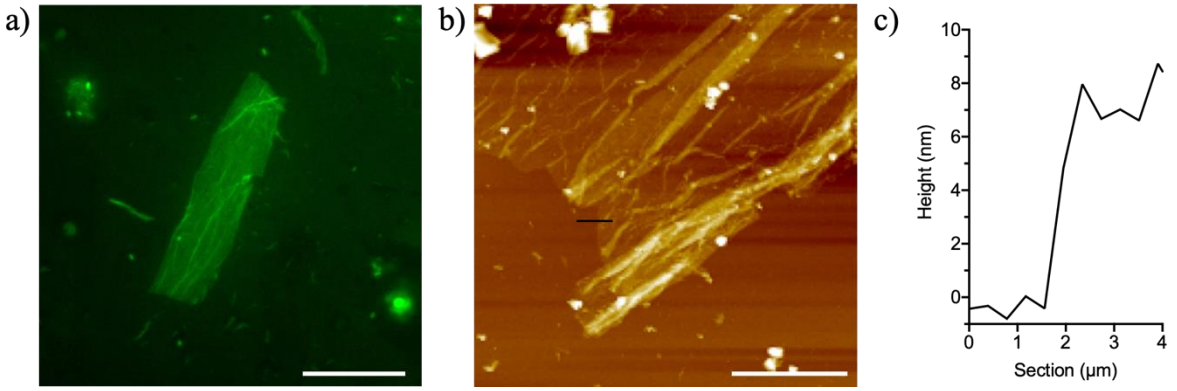

Figure 3.10. a) Epifluorescence micrograph of **2W** assembled following the protocol described (i. 80°C/1.5 h; ii. RT/1h) in sodium phosphate buffer (20 mM, pH 6.5) with ThT (10 μM) Scale bar 50 μm. b) AFM image of a nanosheet. Scale bar 4 μm. c) AFM profile of the section marked.

Finally, we designed two additional cyclic peptides with the hydrophobic domain formed by three residues as explored in previous chapters to promote the bilayer packing observed with **CPx** and variants (Chapter 7.1). In this case, in addition to the variant with Leu-Trp-Leu (**Figure 3.9**: **LWL**), we also prepared one with an Ala instead of Trp (**Figure 3.9**: **LAL**) to reduce steric hindrance due to the smaller size of the hexapeptide backbone. Both variants were designed to have the polar face with a glutamine flanked by complementary ionic glutamic acid and histidine. Both peptides showed higher insolubility than the original **CP6**, complicating their chromatographic purification. However, it was possible to obtain enough product to screen concentrations and pH to evaluate their assembly. Nevertheless, neither of these two variants exhibited assembly in any condition tested (Figure S3.13, Experimental Section 10.3.2).

7.3.3. Conclusions

In this chapter, we have designed a new cyclic peptide monomer (**CP6**) with orthogonal binding motifs whose self-assembly propagates into 3D multilayer nanosheets. In addition to the hydrogen bonding interactions and hydrophobic packing previously used to hierarchically control the propagation in 1D and 2D, respectively, we here introduce additional orthogonal forces: electrostatics to buildup finite 3D structures. The modulation of the charged state of cyclic peptide monomers allowed it to propagate along the third dimension by creating complementary electrostatic interfaces. To do this, we took advantage of the alternating of polar groups with different pKa placed at the surface of the 2D bilayer (i.e., glutamic acid and histidine). The process developed is not exclusively a crystallization, but rather a hierarchical supramolecular 3D construction to form a nanostructure in which the relative growth in the three dimension is precisely controlled. The cyclic peptide diameter was reduced to enhance monomers rigidity and afford a hexagonal close-packed-type lattice. We hypothesized that this geometrical feature would lead to a fully complementary architecture where all amino acids would be matching neighboring monomers, allowing the system to assemble into supramolecular multilayer.

We have demonstrated that this new monomer design is capable to self-assemble in finite 3D structures, by microscopy and diffraction techniques, reaching values of 10 and 20 nm for the height of the nanosheets while NTs were found to measure only 0.9 nm. The pH-dependent behavior has demonstrated the necessity to balance the complementary charges (pH 6.5) to maintain the nanotubes perfectly packed in the afforded multilayers. Moreover, cyclic peptide variants have also probed that both ionizable amino acids (i.e., glutamic acid and histidine) play a key role in directing the assembly. Additionally, we have observed a remarkable consistency in the aspect ratio of nanosheets from the same sample, which is interesting since controlling the assembly size of extended structures is difficult, and usually polydispersity is obtained.

The design of finite nanostructures with specific shape and dimensions is the final goal in bottom-up nanotechnology. In this regard, viral biosynthesis -like that of the tobacco mosaic virus (TMV)- is an excellent example, producing a monodisperse tubular-shaped 3D material simply using one protein (i.e. its capsid) and viral RNA. In this process, viral RNA templates the defined assembly of a protein tube that functions as capsid. In contrast to the use of a template for the ordered assembly of the capsid, we here report a hexapeptide cyclic peptide monomer that encodes all the structural information in is primary sequence towards creating monodisperse defined assemblies. The resulting material features a unique structure made of layers of orthogonal hydrophobic and ionic domains, setting a stepping stone in the rational design of fully synthetic monodisperse bottom-up architectures.

8. GENERAL CONCLUSIONS

In this dissertation, we have explored the potential of cyclic peptides as versatile monomers. By rational design, we strategically incorporated various binding motifs in specific positions of the peptide sequence to bias the self-assembly propagation toward different directions, thereby achieving precise control over the resulting multidimensional nanostructures. A delicate balance between intermolecular forces as well as optimal assembly conditions and geometric precision, were the design motifs employed to effectively direct the assembly process. Overall, we have demonstrated the formation of three different nanosheet architectures by controlled growth across multiple dimensions, from 2D bilayer and monolayer to 3D multilayer.

Firstly, we have explored the influence of the **CP$_x$** sequence in bilayer assembly, which is stabilized by an interplay between attractive and repulsive interactions. Among the attractive, hydrogen bonding drives the 1D nanotube formation while the hydrophobic effect directs the 2D elongation. The polar charged face is exposed to the aqueous environment and the negative net charge generates electrostatic repulsion completing assembly stabilization. For the main objective, we have made strategic modifications to identify the critical amino acids and their optimal positions driving their hierarchical self-assembly from 1D nanotubes to 2D nanosheets. Spectroscopic and imaging characterization have revealed that the hydrophobic domain is more tolerant to changes than the polar domain, highly dependent on the ionized state.

Secondly, we have designed a new cyclic peptide monomer capable of forming monolayered nanosheets. **CP10** with two confronted hydrophobic domains directs the lateral packing of nanotubes toward opposite directions. The monolayer assembly is maintained due to the electrostatic repulsion generated in the polar face. Computational studies have allowed us to understand the mechanism of assembly, deciphering a bias in propagation, and thereby confirming the hierarchical 1D-to-2D self-assembly. Additionally, these studies have also revealed the importance of the "tryptophan hinge" motif, as it imparts the required flexibility in lateral contacts for the maintenance of the monolayers.

Finally, we decided to go beyond 2D nanostructures and designed a cyclic peptide monomer capable of forming 3D multilayer nanosheets. In this new **CP6** monomer, we kept the same binding motifs as in the bilayer design, both the hydrophobic region and the polar charged amino acids, but the assembly conditions were slightly modified. We lowered the pH value to achieve partial protonation of histidines in order to generate electrostatic attraction between polar faces, thus growing the system in a third dimension.

These findings not only demonstrate the versatility of cyclic peptides in self-assembly, but also offer valuable insights for the rational design of nanomaterials with tailored morphologies.

9. BIBLIOGRAPHY

1. Lehn, J. M. Beyond Chemical Synthesis: Self-Organization?! *Israel Journal of Chemistry,* **2018**, *58* (1).
2. Van der Waals, J. D. *On the Continuity of the Gaseous and Liquid States*; Leiden, **1873**.
3. Fischer, E. Influence of Configuration on the Action of Enzymes. *Journal of the American Chemical Society,* **1894**, *3*, 2985–2993.
4. Wendell Latimer, B. M.; Rodebush, W. H. Polarity and Ionization from the Standpoint of the Lewis Theory of Valence. *Journal of the American Chemical Society,* **1920**, *42* (7), 1419–1433.
5. Pauling, L. The application of the quantum mechanics to the structure of the hydrogen molecule and hydrogen molecule-ion and to related problems. *Chemical Reviews,* **1928**, *5* (2), 173–213.
6. Wolf, K. L.; Prahm, H.; Harms, H.. The State of Arrangement of the Molecules in Liquids. *Journal of Physical Chemistry,* **1937**, *36B*(1), 237–287.
7. Werner, A. Beitrag Zur Konstitution Anorganischer Verbindungen. *Journal of Inorganic and General Chemistry,* **1893**, *3*, 267–330.
8. Watson, J. D.; Crick, F. H. C. Molecular Structure of Nucleic Acids: A Structure for Deoxyribose Nucleic Acid, *Nature,* **1953**, *171*, 737–738.
9. Pedersen, C. J. Cyclic Polyethers and Their Complexes with Metal Salts. *Journal of the American Chemical Society***, 1967**, *89* (26), 7017–7036.
10. Dietric, B.; Lehn, J. M.; Sauvage, J. P. Les Cryptands. *Tetrahedron Letters,* **1969**, *10* (34), 2889–2892.
11. Dietrich, B.; Lehn, J. M.; Sauvage, J. P. Diaza-Polyoxa-Macrocycles et Macrobicycles. *Tetrahedron Letters,* **1969**, *10* (34), 2885–2888.
12. Trueblood, K. N.; Knobler, C. B.; Maverick, E.; Helgeson, R. C.; Brown, S. B.; Cram, D. J.; Spherands, the First Ligand Systems Fully Organized during Synthesis Rather than during Complexation. *Journal of American Chemical Society,* **1981**, *103* (18), 5594–5596.
13. Cram, D. J.; Kaneda, T.; Helgeson, R. C.; Lein, G. M. Spherands - Ligands Whose Binding of Cations Relieves Enforced Electron-Electron Repulsions, *Journal of American Chemical Society,* **1979**, *101* (22), 6752–6754.
14. Cram, D. J. *The Design of Molecular Hosts, Guests, and Their Complexes (Nobel Lecture)*, **1988**.
15. Lehn, J. M. *Supramolecular Chemistry-Scope and Perspectives Molecules, Supermolecules, and Molecular Devices (Nobel Lecture)*; **1988**.
16. Rebek, J. Introduction to the Molecular Recognition and Self-Assembly Special Feature. *Proceedings of the National Academy of Science U S A,* **2009**, *106* (26), 10423–10424.
17. Lehn, J. M. *Supramolecular Chemistry-Molecular Information and the Design of Supramolecular Materials*; **1993**, 69, 1–17.
18. Stoddart, J. F. Host-Guest Chemistry. *Organic Chemistry. Annual Reports Section B,* **1988**, *85*, 353–386.
19. Freeman, W. A.; Mock, W. L.; Shih, N. Y. Cucurbituril, *Journal of American Chemical Society,* **1981**, *103*, 7367–7368.
20. Moran, J. R.; Karbach, S.; Cram, D. J. Cavitands: Synthetic Molecular Vessels. *Journal of American Chemical Society,* **1982**, *104* (21), 5573–5856.
21. Tittel, H. W.; Smalley, F. K.; Am, R. E. J.; Lindsey, A. S.; Gutsche, C. D.; Dhawan, B.; No, K. H.; Muthukrishnan, C. D.; Gutsche, B.; Hógberg, A. G. S.; Moran, J. E.; Karbach, S.; Cram, D. J.; Ericson, J. L.; Helgeson, R. C.; Carcerands and Carcaplexes. *Journal of American Chemical Society,* **1988**, *110* (8), 2353–2698.
22. Dietrich-Buchecker, C. O.; Sauvage, J. P.; Kintzingi, J. P. Une Nouvelle Famille De Molecules : Les Metallo-Catenanes, *Tetrahedron Letters,* **1983**, *24* (46), 5095–5098.
23. Anelli, P. L.; Organici, S.; Spencer, I. N.; Stoddart, J. F. Molecular Shuttle. *Journal of American Chemical Society,* **1991**, *113* (1), 5131–5133.
24. Koumura, N.; Zijlstra, R. W. J.; van Delden, R. A.; Harada, N.; Feringa, B. L. Light-Driven Monodirectional Molecular Rotor, *Nature* ,**1999**, *401*, 152–155.

25. Lehn, J. M. *Toward Complex Matter: Supramolecular Chemistry and Self-Organization. Proceedings of the National Academy of Science U S A,* **2002**, *99*, 4763–4768.
26. Lehn, J. M. Supramolecular Chemistry, *Science,* **1993**, *260* (5115), 1762–1763.
27. Lehn, J. M. Supramolecular Chemistry: Where from? Where To? *Chemical Society Reviews*, **2017**, *46* ,2378–2379.
28. Cantrill, S. J.; Fyfe, M. C. T.; Raymo, F. M.; Stoddart, J. F. Synthetic Supramolecular Chemistry. *Current challenges on large supramolecular assemblies. NATO Science Series*; Springer, **1999**; Vol. 519, p 44.
29. Mendes, A. C.; Baran, E. T.; Reis, R. L.; Azevedo, H. S. Self-Assembly in Nature: Using the Principles of Nature to Create Complex Nanobiomaterials, *Wiley Interdisciplinary Reviews: Nanomedicine and Nanobiotechnology,* **2013**, *5* (6), 582–612.
30. Li, H.; LaBean, T. H.; Leong, K. W. Nucleic Acid-Based Nanoengineering: Novel Structures for Biomedical Applications. *Interface Focus*, **2011**, *1*, 702–724.
31. Collier, J.; Messersmith, P.. Phospholipid Strategies in Biomineralization and Biomaterials Research, *Annual Review of Materials Research,* **2001**, *31*, 237–263.
32. Israelachvili, J. N.; Mitchell, D. J.; Ninham, B. W. Theory of Self-Assembly of Lipid Bilayers and Vesicles. *Biochimia et Biophysica Acta,* **1977**, *470* (2), 185–201.
33. Varki, A.. Biological Roles of Oligosaccharides: All of the Theories Are Correct, *Glycobiology,* **1993**, *3* (2), 97–130.
34. Luo, Q.; Hou, C.; Bai, Y.; Wang, R.; Liu, J. Protein Assembly: Versatile Approaches to Construct Highly Ordered Nanostructures. *Chemical Reviews*, **2016**, *116,* 13571–13632.
35. Gautieri, A.; Vesentini, S.; Redaelli, A.; Buehler, M. J. Hierarchical Structure and Nanomechanics of Collagen Microfibrils from the Atomistic Scale Up. *Nano Letters,* **2011**, *11* (2), 757–766.
36. Fletcher, D. A.; Mullins, R. D. Cell Mechanics and the Cytoskeleton. *Nature*, **2010**, *463*, 485–492.
37. Fitzpatrick, A. W. P.; Debelouchina, G. T.; Bayro, M. J.; Clare, D. K.; Caporini, M. A.; Bajaj, V. S.; Jaroniec, C. P.; Wang, L.; Ladizhansky, V.; Müller, S. A.; MacPhee, C. E.; Waudby, C. A.; Mott, H. R.; De Simone, A.; Knowles, T. P. J.; Saibil, H. R.; Vendruscolo, M.; Orlova, E. V.; Griffin, R. G.; Dobson, C. M. Atomic Structure and Hierarchical Assembly of a Cross-ß Amyloid Fibril, *Proceedings of the National Academy of Science U S A,* **2013**, *110* (14), 5468–5473.
38. Petrov, A. S.; Bernier, C. R.; Hsiao, C.; Norris, A. M.; Kovacs, N. A.; Waterbury, C. C.; Stepanov, V. G.; Harvey, S. C.; Fox, G. E.; Wartell, R. M.; Hud, N. V.; Williams, L. D. Evolution of the Ribosome at Atomic Resolution, *Proceedings of the National Academy of Science U S A,* **2014**, *111* (28), 10251–10256.
39. Gad, S.; Ayakar, S. Protein Scaffolds: A Tool for Multi-Enzyme Assembly. *Biotechnology Reports* **2021**, *32.*
40. Insua, I.; Montenegro, J. Synthetic Supramolecular Systems in Life-like Materials and Protocell Models. *Chem*, **2020**, *6,* 1652–1682.
41. Walther, A. Viewpoint: From Responsive to Adaptive and Interactive Materials and Materials Systems: A Roadmap, *Advanced Materials,* **2020**, *32* (20).
42. RP Sijbesma; EW Meijert. Self-Assembly of Well-Defined Structures by Hydrogen Bonding, *Current Opinion in Colloid and Interface Science,* **1999**, *4* (1), 24–32.
43. (43)Knowles, T. P.; Fitzpatrick, A. W.; Meehan, S.; Mott, H. R.; Vendruscolo, M.; Dobson, C. M.; Mark, †; Welland, E. Role of Intermolecular Forces in Defining Material Properties of Protein Nanofibrils. *Science (1979)* **2007**, *318* (5858), 1900–1903.
44. Perutz, M. F.; Johnson, T.; Suzuki, M.; Finch, J. T. Glutamine Repeats as Polar Zippers: Their Possible Role in Inherited Neurodegenerative Diseases. *Proceedings of the National Academy of Science U S A,* **1994**, *91*, 5355–5358.
45. Fleming, S.; Ulijn, R. V. Design of Nanostructures Based on Aromatic Peptide Amphiphiles, *Chemical Society Reviews*, **2014**, *43,* 8150–8177.

46. Gazit, E. A Possible Role For-Stacking in the Self-Assembly of Amyloid Fibrils, *The FASEB Journal,* **2002**, *16*, 77–83.
47. Contorno, S.; Darienzo, R. E.; Tannenbaum, R. Evaluation of Aromatic Amino Acids as Potential Biomarkers in Breast Cancer by Raman Spectroscopy Analysis, *Scientific Reports,* **2021**, *11* (1).
48. Chelli, R.; Gervasio, F. L.; Procacci, P.; Schettino, V. Stacking and T-Shape Competition in Aromatic-Aromatic Amino Acid Interactions, *Journal of American Chemical Society,* **2002**, *124* (21), 6133–6143.
49. Yan, X.; Zhu, P.; Li, J. Self-Assembly and Application of Diphenylalanine-Based Nanostructures. *Chemical Society Reviews,* **2010**, *39* (6), 1877–1890.
50. Tao, K.; Levin, A.; Adler-Abramovich, L.; Gazit, E. Fmoc-Modified Amino Acids and Short Peptides: Simple Bio-Inspired Building Blocks for the Fabrication of Functional Materials, *Chemical Society Reviews*, **2016**, *45*, 3935–3953.
51. Coste, M.; Suárez-Picado, E.; Ulrich, S. Hierarchical Self-Assembly of Aromatic Peptide Conjugates into Supramolecular Polymers: It Takes Two to Tango, *Chemical Science*, **2022**, *13*, 909–933.
52. London, F. The General Theory of Molecular Forces. *Transactions of the Faraday Society,* **1937**, *33*, 8–26.
53. Sung, S. S. Peptide Folding Driven by Van Der Waals Interactions, *Protein Science,* **2015**, *24* (9), 1383–1388.
54. Rehm, T. H.; Schmuck, C. Ion-Pair Induced Self-Assembly in Aqueous Solvents, *Chemical Society Reviews,* **2010**, *39* (10), 3597–3611.
55. Kumar, S.; Nussinov, R. Relationship between Ion Pair Geometries and Electrostatic Strengths in Proteins. *Biophysical Journal,* **2002**, *83* (3), 1595–1612.
56. Chen, C.; Chen, J.; Yu, Q.; Zhang, J.; Niu, X.; Hao, L.; Yang, L.; Zhao, Y. Effects of Salts on the Self-Assembly Behavior and Antibacterial Activity of a Surfactant-like Peptide, *Soft Matter,* **2020**, *16* (42), 9758–9768.
57. Rodnikova, M. N. A New Approach to the Mechanism of Solvophobic Interactions, *Journal of Molecular Liquids,* **2007**, *136* (3), 211–213.
58. David Chandler. Hydrophobicity: Two Faces of Water, *Nature* **2002**, *417*, 491.
59. David Chandler. Interfaces and the Driving Force of Hydrophobic Assembly, *Nature*, **2005**, *437*, 640–647.
60. Li, J.; Wang, J.; Zhao, Y.; Zhou, P.; Carter, J.; Li, Z.; Waigh, T. A.; Lu, J. R.; Xu, H. Surfactant-like Peptides: From Molecular Design to Controllable Self-Assembly with Applications. *Coordination Chemistry Reviews*, **2020**, *421.*
61. Dietzen, D. J. Amino Acids, Peptides, and Proteins. In *Principles and Applications of Molecular Diagnostics*; Elsevier, **2018**; pp 345–380.
62. Lichtenthaler, F.W. Emil Fischer's Proof of the Configuration of Sugars: A Centennial Tribute‡. Angewandte Chemie International Edition, **1992**,*31*, 1541-1556.
63. Wilson, C. J.; Bommarius, A. S.; Champion, J. A.; Chernoff, Y. O.; Lynn, D. G.; Paravastu, A. K.; Liang, C.; Hsieh, M. C.; Heemstra, J. M. Biomolecular Assemblies: Moving from Observation to Predictive Design. *Chemical Reviews*, **2018**, *118,* 11519–11574.
64. Linus Pauling; Robert B. Corey; H. R. Branson. The Structure of Proteins: Two Hydrogen-Bonded Helical Configurations of the Polypeptide Chain, *The Proceedings of the National Academy of Sciences,* **1951**, *37* (4), 205–211.
65. Hutchinson, E. G.; Thornton, J. M. A Revised Set of Potentials for β-Turn Formation in Proteins. *Protein Science,* **1994**, *3*, 2207–2216.
66. Pal, L.; Basu, G.; Chakrabarti, P. Variants of 310-Helices in Proteins. *Proteins: Structure, Function and Genetics,* **2002**, *48* (3), 571–579.
67. Pace, C. N.; Scholtz, J. M. A Helix Propensity Scale Based on Experimental Studies of Peptides and Proteins. *Biophysical Journal,* **1998**, *75* (1), 422–427.
68. Fujiwara, K.; Toda, H.; Ikeguchi, M. Dependence of α-Helical and ß-Sheet Amino Acid Propensities on the Overall Protein Fold Type, *BMC Structural Biology,* **2012**, *12*.

69. Lehmkühler, F.; Forov, Y.; Elbers, M.; Steinke, I.; Sahle, C. J.; Weis, C.; Tsuji, N.; Itou, M.; Sakurai, Y.; Poulain, A.; Sternemann, C. Temperature Dependence of the Hydrogen Bond Network in Trimethylamine: N -Oxide and Guanidine Hydrochloride-Water Solutions, *Physical Chemistry Chemical Physics,* **2017**, *19* (41), 28470–28475.
70. Tiné, M. R.; Alderighi, M.; Duce, C.; Ghezzi, L.; Solaro, R. Effect of Temperature on Self-Assembly of an Ionic Tetrapeptide, *Journal of Thermal Analysis and Calorimetry*, **2011**; *103*, 75–80.
71. Chen, W. Y.; Huang, H. M.; Lin, C. C.; Lin, F. Y.; Chan, Y. C. Effect of Temperature on Hydrophobie Interaction between Proteins and Hydrophobic Adsorbents: Studies by Isothermal Titration Calorimetry and the van't Hoff Equation, *Langmuir,* **2003**, *19* (22), 9395–9403.
72. Henry N. Po; N. M. Senozan. The Henderson-Hasselbalch Equation: Its History and Limitations, *Journal of Chemical Education,* **2001**, *78* (11), 1499.
73. Chagri, S.; Ng, D. Y. W.; Weil, T. Designing Bioresponsive Nanomaterials for Intracellular Self-Assembly. *Nature Reviews Chemistry*, **2022**, *78,* 320–338.
74. Li, Z.; Zhu, Y.; Matson, J. B. PH-Responsive Self-Assembling Peptide-Based Biomaterials: Designs and Applications, *ACS Applied Bio Materials,* **2022**, *5* (10), 4635–4651.
75. Wang, J.; Liu, K.; Yan, L.; Wang, A.; Bai, S.; Yan, X. Trace Solvent as a Predominant Factor to Tune Dipeptide Self-Assembly, *ACS Nano,* **2016**, *10* (2), 2138–2143.
76. Lin, Y.; Penna, M.; Thomas, M. R.; Wojciechowski, J. P.; Leonardo, V.; Wang, Y.; Pashuck, E. T.; Yarovsky, I.; Stevens, M. M. Residue-Specific Solvation-Directed Thermodynamic and Kinetic Control over Peptide Self-Assembly with 1D/2D Structure Selection, *ACS Nano,* **2019**, *13* (2), 1900–1909.
77. Méndez-Ardoy, A.; Bayón-Fernández, A.; Yu, Z.; Abell, C.; Granja, J. R.; Montenegro, J. Spatially Controlled Supramolecular Polymerization of Peptide Nanotubes by Microfluidics, *Angewandte Chemie - International Edition,* **2020**, *59* (17), 6902–6908.
78. Pierandrea Lo Nostro, Barry W. Ninham, *Chemical Reviews*, **2012**, *112* (4), 2286-2322.
79. Chen, Y.; Tao, K.; Ji, W.; Kumar, V. B.; Rencus-Lazar, S.; Gazit, E. Histidine as a Key Modulator of Molecular Self-Assembly: Peptide-Based Supramolecular Materials Inspired by Biological Systems, *Materials Today*, **2022**, *60,* 106–127.
80. Novo, M.; Freire, S.; Al-Soufi, W. Critical Aggregation Concentration for the Formation of Early Amyloid-ß (1-42) Oligomers. *Scientific Reports,* **2018**, *8* (1).
81. Tantakitti, F.; Boekhoven, J.; Wang, X.; Kazantsev, R. V.; Yu, T.; Li, J.; Zhuang, E.; Zandi, R.; Ortony, J. H.; Newcomb, C. J.; Palmer, L. C.; Shekhawat, G. S.; De La Cruz, M. O.; Schatz, G. C.; Stupp, S. I. Energy Landscapes and Functions of Supramolecular Systems. *Nature Materials,* **2016**, *15* (4), 469–476.
82. Ghosh, G.; Barman, R.; Mukherjee, A.; Ghosh, U.; Ghosh, S.; Fernández, G. Control over Multiple Nano- and Secondary Structures in Peptide Self-Assembly. *Angewandte Chemie - International Edition,* **2022**, *61* (5).
83. Pappas, C. G.; Mutasa, T.; Frederix, P. W. J. M.; Fleming, S.; Bai, S.; Debnath, S.; Kelly, S. M.; Gachagan, A.; Ulijn, R. V. Transient Supramolecular Reconfiguration of Peptide Nanostructures Using Ultrasound. *Materials Horizons,* **2014**, *2* (2), 198–202.
84. Vilela-Picos, M.; Novelli, F.; Pazó, A.; Méndez-Ardoy, A.; Marafon, G.; Amorín, M.; Moretto, A.; Granja, J. R. Photo-Assembling Cyclic Peptides for Dynamic Light-Driven Peptide Nanotubes. *Chem,* **2023**, *9* (11), 3365–3378.
85. Kelly, C. M.; Northey, T.; Ryan, K.; Brooks, B. R.; Kholkin, A. L.; Rodriguez, B. J.; Buchete, N. V. Conformational Dynamics and Aggregation Behavior of Piezoelectric Diphenylalanine Peptides in an External Electric Field. *Biophysical Chemistry,* **2015**, *196*, 16–24.
86. Hashim, P. K.; Bergueiro, J.; Meijer, E. W.; Aida, T. Supramolecular Polymerization: A Conceptual Expansion for Innovative Materials. *Progress in Polymer Science*, **2020**, *105.*
87. Matern, J.; Dorca, Y.; Sánchez, L.; Fernández, G. Revision Komplexer Supramolekularer Polymerisation Unter Kinetischer Und Thermodynamischer Kontrolle. *Angewandte Chemie,* **2019**, *131* (47), 16884–16895.

88. De Greef, T. F. A.; Smulders, M. M. J.; Wolffs, M.; Schenning, A. P. H. J.; Sijbesma, R. P.; Meijer, E. W. Supramolecular Polymerization. *Chemical Reviews,* **2009**, *109* (11), 5687–5754.
89. Sorrenti, A.; Leira-Iglesias, J.; Markvoort, A. J.; De Greef, T. F. A.; Hermans, T. M. Non-Equilibrium Supramolecular Polymerization. *Chemical Society Reviews*. **2017**, *46*, 5476–5490.
90. Mattia, E.; Otto, S. Supramolecular Systems Chemistry. *Nature Nanotechnology*, **2015**, *10,* 111–119.
91. Fukui, T.; Kawai, S.; Fujinuma, S.; Matsushita, Y.; Yasuda, T.; Sakurai, T.; Seki, S.; Takeuchi, M.; Sugiyasu, K. Control over Differentiation of a Metastable Supramolecular Assembly in One and Two Dimensions. *Nature Chemistry,* **2017**, *9* (5), 493–499.
92. Hartlieb, M.; Mansfield, E. D. H.; Perrier, S. A Guide to Supramolecular Polymerizations. *Polymer Chemistry*, **2020**, *11*, 1083–1110.
93. Zhao, D.; Moore, J. S. Nucleation-Elongation: A Mechanism for Cooperative Supramolecular Polymerization. *Organic and Biomolecular Chemistry*, **2003**, *1*, 3471–3491.
94. Smulders, M. M. J.; Nieuwenhuizen, M. M. L.; De Greef, T. F. A.; Van Der Schoot, P.; Schenning, A. P. H. J.; Meijer, E. W. How to Distinguish Isodesmic from Cooperative Supramolecular Polymerisation. *Chemistry - A European Journal,* **2010**, *16* (1), 362–367.
95. Van Der Zwaag, D.; Pieters, P. A.; Korevaar, P. A.; Markvoort, A. J.; Spiering, A. J. H.; De Greef, T. F. A.; Meijer, E. W. Kinetic Analysis as a Tool to Distinguish Pathway Complexity in Molecular Assembly: An Unexpected Outcome of Structures in Competition. *Journal of the American Chemical Society,* **2015**, *137* (39), 12677–12688.
96. Grubbs, R. B.; Grubbs, R. H. 50th Anniversary Perspective: Living Polymerization - Emphasizing the Molecule. *Macromolecules*, **2017**, *50*, 6979–6997.
97. Wehner, M.; Würthner, F. Supramolecular Polymerization through Kinetic Pathway Control and Living Chain Growth. *Nature Reviews Chemistry*, **2020**, *4*, 38–53.
98. Markvoort, A. J.; Ten Eikelder, H. M. M.; Hilbers, P. A. J.; De Greef, T. F. A. Fragmentation and Coagulation in Supramolecular (Co)Polymerization Kinetics. *ACS Central Science,* **2016**, *2* (4), 232–241.
99. Bruckner, E. P.; Stupp, S. I. Designing Supramolecular Polymers with Nucleation and Growth Processes. *Polymer International*, **2022**, *71*, 590–595.
100. Ogi, S.; Sugiyasu, K.; Manna, S.; Samitsu, S.; Takeuchi, M. Living Supramolecular Polymerization Realized through a Biomimetic Approach. *Nature Chemistry,* **2014**, *6* (3), 188–195.
101. Kang, J; Miyajima, D; Mori, T; Inoue Y; Itoh Y; Aida T. A Rational Strategy for the Realization of Chain-Growth Supramolecular Polymerization. *Science,* **2015**, *347* (6222), 646–651.
102. Ganda, S.; Stenzel, M. H. Concepts, Fabrication Methods and Applications of Living Crystallization-Driven Self-Assembly of Block Copolymers. *Progress in Polymer Science*, **2020**, *101.*
103. Wang, X.; Guerin, G.; Wang, H.; Wang, Y.; Manners, I.; Winnik, M. A. Cylindrical Block Copolymer Micelles and Co-Micelles of Controlled Length and Architecture. *Science,* **2007**, *317* (5838), 644–647.
104. Guérin, G.; Wang, H.; Manners, I.; Winnik, M. A. Fragmentation of Fiberlike Structures: Sonication Studies of Cylindrical Block Copolymer Micelles and Behavioral Comparisons to Biological Fibrils. *Journal of the American Chemical Society,* **2008**, *130* (44), 14763–14771.
105. Gilroy, J. B.; Gädt, T.; Whittell, G. R.; Chabanne, L.; Mitchels, J. M.; Richardson, R. M.; Winnik, M. A.; Manners, I. Monodisperse Cylindrical Micelles by Crystallization-Driven Living Self-Assembly. *Nature Chemistry,* **2010**, *2* (7), 566–570.
106. Qian, J.; Lu, Y.; Chia, A.; Zhang, M.; Rupar, P. A.; Gunari, N.; Walker, G. C.; Cambridge, G.; He, F.; Guerin, G.; Manners, I.; Winnik, M. A. Self-Seeding in One Dimension: A Route to Uniform Fiber-like Nanostructures from Block Copolymers with a Crystallizable Core-Forming Block. *ACS Nano,* **2013**, *7* (5), 3754–3766.

107. Hudson, Z. M.; Boott, C. E.; Robinson, M. E.; Rupar, P. A.; Winnik, M. A.; Manners, I. Tailored Hierarchical Micelle Architectures Using Living Crystallization-Driven Self-Assembly in Two Dimensions. *Nature Chemistry,* **2014**, *6* (10), 893–898.
108. Deng, R.; Mao, X.; Pearce, S.; Tian, J.; Zhang, Y.; Manners, I. Role of Competitive Crystallization Kinetics in the Formation of 2D Platelets with Distinct Coronal Surface Patterns via Seeded Growth. *Journal of the American Chemical Society,* **2022**, *144* (41), 19051–19059.
109. He, X.; Hsiao, M. S.; Boott, C. E.; Harniman, R. L.; Nazemi, A.; Li, X.; Winnik, M. A.; Manners, I. Two-Dimensional Assemblies from Crystallizable Homopolymers with Charged Termini. *Nature Materials,* **2017**, *16* (4), 481–488.
110. Qiu, H.; Hudson, Z. M.; Winnik, M. A.; Manners, I. Multidimensional Hierarchical Self-Assembly of Amphiphilic Cylindrical Block Comicelles. *Science,* **2015**, *347* (6228), 1329–1332.
111. MacFarlane, L.; Zhao, C.; Cai, J.; Qiu, H.; Manners, I. Emerging Applications for Living Crystallization-Driven Self-Assembly. *Chemical Science*, **2021**, *12*, 4661–4682.
112. Ozin, G. A.; Cademartiri, L. Nanochemistry: What Is Next? *Small,* **2009**, *5* (11), 1240–1244.
113. Abid, N.; Khan, A. M.; Shujait, S.; Chaudhary, K.; Ikram, M.; Imran, M.; Haider, J.; Khan, M.; Khan, Q.; Maqbool, M. Synthesis of Nanomaterials Using Various Top-down and Bottom-up Approaches, Influencing Factors, Advantages, and Disadvantages: A Review. *Advances in Colloid and Interface Science*, **2022**, *300.*
114. Lombardo, D.; Calandra, P.; Pasqua, L.; Magazù, S. Self-Assembly of Organic Nanomaterials and Biomaterials: The Bottom-up Approach for Functional Nanostructures Formation and Advanced Applications. *Materials,* **2020**, *13* (5).
115. Bai, Y.; Luo, Q.; Liu, J. Protein Self-Assembly: Via Supramolecular Strategies. *Chemical Society Reviews*, **2016**, *45*, 2756–2767.
116. Bayda, S.; Adeel, M.; Tuccinardi, T.; Cordani, M.; Rizzolio, F. The History of Nanoscience and Nanotechnology: From Chemical-Physical Applications to Nanomedicine. *Molecules*, **2020**, *25.*
117. Tateishi, T.; Yoshimura, M.; Tokuda, S.; Matsuda, F.; Fujita, D.; Furukawa, S. Coordination/metal-organic cages inside out. *Coordination Chemistry Reviews,* **2022**, *467*, 214612.
118. Baig, N. Two-Dimensional Nanomaterials: A Critical Review of Recent Progress, Properties, Applications, and Future Directions. *Composites Part A: Applied Science and Manufacturing*, **2023**, *165.*
119. Insua, I.; Bergueiro, J.; Méndez-Ardoy, A.; Lostalé-Seijo, I.; Montenegro, J. Bottom-up Supramolecular Assembly in Two Dimensions. *Chemical Science*, **2022**, *13*, 3057–3068.
120. Knowles, T. P. J.; Vendruscolo, M.; Dobson, C. M. The Amyloid State and Its Association with Protein Misfolding Diseases. *Nature Reviews Molecular Cell Biology*, **2014**, *15*, 384–396.
121. Härd, T. Amyloid Fibrils: Formation, Polymorphism, and Inhibition. *Journal of Physical Chemistry Letters*, **2014**, *5*, 607–614.
122. Cherny, I.; Gazit, E. Amyloids: Not Only Pathological Agents but Also Ordered Nanomaterials. *Angewandte Chemie - International Edition*, **2008**, *47*, 4062–4069.
123. Sipe, J. D.; Cohen, A. S. Review: History of the Amyloid Fibril. *Journal of Structural Biology*, **2000**, *130*, 88–98.
124. Knowles, T. P. J.; Mezzenga, R. Amyloid Fibrils as Building Blocks for Natural and Artificial Functional Materials. *Advanced Materials*, **2016**, *28*, 6546–6561.
125. Lai, Y.; Li, F.; Zou, Z.; Saeed, M.; Xu, Z.; Yu, H. Bio-Inspired Amyloid Polypeptides: From Self-Assembly to Nanostructure Design and Biotechnological Applications. *Applied Materials Today*, **2021**, *22.*
126. Zhang, S.; Holmest, T.; Lockshin, C.; Rich, A. Spontaneous Assembly of a Self-Complementary Oligopeptide to Form a Stable Macroscopic Membrane (,B-Sheet/Insoluble Filaments/Ionic Bonds/Origin of Life/Zuotin). *Proceedings of the National Academy of Science USA,* **1993**, *90*, 3334–3338.

127. Dai, B.; Li, D.; Xi, W.; Luo, F.; Zhang, X.; Zou, M.; Cao, M.; Hu, J.; Wang, W.; Wei, G.; Zhang, Y.; Liua, C. Tunable Assembly of Amyloid-Forming Peptides into Nanosheets as a Retrovirus Carrier. *Proceedings of the National Academy of Science U S A,* **2015**, *112* (10), 2996–3001.

128. Jia, B.; Sun, Y.; Yang, L.; Yu, Y.; Fan, H.; Ma, G. A Structural Model of the Hierarchical Assembly of an Amyloid Nanosheet by an Infrared Probe Technique. *Physical Chemistry Chemical Physics,* **2018**, *20* (43), 27261–27271.

129. Adamcik, J.; Sánchez-Ferrer, A.; Ait-Bouziad, N.; Reynolds, N. P.; Lashuel, H. A.; Mezzenga, R. Microtubule-Binding R3 Fragment from Tau Self-Assembles into Giant Multistranded Amyloid Ribbons. *Angewandte Chemie,* **2016**, *128* (2), 628–632.

130. Pan, Y. X.; Liu, C. J.; Zhang, S.; Yu, Y.; Dong, M. 2D-Oriented Self-Assembly of Peptides Induced by Hydrated Electrons. *Chemistry - A European Journal,* **2012**, *18* (46), 14614–14617.

131. Lee, J.; Ju, M.; Cho, O. H.; Kim, Y.; Nam, K. T. Tyrosine-Rich Peptides as a Platform for Assembly and Material Synthesis. *Advanced Science*, **2019**, *6*.

132. Jang, H. S.; Lee, J. H.; Park, Y. S.; Kim, Y. O.; Park, J.; Yang, T. Y.; Jin, K.; Lee, J.; Park, S.; You, J. M.; Jeong, K. W.; Shin, A.; Oh, I. S.; Kwon, M. K.; Kim, Y. Il; Cho, H. H.; Han, H. N.; Kim, Y.; Chang, Y. H.; Paik, S. R.; Nam, K. T.; Lee, Y. S. Tyrosine-Mediated Two-Dimensional Peptide Assembly and Its Role as a Bio-Inspired Catalytic Scaffold. *Nature Communications,* **2014**, *5*.

133. Lee, J.; Choe, I. R.; Kim, N. K.; Kim, W. J.; Jang, H. S.; Lee, Y. S.; Nam, K. T. Water-Floating Giant Nanosheets from Helical Peptide Pentamers. *ACS Nano,* **2016**, *10* (9), 8263–8270.

134. Guo, C.; Luo, Y.; Zhou, R.; Wei, G. Probing the Self-Assembly Mechanism of Diphenylalanine-Based Peptide Nanovesicles and Nanotubes. *ACS Nano,* **2012**, *6* (5), 3907–3918.

135. Reches, M.; Gazit, E. Controlled Patterning of Aligned Self-Assembled Peptide Nanotubes. *Nature Nanotechnology,* **2006**, *1* (3), 195–200.

136. Hill, R. J. A.; Sedman, V. L.; Allen, S.; Williams, P. M.; Paoli, M.; Adler-Abramovich, L.; Gazit, E.; Eaves, L.; Tendler, S. J. B. Alignment of Aromatic Peptide Tubes in Strong Magnetic Fields. *Advanced Materials,* **2007**, *19* (24), 4474–4479.

137. Hartgerink, J. D.; Beniash, E.; Stupp, S. I. Self-Assembly and Mineralization of Peptide-Amphiphile Nanofibers. *Science,* **2001**, *294* (5547), 1684–1688.

138. Hendricks, M. P.; Sato, K.; Palmer, L. C.; Stupp, S. I. Supramolecular Assembly of Peptide Amphiphiles. *Accounts of Chemical Research,* **2017**, *50* (10), 2440–2448.

139. Cui, H.; Cheetham, A. G.; Pashuck, E. T.; Stupp, S. I. Amino Acid Sequence in Constitutionally Isomeric Tetrapeptide Amphiphiles Dictates Architecture of One-Dimensional Nanostructures. *Journal of the America Chemical Society,* **2014**, *136* (35), 12461–12468.

140. Dasgupta, A.; Das, D. Designer Peptide Amphiphiles: Self-Assembly to Applications. *Langmuir* **2019**, *35* (33), 10704–10724.

141. Webber, M. J.; Tongers, J.; Newcomb, C. J.; Marquardt, K.-T.; Bauersachs, J.; Losordo, D. W.; Stupp, S. I. Supramolecular Nanostructures That Mimic VEGF as a Strategy for Ischemic Tissue Repair. *Proceedings of the National Academy of Science U S A,* **2011**, *108* (33), 13438–13443.

142. Toft, D. J.; Moyer, T. J.; Standley, S. M.; Ruff, Y.; Ugolkov, A.; Stupp, S. I.; Cryns, V. L. Coassembled Cytotoxic and Pegylated Peptide Amphiphiles Form Filamentous Nanostructures with Potent Antitumor Activity in Models of Breast Cancer. *ACS Nano,* **2012**, *6* (9), 7956–7965.

143. Capito, R. M.; Azevedo, H. S.; Velichko, Y. S.; Mata, A.; Stupp, S. I. Self-Assembly of Large and Small Molecules into Hierarchically Ordered Sacs and Membranes. *Science,* **2008**, *319* (5871), 1812–1816.

144. Cui, H.; Muraoka, T.; Cheetham, A. G.; Stupp, S. I. Self-Assembly of Giant Peptide Nanobelts. *Nano Letters,* **2009**, *9* (3), 945–951.

145. Moyer, T. J.; Cui, H.; Stupp, S. I. Tuning Nanostructure Dimensions with Supramolecular Twisting. *Journal of Physical Chemistry B,* **2013**, *117* (16), 4604–4610.

146. Chen, Y.; Gan, H. X.; Tong, Y. W. PH-Controlled Hierarchical Self-Assembly of Peptide Amphiphile. *Macromolecules,* **2015**, *48* (8), 2647–2653.

147. Lin, Y.; Thomas, M. R.; Gelmi, A.; Leonardo, V.; Pashuck, E. T.; Maynard, S. A.; Wang, Y.; Stevens, M. M. Self-Assembled 2D Free-Standing Janus Nanosheets with Single-Layer Thickness. *Journal of the American Chemical Society,* **2017**, *139* (39), 13592–13595.

148. Vauthey, S.; Santoso, S.; Gong, H.; Watson, N.; Zhang, S. Molecular Self-Assembly of Surfactant-like Peptides to Form Nanotubes and Nanovesicles. *Proceedings of the National Academy of Science,* **2002**, *99* (8), 5355–5360.

149. Santoso, S.; Hwang, W.; Hartman, H.; Zhang, S. Self-Assembly of Surfactant-like Peptides with Variable Glycine Tails to Form Nanotubes and Nanovesicles. *Nano Letters,* **2002**, *2* (7), 687–691.

150. Xu, H.; Wang, J.; Han, S.; Wang, J.; Yu, D.; Zhang, H.; Xia, D.; Zhao, X.; Waigh, T. A.; Lu, J. R. Hydrophobic-Region-Induced Transitions in Self-Assembled Peptide Nanostructures. *Langmuir,* **2009**, *25* (7), 4115–4123.

151. Cenker, Ç. Ç.; Bucak, S.; Olsson, U. Nanotubes and Bilayers in a Model Peptide System. *Journal of Soft Matter* **2011**, *7* (10), 4868–4875.

152. Hamley, I. W.; Dehsorkhi, A.; Castelletto, V. Self-Assembled Arginine-Coated Peptide Nanosheets in Water. *Chemical Communications* **2013**, *49* (18), 1850–1852.

153. Wang, M.; Wang, J.; Zhou, P.; Deng, J.; Zhao, Y.; Sun, Y.; Yang, W.; Wang, D.; Li, Z.; Hu, X.; King, S. M.; Rogers, S. E.; Cox, H.; Waigh, T. A.; Yang, J.; Lu, J. R.; Xu, H. Nanoribbons Self-Assembled from Short Peptides Demonstrate the Formation of Polar Zippers between ß-Sheets. *Nature Communications,* **2018**, *9* (1).

154. Zhao, Y.; Deng, L.; Yang, W.; Wang, D.; Pambou, E.; Lu, Z.; Li, Z.; Wang, J.; King, S.; Rogers, S.; Xu, H.; Lu, J. R. Tuning One-Dimensional Nanostructures of Bola-Like Peptide Amphiphiles by Varying the Hydrophilic Amino Acids. *Chemistry - A European Journal,* **2016**, *22* (32), 11394–11404.

155. Hulgan, S. A. H.; Hartgerink, J. D. Recent Advances in Collagen Mimetic Peptide Structure and Design. *Biomacromolecules*, **2022**, *23*, 1475–1489.

156. Bretscher, L. E.; Jenkins, C. L.; Taylor, K. M.; DeRider, M. L.; Raines, R. T. Conformational Stability of Collagen Relies on a Stereoelectronic Effect. *Journal of the American Chemical Society*, **2001**, *123*, 777–778.

157. Holmgren, S. K.; Taylor, K. M.; Bretscher, L. E.; Raines, R. T. Code for Collagen's Stability Deciphered. *Nature,* **1998**, *392*, 666–667.

158. Rele, S.; Song, Y.; Apkarian, R. P.; Qu, Z.; Conticello, V. P.; Chaikof, E. L. D-Periodic Collagen-Mimetic Microfibers. *Journal of the American Chemical Society,* **2007**, *129* (47), 14780–14787.

159. O'Leary, L. E. R.; Fallas, J. A.; Bakota, E. L.; Kang, M. K.; Hartgerink, J. D. Multi-Hierarchical Self-Assembly of a Collagen Mimetic Peptide from Triple Helix to Nanofibre and Hydrogel. *Nature Chemistry,* **2011**, *3* (10), 821–828.

160. Babu, I. R.; Ganesh, K. N. Enhanced Triple Helix Stability of Collagen Peptides with 4R-Aminoprolyl (Amp) Residues: Relative Roles of Electrostatic and Hydrogen Bonding Effects. *Journal of the American Chemical Society*, **2001**, *123*, 2079–2080.

161. Umashankara, M.; Ramesh Babu, I.; Ganesh, K. N. Two Prolines with a Difference: Contrasting Stereoelectronic Effects of 4R/S-Aminoproline on Triplex Stability in Collagen Peptides. *Chemical Communications,* **2003**, *3* (20), 2606–2607.

162. Jiang, T.; Xu, C.; Liu, Y.; Liu, Z.; Wall, J. S.; Zuo, X.; Lian, T.; Salaita, K.; Ni, C.; Pochan, D.; Conticello, V. P. Structurally Defined Nanoscale Sheets from Self-Assembly of Collagen-Mimetic Peptides. *Journal of the American Chemical Society,* **2014**, *136* (11), 4300–4308.

163. Jiang, T.; Xu, C.; Zuo, X.; Conticello, V. P. Structurally Homogeneous Nanosheets from Self-Assembly of a Collagen-Mimetic Peptide. *Angewandte Chemie - International Edition,* **2014**, *53* (32), 8367–8371.

164. Jiang, T.; Magnotti, E. L.; Conticello, V. P. Geometrical Frustration as a Potential Design Principle for Peptide-Based Assemblies. *Interface Focus*, **2017**, *7*.
165. Merg, A. D.; Touponse, G.; van Genderen, E.; Zuo, X.; Bazrafshan, A.; Blum, T.; Hughes, S.; Salaita, K.; Abrahams, J. P.; Conticello, V. P. 2D Crystal Engineering of Nanosheets Assembled from Helical Peptide Building Blocks. *Angewandte Chemie,* **2019**, *131* (38), 13641–13646.
166. (164)Merg, A. D.; Van Genderen, E.; Bazrafshan, A.; Su, H.; Zuo, X.; Touponse, G.; Blum, T. B.; Salaita, K.; Abrahams, J. P.; Conticello, V. P. Seeded Heteroepitaxial Growth of Crystallizable Collagen Triple Helices: Engineering Multifunctional Two-Dimensional Core-Shell Nanostructures. *Journal of the American Chemical Society,* **2019**, *141* (51), 20107–20117.
167. Zhang, W.; Mo, S.; Liu, M.; Liu, L.; Yu, L.; Wang, C. Rationally Designed Protein Building Blocks for Programmable Hierarchical Architectures. *Frontiers in Chemistry*, **2020**, *8*.
168. Woolfson, D. N. Understanding a Protein Fold: The Physics, Chemistry, and Biology of α-Helical Coiled Coils. *Journal of Biological Chemistry*, **2023**, *299*.
169. Woolfson, D. N.; Bartlett, G. J.; Bruning, M.; Thomson, A. R. New Currency for Old Rope: From Coiled-Coil Assemblies to α-Helical Barrels. *Current Opinion in Structural Biology*, **2012**, *22*, 432–441.
170. Dawson, W. M.; Martin, F. J. O.; Rhys, G. G.; Shelley, K. L.; Brady, R. L.; Woolfson, D. N. Coiled Coils 9-to-5: Rational: De Novo Design of α-Helical Barrels with Tunable Oligomeric States. *Chemical Science,* **2021**, *12* (20), 6923–6928.
171. Kumar, P.; Paterson, N. G.; Clayden, J.; Woolfson, D. N. De Novo Design of Discrete, Stable 310-Helix Peptide Assemblies. *Nature,* **2022**, *607* (7918), 387–392.
172. Thomson, A. R.; Wood, C. W.; Burton, A. J.; Bartlett, G. J.; Sessions, R. B.; Brady, R. L.; Woolfson, D. N. Computational Design of Water-Soluble α-Helical Barrels. *Science,* **2014**, *346* (6208), 485–488.
173. Zhang, H. V.; Polzer, F.; Haider, M. J.; Tian, Y.; Villegas, J. A.; Kiick, K. L.; Pochan, D. J.; Saven, J. G. Computationally Designed Peptides for Self-Assembly of Nanostructured Lattices. *Science Advances,* **2016**, *2* (9).
174. Tian, Y.; Zhang, H. V.; Kiick, K. L.; Saven, J. G.; Pochan, D. J. Transition from Disordered Aggregates to Ordered Lattices: Kinetic Control of the Assembly of a Computationally Designed Peptide. *Organic and Biomolecular Chemistry,* **2017**, *15* (29), 6109–6118.
175. Tian, Y.; Polzer, F. B.; Zhang, H. V.; Kiick, K. L.; Saven, J. G.; Pochan, D. J. Nanotubes, Plates, and Needles: Pathway-Dependent Self-Assembly of Computationally Designed Peptides. *Biomacromolecules* **2018**, *19* (11), 4286–4298.
176. Chen, X.; Xia, C.; Guo, P.; Wang, C.; Zuo, X.; Jiang, Y. B.; Jiang, T. Preserving Structurally Labile Peptide Nanosheets After Molecular Functionalization of the Self-Assembling Peptides. *Angewandte Chemie - International Edition* **2023**, *63*.
177. Galloway, J. M.; Bray, H. E. V.; Shoemark, D. K.; Hodgson, L. R.; Coombs, J.; Mantell, J. M.; Rose, R. S.; Ross, J. F.; Morris, C.; Harniman, R. L.; Wood, C. W.; Arthur, C.; Verkade, P.; Woolfson, D. N. De Novo Designed Peptide and Protein Hairpins Self-Assemble into Sheets and Nanoparticles. *Small,* **2021**, *17* (10).
178. Magnotti, E. L.; Hughes, S. A.; Dillard, R. S.; Wang, S.; Hough, L.; Karumbamkandathil, A.; Lian, T.; Wall, J. S.; Zuo, X.; Wright, E. R.; Conticello, V. P. Self-Assembly of an α-Helical Peptide into a Crystalline Two-Dimensional Nanoporous Framework. *Journal of the American Chemical Society,* **2016**, *138* (50), 16274–16282.
179. De Santis, P.; Morosetti, S.; Rizzo, R. Conformational Analysis of Regular Enantiomeric Sequences. *Macromolecules,* **1974**, *7* (1), 52–58.
180. M. Reza Ghadiri; Juan R. Granja; Ronald A. Milligan; Duncan E. McRee; Nina Khazanovich. Self-Assembling Organic Nanotubes Based on Cyclic Peptide Architecture. *Nature*. **1993**, *366*, 324–327.
181. Engels, M.; Bashford, D.; Ghadiri, M. R. Structure and Dynamics of Self-Assembling Peptide Nanotubes and the Channel-Mediated Water Organization and Self-Diffusion. A

Molecular Dynamics Study. *Journal of the American Chemical Society,* **1995**, *117*, 9151–9158.

182. Baughman, R. H.; Zakhidov, A. A.; De Heer, W. A. Carbon Nanotubes - The Route toward Applications. *Science*, **2002**, *354*, 787–792.
183. Iijima, S. Helical Microtubules of Graphitic Carbon. *Nature,* **1991**, *354*, 56–58.
184. Song, Q.; Cheng, Z.; Kariuki, M.; Hall, S. C. L.; Hill, S. K.; Rho, J. Y.; Perrier, S. Molecular Self-Assembly and Supramolecular Chemistry of Cyclic Peptides. *Chemical Reviews*, **2021**, *121*, 13936–13995.
185. Khazanovich, N.; Granja, J. R.; McRee, D. E.; Milligan, R. A.; Reza Ghadiri, M.; Sloan, A. P. Nanoscale Tubular Ensembles with Specified Internal Diameters. Design of a Self-Assembled Nanotube with a 13-.ANG. Pore. *Journal of the American Chemical Society,* **1994**, *116* (1), 6011–6012.
186. Clark, T. D.; Buriak, J. M.; Kobayashi, K.; Isler, M. P.; Mcree, D. E.; Ghadiri, M. R. Cylindrical-Sheet Peptide Assemblies. *Journal of the American Chemical Society,* **1998**, *120* (35), 8949–8962.
187. Hartgerink, J. D.; Granja, J. R.; Milligan, R. A.; Ghadiri, M. R. Self-Assembling Peptide Nanotubes. *Journal of the American Chemical Society,* **1996**, *118,* 43-50.
188. Kobayashi, K.; Granja, J. R.; Ghadiri M. R. ß-Sheet Peptide Architecture: Measuring the Relative Stability of Parallel vs. Antiparallel ß-Sheets. *Angewandte Chemie International Edition,* **1995**, *34* (1), 95–98.
189. Rubin, D. J.; Amini, S.; Zhou, F.; Su, H.; Miserez, A.; Joshi, N. S. Structural, Nanomechanical, and Computational Characterization of D,L-Cyclic Peptide Assemblies. *ACS Nano,* **2015**, *9* (3), 3360–3368.
190. Rubin, D. J.; Nia, H. T.; Desire, T.; Nguyen, P. Q.; Gevelber, M.; Ortiz, C.; Joshi, N. S. Mechanical Reinforcement of Polymeric Fibers through Peptide Nanotube Incorporation. *Biomacromolecules,* **2013**, *14* (10), 3370–3375.
191. Shaikh, H.; Rho, J. Y.; Macdougall, L. J.; Gurnani, P.; Lunn, A. M.; Yang, J.; Huband, S.; Mansfield, E. D. H.; Peltier, R.; Perrier, S. Hydrogel and Organogel Formation by Hierarchical Self-Assembly of Cyclic Peptides Nanotubes. *Chemistry - A European Journal,* **2018**, *24* (71), 19066–19074.
192. Lim, Y. B.; Lee, M. Nanostructures of ß-Sheet Peptides: Steps towards Bioactive Functional Materials. *Journal of Materials Chemistry,* **2008**, *18* (7), 723–727.
193. Silk, M. R.; Newman, J.; Ratcliffe, J. C.; White, J. F.; Caradoc-Davies, T.; Price, J. R.; Perrier, S.; Thompson, P. E.; Chalmers, D. K. Parallel and Antiparallel Cyclic d/l Peptide Nanotubes. *Chemical Communications,* **2017**, *53* (49), 6613–6616.
194. Seebacb, D.; Matthewsl, J. L.; Meden2, A.; Wessels, T.; Baerlocher, C.; Mccusker, L. B. Cyclo-B-Peptides: Structure and Tubular Stacking of Cyclic Tetramers of 3-Aminobutanoic Acid as Determined from Powder Diffraction Data. *Helvetica Chimica Acta,* **1997**, *80*.
195. Amorín, M.; Castedo, L.; Granja, J. R. New Cyclic Peptide Assemblies with Hydrophobic Cavities: The Structural and Thermodynamic Basis of a New Class of Peptide Nanotubes. *Journal of the American Chemical Society,* **2003**, *125* (10), 2844–2845.
196. Gauthier, D.; Baillargeon, P.; Drouin, M.; Dory, Y. L. Self-Assembly of Cyclic Peptides into Nanotubes and Then into Highly Anisotropic Crystalline Materials. *Angewandte Chemie - International Edition,* **2001**, *40* (24), 4635–4638.
197. Horne, W. S.; Stout, C. D.; Ghadiri, M. R. A Heterocyclic Peptide Nanotube. *Journal of the American Chemical Society,* **2003**, *125* (31), 9372–9376.
198. Van Maarseveen, J. H.; Horne, W. S.; Ghadiri, M. R.; Lett, O. Efficient Route to C 2 Symmetric Heterocyclic Backbone Modified Cyclic Peptides. *Organic Letters,* **2005**, *7* (20), 4503–4506.
199. Calvelo, M.; Lamas, A.; Guerra, A.; Amorín, M.; Garcia-Fandino, R.; Granja, J. R. Parallel Versus Antiparallel ß-Sheet Structure in Cyclic Peptide Hybrids Containing γ- or δ-Cyclic Amino Acids. *Chemistry - A European Journal,* **2020**, *26* (26), 5846–5858.

200. Brea, R. J.; Castedo, L.; Granja, J. R. Large-Diameter Self-Assembled Dimers of α,γ-Cyclic Peptides, with the Nanotubular Solid-State Structure of Cyclo-[(L-Leu-D-^{Me}N-γ-Acp)$_4$-] ·4CHCl$_2$COOH. *Chemical Communications,* **2007**, *31*, 3267–3269.
201. Reza Ghadiri, M.; Granja, J. R.; Buehler, L. K. Artificial Transmembrane Ion Channels from Self-Assembling Peptide Nanotubes. *Nature,* **1994**, *369* (6478), 301–304.
202. García-Fandiño, R.; Amorín, M.; Castedo, L.; Granja, J. R. Transmembrane Ion Transport by Self-Assembling α,γ-Peptide Nanotubes. *Chemical Science,* **2012**, *3* (11), 3280–3285.
203. Horne, W. S.; Wiethoff, C. M.; Cui, C.; Wilcoxen, K. M.; Amorin, M.; Ghadiri, M. R.; Nemerow, G. R. Antiviral Cyclic D,L-α-Peptides: Targeting a General Biochemical Pathway in Virus Infections. *Bioorganic and Medicinal Chemistry,* **2005**, *13* (17), 5145–5153.
204. Lamas, A.; Guerra, A.; Amorín, M.; Granja, J. R. New Self-Assembling Peptide Nanotubes of Large Diameter Using δ-Amino Acids. *Chemical Science,* **2018**, *9* (43), 8228–8233.
205. Rodríguez-Vázquez, N.; García-Fandiño, R.; Aldegunde, M. J.; Brea, J.; Loza, M. I.; Amorín, M.; Granja, J. R. Cis-Platinum Complex Encapsulated in Self-Assembling Cyclic Peptide Dimers. *Organic Letters,* **2017**, *19* (10), 2560–2563.
206. Darnall, S. M.; Li, C.; Dunbar, M.; Alsina, M.; Keten, S.; Helms, B. A.; Xu, T. Organic Nanotube with Subnanometer, PH-Responsive Lumen. *Journal of the American Chemical Society,* **2019**, *141* (28), 10953–10957.
207. Horne, W. S.; Ashkenasy, N.; Ghadiri, M. R. Modulating Charge Transfer Through Cyclic D,L α-Peptide Self-Assembly. *Chemistry - A European Journal,* **2005**, *11*, 1137–1144.
208. Montenegro, J.; Vázquez-Vázquez, C.; Kalinin, A.; Geckeler, K. E.; Granja, J. R. Coupling of Carbon and Peptide Nanotubes. *Journal of the American Chemical Society,* **2014**, *136* (6), 2484–2491.
209. Cuerva, M.; García-Fandiño, R.; Vázquez-Vázquez, C.; López-Quintela, M. A.; Montenegro, J.; Granja, J. R. Self-Assembly of Silver Metal Clusters of Small Atomicity on Cyclic Peptide Nanotubes. *ACS Nano,* **2015**, *9* (11), 10834–10843.
210. Méndez-Ardoy, A.; Granja, J. R.; Montenegro, J. PH-Triggered Self-Assembly and Hydrogelation of Cyclic Peptide Nanotubes Confined in Water Micro-Droplets. *Nanoscale Horizons,* **2018**, *3* (4), 391–396.
211. Couet, J.; Biesalski, M. Polymer-Wrapped Peptide Nanotubes: Peptide-Grafted Polymer Mass Impacts Length and Diameter. *Small,* **2008**, *4* (7), 1008–1016.
212. Chapman, R.; Jolliffe, K. A.; Perrier, S. Modular Design for the Controlled Production of Polymeric Nanotubes from Polymer/Peptide Conjugates. *Polymer Chemistry,* **2011**, *2* (9), 1956–1963.
213. Chapman, R.; Bouten, P. J. M.; Hoogenboom, R.; Jolliffe, K. A.; Perrier, S. Thermoresponsive Cyclic Peptide – Poly(2-Ethyl-2-Oxazoline) Conjugate Nanotubes. *Chemical Communications,* **2013**, *49* (58), 6522–6524.
214. Chapman, R.; Warr, G. G.; Perrier, S.; Jolliffe, K. A. Water-Soluble and PH-Responsive Polymeric Nanotubes from Cyclic Peptide Templates. *Chemistry - A European Journal,* **2013**, *19* (6), 1955–1961.
215. Yang, J.; Song, J. I.; Song, Q.; Rho, J. Y.; Mansfield, E. D. H.; Hall, S. C. L.; Sambrook, M.; Huang, F.; Perrier, S. Hierarchical Self-Assembled Photo-Responsive Tubisomes from a Cyclic Peptide-Bridged Amphiphilic Block Copolymer. *Angewandte Chemie - International Edition,* **2020**, *59* (23), 8860–8863.
216. Rho, J. Y.; Cox, H.; Mansfield, E. D. H.; Ellacott, S. H.; Peltier, R.; Brendel, J. C.; Hartlieb, M.; Waigh, T. A.; Perrier, S. Dual Self-Assembly of Supramolecular Peptide Nanotubes to Provide Stabilisation in Water. *Nature Communications,* **2019**, *10* (1).
217. Mansfield, E. D. H.; Hartlieb, M.; Catrouillet, S.; Rho, J. Y.; Larnaudie, S. C.; Rogers, S. E.; Sanchis, J.; Brendel, J. C.; Perrier, S. Systematic Study of the Structural Parameters Affecting the Self-Assembly of Cyclic Peptide-Poly(Ethylene Glycol) Conjugates. *Soft Matter Journal,* **2018**, *14* (30), 6320–6326.
218. Danial, M.; My-Nhi Tran, C.; Young, P. G.; Perrier, S.; Jolliffe, K. A. Janus Cyclic Peptide-Polymer Nanotubes. *Nature Communications,* **2013**, *4*.

219. Brendel, J. C.; Sanchis, J.; Catrouillet, S.; Czuba, E.; Chen, M. Z.; Long, B. M.; Nowell, C.; Johnston, A.; Jolliffe, K. A.; Perrier, S. Secondary Self-Assembly of Supramolecular Nanotubes into Tubisomes and Their Activity on Cells. *Angewandte Chemie - International Edition,* **2018**, *57* (51), 16678–16682.

220. Fernandez-Lopez, S; Kim, H. S; Choi, E. C; Delgado, M; Granja, J.R; Khasanov, A; Kraehenbuehl, K; Long, G; Weinberger, D. A; Wilcoxen, K. M; Ghadiri, M. R. Antibacterial Agents Based on the Cyclic D,L-α-Peptide Architecture. *Nature,* **2001**, *412*, 452–455.

221. Claro, B.; González-Freire, E.; Calvelo, M.; Bessa, L. J.; Goormaghtigh, E.; Amorín, M.; Granja, J. R.; Garcia-Fandiño, R.; Bastos, M. Membrane Targeting Antimicrobial Cyclic Peptide Nanotubes – an Experimental and Computational Study. *Colloids and Surfaces B: Biointerfaces,* **2020**, *196*.

222. Dartois, V.; Sanchez-Quesada, J.; Cabezas, E.; Chi, E.; Dubbelde, C.; Dunn, C.; Granja, J.; Gritzen, C.; Weinberger, D.; Ghadiri, M. R.; Parr, T. R. Systemic Antibacterial Activity of Novel Synthetic Cyclic Peptides. *Antimicrobial Agents Chemotherapy,* **2005**, *49* (8), 3302–3310.

223. Chen, J.; Zhang, B.; Xia, F.; Xie, Y.; Jiang, S.; Su, R.; Lu, Y.; Wu, W. Transmembrane Delivery of Anticancer Drugs through Self-Assembly of Cyclic Peptide Nanotubes. *Nanoscale,* **2016**, *8* (13), 7127–7136.

224. Insua, I.; Montenegro, J. 1D to 2D Self Assembly of Cyclic Peptides. *Journal of the American Chemical Society,* **2020**, *142* (1), 300–307.

225. El-Faham, A.; Albericio, F. Peptide Coupling Reagents, More than a Letter Soup. *Chemical Reviews*, **2011**, *111*, 6557–6602.

226. Palomo, J. M. Solid-Phase Peptide Synthesis: An Overview Focused on the Preparation of Biologically Relevant Peptides. *RSC Advances*, **2014**, *4*, 32658–32672.

227. Coppock, M. B.; Winton Editors, A. J. *Peptide Macrocycles Methods and Protocols Methods in Molecular Biology,* Vol. 2371, Winton Editors, **2022**, pp. 467-469.

228. Wolfe, L. S.; Calabrese, M. F.; Nath, A.; Blaho, D. V; Miranker, A. D.; Xiong, Y. Protein-Induced Photophysical Changes to the Amyloid Indicator Dye Thioflavin T. *Proceedings of the National Academy of Science U.S.A,* **2010**, *107* (39), 16863–16868.

229. Singh, P. K.; Mora, A. K.; Nath, S. Ultrafast Fluorescence Spectroscopy Reveals a Dominant Weakly-Emissive Population of Fibril Bound Thioflavin-T. *Chemical Communications,* **2015**, *51* (74), 14042–14045.

230. Groenning, M. Binding Mode of Thioflavin T and Other Molecular Probes in the Context of Amyloid Fibrils-Current Status. *Journal of Chemical Biology*, **2010**, *3*, 1–18.

231. Khurana, R.; Coleman, C.; Ionescu-Zanetti, C.; Carter, S. A.; Krishna, V.; Grover, R. K.; Roy, R.; Singh, S. Mechanism of Thioflavin T Binding to Amyloid Fibrils. *Journal of Structural Biology,* **2005**, *151* (3), 229–238.

232. Schneider, C. A.; Rasband, W. S.; Eliceiri, K. W. NIH Image to ImageJ: 25 Years of Image Analysis. *Nature Methods*, **2012**, *9*, 671–675.

233. Schindelin, J.; Arganda-Carreras, I.; Frise, E.; Kaynig, V.; Longair, M.; Pietzsch, T.; Preibisch, S.; Rueden, C.; Saalfeld, S.; Schmid, B.; Tinevez, J. Y.; White, D. J.; Hartenstein, V.; Eliceiri, K.; Tomancak, P.; Cardona, A. Fiji: An Open-Source Platform for Biological-Image Analysis. *Nature Methods*, **2012**, *9*, 676–682.

234. Nečas, D.; Klapetek, P. Gwyddion: An Open-Source Software for SPM Data Analysis. *Central European Journal of Physics*, **2012**, *10*, 181–188.

235. Kay, C.; Lorthioir, O. E.; Parr, N. J.; Congreve, M.; Mckeown, S. C.; Scicinski, J. J.; Ley, S. V. Solid-Phase Reaction Monitoring-Chemical Derivatization and Off-Bead Analysis. *Biotechnology and Bioengineering,* **2001**, *71*, 110-118.

236. Xue, C.; Lin, T. Y.; Chang, D.; Guo, Z. Thioflavin T as an Amyloid Dye: Fibril Quantification, Optimal Concentration and Effect on Aggregation. *Royal Society Open Science,* **2017**, *4* (1).

237. Sarroukh, R.; Goormaghtigh, E.; Ruysschaert, J. M.; Raussens, V. ATR-FTIR: A "Rejuvenated" Tool to Investigate Amyloid Proteins. *Biochimica et Biophysica Acta – Biomembranes*, **2013**, *1828*, 2328–2338.

238. Reza Ghadiri, M.; Kobayashi, K.; Granja, J. R.; Chadha, R. K.; McRee, D. E. The Structural and Thermodynamic Basis for the Formation of Self-Assembled Peptide Nanotubes. *Angewandte Chemie International Edition English,* **1995**, *34*, 93–95.

239. Amorín, M.; Castedo, L.; Granja, J. R. Folding Control in Cyclic Peptides through N-Methylation Pattern Selection: Formation of Antiparallel ß-Sheet Dimers, Double Reverse Turns and Supramolecular Helices by 3α,γ Cyclic Peptides. *Chemistry - A European Journal,* **2008**, *14* (7), 2100–2111.

240. González-Freire, E.; Novelli, F.; Pérez-Estévez, A.; Seoane, R.; Amorín, M.; Granja, J. R. Double Orthogonal Click Reactions for the Development of Antimicrobial Peptide Nanotubes. *Chemistry - A European Journal,* **2021**, *27* (9), 3029–3038.

241. Zou, Y.; Li, Y.; Hao, W.; Hu, X.; Ma, G. Parallel ß-Sheet Fibril and Antiparallel ß-Sheet Oligomer: New Insights into Amyloid Formation of Hen Egg White Lysozyme under Heat and Acidic Condition from FTIR Spectroscopy. *Journal of Physical Chemistry B,* **2013**, *117* (15), 4003–4013.

242. Clark, T. D.; Buriak, J. M.; Kobayashi, K.; Isler, M. P.; Mcree, D. E.; Ghadiri, M. R. Cylindrical-Sheet Peptide Assemblies. *Journal of the American Chemical Society,* **1998**, *120,* 8949–8962.

243. Mendez-Ardoy, A.; Bayón-Fernández, A.; Yu, Z.; Abell, C.; Granja, J. R.; Montenegro, J. Spatially Controlled Supramolecular Polymerization of Peptide Nanotubes by Microfluidics. *Angewandte Chemie - International Edition,* **2020**, *59* (17), 6902–6908.

244. Méndez-Ardoy, A.; Granja, J. R.; Montenegro, J. PH-Triggered Self-Assembly and Hydrogelation of Cyclic Peptide Nanotubes Confined in Water Micro-Droplets. *Nanoscale Horizons,* **2018**, *3* (4), 391–396.

245. Díaz, S.; Insua, I.; Bhak, G.; Montenegro, J. Sequence Decoding of 1D to 2D Self-Assembling Cyclic Peptides. *Chemistry - A European Journal,* **2020**, *26* (64), 14765–14770.

246. Panciera, M.; Gonzalez-Freire, E.; Calvelo, M.; Amorín, M.; Granja, J. R. Induced α,γ-Cyclic Peptide Rotodimer Recognition by Nucleobase Scaffolds. *Peptide Science,* **2020**, *112* (1).

247. Cochran, A. G.; Skelton, N. J.; Starovasnik, M. A. Tryptophan Zippers: Stable, Monomeric-Hairpins. *Proceedings of the National Academy of Science,* **2001**, *8* (10), 5578–5583.

248. Bochicchio, D.; Kwangmettatam, S.; Kudernac, T.; Pavan, G. M. How Defects Control the Out-of-Equilibrium Dissipative Evolution of a Supramolecular Tubule. *ACS Nano,* **2019**, *13* (4), 4322–4334.

249. de Marco, A. L.; Bochicchio, D.; Gardin, A.; Doni, G.; Pavan, G. M. Controlling Exchange Pathways in Dynamic Supramolecular Polymers by Controlling Defects. *ACS Nano,* **2021**, *15* (9), 14229–14241.

250. Barducci, A.; Bussi, G.; Parrinello, M. Well-Tempered Metadynamics: A Smoothly Converging and Tunable Free-Energy Method. *Physical Review Letters,* **2008**, *100* (2).

251. Marrink, S. J.; Risselada, H. J.; Yefimov, S.; Tieleman, D. P.; De Vries, A. H. The MARTINI Force Field: Coarse Grained Model for Biomolecular Simulations. *Journal of Physical Chemistry B,* **2007**, *111* (27), 7812–7824.

252. Empereur-Mot, C.; Pesce, L.; Doni, G.; Bochicchio, D.; Capelli, R.; Perego, C.; Pavan, G. M. Swarm-CG: Automatic Parametrization of Bonded Terms in MARTINI-Based Coarse-Grained Models of Simple to Complex Molecules via Fuzzy Self-Tuning Particle Swarm Optimization. *ACS Omega,* **2020**, *5* (50), 32823–32843.

253. Bochicchio, D.; Salvalaglio, M.; Pavan, G. M. Into the Dynamics of a Supramolecular Polymer at Submolecular Resolution. *Nature Communications,* **2017**, *8* (1).

254. Bochicchio, D.; Pavan, G. M. From Cooperative Self-Assembly to Water-Soluble Supramolecular Polymers Using Coarse-Grained Simulations. *ACS Nano,* **2017**, *11* (1), 1000–1011.

255. Bochicchio, D.; Pavan, G. M. Effect of Concentration on the Supramolecular Polymerization Mechanism via Implicit-Solvent Coarse-Grained Simulations of Water-Soluble 1,3,5-Benzenetricarboxamide. *J. Phys. Chem. Lett.,* **2017**, *8* (16), 3813–3819.

256. Insua, I.; Cardellini, A.; Díaz, S.; Bergueiro, J.; Capelli, R.; Pavan, G. M.; Montenegro, J. Self-Assembly of Cyclic Peptide Monolayers by Hydrophobic Supramolecular Hinges. *Chemical Science,* **2023**, *14* (48), 14074–14081.

257. Yuan, C.; Ji, W.; Xing, R.; Li, J.; Gazit, E.; Yan, X. Hierarchically Oriented Organization in Supramolecular Peptide Crystals. *Nature Reviews Chemistry*, **2019**, *3*, 567–588.

258. Pedersen, J. S. *Analysis of Small-Angle Scattering Data from Colloids and Polymer Solutions: Modeling and Least-Squares Fitting I*; ELSEVIER, **1997**; Vol. 70.

259. Biancalana, M.; Makabe, K.; Koide, A.; Koide, S. Molecular Mechanism of Thioflavin-T Binding to the Surface of β-Rich Peptide Self-Assemblies. *Journal of Molecular Biology,* **2009**, *385* (4), 1052–1063.

260. Babenko, V.; Dzwolak, W. Thioflavin T Forms a Non-Fluorescent Complex with α-Helical Poly-l-Glutamic Acid. *Chemical Communications,* **2011**, *47* (38), 10686–10688.

261. Abbas, M.; Lipiński, W. P.; Nakashima, K. K.; Huck, W. T. S.; Spruijt, E. A Short Peptide Synthon for Liquid–Liquid Phase Separation. *Nature Chemistry,* **2021**, *13* (11), 1046–1054.

10. EXPERIMENTAL SECTION

10.1.SEQUENCE DECODING OF 1D-TO-2D SELF-ASSEMBLING CYCLIC PEPTIDES

10.1.1. Characterization

10.1.1.1. CP_A

UHPLC-MS (C18-ESI, +eV) A = H_2O + 0.1% TFA; B = ACN + 0.1% TFA; Gradient (A:B): 100:0 (0 min) → 25:75 (21 min); R_t = 9.5 min. Product after HPLC purification: white solid (35 mg, 36%) m/z = 958.5 ($[M+H]^+$), 479.8 ($[M+2H]^{2+}$).

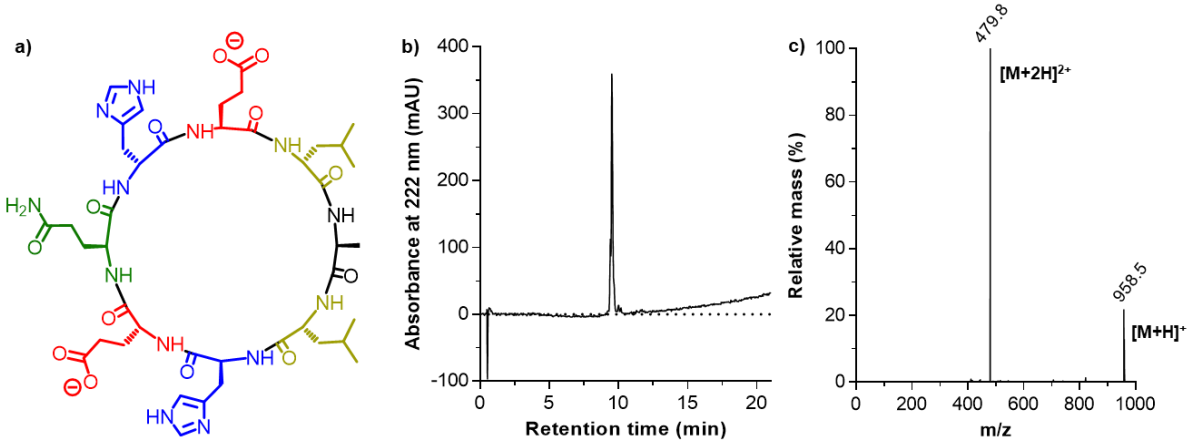

Figure S1.1. a) Structure of CP_A; b) Chromatogram after purification; c) MS spectrum.

HR-MS (ESI, +eV) m/z = 958.4741 (calculated for $[M+H]^+$); 958.4744 (found).

^{1}H-NMR (300 MHz, D_2O) δ: 0.78-0.95 (m, 17H, Leu *i*-Bu x2, Ala-CH_3), 1.31-1.38 (m, 4H, Leu-CH_2), 1.49-1.69 (m, 4H, Glu-CH_2- x2), 1.82-2.13 (m, 4H, Gln x2), 2.27-2.34 (m, 4H, Glu-CH_2- x2), 3.01-3.43 (m, 4H, His-CH_2- x2), 4.17-4.47 (m, 8H, H_α), 7.28 (s, 2H, His-CH= x2), 8.65 (s, 2H, His-CH= x2) ppm.

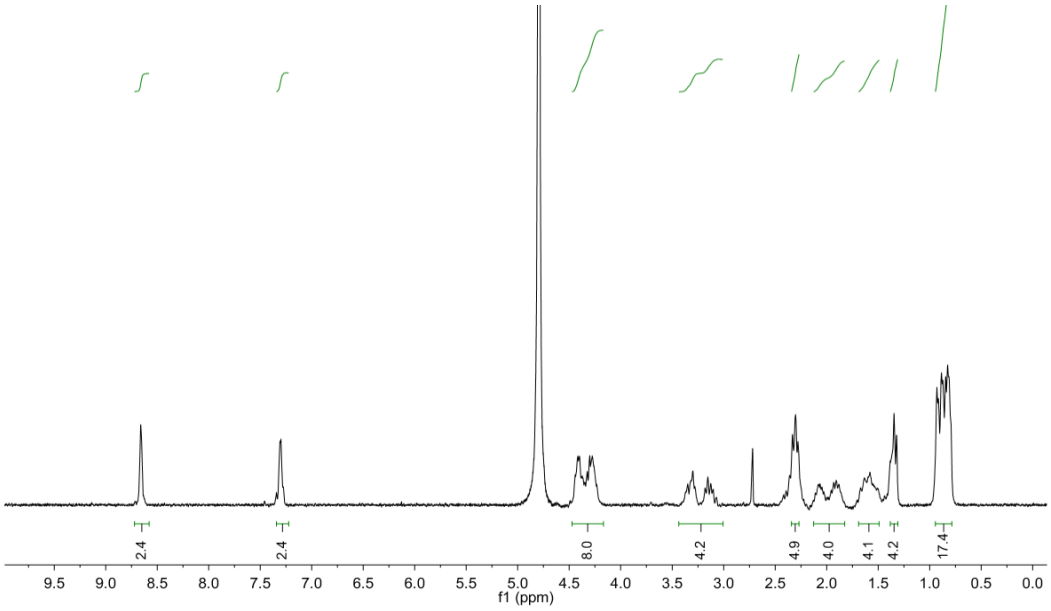

Figure S1.2. ^{1}H NMR (300 MHz) of CP_A in D_2O.

10.1.1.2. CP_L

UHPLC-MS (C18-ESI, +eV) A = H_2O + 0.1% TFA; B = ACN + 0.1% TFA; Gradient (A:B): 100:0 (0 min) → 25:75 (21 min); R_t =11.1 min. Product after HPLC purification: white solid (40 mg, 40%); m/z = 1000.5 ($[M+H]^+$), 500.8 ($[M+2H]^{2+}$).

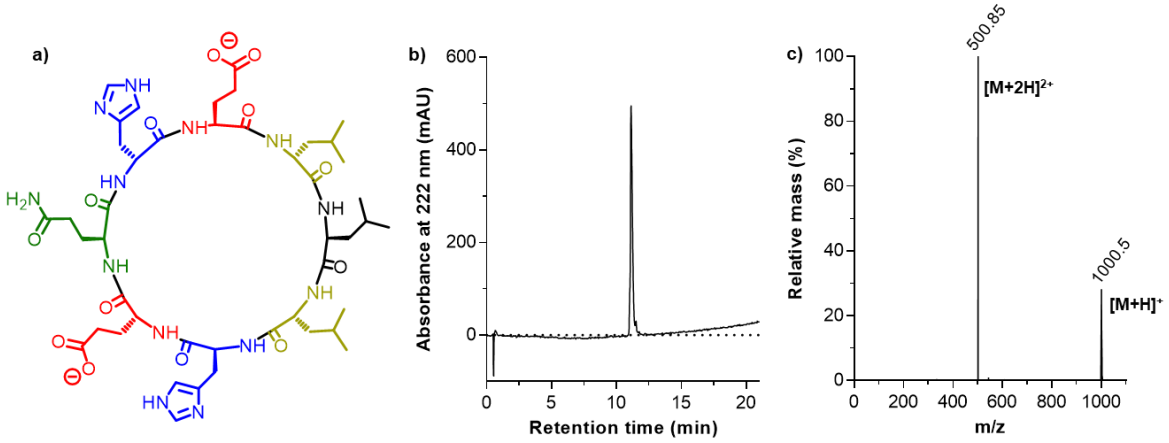

Figure S1.3. a) Structure of **CP_L**; b) Chromatogram after purification; c) MS spectrum.

HR-MS (ESI, +eV): m/z = 1000.5211 (calculated for $[M+H]^+$); 1000.5206 (found).

^{1}H-NMR (300 MHz, D_2O) δ: 0.78-0.95 (m, 27H, Leu x3), 1.49-2.37 (m, 12H, Glu x2, Gln), 3.01-3.44 (m, 4H, His-CH_2- x2), 4.18-4.76 (m, 8H, H_α), 7.29 (s, 2H, His-CH= x2), 8.65 (s, 2H, His-CH= x2) ppm.

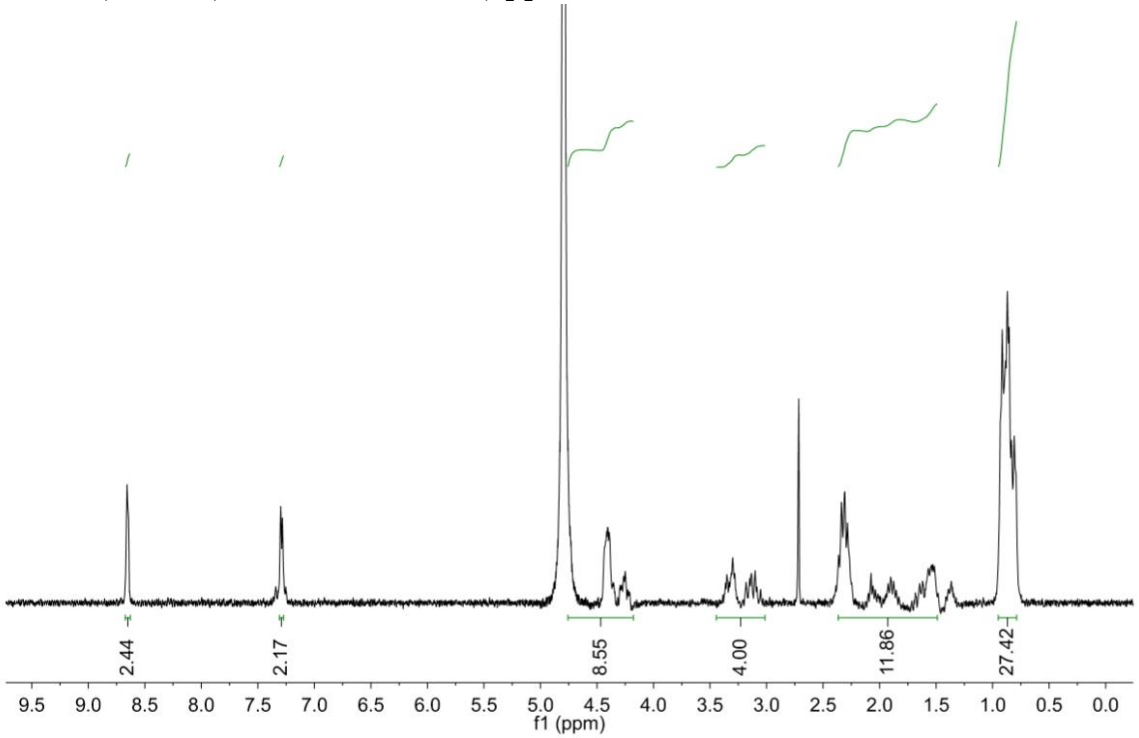

Figure S1.4. ^{1}H NMR (300 MHz) of **CP_L** in D_2O.

10.1.1.3. CP_F

UHPLC-MS (C18-ESI, +eV) A = H_2O + 0.1% TFA; B = ACN + 0.1% TFA; Gradient (A:B): 100:0 (0 min) → 25:75 (21 min); R_t = 11.4 min. Product after HPLC purification: white solid (41 mg, 39%); m/z = 1034.5 ($[M+H]^+$), 517.8 ($[M+2H]^{2+}$).

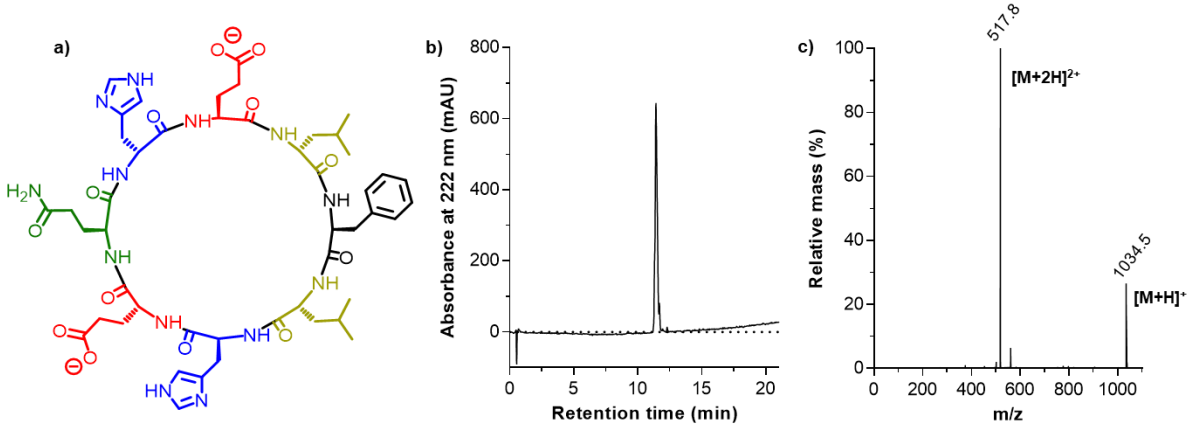

Figure S1.5. a) Structure of CP_F; b) Chromatogram after purification; c) MS spectrum.

HR-MS (ESI, +eV): m/z = 1034.5054 (calculated for $[M+H]^+$); 1034.5048 (found).

^{1}H-NMR (300 MHz, D_2O) δ: 0.67-0.90 (m, 16H, Leu *i*-Bu x2, Leu-CH_2- x2), 1.22-1.38 (m, 2H, Leu-CH- x2), 1.69-2.41 (m, 12H, Glu x2, Gln), 2.88-3.25 (m, 4H, His-CH_2- x2), 3.25-3.42 (m, 2H, Phe-CH_2-), 4.01-4.68 (m, 8H, H_α), 7.19-7.35 (m, 7H, His-CH= x2, Phe-CH= x2), 8.64 (s, 2H, His-CH= x2) ppm

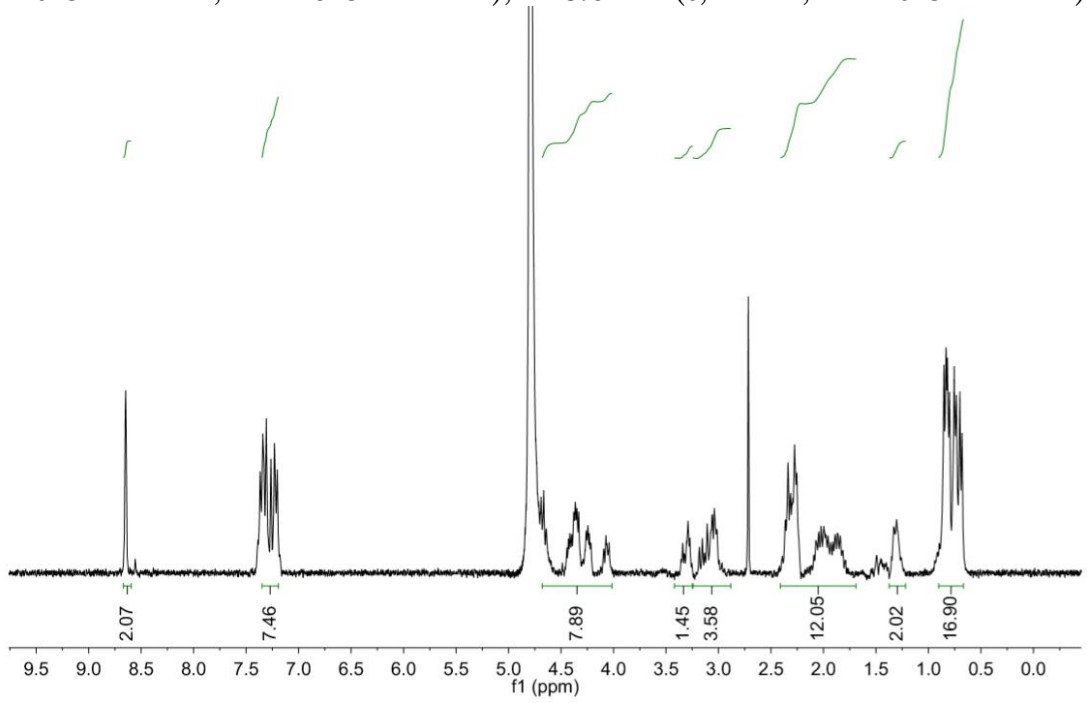

Figure S1.6. ^{1}H NMR (300 MHz) of CP_F in D_2O.

10.1.1.4. CP_{2F}

UHPLC-MS (C18-ESI, +eV) A = H_2O + 0.1% TFA; B = ACN + 0.1% TFA; Gradient (A:B): 100:0 (0 min) → 25:75 (21 min); R_t = 11.9 min. Product after HPLC purification: white solid (44 mg, 38%); m/z = 1141.5 ($[M+H]^+$), 571.3 ($[M+2H]^{2+}$).

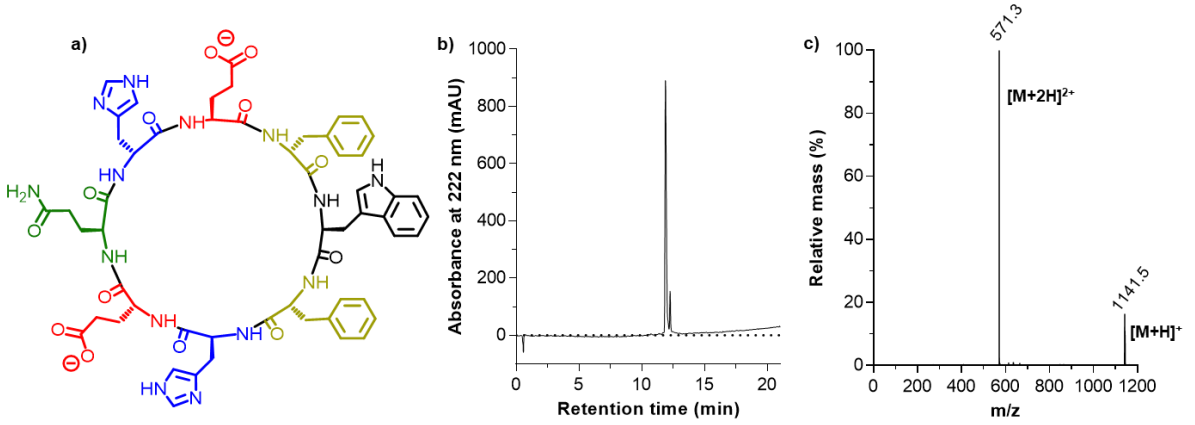

Figure S1.7. a) Structure of CP_{2F}; b) Chromatogram after purification; c) MS spectrum.

HR-MS (ESI, +eV): m/z = 1141.4850 (calculated for $[M+H]^+$); 1141.4845 (found):

^{1}H-NMR (300 MHz, D_2O) δ: 1.77-2.02 (m, 8H, Gln, Glu-CH_2- x2), 2.13-2.22 (m, 4H, Glu-CH_2- x2), 2.76-3.26 (m, 10H, Phe-CH_2- x2, Trp-CH_2-, His-CH_2- x2), 4.11-4.70 (m, 8H, H_α), 7.02-7.45 (m, 17H, Phe-CH= x15, His-CH= x2), 8.60 (d, J = 11.6 Hz, 2H, His-CH= x2) ppm.

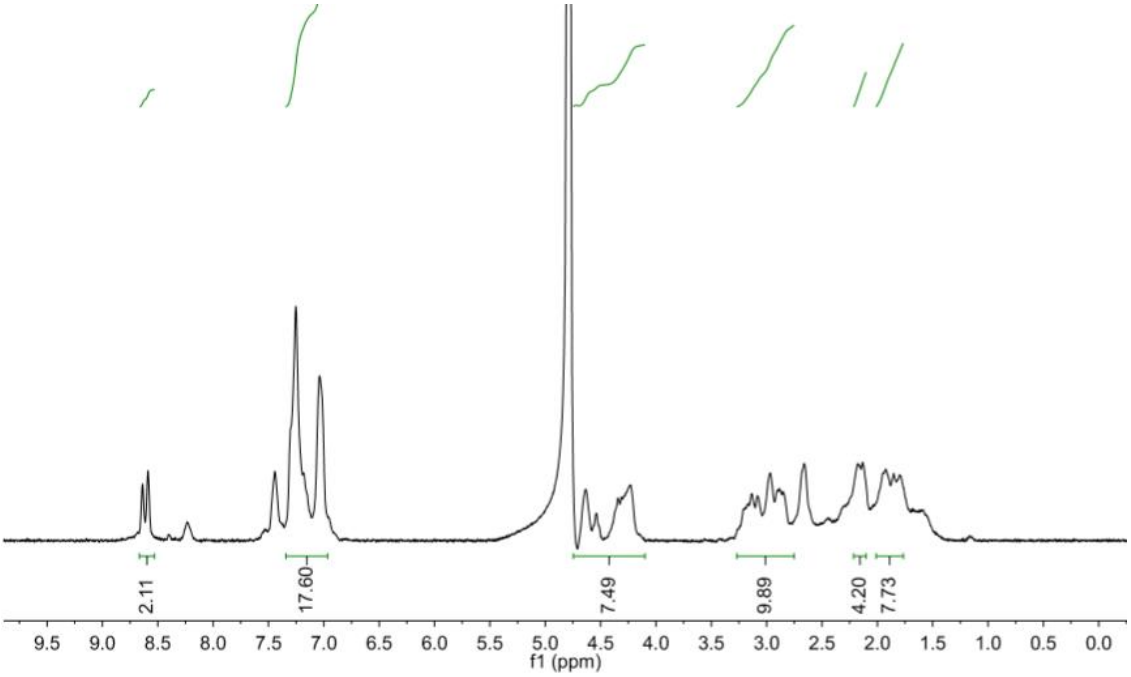

Figure S1.8. ^{1}H NMR (300 MHz) of CP_{2F} in D_2O.

10.1.1.5. CP_{3F}

UHPLC-MS (C18-ESI, +eV) A = H_2O + 0.1% TFA; B = ACN + 0.1% TFA; Gradient (A:B): 100:0 (0 min) → 25:75 (21 min); R_t = 12.2 min. Product after HPLC purification: white solid (39 mg, 35%); m/z = 1102.5 ($[M+H]^+$), 551.8 ($[M+2H]^{2+}$).

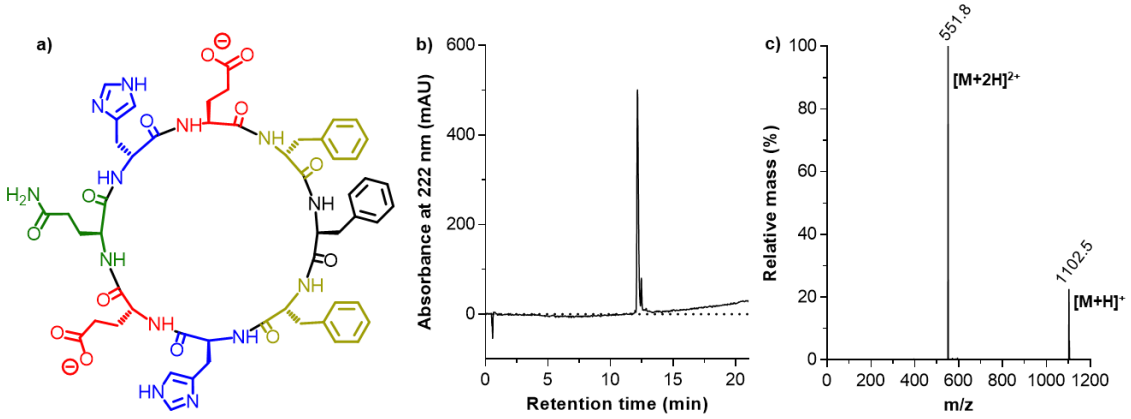

Figure S1.9 a) Structure of **CP_{3F}**; b) Chromatogram after purification; c) MS spectrum.

HR-MS (ESI, +eV): m/z = 1102.4741 (calculated for $[M+H]^+$), 1102.4737 (found).

^{1}H NMR (300 MHz, D_2O) δ: 1.36-2.15 (m, 12 H, Glu, Gln), 2.62-3.25 (m, 10 H, His-CH_2- x2, Phe-CH_2- x2, Trp-CH_2-), 4.19-4.80 (m, 8H, H_α), 6.98-7.41 (m, 17H, Phe x3, His x2), 8.62 (s, 2H, His x2) ppm.

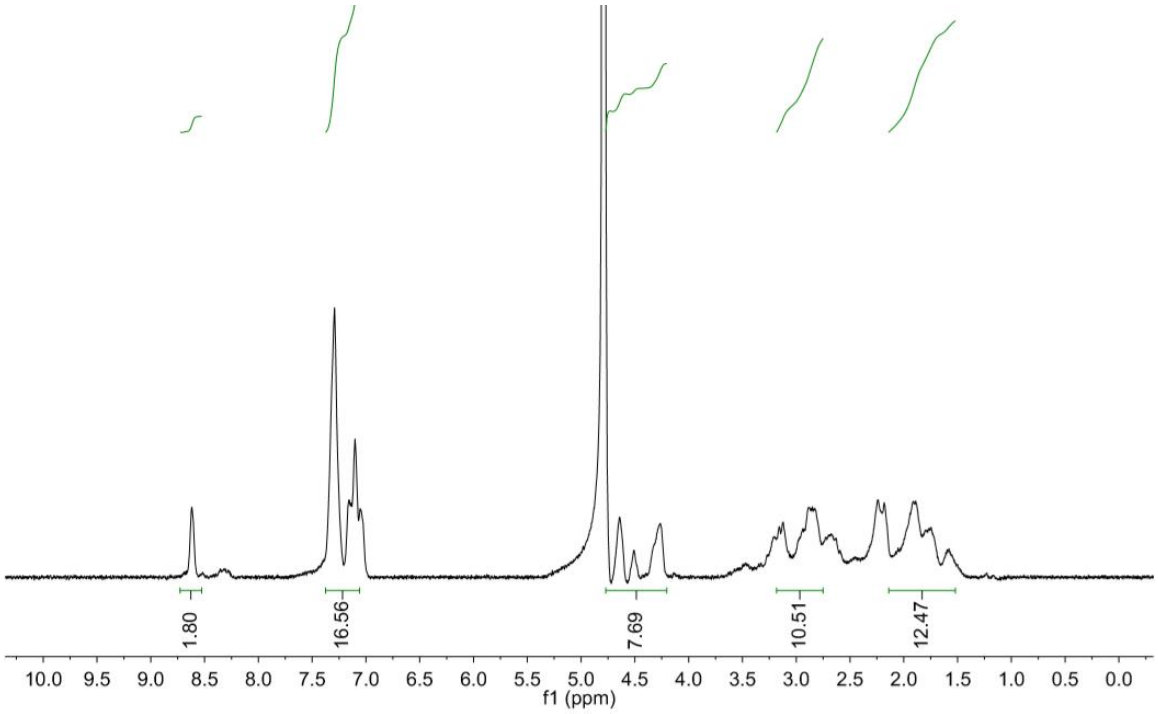

Figure S10. ^{1}H NMR (300 MHz) of **CP_{3F}** in D_2O.

10.1.1.6. CP_{oE}

UHPLC-MS (C18-ESI, +eV) A = H_2O + 0.1% TFA; B = ACN + 0.1% TFA; Gradient (A:B): 100:0 (0 min) → 25:75 (21 min); R_t = 10.9 min. Product after HPLC purification: white solid (41 mg, 38%); m/z = 1073.5 ($[M+H]^+$), 537.3 ($[M+2H]^{2+}$).

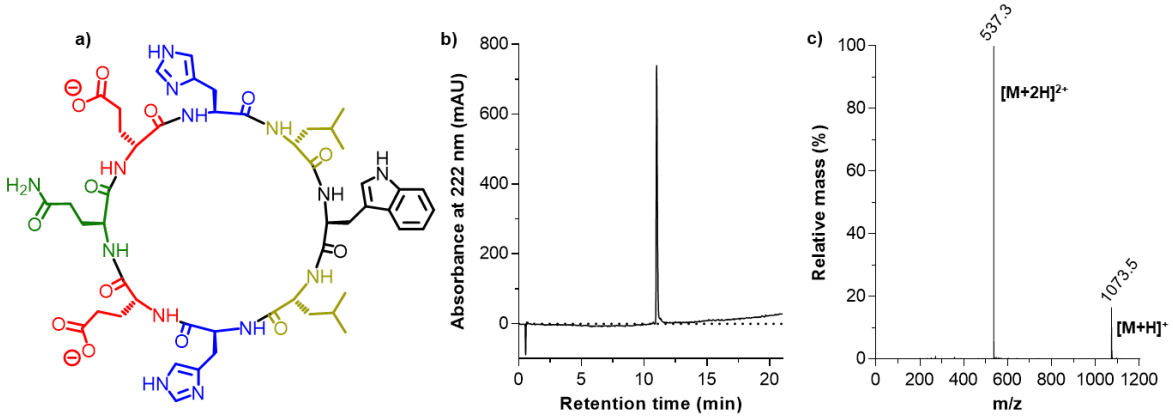

Figure S1.11. a) Structure of **CP_{oE}**; b) Chromatogram after purification; c) MS spectrum.

HR-MS (ESI, +eV): m/z = 1073.5163 (calculated for $[M+H]^+$); 1073.5172 (found).

^{1}H-NMR (300 MHz, D_2O) δ: 0.59-0.84 (m, 14H, Leu i-Bu x2, Leu-CH- x2), 1.15-1.35 (m, 4H, Leu-CH_2- x2), 1.85-2.38 (m, 12H, Glu x2, Gln), 2.97-3.43 (m, 6H, His-CH_2- x2, Trp-CH_2-), 3.80-4.70 (m, 8H, H_α), 7.13 (s, 2H, His-CH= x2), 7.31 (s, 1H, Trp-CH=), 7.42 (d, J = 7.18 Hz, 2H, Trp-CH= x2, 7.55 (d, J = 6.8 Hz, 2H, Trp-CH= x2), 8.64 (s, 2H, His-CH= x2) ppm.

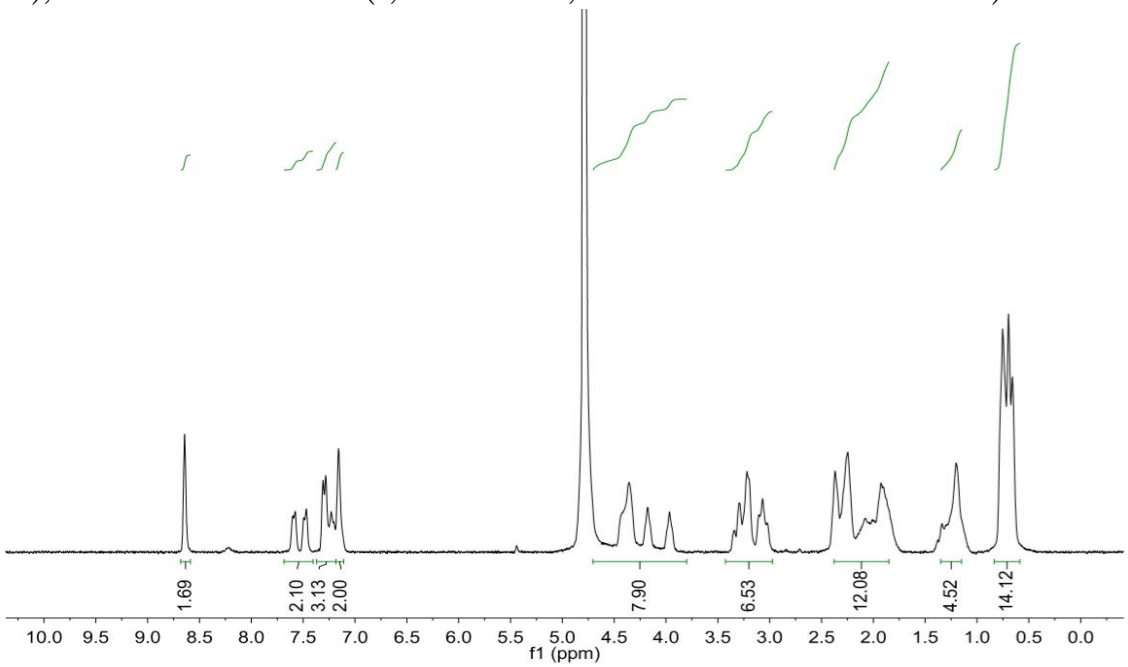

Figure S1.12. ^{1}H NMR (300 MHz) of **CP_{oE}** in D_2O.

10.1.1.7. CP_{2E2H}

UHPLC-MS (C18-ESI, +eV) A = H_2O + 0.1% TFA; B = ACN + 0.1% TFA; Gradient (A:B): 100:0 (0 min) → 25:75 (21 min); R_t = 11.0 min. Product after HPLC purification: white solid (38, 35%); m/z = 1073.5 ($[M+H]^+$), 537.4 ($[M+2H]^{2+}$).

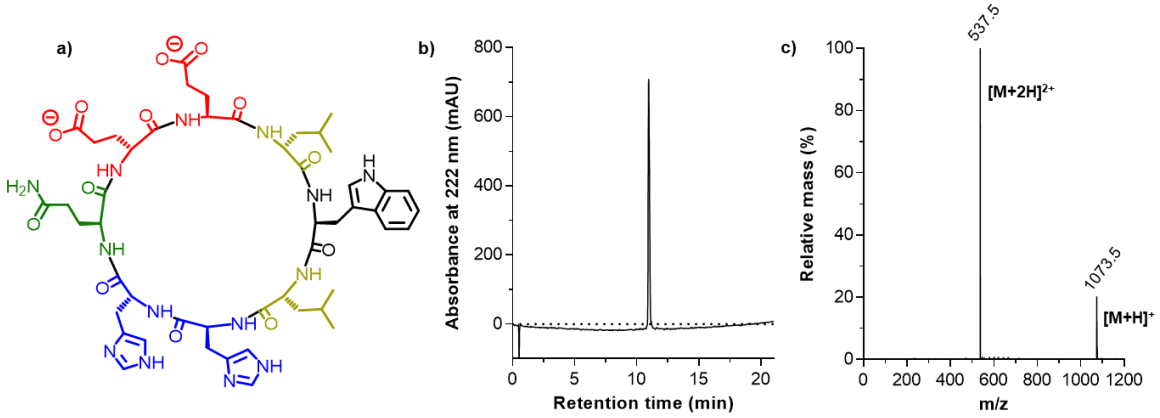

Figure S1.13. a) Structure of **CP_{2E2H}**; b) Chromatogram after purification; c) MS spectrum.

HR-MS (ESI, +eV): m/z = 1073.5163 (calculated for $[M+H]^+$); 1073.5155 (found).

^{1}H-NMR (300 MHz, D_2O) δ: 0.49-0.82 (m, 14H, Leu *i*-Bu x2, Leu-CH- x2), 1.18-1.37 (m, 4H, Leu-CH_2- x2), 1.86-2.38 (m, 12H, Glu x2, Gln), 2.87-3.38 (m, 6H, His-CH_2- x2, Trp-CH_2-), 3.83-4.69 (m, 8H, H_α), 6.95-7.37 (m, 2H, His-CH= x2, 3H, Trp-CH= x3), 7.55 (d, J = 7.04 Hz, 2H, Trp-CH= x2) 8.62 (s, 2H, His-CH= x2) ppm.

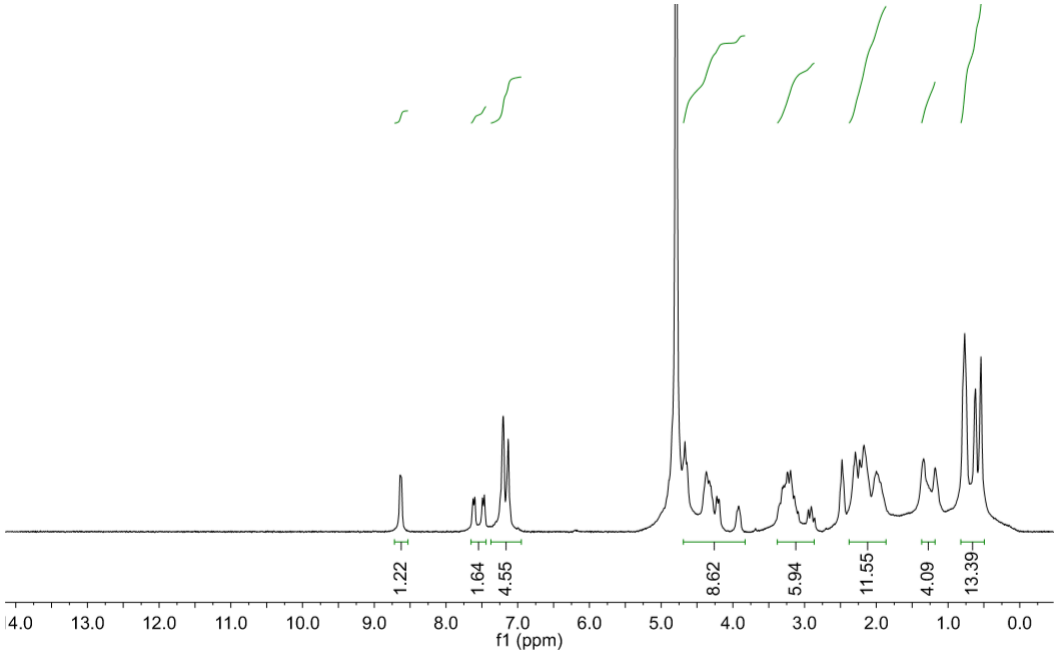

Figure S1.14. ^{1}H NMR (300 MHz) of **CP_{2E2H}** in D_2O.

10.1.1.8. CP_K

UHPLC-MS (C18-ESI, +eV) A = H_2O + 0.1% TFA; B = ACN + 0.1% TFA; Gradient (A:B): 100:0 (0 min) → 25:75 (21 min); R_t = 11.2 min. Product after HPLC purification: white solid (22 mg, 21%); m/z = 1055.6 ($[M+H]^+$), 528.4 ($[M+2H]^{2+}$).

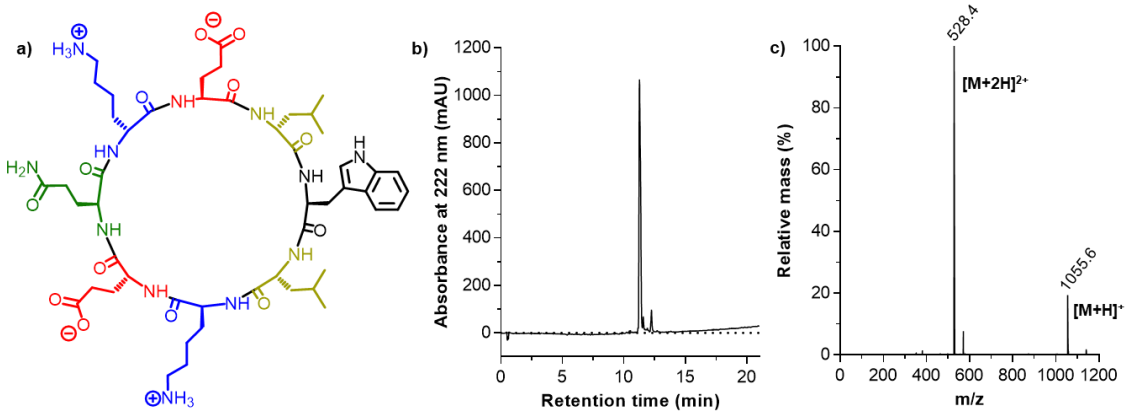

Figure S1.15. a) Structure of **CP_K**; b) Chromatogram after purification; c) MS spectrum.

HR-MS (ESI, +eV): m/z = 1055.5884 (calculated for $[M+H]^+$); 1055.5877 (found).

^{1}H-NMR (300 MHz, D_2O) δ: 0.41-0.91 (m, 12H, Leu *i*-Bu x2), 1.15-1.28 (m, 2H, Leu-CH- x2), 1.32-1.46 (m, 4H, Leu-CH_2- x2), 1.47-2.38 (m, 24H, Glu x2, Lys-CH_2- x6, Gln), 2.88-3.02 (m, 4H, Lys-CH_2- x2), 3.19-3.35 (m, 2H, Trp-CH_2-), 4.10-4.66 (m, 8H, H_α), 7.04-7.29 (m, 3H, Trp-CH= x3), 7.58 (d, J = 7.02 Hz, 2H, Trp-CH= x2) ppm.

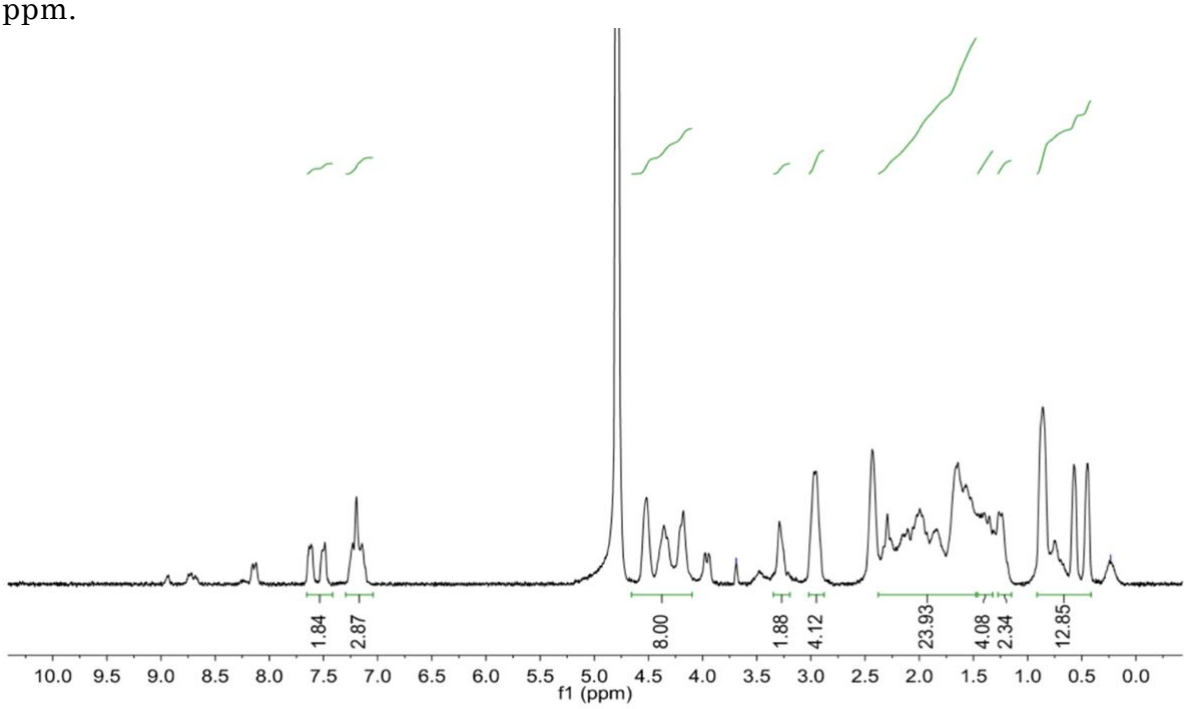

Figure S1.16. ^{1}H NMR (300 MHz) of **CP_K** in D_2O.

10.1.1.9. CP_{4E}

UHPLC-MS (C18-ESI, +eV) A = H_2O + 0.1% TFA; B = ACN + 0.1% TFA; 100:0 (0 min) → 25:75 (21 min); R_t = 12.2 min. Product after HPLC purification: white solid (24 mg, 22%); m/z = 1057.5 ($[M+H]^+$), 529.4 ($[M+2H]^{2+}$).

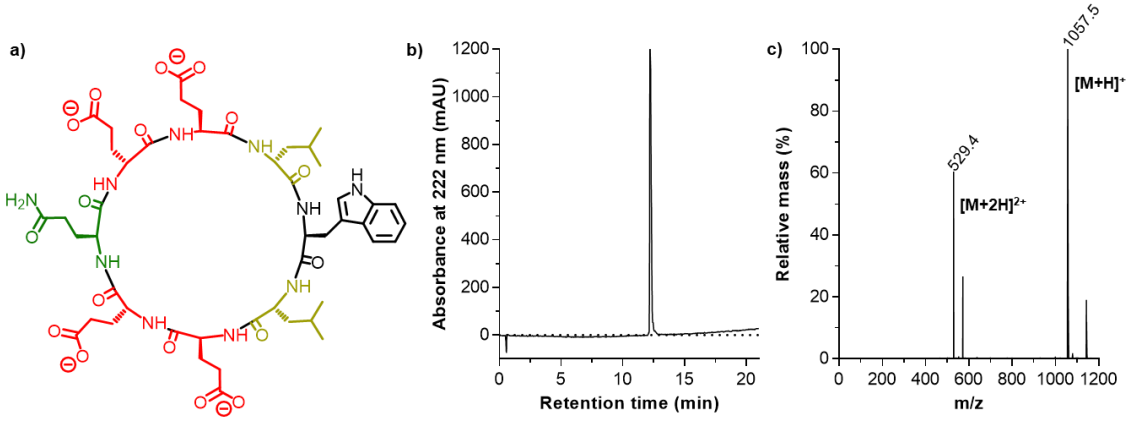

Figure S1.17. a) Structure of **CP_{4E}**; b) Chromatogram after purification; c) MS spectrum.

HR-MS (ESI, +eV): m/z = 1057.4837 (calculated for $[M+H]^+$); 1057.4836 (found).

^{1}H-NMR (300 MHz, D_2O) δ: 0.65-0.81 (m, 12H, Leu *i*-Bu x2), 1.20-1.29 (m, 2H, Leu-CH- x2), 1.34-1.46 (m, 4H, Leu-CH_2- x2), 1.87-2.43 (m, 20H, Glu x4, Gln), 3.12-3.36 (m, 2H, Trp-CH_2-), 4.01-4.43 (m, 8H, H_α), 7.03-7.34 (m, 3H, Trp-CH= x3), 7.58 (d, *J* = 6.94 Hz, 2H, Trp-CH= x2) ppm.

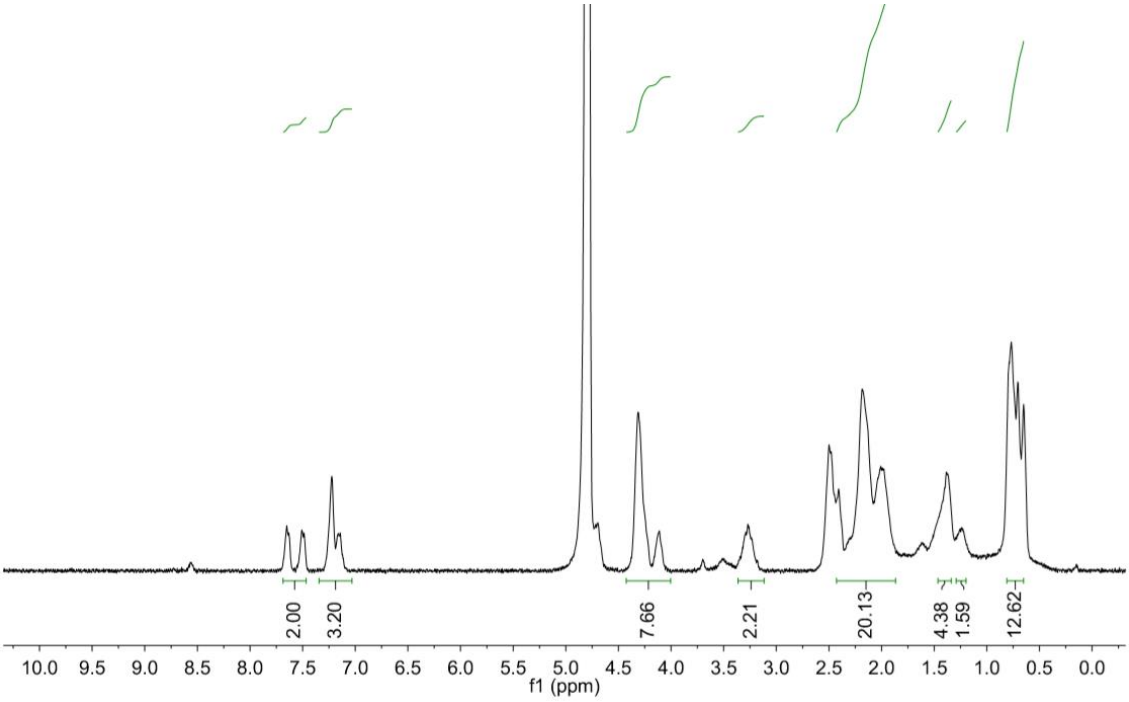

Figure S1.18. ^{1}H NMR (300 MHz) of **CP_{4E}** in D_2O.

10.1.2. Supplementary figures

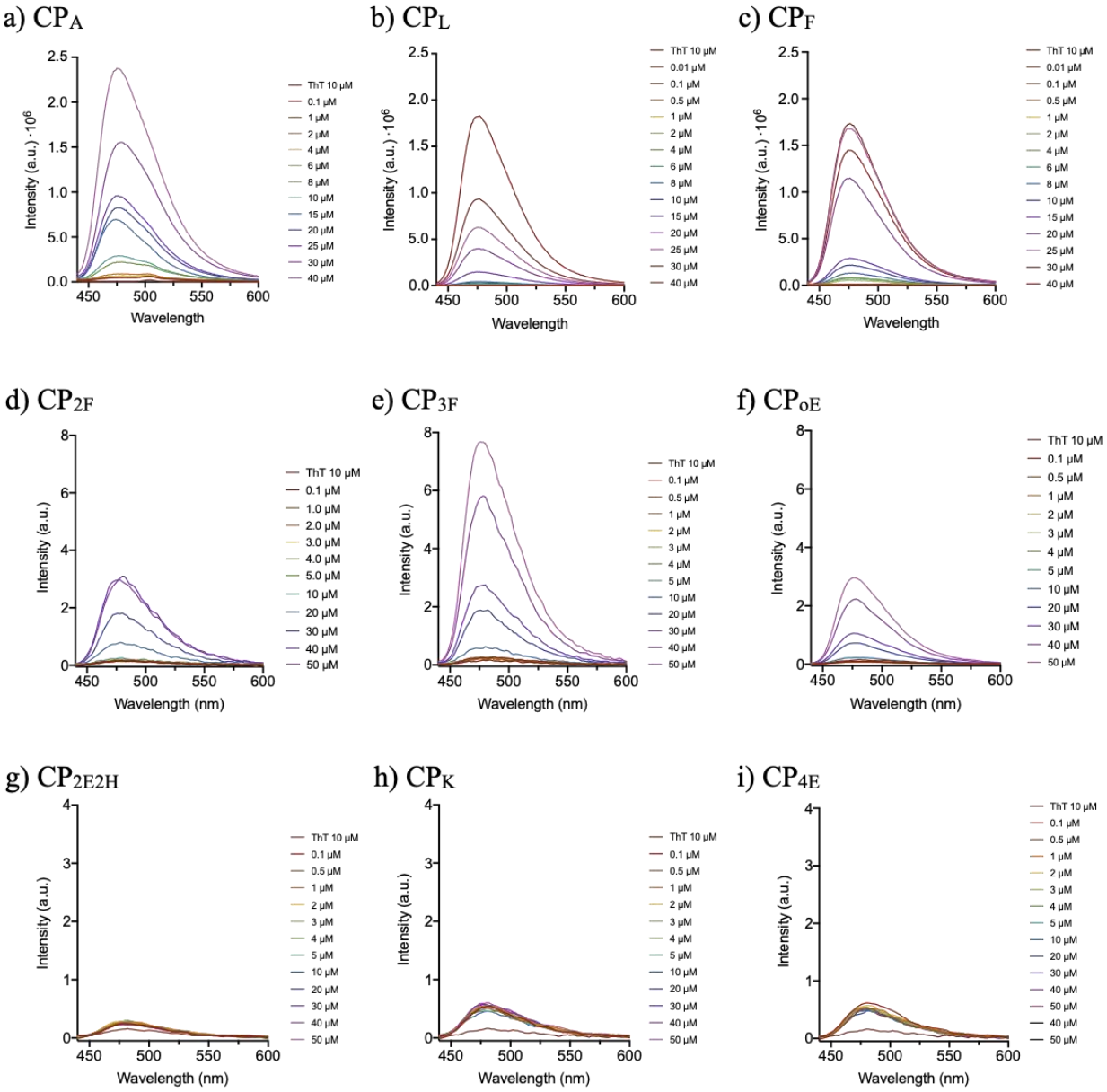

Figure S1.19. Overlay ThT fluorescence emission spectra at different cyclic peptide concentrations. Spectra were recorded after annealed samples (i. 80°C/1.5 h; ii. RT/1 h) in sodium phosphate buffer (20 mM; pH 7,4) with ThT (10 µM). λ_{exc} = 420 nm at T = 20°C.

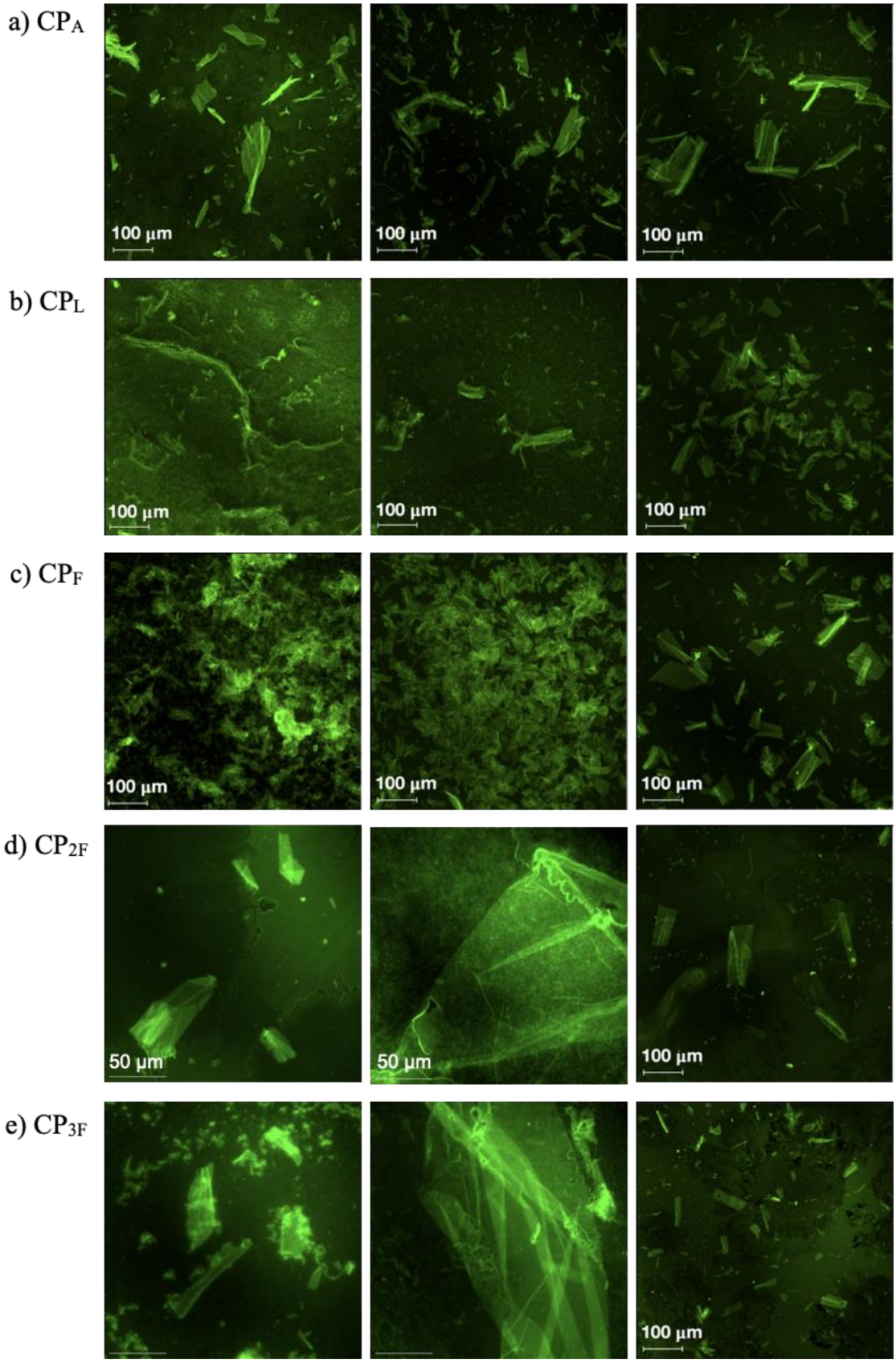

Figure S1.20. Epifluorescence micrographs of cyclic peptides with mutations in the hydrophobic region. Samples were annealed following the self-assembly protocol (i. 80°C/1.5 h; ii. RT/1 h) in sodium phosphate buffer (20 mM; pH 7,4) with ThT (10 µM). From left to right: 10 – 50 – 100 µM.

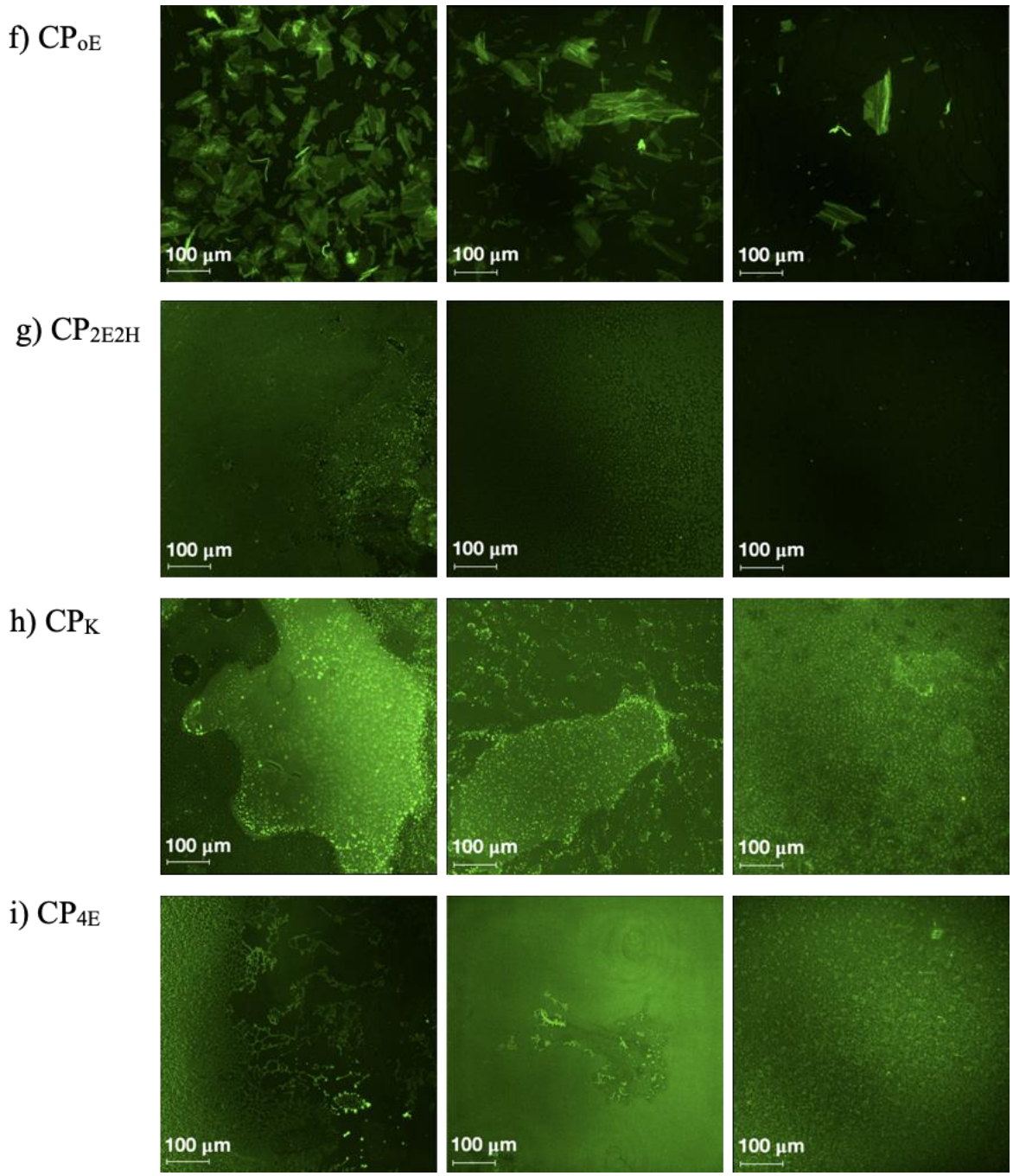

Figure S1.21. Epifluorescence micrographs of cyclic peptides with mutations in the polar region. Samples were annealed following the self-assembly protocol (i. 80°C/1.5 h; ii. RT/1 h) in sodium phosphate buffer (20 mM; pH 7,4) with ThT (10 µM). From left to right: 10 – 50 – 100 µM.

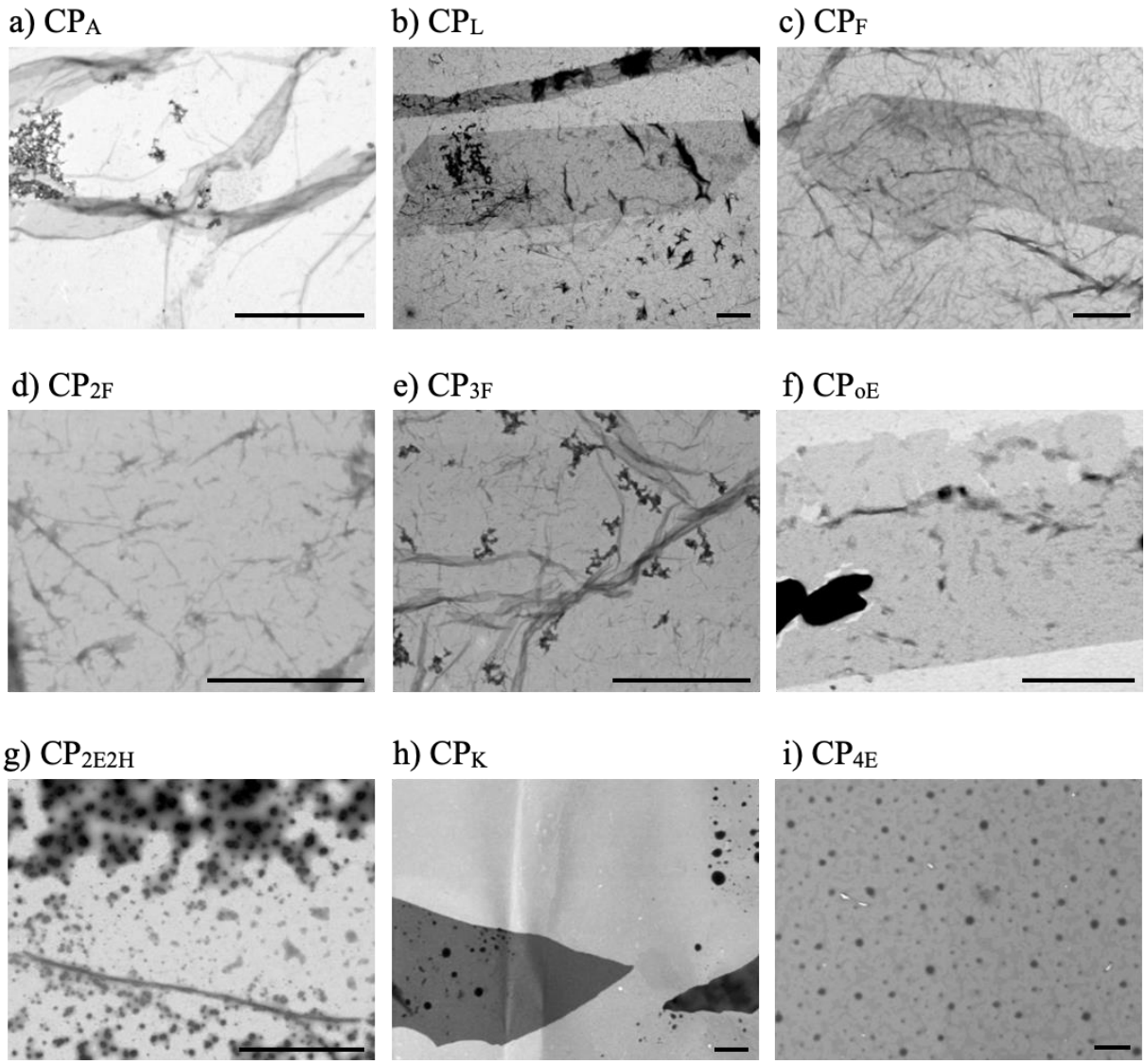

Figure S1.22. STEM micrographs of cyclic peptides (50 μM) annealed for 2D self-assembly (i. 80°C/1.5 h; ii. RT/1 h) in sodium phosphate buffer (20 mM; pH 7,4) without ThT. Scale bar 1 μm-

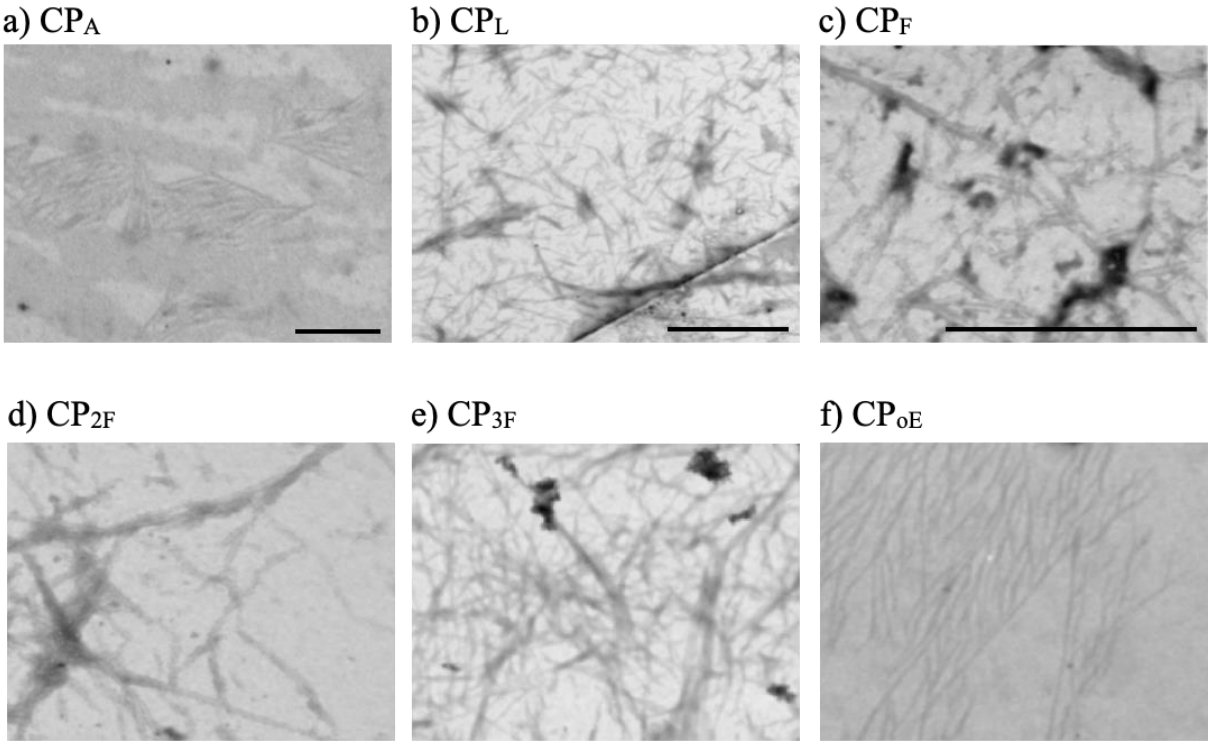

Figure S1.23. STEM micrographs of sonicated samples (30 min) of pre-assemble 2D nanosheets. Scale bars: a) 200 nm, b) 1 μm, c) 500 nm, d) 200 nm, e) 200 nm and f) 200 nm.

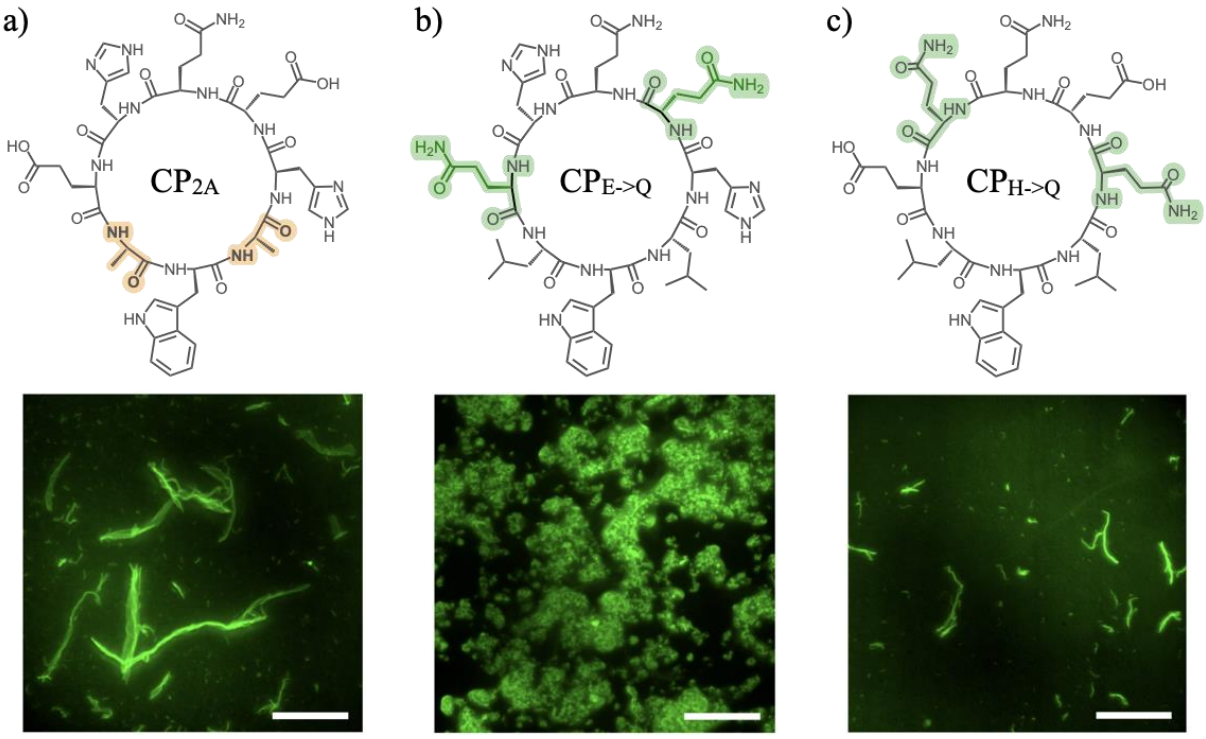

Figure S1.24. Chemical structures (top) and epifluorescence micrographs (bottom) of a) **CP$_{2A}$**, b) **CP$_{E->Q}$** and c) **CP$_{H->Q}$** at 100 μM. Samples were submitted to the assembly protocol described (i. 80°C/1.5 h; ii. RT/1 h) in sodium phosphate buffer (20 mM; pH 7,4) with ThT (10 μM). Scale bar 50 μm.

10.2.SELF-ASSEMBLY OF CYCLIC PEPTIDE MONOLAYERS BY HYDROPHOBIC SUPRAMOLECULAR HINGES

10.2.1. Characterization

10.2.1.1. CP10

UHPLC-MS (C18-ESI, +eV) gradient of H_2O + 0.1% TFA: CH_3CN + 0.1% TFA → 95:5 (0 min) to 5:95 (12 min) R_t = 8.6 min. Product after HPLC purification: white solid (26 mg, 19%); m/z = 1357.6 ($[M+H]^+$), 679.6($[M+2H]^{2+}$)

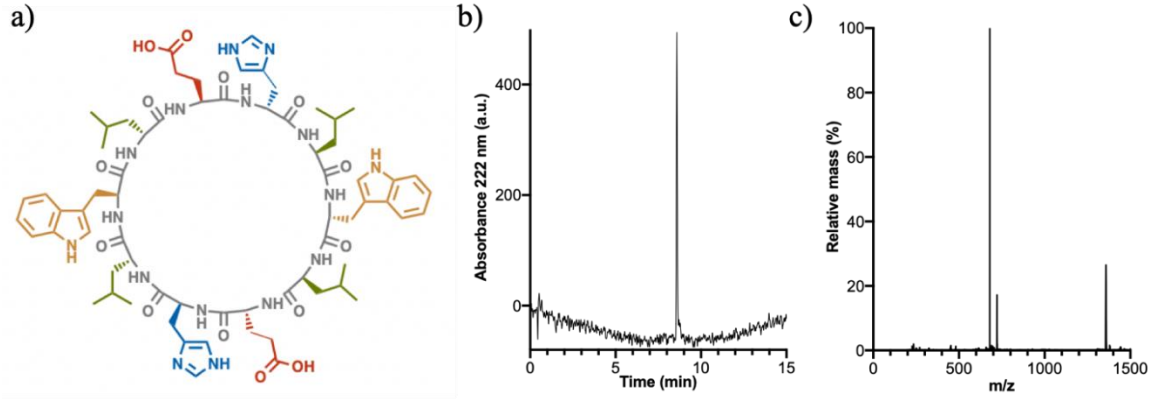

Figure S2.1. a) Structure of **CP10**; b) Chromatogram after purification; c) MS spectrum.

HR-MS (ESI, +eV) Calculated for $C_{68}H_{93}N_{16}O_{14}$ ($[M+H]^+$): 1357.6800; found: 1357.7050.

^{1}H-NMR (500 MHz, CD_3OH) δ: 0.43-0.52 (m, 5H, Leu), 0.59-0.66 (m, 5H, Leu), 0.8-0.92 (m, 14H, Leu), 1.2-1.5 (m, 12H, Leu), 2.0-2.5 (m, 8H, Glu -CH_2-), 2.9-3.2 (m, 8H, His -CH_2-, Trp -CH_2-), 3.9-5.3 (m, 10H, H_a), 6.9-7.03 (m, 2H, Trp -CH=), 7.04-7.1 (m, 4H, Trp -CH=), 7.18 (s, 1H, His -CH=), 7.25 (s, 1H, His -CH=), 7.32 (dd, 2H, $J_{h,h}$ = 8.17, 3.23 Hz, Trp -CH=), 7.52 (dd, 2H, $J_{h,h}$ = 7.44, 2.99 Hz, Trp -CH=), 8.76 (s, 1H, His -CH=), 8.81 (s, 1H, His -CH=).

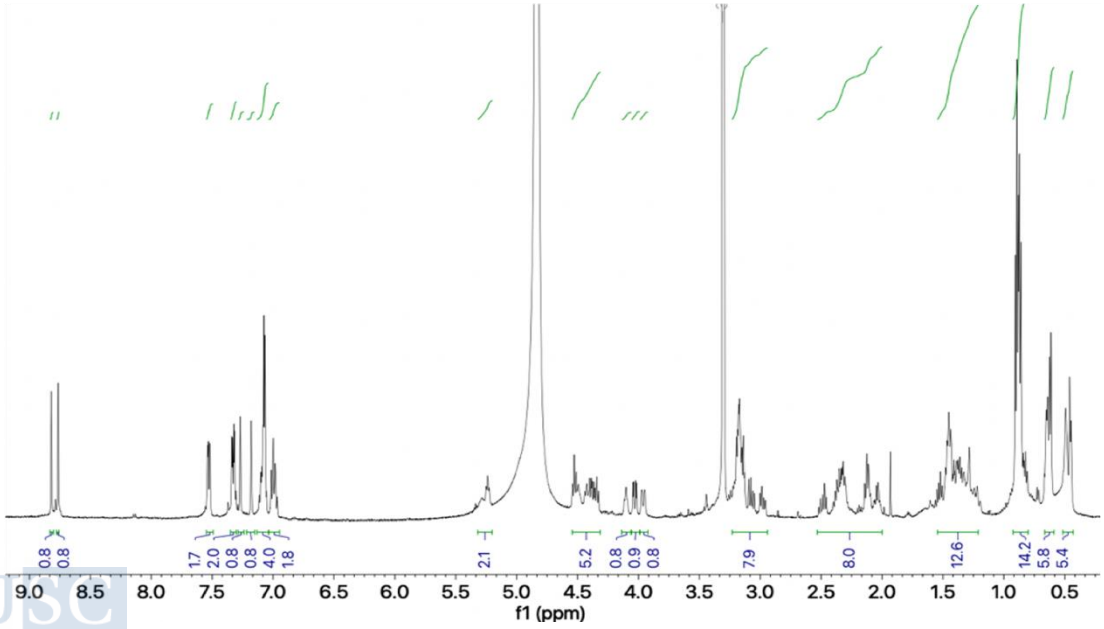

Figure S2.2. ^{1}H NMR (500 MHz) of **CP10** in CD_3OH.

10.2.1.2. 3L

UHPLC-MS (C18-ESI, +eV) gradient of H_2O + 0.1% TFA: CH_3CN + 0.1% TFA → 95:5 (5 min) to 5:95 (12 min) R_t = 8.6 min. Product after HPLC purification: white solid (18 mg, 15%); m/z = 1211.7 ($[M+H]^+$), 606.45($[M+2H]^{2+}$).

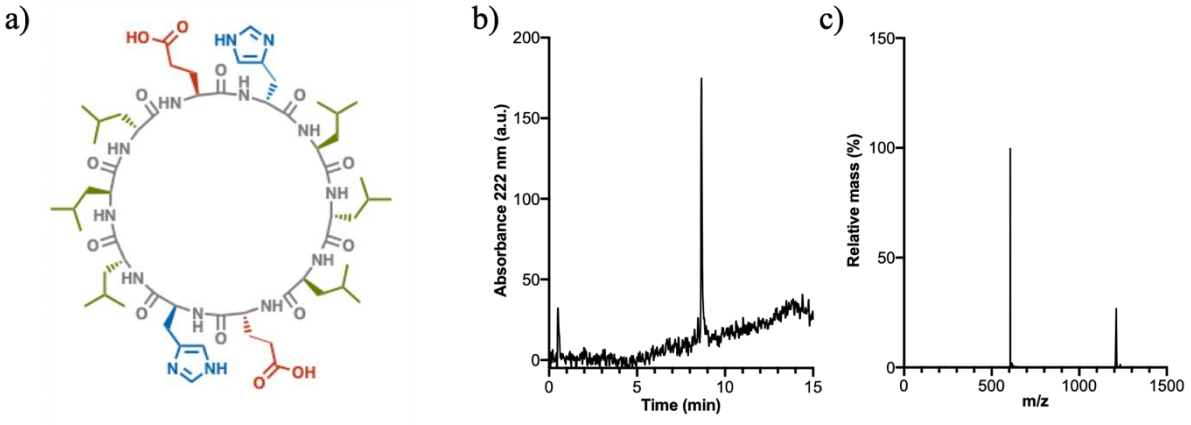

Figure S2.3. a) Structure of **3L**; b) Chromatogram after purification; c) MS spectrum of the peak.

HR-MS (ESI, +eV): Calculated for $C_{58}H_{94}N_{14}O_{14}$ ($[M+H]^+$): 1211.7100; found: 1211.7134

^{1}H-NMR (500 MHz, CD_3OH) δ: 0.79-0.99 (m, 37H, Leu), 1.5-1.7 (m, 17H, Leu), 1.8-2.2 (m, 4H, Glu -CH_2-), 2.2-2.4 (m, 4H, Glu, -CH_2-), 3.1- 3.4 (m, 4H, His -CH_2-), 4.3-4.4 (m, 7H, H_a), 4.6-4.7 (m, 3H, H_a), 7.35 (s, 2H, His -CH=), 8.75 (s, 2H, His -CH=).

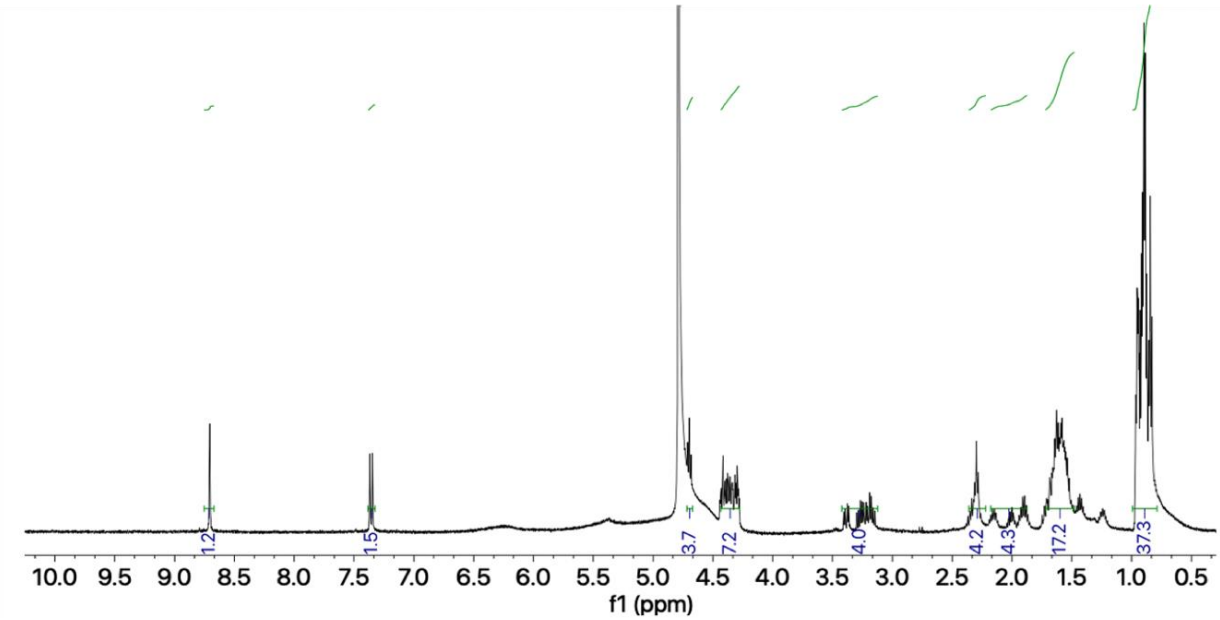

Figure S2.4. ^{1}H NMR (500 MHz) of **3L** in CD_3OH.

10.2.1.3. LW

UHPLC-MS (C18-ESI, +eV) gradient of H_2O + 0.1% TFA: CH_3CN + 0.1% TFA → 95:5 (0 min) to 5:95 (20 min) R_t = 11.9 min. Product after HPLC purification: white solid (22 mg, 16%); m/z = 699.4 ($[M+2H]^{2+}$), 466.8($[M+3H]^{3+}$).

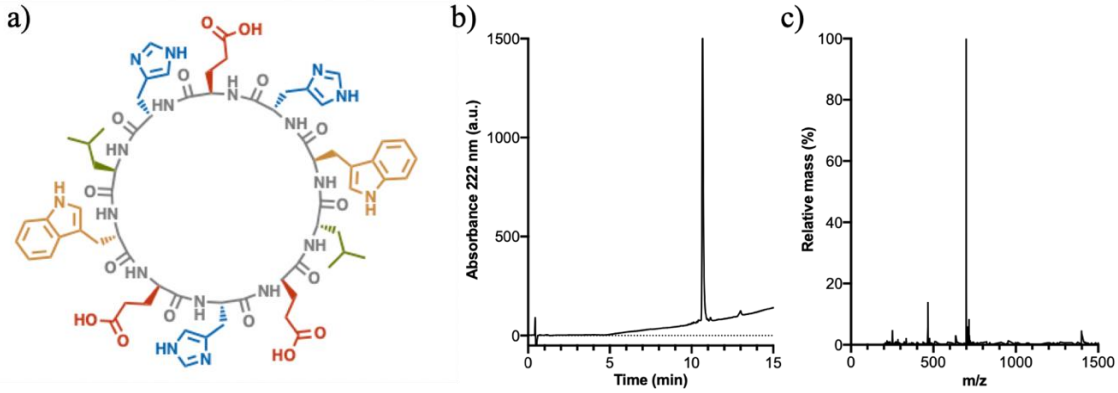

Figure S2.5. a) Structure of **LW**; b) Chromatogram after purification; c) MS spectrum.

HR-MS (ESI, +eV): Calculated for $C_{67}H_{84}N_{18}O_{16}$ ($[M+H]^+$): 1396.6300; found: 1397.6352.

^{1}H-NMR (500 MHz, CD_3OH) δ: 0.58-0.65 (m, 9H, Leu), 0.70-0.73 (m, 2H, Leu), 1.2-1.3 (m, 2H, Leu), 1.3-1.4 (m, 2H, Leu), 1.7-2.3 (m, 12H, Glu -CH_2-), 2.9-3.3 (m, 10H, His -CH_2-, Trp -CH_2-, overlapped), 4.0-4.7 (m, 10H, H_a, overlapped with solvent signal), 6.85 (s, 1H, His -CH=), 7.05 (d, 2H, $J_{h,h}$ = 7.07 Hz Trp -CH=), 7.1-7.3 (m, 4H, Trp -CH= overlapped with 2H, His -CH=), 7.45 (d, 1H, $J_{h,h}$ = 7.46 Hz, Trp =CH_2=), 7.53 (d, 1H, $J_{h,h}$ = 7.52 Hz, Trp -CH=), 7.58 (d, 1H, $J_{h,h}$ = 7.58 Hz, Trp -CH=), 7.65 (d, 1H, $J_{h,h}$ = 7.66 Hz, Trp -CH=), 7.75 (s, 1H, His -CH=), 8.05 (s, 2H,His,-CH=).

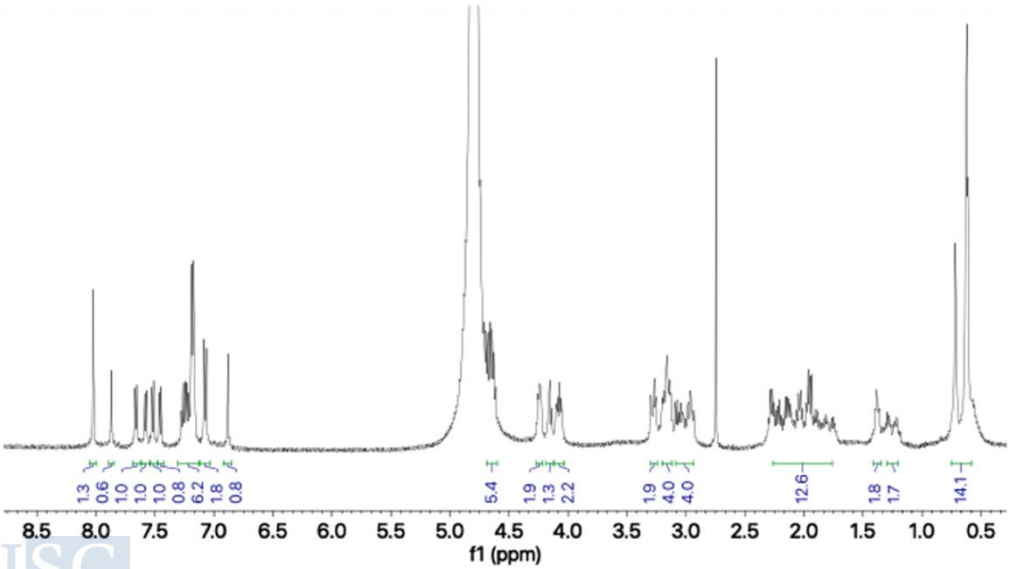

Figure S2.6. ^{1}H NMR (500 MHz) of **LW** in CD_3OH.

10.2.1.4. 2L

UHPLC-MS (C18-ESI, +eV) gradient of H_2O + 0.1% TFA: CH_3CN + 0.1% TFA → 95:5 (0 min) to 25:75 (21 min) R_t = 13.1 min. Product after HPLC purification: white solid (28 mg, 22.4%); m/z = 1251.65 ($[M+H]^+$), 626.4($[M+2H]^{2+}$).

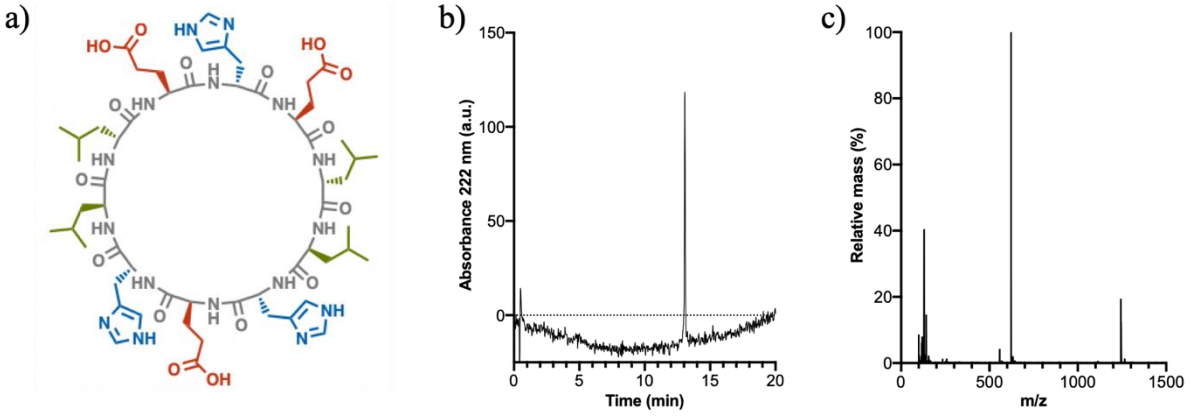

Figure S2.7. a) Structure of **2L**; b) Chromatogram after purification; c) MS spectrum.

10.2.1.5. 2W

UHPLC-MS (C18-ESI, +eV) gradient of H_2O + 0.1% TFA: CH_3CN + 0.1% TFA → 95:5 (0 min) to 25:75 (12 min) R_t = 8.01 min. Product after HPLC purification: white solid (18 mg, 11.7%); m/z = 772.6 ($[M+2H]^{2+}$)

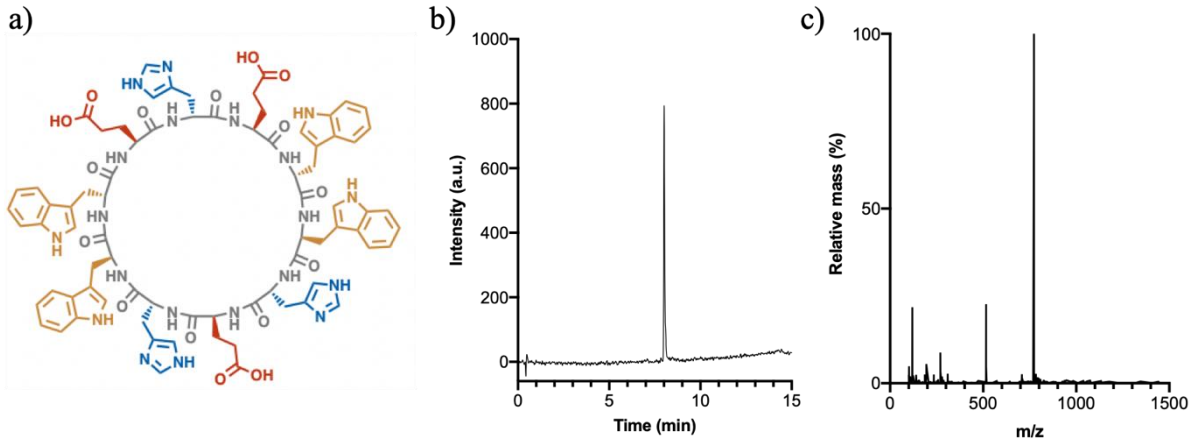

Figure S2.8. a) Structure of **2W**; b) Chromatogram after purification; c) MS spectrum.

10.2.1.6. EHEH

UHPLC-MS (C18-ESI, +eV) gradient of H_2O + 0.1% TFA: CH_3CN + 0.1% TFA → 95:5 (0 min) to 5:95 (21 min) R_t = 13.9 min. Product after HPLC purification: white solid (22 mg, 16.2%); m/z = 679.45 $([M+2H]^{2+})$

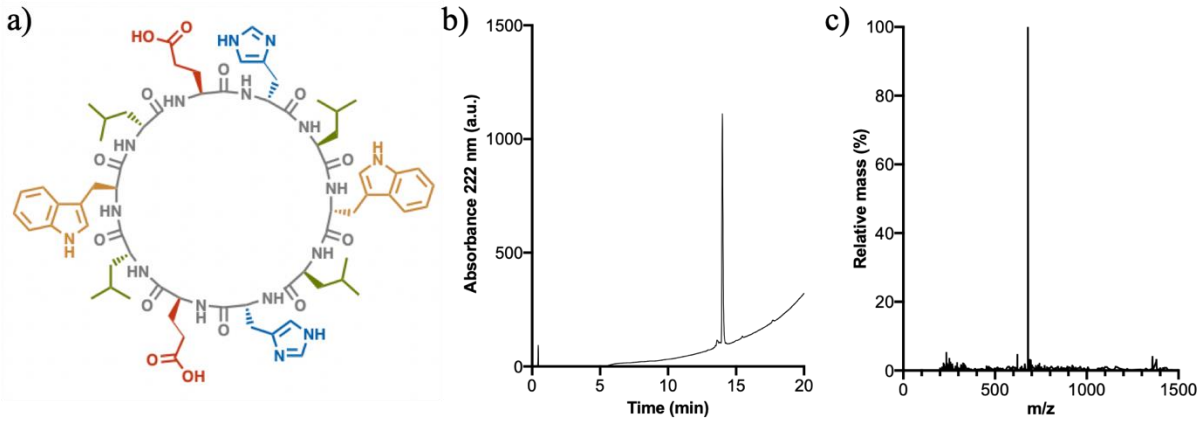

Figure S2.9. a) Structure of **EHEH**; b) Chromatogram after purification; c) MS spectrum.

10.2.1.7. 2E2H

UHPLC-MS (C18-ESI, +eV) gradient of H_2O + 0.1% TFA: CH_3CN + 0.1% TFA → 95:5 (0 min) to 5:95 (21 min) R_t = 13.8 min. Product after HPLC purification: white solid (15 mg, 11.1%); m/z = 1357.7 $([M+H]^+)$, 679.4 $([M+2H]^{2+})$

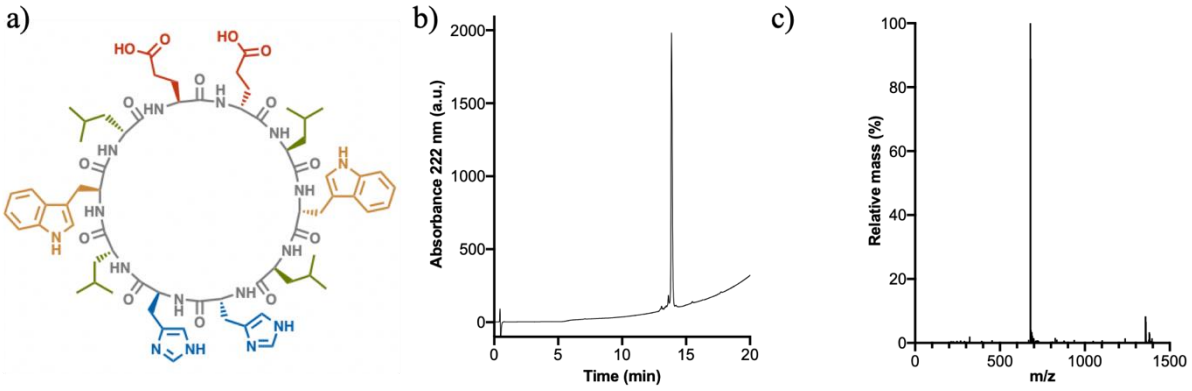

Figure S2.10. a) Structure of **2E2H**; b) Chromatogram after purification; c) MS spectrum.

10.2.2. Supporting figures

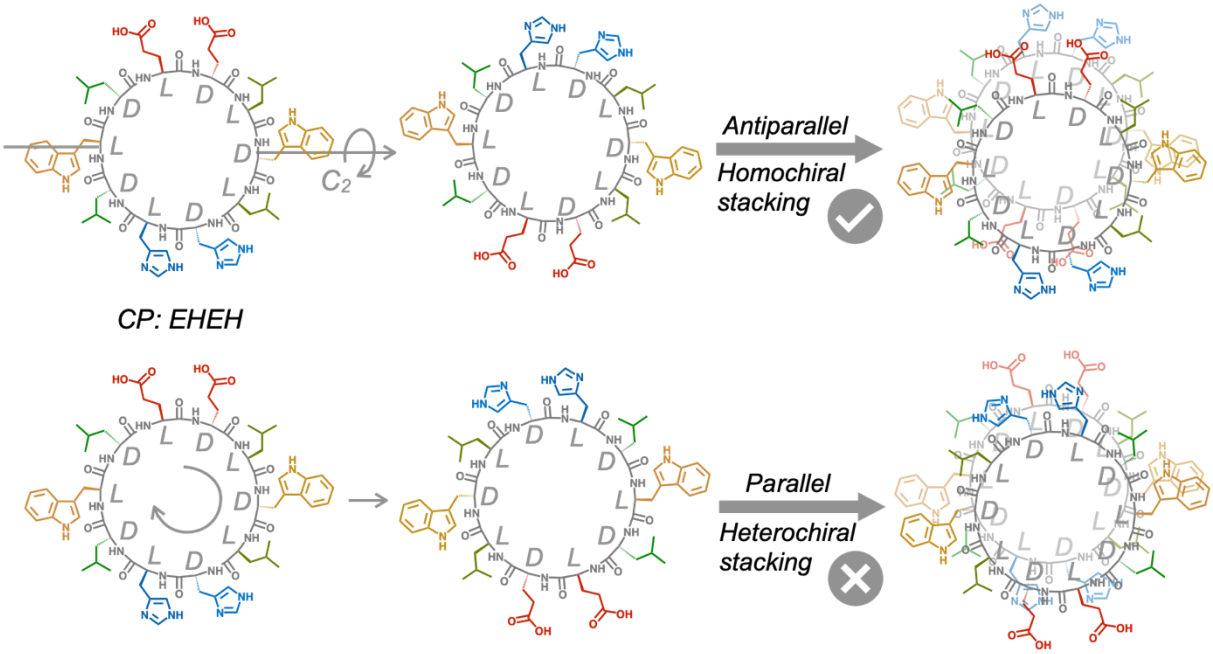

Figure S2.11. Comparison of both different conformations illustrating the dimerization of **EHEH**. At the top a C2 turn is depicted, leaving homochiral residues in the same position and leading to an allowed antiparallel conformation. At the bottom, a 180º rotation is depicted, leaving heterochiral residues in the same position which leads to a forbidden stacking (parallel conformation).

10.3.3D SELF-ASSEMBLY OF CYCLIC PEPTIDES INTO MULTILAYERED NANOSHEETS

10.3.1. Characterization

10.3.1.1. CP6

UHPLC-MS (C18-ESI, +eV) A = H_2O + 0.1% TFA; B = ACN + 0.1% TFA; Gradient (A:B): 95:5 (0 min) → 5:95 (12 min); R_t = 5.45 min. Product after HPLC purification: white solid (36 mg, 23.7%); m/z = 759.45 ($[M+H]^+$), 380.30 ($[M+2H]^{2+}$).

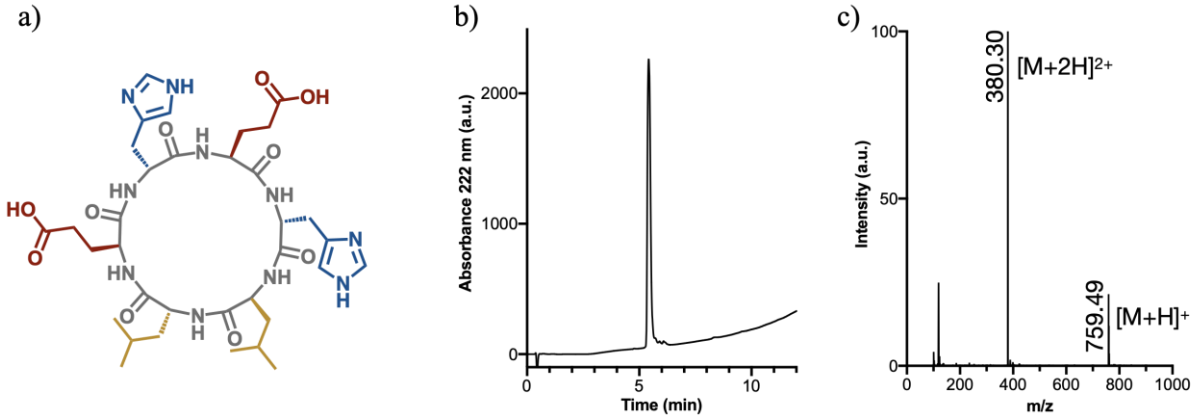

Figure S3.1. a) Structure of **CP6**; b) Chromatogram after purification; c) MS spectrum.

^{1}H-NMR (300 MHz, CD_3OD) δ: 0.86-0.98 (m, 12H, Leu *i*-Bu x2), 1.53-1.65 (m, 6H, Leu-CH_2, Leu-CH-), 1.94-2.42 (m, 8H, Glu-CH_2-), 3.05-3.37 (m, 4H, His-CH_2-), 4.23-4.77 (m, 6H, H_α), 7.35 (dd, *J*=13.25 Hz, 1.33, 2H, His-CH=), 8.80 (dd, *J*=5.75 Hz, 1.39, 2H, His-CH= x2) ppm.

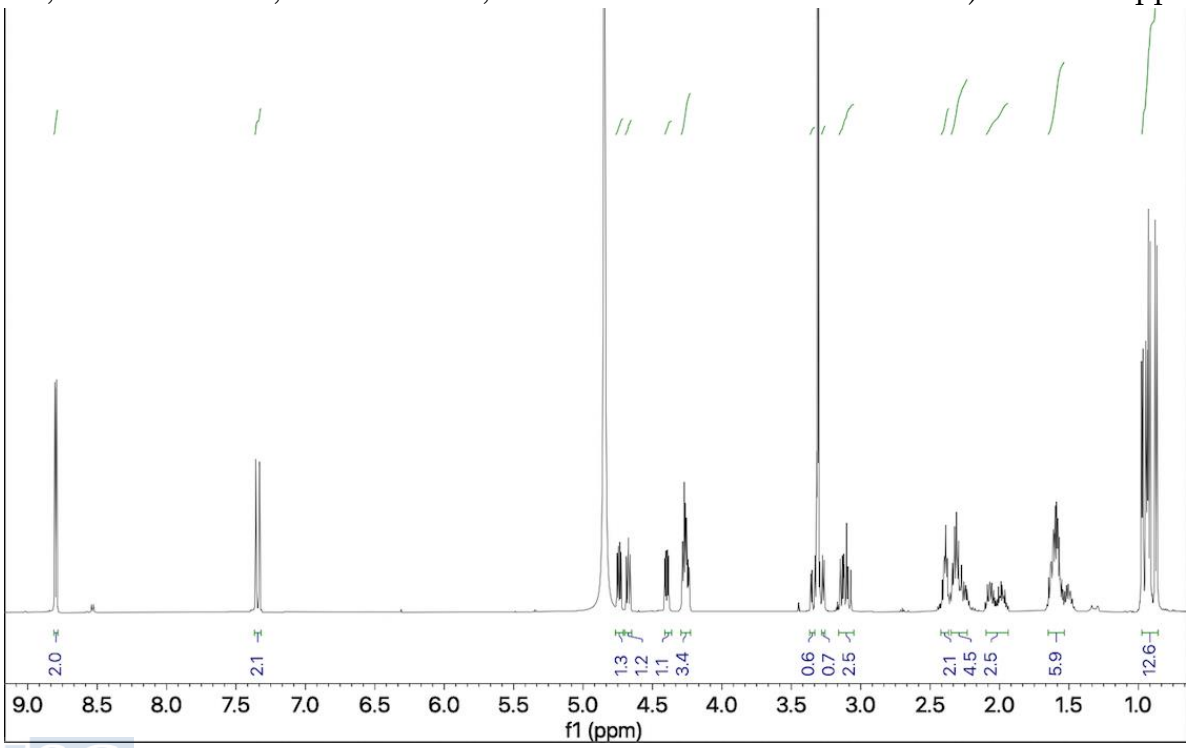

Figure S3.2. ^{1}H NMR (300 MHz) of **CP6** in CD_3OD.

10.3.1.2. 2W

UHPLC-MS (C18-ESI, +eV) A = H_2O + 0.1% TFA; B = ACN + 0.1% TFA; Gradient (A:B): 95:5 (0 min) → 5:95 (12 min); R_t = 8.7 min. Product after HPLC purification: white solid (28 mg, 15.5%); m/z = 905.45 ($[M+H]^+$), 453.25 ($[M+2H]^{2+}$).

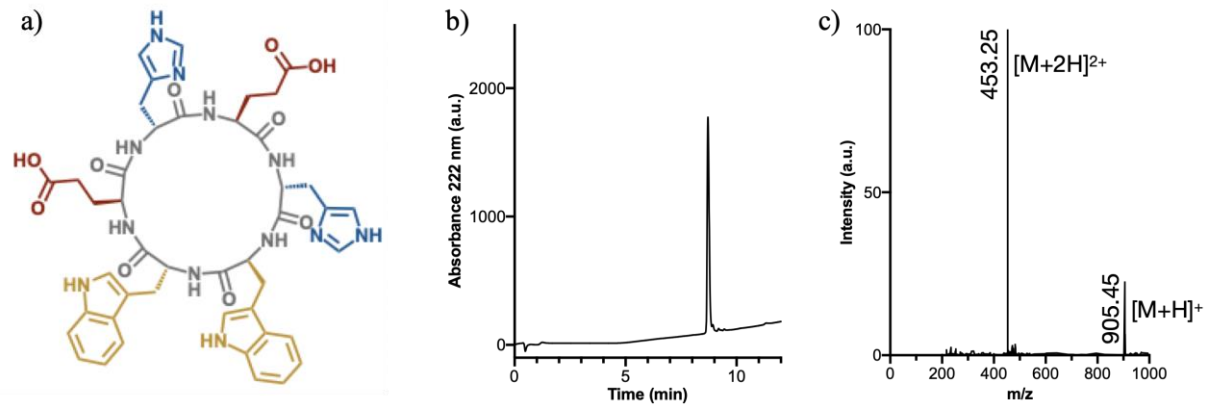

Figure S3.3. a) Structure of **2W**; b) Chromatogram after purification; c) MS spectrum.

10.3.1.3. EQEQ

UHPLC-MS (C18-ESI, +eV) A = H_2O + 0.1% TFA; B = ACN + 0.1% TFA; Gradient (A:B): 95:5 (0 min) → 5:95 (15 min); R_t = 7.9 min. Product after HPLC purification: white solid (32 mg, 21.6%); m/z = 741.37 ($[M+H]^+$), 371.05 ($[M+2H]^{2+}$).

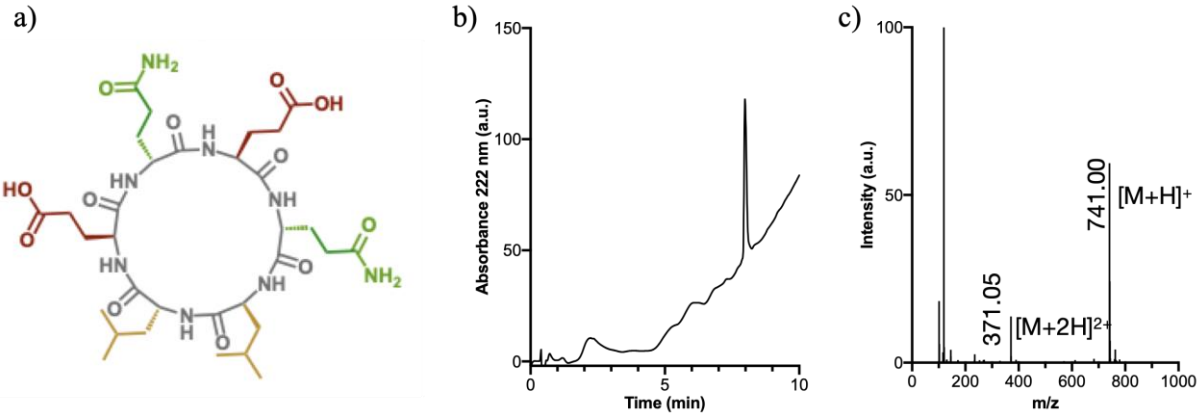

Figure S3.4. a) Structure of **EQEQ**; b) Chromatogram after purification; c) MS spectrum.

10.3.1.4. EQQH

UHPLC-MS (C18-ESI, +eV) A = H_2O + 0.1% TFA; B = ACN + 0.1% TFA; Gradient (A:B): 95:5 (0 min) → 5:95 (15 min); R_t = 7.33 min. Product after HPLC purification: white solid (38 mg, 25.4%); m/z = 749.40 ($[M+H]^+$), 375.30 ($[M+2H]^{2+}$).

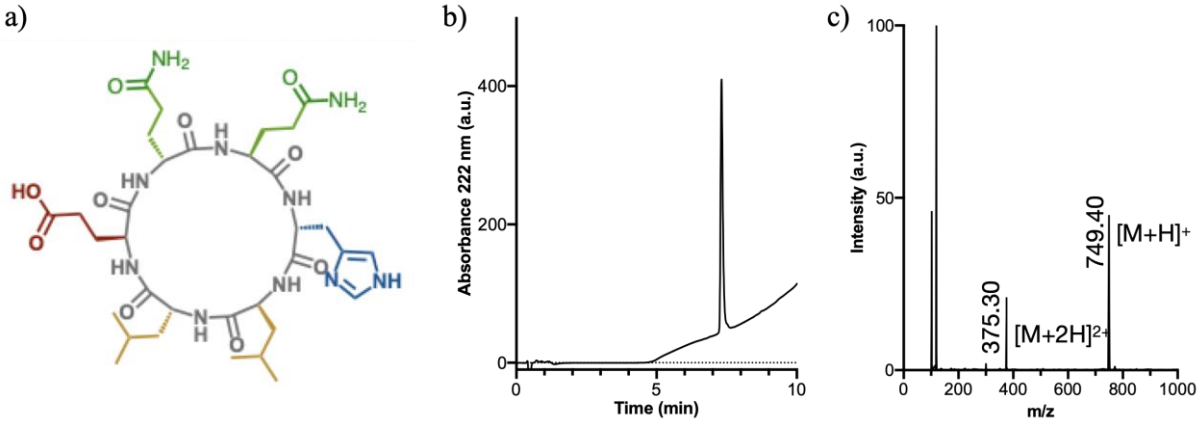

Figure S3.5. a) Structure of **EQQH**; b) Chromatogram after purification; c) MS spectrum.

10.3.1.5. LAL

UHPLC-MS (C18-ESI, +eV) A = H_2O + 0.1% TFA; B = ACN + 0.1% TFA; Gradient (A:B): 95:5 (0 min) → 5:95 (10 min); R_t = 7.45 min. Product after HPLC purification: white solid (16 mg, 11.6%); m/z = 692.30 ($[M+H]^+$).

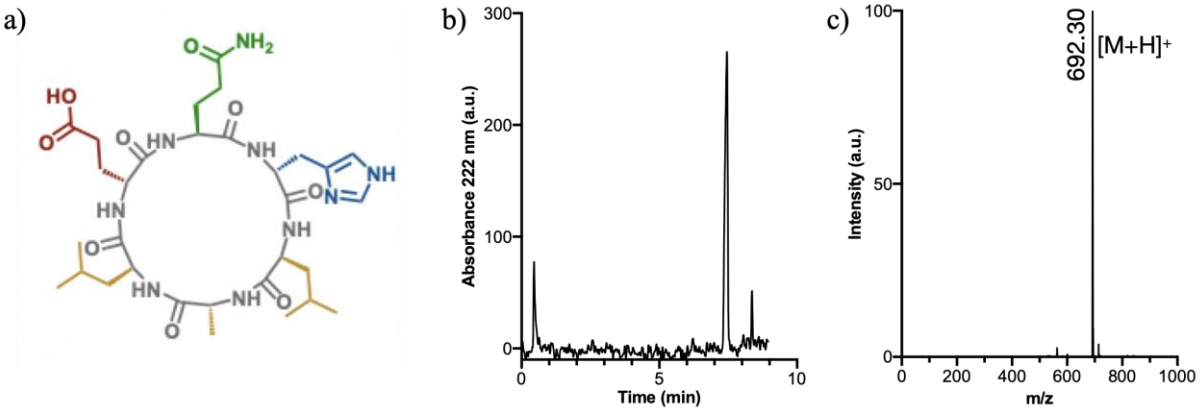

Figure S3.6. a) Structure of **LAL**; b) Chromatogram after purification; c) MS spectrum.

10.3.1.6. LWL

UHPLC-MS (C18-ESI, +eV) A = H_2O + 0.1% TFA; B = ACN + 0.1% TFA; Gradient (A:B): 95:5 (0 min) → 5:95 (15 min); R_t = 12.8 min. Product after HPLC purification: white solid (12 mg, 7.4%); m/z = 807.25 ($[M+H]^+$), 404.25 ($[M+2H]^{2+}$).

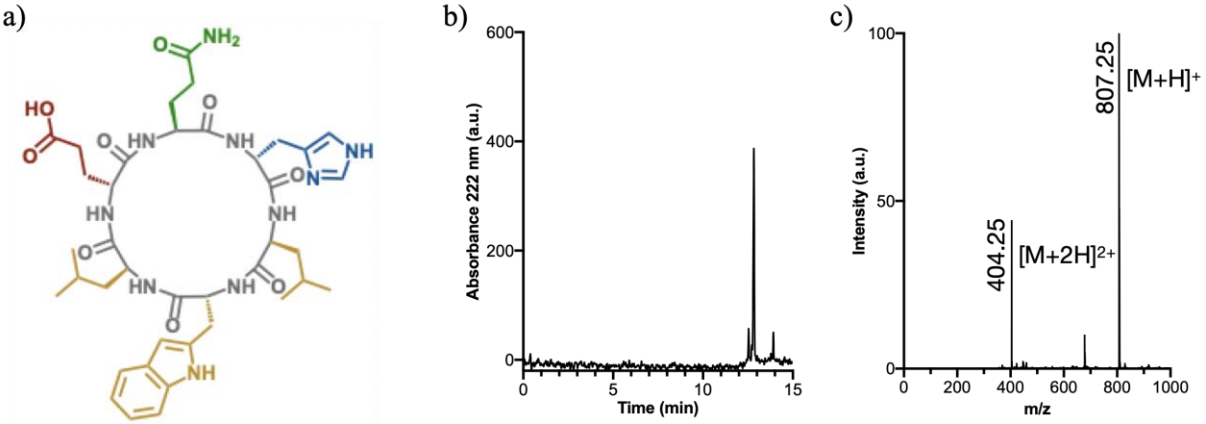

Figure S3.7. a) Structure of **LWL**; b) Chromatogram after purification; c) MS spectrum.

10.3.2. Supplementary figures

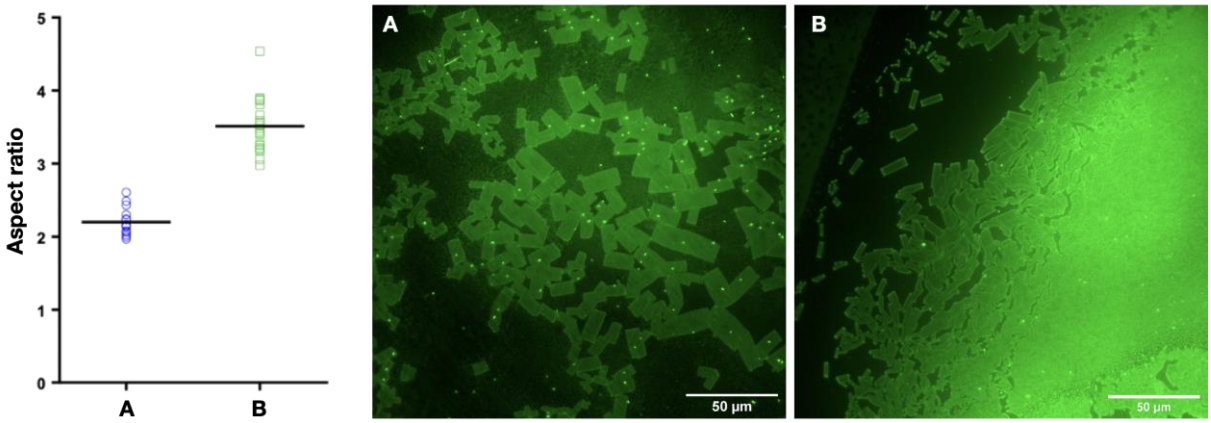

Figure S3.8. Histogram of the distribution of aspect ratio for the populations showed in the epifluorescence micrographs (the number of nanosheets measured was 20)

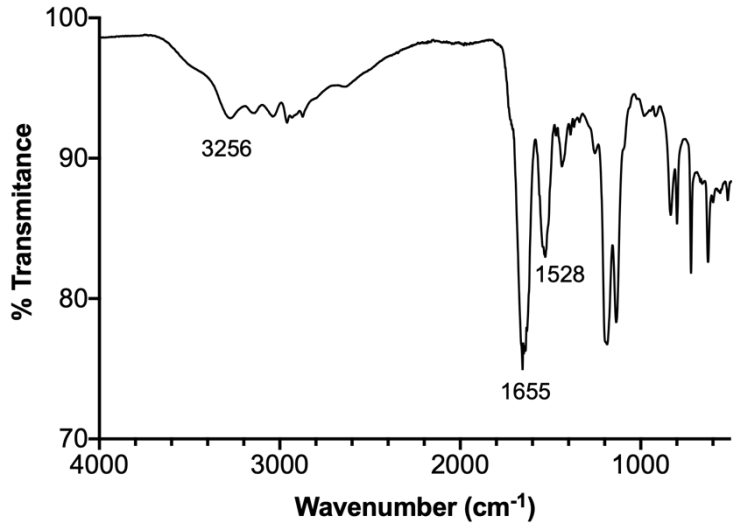

Figure S3.9. FTIR-ATR of **CP6** powder.

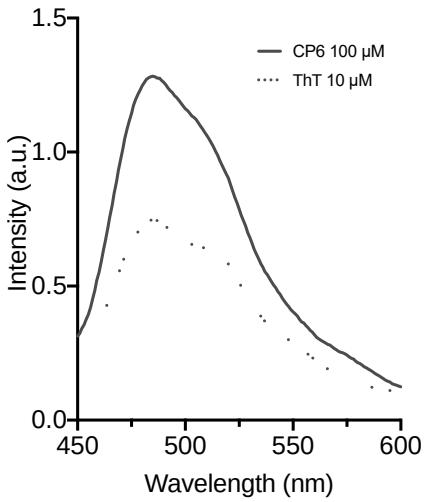

Figure S3.10. Fluorescence of ThT in an assembled sample of **CP6** (black line) in phosphate buffer (20 mM, pH 6.5) with ThT at 10 μM. The dotted line is the emission of a solution of ThT (10 μM) in phosphate buffer (20 mM, pH 6.5).

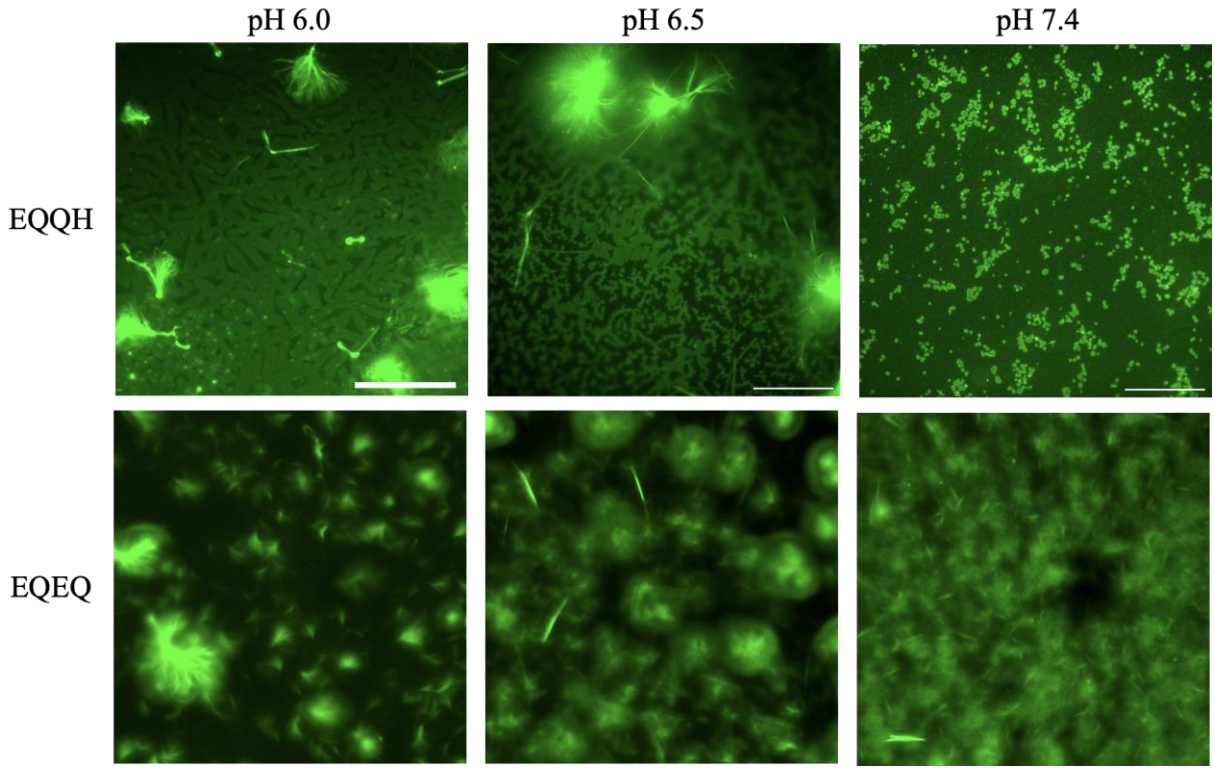

Figure S3.11. Epifluorescence micrographs of **EQQH** and **EQEQ** at different pH (50 μM in sodium phosphate buffer 20 mM with ThT 10 μM). Each sample at each condition was prepared following the assembly protocol separately. Scale bars 50 μm

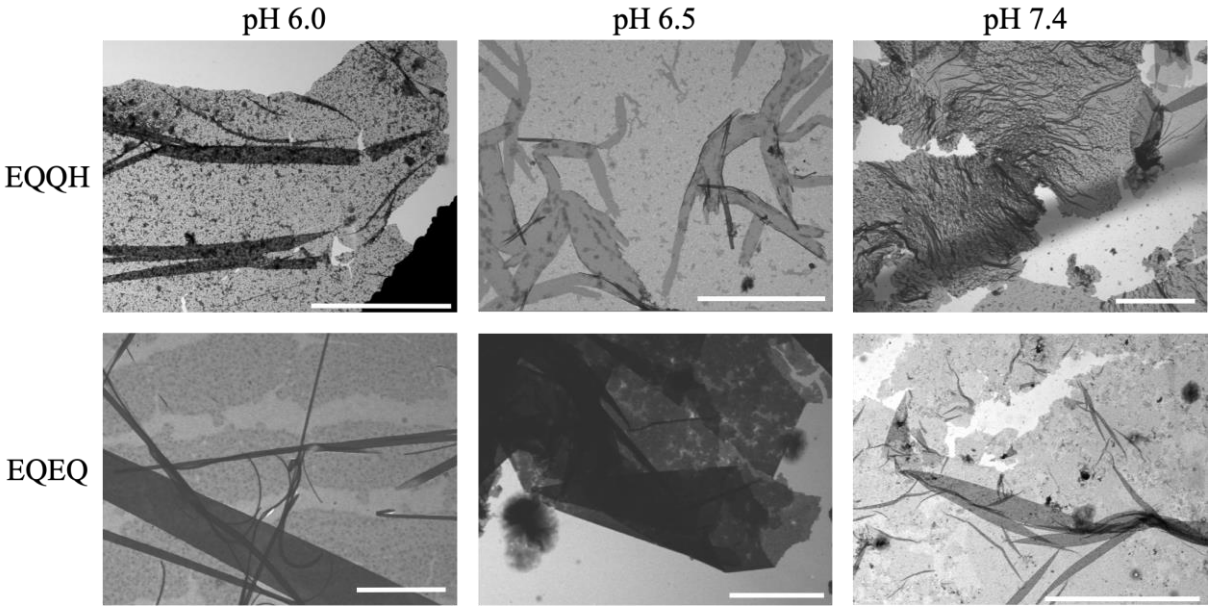

Figure S3.12. STEM micrographs of **EQQH** and **EQEQ** at different pH (50 μM in sodium phosphate buffer 20 mM). Each sample at each condition was prepared following the assembly protocol separately. Samples were stained after being deposited. Scale bars 5 μm.

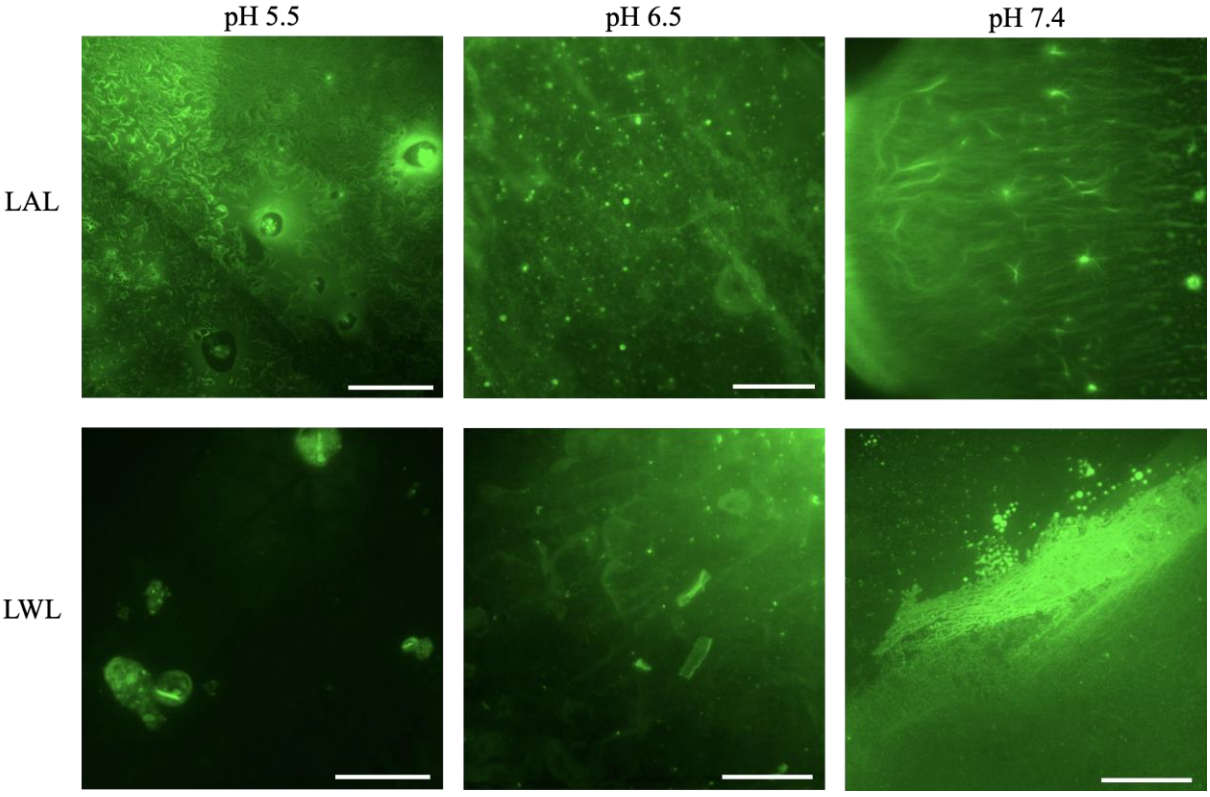

Figure S3.13. Epifluorescence micrographs of **LAL** and **LWL** at different pH (50 μM in sodium phosphate buffer 20 mM with ThT 10 μM). Each sample at each condition was prepared following the assembly protocol separately. Scale bars 50 μm

11. ANNEX

11.1.List of publications

11.1.1. Sequence Decoding of 1D to 2D Self-Assembling Cyclic Peptides

Sandra Díaz, Dr. Ignacio Insua, Dr. Ghibom Bhak, Dr. Javier Montenegro. Sequence Decoding of 1D to 2D Self-Assembling Cyclic Peptides. *Chemistry A European Journal,* ***2020***, *26*, 14765-14770.

Quality indexes:

Journal Impact Factor: 4.3 (2-year IF; 2022)
CiteScore: 8.8 (Scopus; 2022)
SJR: 1.06 (2023)
Quartile Q1 for Chemistry (Multidisciplinary)

Author contribution:

The author of this Thesis contributed to the synthesis and characterization of all the compounds as well as to the spectroscopy and microscopy experiments. The results obtained were discussed with all the co-authors.

Authorization from the journal:

Order Completed

Thank you for your order.

This Agreement between Miss. Sandra Diaz ("You") and John Wiley and Sons ("John Wiley and Sons") consists of your license details and the terms and conditions provided by John Wiley and Sons and Copyright Clearance Center.

Your confirmation email will contain your order number for future reference.

License Number	5767181275383
License date	Apr 13, 2024

Printable Details

Licensed Content

Licensed Content Publisher	John Wiley and Sons
Licensed Content Publication	Chemistry - A European Journal
Licensed Content Title	Sequence Decoding of 1D to 2D Self-Assembling Cyclic Peptides
Licensed Content Author	Javier Montenegro, Ghibom Bhak, Ignacio Insua, et al
Licensed Content Date	Oct 12, 2020
Licensed Content Volume	26
Licensed Content Issue	64
Licensed Content Pages	6

Order Details

Type of use	Dissertation/Thesis
Requestor type	Author of this Wiley article
Format	Print and electronic
Portion	Full article
Will you be translating?	No

About Your Work

Title of new work	Dissertation Sandra Diaz
Institution name	USC
Expected presentation date	Jun 2024

Additional Data

11.1.2. Self-Assembly of Cyclic Peptide Monolayers by Hydrophobic Supramolecular Hinges

Ignacio Insua, Annalisa Cardellini, Sandra Díaz, Julian Bergueiro, Riccardo Capelli, Giovanni M. Pavan and Javier Montenegro. Self-assembly of cyclic peptide monolayers by hydrophobic supramolecular hinges. *Chemical Science*, **2023**, *14*, 14074-14081.

Quality indexes:

- Journal Impact Factor: 8.4 (2-year IF; 2022)
- CiteScore: 15.2 (Scopus; 2022)
- SJR: 2.33 (2023)
- Quartile Q1 for Chemistry (Multidisciplinary)

Author contribution:

The author of this Thesis contributed to the synthesis and characterization of all the compounds as well as to the spectroscopy and microscopy experiments. The author has participated in the discussion of the results with all the coauthors and reviewed and approved the final version of the manuscript.

Authorization from the journal:

As it can be read in the following text for thesis and dissertation not permission is required if you are an author of the article.

> If you are **the author of this article, you do not need to request permission to reproduce figures and diagrams** provided correct acknowledgement is given. If you want to reproduce the whole article in a third-party commercial publication (excluding your thesis/dissertation for which permission is not required) please go to the Copyright Clearance Center request page.

Relationship of publications to chapters

The article "Sequence Decoding of 1D to 2D Self-Assembling Cyclic Peptides" (Section 11.1.1) was reproduced in the first Chapter of this thesis under the same title "Sequence Decoding of 1D to 2D Self-Assembling Cyclic Peptides". The data presented in the sections related to this chapter (Sections 6.1, 7.1, 10.1) were derived from both the article and from additional experiments conducted in the laboratory which were not include in the manuscript.

The article "Self-Assembly of Cyclic Peptide Monolayers by Hydrophobic Supramolecular Hinges" (Section 11.1.2) was reproduced in the second Chapter of this thesis under the same title "Self-Assembly of Cyclic Peptide Monolayers by Hydrophobic Supramolecular Hinges". The data presented in the sections related to this chapter (Section 6.2, 7.2, 10.2) were derived from both the article and from additional experiments conducted in the laboratory which were not include in the manuscript.

Additionally, in Section 11.1 the author contribution for each article was specified with a list of quality indexes regarding the journal and the authorization to include the data as part of the thesis.

11.2.Conflict of interest

The PhD candidate Sandra Natalia Díaz Arias declares no conflict of interest in relation to the doctoral thesis.

Santiago de Compostela, April 2024.

11.3.Rights and permissions of the images

All images taken from articles published in Proceedings of the National Academy of Science (Proc. Natl. Acad. Sci.) do not require permission (license number) as detailed in the text:

Anyone may, without requesting permission, use original figures or tables from PNAS articles that published under the exclusive license to publish for noncommercial and educational use (i.e., in a review article, in a book that is not for sale), provided that the full journal reference is cited and, for articles published in volumes 90–105 (1993–2008), "Copyright (copyright year) National Academy of Sciences." Commercial reuse of figures and tables (i.e., in promotional materials, in a textbook for sale) requires permission from PNAS.

All images taken from American Chemical Society (ACS) journals:

PERMISSION/LICENSE IS GRANTED FOR YOUR ORDER AT NO CHARGE

This type of permission/license, instead of the standard Terms and Conditions, is sent to you because no fee is being charged for your order. Please note the following:

- Permission is granted for your request in both print and electronic formats, and translations.
- If figures and/or tables were requested, they may be adapted or used in part.
- Please print this page for your records and send a copy of it to your publisher/graduate school.
- Appropriate credit for the requested material should be given as follows: "Reprinted (adapted) with permission from {COMPLETE REFERENCE CITATION}. Copyright {YEAR} American Chemical Society." Insert appropriate information in place of the capitalized words.
- One-time permission is granted only for the use specified in your RightsLink request. No additional uses are granted (such as derivative works or other editions). For any uses, please submit a new request.

If credit is given to another source for the material you requested from RightsLink, permission must be obtained from that source.

All images that belong to the American Association for the Advancement of Science (AAAS) can be used in this thesis without specific requested permission if the articles meet the following criteria:

Can I use AAAS material in a thesis or dissertation?

Yes, different criteria apply depending upon whether you are the author of the AAAS article being reproduced.

Authors:

If you are the author of the AAAS article being reproduced, please refer to your License to Publish for rules on reproducing your paper in a dissertation or thesis.

Others:

AAAS permits the use of content published in its journals *Science*, *Science Immunology*, *Science Robotics*, *Science Signaling*, and *Science Translational Medicine* to be used in a thesis or dissertation, but only provided the following criteria are met:

1. If you are using figure(s)/table(s), permission is granted for use in print and electronic versions of your dissertation or thesis.
2. A full-text article may be used only in print versions of a dissertation or thesis. AAAS does not permit the reproduction of full-text articles in electronic versions of theses or dissertations.
3. The following credit line must be printed along with the AAAS material: "From [Full Reference Citation]. Reprinted with permission from AAAS."
4. All required credit lines and notices must be visible any time a user accesses any part of the AAAS material and must appear on any printed copies that an authorized user might make.
5. The AAAS material may not be modified or altered, with the exception that figures and tables may be modified with permission from the author. Author permission for any such changes must be secured prior to your use.
6. AAAS must publish the full paper prior to your use of any of its text or figures.
7. If the AAAS material covered by this permission was published in *Science* during the years 1974–1994, you must also obtain permission from the author, who may grant or withhold permission, and who may or may not charge a fee if permission is granted. See original article for author's address. This condition does not apply to news articles.
8. If you are an original author of the AAAS article being reproduced, please refer to your License to Publish for rules on reproducing your paper in a dissertation or thesis.
9. Permission covers the distribution of your dissertation or thesis on demand by a third-party distributor (e.g., ProQuest/UMI), provided the AAAS material covered by this permission remains in situ and is not distributed by that third party outside of the context of your thesis/dissertation.
10. Permission does not apply to figures/photos/artwork or any other content or materials included in your work that are credited to non-AAAS sources. If the requested material is sourced to or references non-AAAS sources, you must obtain authorization from that source as well before using that material. You agree to hold harmless and indemnify AAAS against any claims arising from your use of any content in your work that is credited to non-AAAS sources.
11. By using the AAAS material identified in your request, you agree to abide by all the terms and conditions herein.
12. AAAS makes no representations or warranties as to the accuracy of any information contained in the AAAS material covered by this permission, including any warranties of merchantability or fitness for a particular purpose.

Figure 8

1. Polymer Chemistry — 0,00 EUR

Article: A Guide to Supramolecular Polymerizations

Order License ID	Pending	Publisher	Royal Society of Chemistry
ISSN	1759-9954	Portion	Image/photo/illustration
Type of Use	Republish in a thesis/dissertation		

View Details — Print License

Figure 9

License Number	5754930520737
License date	Mar 23, 2024

Licensed Content

Licensed Content Publisher	John Wiley and Sons
Licensed Content Publication	Chemistry - A European Journal
Licensed Content Title	How to Distinguish Isodesmic from Cooperative Supramolecular Polymerisation
Licensed Content Author	Maarten M. J. Smulders, Marko M. L. Nieuwenhuizen, Tom F. A. de Greef, et al
Licensed Content Date	Dec 23, 2009
Licensed Content Volume	16
Licensed Content Issue	1
Licensed Content Pages	6

Order Details

Type of use	Dissertation/Thesis
Requestor type	University/Academic
Format	Print and electronic
Portion	Figure/table
Number of figures/tables	1
Will you be translating?	No

Figure 10

M. Coste, E. Suárez-Picado and S. Ulrich, *Chem. Sci.*, 2022, **13**, 909 **DOI:** 10.1039/D1SC05589E

Fragmentation and Coagulation in Supramolecular (Co)polymerization Kinetics

Your permission requested is granted as long as your thesis won't be sold, and there is no fee for this reuse. In your planned reuse, you must cite the ACS article as the source, add this direct link <https://pubs.acs.org/doi/10.1021/acscentsci.6b00009>.

Figure 11
11b is AAAS image and the permission for 11b:

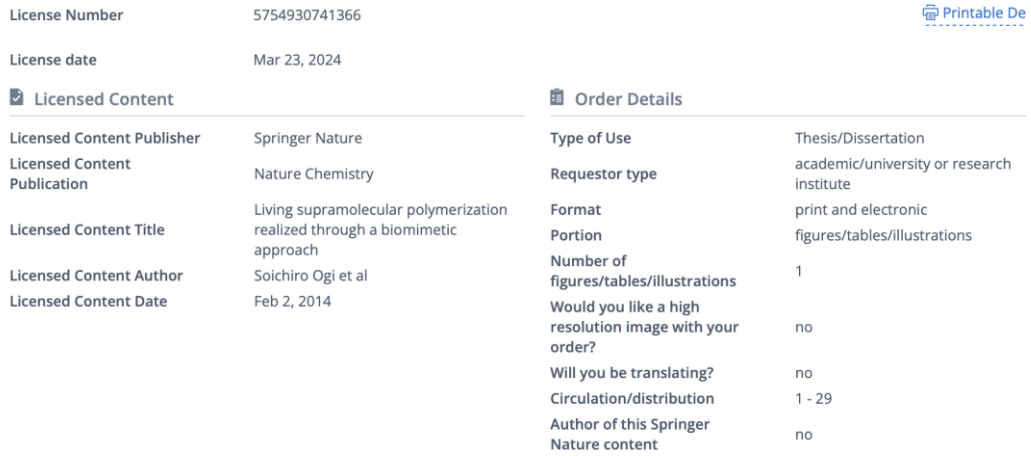

License Number	5754930741366
License date	Mar 23, 2024

Licensed Content

Licensed Content Publisher	Springer Nature
Licensed Content Publication	Nature Chemistry
Licensed Content Title	Living supramolecular polymerization realized through a biomimetic approach
Licensed Content Author	Soichiro Ogi et al
Licensed Content Date	Feb 2, 2014

Order Details

Type of Use	Thesis/Dissertation
Requestor type	academic/university or research institute
Format	print and electronic
Portion	figures/tables/illustrations
Number of figures/tables/illustrations	1
Would you like a high resolution image with your order?	no
Will you be translating?	no
Circulation/distribution	1 - 29
Author of this Springer Nature content	no

Figure 12

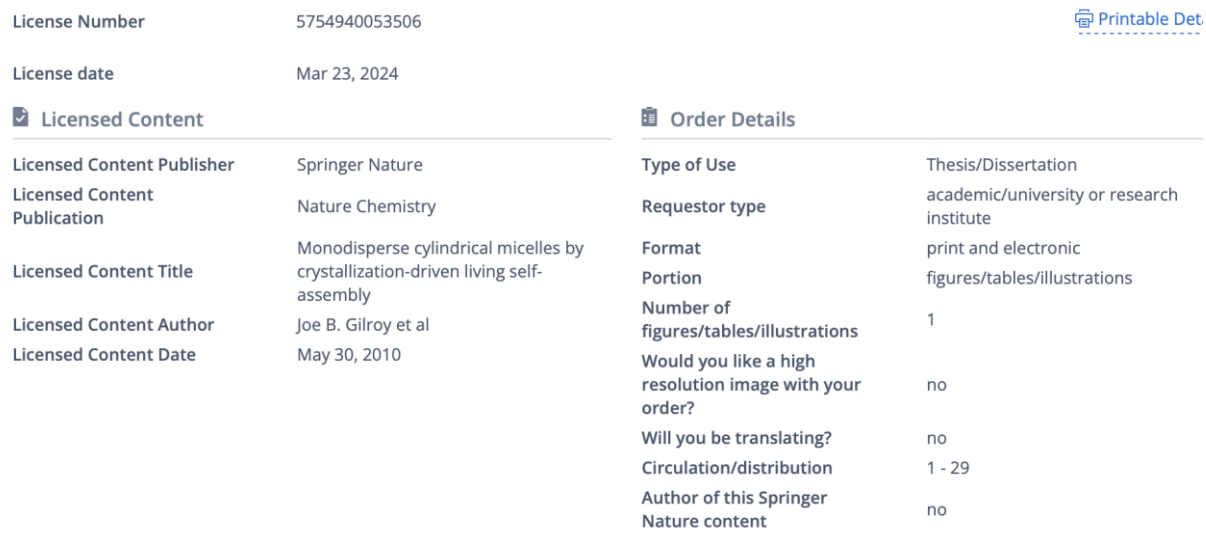

License Number	5754940053506
License date	Mar 23, 2024

Licensed Content

Licensed Content Publisher	Springer Nature
Licensed Content Publication	Nature Chemistry
Licensed Content Title	Monodisperse cylindrical micelles by crystallization-driven living self-assembly
Licensed Content Author	Joe B. Gilroy et al
Licensed Content Date	May 30, 2010

Order Details

Type of Use	Thesis/Dissertation
Requestor type	academic/university or research institute
Format	print and electronic
Portion	figures/tables/illustrations
Number of figures/tables/illustrations	1
Would you like a high resolution image with your order?	no
Will you be translating?	no
Circulation/distribution	1 - 29
Author of this Springer Nature content	no

Figure 15

I. Insua, J. Bergueiro, A. Méndez-Ardoy, I. Lostalé-Seijo and J. Montenegro, *Chem. Sci.*, 2022, **13**, 3057 **DOI:** 10.1039/D1SC05667K

Figure 17

Images in 17 a and b are adapted from PNAS, permission for 17c:

License Number	5747580160585
License date	Mar 14, 2024

Licensed Content

Licensed Content Publisher	John Wiley and Sons
Licensed Content Publication	Angewandte Chemie International Edition
Licensed Content Title	Microtubule-Binding R3 Fragment from Tau Self-Assembles into Giant Multistranded Amyloid Ribbons
Licensed Content Author	Raffaele Mezzenga, Hilal A. Lashuel, Nicholas P. Reynolds, et al
Licensed Content Date	Dec 4, 2015
Licensed Content Volume	55
Licensed Content Issue	2
Licensed Content Pages	5

Order Details

Type of use	Dissertation/Thesis
Requestor type	University/Academic
Format	Print and electronic
Portion	Figure/table
Number of figures/tables	2
Will you be translating?	No

Figure 18a

License Number	5747710825063
License date	Mar 14, 2024

Printable Details

Licensed Content

Licensed Content Publisher	Springer Nature
Licensed Content Publication	Nature Communications
Licensed Content Title	Tyrosine-mediated two-dimensional peptide assembly and its role as a bio-inspired catalytic scaffold
Licensed Content Author	Hyung-Seok Jang et al
Licensed Content Date	Apr 11, 2014

Order Details

Type of Use	Thesis/Dissertation
Requestor type	academic/university or research institute
Format	print and electronic
Portion	figures/tables/illustrations
Number of figures/tables/illustrations	2
Would you like a high resolution image with your order?	no
Will you be translating?	no
Circulation/distribution	1 - 29
Author of this Springer Nature content	no

Figure 18b

License Number	5747721022180
License date	Mar 14, 2024

Printable Details

Licensed Content

Licensed Content Publisher	Springer Nature
Licensed Content Publication	Nature Nanotechnology
Licensed Content Title	Controlled patterning of aligned self-assembled peptide nanotubes
Licensed Content Author	Meital Reches et al
Licensed Content Date	Dec 5, 2006

Order Details

Type of Use	Thesis/Dissertation
Requestor type	academic/university or research institute
Format	print and electronic
Portion	figures/tables/illustrations
Number of figures/tables/illustrations	1
Would you like a high resolution image with your order?	no
Will you be translating?	no
Circulation/distribution	1 - 29
Author of this Springer Nature content	no

Figure 19

Adapted with the permission:

Supramolecular Assembly of Peptide Amphiphiles-se images

Your permission requested is granted as long as your thesis won't be sold, and there is no fee for this reuse. In your planned reuse, you must cite the ACS article as the source, add this direct link <https://pubs.acs.org/doi/10.1021/acs.accounts.7b00297>.

Figure 20
Images in 20a are adapted from AAAS and in 20b are adapted from ACS.

Figure 21
Adapted from ACS

Figure 22
Adapted from ACS

Figure 23
Images in 23a are adapted from ACS, permission for 23 b and c are:

SPRINGER NATURE

Nanoribbons self-assembled from short peptides demonstrate the formation of polar zippers between β-sheets

Author: Meng Wang et al
Publication: Nature Communications
Publisher: Springer Nature
Date: Nov 30, 2018

Copyright © 2018, The Author(s)

Creative Commons

This is an open access article distributed under the terms of the Creative Commons CC BY license, which permits unrestricted use, distribution, and reproduction in any medium, provided the original work is properly cited.

You are not required to obtain permission to reuse this article.
To request permission for a type of use not listed, please contact Springer Nature

Figure 24b

License Number	5750380537126
License date	Mar 15, 2024

Licensed Content

Licensed Content Publisher	John Wiley and Sons
Licensed Content Publication	Chemistry - A European Journal
Licensed Content Title	Tuning One-Dimensional Nanostructures of Bola-Like Peptide Amphiphiles by Varying the Hydrophilic Amino Acids
Licensed Content Author	Jian R. Lu, Hai Xu, Sarah Rogers, et al
Licensed Content Date	Jun 30, 2016
Licensed Content Volume	22
Licensed Content Issue	32
Licensed Content Pages	11

Order Details

Type of use	Dissertation/Thesis
Requestor type	University/Academic
Format	Print and electronic
Portion	Figure/table
Number of figures/tables	1
Will you be translating?	No

Figure 25
Both images are adapted from ACS

Figures 26 and 27
Images are adapted from ACS and Angewandte Journal with the permission:

License Number	5750931040202
License date	Mar 16, 2024

Licensed Content

Licensed Content Publisher	John Wiley and Sons
Licensed Content Publication	Angewandte Chemie International Edition
Licensed Content Title	2D Crystal Engineering of Nanosheets Assembled from Helical Peptide Building Blocks
Licensed Content Author	Andrea D. Merg, Gavin Touponse, Eric van Genderen, et al
Licensed Content Date	Aug 12, 2019
Licensed Content Volume	58
Licensed Content Issue	38
Licensed Content Pages	6

Order Details

Type of use	Dissertation/Thesis
Requestor type	University/Academic
Format	Print and electronic
Portion	Figure/table
Number of figures/tables	2
Will you be translating?	No

Figure 28

Figure 29
Images in 29 a and b are adapted from AAAS and ACS respectively. Permission for 29c:

License Number	5751030980449
License date	Mar 16, 2024

Licensed Content

Licensed Content Publisher	John Wiley and Sons
Licensed Content Publication	Angewandte Chemie International Edition
Licensed Content Title	Preserving Structurally Labile Peptide Nanosheets After Molecular Functionalization of the Self-Assembling Peptides
Licensed Content Author	Xin Chen, Cai Xia, Pan Guo, et al
Licensed Content Date	Dec 6, 2023
Licensed Content Volume	63
Licensed Content Issue	2
Licensed Content Pages	8

Order Details

Type of use	Dissertation/Thesis
Requestor type	University/Academic
Format	Print and electronic
Portion	Figure/table
Number of figures/tables	1
Will you be translating?	No

Figure 30
Images in 30a are adapted from an Open Access article (Small):

Open Access Article

This is an open access article distributed under the terms of the Creative Commons CC BY license, which permits unrestricted use, distribution, and reproduction in any medium, provided the original work is properly cited.

You are not required to obtain permission to reuse this article.

For an understanding of what is meant by the terms of the Creative Commons License, please refer to Wiley's Open Access Terms and Conditions.

Permission is not required for this type of reuse.

Images in 30b are adapted from ACS

Figure 31

License Number	5754300562374
License date	Mar 22, 2024

Printable Details

Licensed Content

Licensed Content Publisher	Springer Nature
Licensed Content Publication	Nature
Licensed Content Title	Self-assembling organic nanotubes based on a cyclic peptide architecture
Licensed Content Author	M. Reza Ghadiri et al
Licensed Content Date	Dec 25, 1993

Order Details

Type of Use	Thesis/Dissertation
Requestor type	academic/university or research institute
Format	print and electronic
Portion	figures/tables/illustrations
Number of figures/tables/illustrations	2
Will you be translating?	no
Circulation/distribution	1 - 29
Author of this Springer Nature content	no

Figure 32
Images adapted from ACS

Figure 33

License Number	5754300914152
License date	Mar 22, 2024

Licensed Content

Licensed Content Publisher	John Wiley and Sons
Licensed Content Publication	Angewandte Chemie International Edition
Licensed Content Title	β-Sheet Peptide Architecture: Measuring the Relative Stability of Parallel vs. Antiparallel β-Sheets
Licensed Content Author	M. Reza Ghadiri, Juan R. Granja, Kenji Kobayashi
Licensed Content Date	Dec 22, 2003
Licensed Content Volume	34
Licensed Content Issue	1
Licensed Content Pages	4

Order Details

Type of use	Dissertation/Thesis
Requestor type	University/Academic
Format	Print and electronic
Portion	Figure/table
Number of figures/tables	1
Will you be translating?	No

Figure 34

Images adapted with the following permission:

1. Journal of materials chemistry 0,00 EUR

Article: Nanostructures of β-sheet peptides: steps towards bioactive functional materials

Order License ID	Pending
ISSN	1364-5501
Type of Use	Republish in a thesis/dissertation
Publisher	ROYAL SOCIETY OF CHEMISTRY,
Portion	Image/photo/illustration

1. Chemical communications : Chem comm 0,00 EUR

Article: Parallel and antiparallel cyclic d/l peptide nanotubes.

Order License ID	Pending
ISSN	1359-7345
Type of Use	Republish in a thesis/dissertation
Publisher	THE SOCIETY,
Portion	Image/photo/illustration

Figure 35
Images adapted from ACS

Figure 36

A. Lamas, A. Guerra, M. Amorín and J. R. Granja, *Chem. Sci.*, 2018, **9**, 8228 **DOI:** 10.1039/C8SC02276C

This article is licensed under a Creative Commons Attribution-NonCommercial 3.0 Unported Licence. **You can use material from this article in other publications, without requesting further permission** from the RSC, provided that the correct acknowledgement is given and it is not used for commercial purposes.

Figure 37
Image in 37a was taken from ACS and the permission for 37b:

License Number	5754360069676
License date	Mar 22, 2024

Licensed Content

Licensed Content Publisher	John Wiley and Sons
Licensed Content Publication	Angewandte Chemie International Edition
Licensed Content Title	Spatially Controlled Supramolecular Polymerization of Peptide Nanotubes by Microfluidics
Licensed Content Author	Javier Montenegro, Juan R. Granja, Chris Abell, et al
Licensed Content Date	Feb 28, 2020
Licensed Content Volume	59
Licensed Content Issue	17
Licensed Content Pages	7

Order Details

Type of use	Dissertation/Thesis
Requestor type	University/Academic
Format	Print and electronic
Portion	Figure/table
Number of figures/tables	2
Will you be translating?	No

Figure 38

License Number	5754360491065
License date	Mar 22, 2024

Licensed Content

Licensed Content Publisher	John Wiley and Sons
Licensed Content Publication	Angewandte Chemie International Edition
Licensed Content Title	Secondary Self-Assembly of Supramolecular Nanotubes into Tubisomes and Their Activity on Cells
Licensed Content Author	Angus Johnston, Katrina A. Jolliffe, Sébastien Perrier, et al
Licensed Content Date	Nov 21, 2018
Licensed Content Volume	57
Licensed Content Issue	51
Licensed Content Pages	5

Order Details

Type of use	Dissertation/Thesis
Requestor type	University/Academic
Format	Print and electronic
Portion	Figure/table
Number of figures/tables	1
Will you be translating?	No

License Number	5754360847553
License date	Mar 22, 2024

Licensed Content

Licensed Content Publisher	John Wiley and Sons
Licensed Content Publication	Angewandte Chemie International Edition
Licensed Content Title	Hierarchical Self-Assembled Photo-Responsive Tubisomes from a Cyclic Peptide-Bridged Amphiphilic Block Copolymer
Licensed Content Author	Jie Yang, Ji-Inn Song, Qiao Song, et al
Licensed Content Date	Mar 25, 2020
Licensed Content Volume	59
Licensed Content Issue	23
Licensed Content Pages	4

Order Details

Type of use	Dissertation/Thesis
Requestor type	University/Academic
Format	Print and electronic
Portion	Figure/table
Number of figures/tables	1
Will you be translating?	No

Figure 39
Image from ACS

Figure 40
Image from ACS

Self-assembly is a fundamental process whereby individual molecules spontaneously associate into well-defined structures. Nature employs self-assembly to create complex architectures with remarkable structural and functional precision. This natural sophistication has inspired scientists to rationally design synthetic analogues for the fabrication of structures and functions not evolved in nature. Despite important developments in this field, the design of synthetic molecules with hierarchical levels of self-assembly remains a challenging task. In this doctoral thesis, synthetic cyclic peptides are explored as customizable building blocks for the hierarchical self-assembly of multidimensional nanostructures. Key design principles are presented to direct hierarchical stages of self-assembly by rational molecular design.